

1-2-2013

Methodologies For Attaching Polypyridyl Ligands Into Amino Acids And Synthesis And Biological Evaluation Of Novel Light Activated Peptidomimetic Cysteine Protease Inhibitors Caged By Ru(II)(bpy)₂

Tomasz Respondek
Wayne State University,

Follow this and additional works at: http://digitalcommons.wayne.edu/oa_dissertations

 Part of the [Chemistry Commons](#)

Recommended Citation

Respondek, Tomasz, "Methodologies For Attaching Polypyridyl Ligands Into Amino Acids And Synthesis And Biological Evaluation Of Novel Light Activated Peptidomimetic Cysteine Protease Inhibitors Caged By Ru(II)(bpy)₂" (2013). *Wayne State University Dissertations*. Paper 792.

This Open Access Dissertation is brought to you for free and open access by DigitalCommons@WayneState. It has been accepted for inclusion in Wayne State University Dissertations by an authorized administrator of DigitalCommons@WayneState.

**METHODOLOGIES FOR ATTACHING POLYPYRIDYL LIGANDS INTO AMINO
ACIDS
AND
SYNTHESIS AND BIOLOGICAL EVALUATION OF NOVEL LIGHT ACTIVATED
PEPTIDOMIMETIC CYSTEINE PROTEASE INHIBITORS
CAGED BY Ru^{II}(bpy)₂**

by

TOMASZ RESPONDEK

DISSERTATION

Submitted to the Graduate School

of Wayne State University,

Detroit, Michigan

in partial fulfillment of the requirements

for the degree of

DOCTOR OF PHILOSOPHY

2013

MAJOR: CHEMISTRY (Organic)

Approved by:

Advisor Date

© COPYRIGHT BY
TOMASZ RESPONDEK
2013
All Rights Reserved

DEDICATION

*This thesis is dedicated to my parents, grandparents and godfather
for their never-ending commitment to make me a better person*

ACKNOWLEDGMENTS

I would like to express my deepest gratitude to Prof Jeremy Kodanko, for his guidance and mentorship throughout the duration of my studies in his laboratory. He has been an incredible source of help, motivation, knowledge and inspiration which resulted in a great learning environment for me and the other students in the group. Prof Kodanko has never given up on me, and his support has been constant, despite my difficult and stubborn character. I don't know if I will ever be able to express how thankful I am for that.

I would like to extend my acknowledgments to my committee members, Prof Firestine, Prof Guo and Prof Hendrickson. Thank you for all the time and advice that you have given me. Most of all, I do not know if I would have been able to schedule any of the required meetings without your complete cooperation and flexibility.

None of the results presented in the second part of this dissertation would have been possible without the help of our collaborators. I wish to express my deepest appreciation for the time and money that Prof Podgorski and Prof Turro have spent to help me carry out my research. I must in particular thank Izabela for welcoming me in her laboratory and making me feel as one of her students from the second I entered the premises. She has been a great mentor and a great person.

I would like to thank all of the students that I had the opportunity to work with. I am in particular grateful to my labmates: Ashley, Mirvat, Nadiya, Selma, Ahmed, Anil, Casey, Eric, Jai, Nitin and Raj. The results presented in the first part of this dissertation were only possible because of a collaborative effort with Selma, Nitin and Eric. Thanks guys! Any of the work done at the Pharmacology department wouldn't have been possible without Mackenzie, Aimalie and Erandi. You guys made biochemistry easy for me, and that wasn't given. Thank you so much.

I also would like to thank all the other students that I had the opportunity to meet at Wayne State, including all the undergraduate students that were an important part of my life over those five years as well as all the staff members from the Science Stores, the CIF and Nestor, Marty, Lew, Bashar and Brian in particular.

A special note goes to all my friends that I met here in Detroit. Being surrounded by great people, made difficult moments a lot easier to deal with but most importantly made me feel like Detroit was my home. Stephane, Ivan, Ben and Jeremy thank you for being my chemistry mentors. You always had time and unlimited advice. Mark and Jean-Paul, thanks for all the great moments that we had at 720 East Second. Sharing my life with you was an honor and a blast. Anaïs, Anne-Cécile and Myriame, thank you for bringing the feminine touch into my life over those years.

Finally, none of this would have been possible without my family. Your support, help and understanding is without measure.

TABLE OF CONTENTS

Dedication	ii
Acknowledgments	iii
List of Schemes	ix
List of Figures	x
List of Tables	xiii
List of Abbreviations	xiv
Part I : Methodologies for attaching polypyridyl ligands into amino acid side chains	1
Chapter 1. Introduction	1
I.1.A. Peptide ligand conjugates	3
I.1.A.a. Ligand attachment through amino acid side chains	5
I.1.A.b. Preparation of metal chelating unnatural amino acids	7
I.1.B. Biomedical applications of peptide ligand conjugates	9
I.1.C. Ferryl chemistry	13
I.1.D. Solid phase chemistry/peptide synthesis	16
I.1.E. Unnatural amino acid synthesis strategies	23
I.1.F. Enantioselective alkylation of glycine imine derivatives	27
I.1.F.a. Strategies	27
I.1.F.b. Substrate and catalyst optimization	28
I.1.G. Thesis statement (Part I)	31
Chapter 2. Novel, divergent strategy for the synthesis of peptide polypyridyl ligand conjugates and its applications to SPPS	34
I.2.A. Background and project design	34
I.2.B. Results and discussion	36
I.2.B.a. Fmoc-HPMA-OH	36

I.2.B.b. Applications to SPPS	41
I.2.C. Conclusion.....	44
I.2.D. Experimental section	45
I.2.D.a. General considerations.....	45
I.2.D.b. Experimental procedures and tabulated characterization data.....	46
Chapter 3. Development of an “optimal substrate” for the enantioselective alkylation of benzophenone imine	60
I.3.A. Background and project design	60
I.3.B. Results and discussion.....	63
I.3.B.a. Synthesis of cumyl ester protected benzophenone imine	63
I.3.B.b. Enantioselective alkylation conditions optimization	64
I.3.B.c. Reaction scope	65
I.3.B.d. Hydrogenolysis of 89b and synthesis of Fmoc-HPA-OH 62	67
I.3.B.e. Synthesis of Fmoc-HPN-OH 60	68
I.3.C. Conclusion.....	69
I.3.D. Experimental section	71
I.3.D.a. General considerations.....	71
I.3.D.b. Experimental procedures and tabulated characterization data.....	72
Part II : Synthesis and biological evaluation of novel light activated cysteine proteases inhibitors caged by Ru ^{II} (bpy) ₂	83
Chapter 1. Introduction:	83
II.1.A. Proteases.....	83
II.1.B. Cysteine cathepsins and cancer	84
II.1.C. Cysteine cathepsin inhibitors	85
II.1.D. Metals as therapeutic or biologically relevant agents	85

II.1.D.a. Platinum anticancer drugs.....	86
II.1.D.b. Ruthenium anticancer drugs	87
II.1.E. Kinetic and spatial control over drug delivery	92
II.1.E.a. Photodynamic therapy (PDT) and chromophore-assisted laser inactivation (CALI) strategies.....	92
II.1.E.b. Caging strategies using Ru complexes	94
II.1.F. Photodissociation of $[\text{Ru}(\text{bpy})_2(\text{X})_2](\text{Y})_2$ complexes	98
II.1.G. Thesis statement (Part II)	99
Chapter 2. Synthesis and biological testing of the first nitrile containing cysteine protease inhibitor caged by $\text{Ru}^{\text{II}}(\text{bpy})_2$ and activated by light	101
II.2.A. Background and project design	101
II.2.B. Results and discussion.....	103
II.2.B.a. Synthesis of nitrile cathepsin inhibitor 119	103
II.2.B.b. Synthesis of <i>cis</i> - $[\text{Ru}(\text{bpy})_2(\mathbf{119})_2](\text{PF}_6)_2$	104
II.2.B.c. Characterization of <i>cis</i> - $[\text{Ru}(\text{bpy})_2(\mathbf{119})_2](\text{PF}_6)_2$	105
II.2.B.d. Stability in the dark and release using light.....	106
II.2.B.e. Biological evaluation of nitrile containing cysteine protease inhibitor caged by $\text{Ru}^{\text{II}}(\text{bpy})_2$ against papain.....	109
II.2.B.f. Biological evaluation of nitrile containing cysteine protease inhibitor caged by $\text{Ru}^{\text{II}}(\text{bpy})_2$ against isolated human cathepsins	111
II.2.B.g. Biological evaluation of nitrile containing cysteine protease inhibitor caged by $\text{Ru}^{\text{II}}(\text{bpy})_2$ against cathepsins B in cancer cell lysates	112
II.2.C. Conclusions and further directions.....	113
II.2.D. Experimental section.....	114
II.2.D.a. General considerations.....	114
II.2.D.b. Experimental procedures and tabulated characterization data.....	115
II.2.D.c. Enzyme Inhibition Studies.....	120

Chapter 3. Synthesis and biological testing of a second generation nitrile containing cathepsin K inhibitor caged by Ru ^{II} (bpy) ₂ and live cell assays	129
II.3.A. Background and project design	129
II.3.B. Results and discussion.....	130
II.3.B.a. Synthesis of nitrile cathepsin K inhibitor 124	130
II.3.B.b. Synthesis of <i>cis</i> -[Ru(bpy) ₂ (124) ₂]Cl ₂	131
II.3.B.c. Characterization of <i>cis</i> -[Ru ^{II} (bpy) ₂ (124) ₂]Cl ₂	132
II.3.B.d. Stability in the dark and release using light.....	133
II.3.B.e. Biological evaluation of a nitrile containing cathepsin K inhibitor 124 caged by Ru ^{II} (bpy) ₂ (126) against isolated human cathepsin K	135
II.3.B.f. Biological evaluation of a nitrile containing cathepsin K inhibitor 124 caged by Ru ^{II} (bpy) ₂ (126) in live cells.....	137
II.3.B.g. Toxicity evaluation of a nitrile containing cathepsin K inhibitor 124 caged by Ru ^{II} (bpy) ₂ (126)	141
II.3.C. Conclusions and further directions.....	143
II.3.D. Experimental section	145
II.3.D.a. General considerations.....	145
II.3.D.b. Experimental procedures and tabulated characterization data.....	146
II.3.D.c. Cathepsin K inhibition studies.....	151
II.3.D.d. Cell Viability Determinations.....	153
References.....	186
Abstract.....	208
Autobiographical Statement.....	210

LIST OF SCHEMES

Scheme 1: Retrosynthetic approach to HPMA using L-serine as a starting material	37
Scheme 2: Synthesis of the 2,5-substituted pyridine derivatives	37
Scheme 3: Serine as the nucleophilic partner in one phase alkylation reactions	38
Scheme 4: Serine as the nucleophilic partner in PTC alkylation trials	39
Scheme 5: Hydrogenation of the <i>O</i> -alkylation product 66c and subsequent Fmoc protection....	40
Scheme 6: Construction of polypyridyl ligand-peptide conjugates by SPPS on Rink amide resin.....	42
Scheme 7: Construction of heptapeptide 77 by SPPS.....	44
Scheme 8: Retrosynthetic analysis of HPA and HPN unnatural amino acids	60
Scheme 9: N. Jabre's synthesis of Fmoc-HPA(OTBS)-OH 62	61
Scheme 10: S. Ulku's synthesis of Fmoc-HPN(OTBS)-OH 60	62
Scheme 11: Synthesis of cumyl ester protected benzophenone imine.....	64
Scheme 12: Optimization of the asymmetric alkylation conditions with the cumyl ester 88	65
Scheme 13: Scope of the asymmetric alkylation reaction with the cumyl ester 88	66
Scheme 14: Synthesis of Fmoc-HPA-OH 62 from product 89b	68
Scheme 15: Synthesis of Fmoc-HPN-OH 60 from 89f	69
Scheme 16: Synthesis of nitrile inhibitor Ac-Phe-Gly-ψ[C≡N] 119	104
Scheme 17: Synthesis of <i>cis</i> -[Ru ^{II} (bpy) ₂ (119) ₂] ²⁺	104
Scheme 18: Synthesis of cathepsin K nitrile inhibitor Cbz-Leu-Gly-ψ[C≡N] 124	130
Scheme 19: Synthesis of <i>cis</i> -[Ru ^{II} (bpy) ₂ (124) ₂]Cl ₂	132

LIST OF FIGURES

Figure 1: Strategies for attaching metals to peptides by SPPS	3
Figure 2: Different modes of attachment of metal ligands to peptides.....	5
Figure 3: Examples of amino acids bearing metal ligands prepared from lysine.....	6
Figure 4: Examples of amino acids bearing metal ligands prepared from natural amino acids	7
Figure 5: Examples of unnatural amino acids bearing metal ligands attached to the backbone ...	9
Figure 6: ¹¹¹ In-DTPA-octreotide or OctreoScan®: the first FDA approved radiolabelled peptide for cancer imaging.....	10
Figure 7: Commonly used radiometal chelators	11
Figure 8: VEGF antagonist (Ru ^{II} (bpy) ₃ ²⁺)-GU40C metal peptoid conjugate.....	13
Figure 9: The oxidation chemistry of ferryl complexes	15
Figure 10: Merrifield's first solid phase synthesis sequence of a tetrapeptide.....	18
Figure 11: Boc and Fmoc deprotection.....	20
Figure 12: Commonly used resins and linkers in SPPS.....	20
Figure 13: Formation of an intermediate oxazolone that epimerizes the R ₂ α-carbon geometry while building a peptide from the N-terminus (example on PEG resin)	21
Figure 14: Absence of formation of an intermediate oxazolone while peptide is built from the C-terminus (use of carbamate protection) (example on PEG resin).....	22
Figure 15: Commonly used peptide coupling agents.....	23
Figure 16: Different approaches to build α-AAs ⁸⁰	25
Figure 17: Asymmetric hydrogenation of α-β-dehydro α-AAs with Rh complexes.....	26
Figure 18: Asymmetric hydrogenation of α-β carbon-nitrogen double bonds with bidentate phosphine ligand-metal complexes.....	26
Figure 19: Strecker type asymmetric α-AA synthesis	27
Figure 20: Phase transfer catalysis of α-aminoacid ester imines.....	28
Figure 21: First example of <i>Cinchona</i> derived PTC of glycine imines by O'Donnell.....	29

Figure 22: Optimized cinchonidinium PTC for the asymmetric alkylation of glycine imines.....	30
Figure 23: C ₂ -symmetric quaternary salts derived from (R)-or (S)-Binol.....	31
Figure 24: Design of the HPA(OTBS) unnatural amino acid leading to the synthesis of dipeptide Ac-HPA(Fe ^{IV} (O)(N ₃ Py))-Gly-OBn	34
Figure 25: Design of the second generation unnatural amino acids HPN and HPMA.....	35
Figure 26: Solid phase, divergent and combinatorial, synthesis of peptide-ferryl conjugates	36
Figure 27: Examples of phase transfer catalysts used in the alkylation of glycine benzophenone imine reaction	63
Figure 28: FDA approved platinum complexes for cancer treatment	86
Figure 29: Early Ru based complexes with anticancer activity.....	87
Figure 30: Ru complexes being investigated in clinical trials.....	88
Figure 31: Examples of Ru-arene complexes with anticancer activity	89
Figure 32: Examples of Ru-polypyridyl complexes mimicking cisplatin	90
Figure 33: New classes of polypyridyl ruthenium complexes that lack labile ligands.....	91
Figure 34: Ru(bpy) ₃ ²⁺ used as a CALI photosensitizer	93
Figure 35: [Ru(bpy) ₃] ²⁺ -GU40C CALI agent.....	94
Figure 36: Ru complexes used as cages: prodrugs of Ru based, cisplatin like anticancer agents	95
Figure 37: Double directing strategy of a potential anticancer Ru complex [(p-cym)Ru(bpm)(py-linker-peptide)] ²⁺	96
Figure 38: Ru based caging of amine based neurotransmitters	97
Figure 39: Light activated release of nitrile containing cysteine proteases.....	102
Figure 40: Δ- <i>cis</i> -[Ru(bpy) ₂ (119) ₂](PF ₆) ₂ and Λ- <i>cis</i> -[Ru(bpy) ₂ (119) ₂](PF ₆) ₂	105
Figure 41: Plot of ln A vs t for complex 123 in 0.1M phosphate pH 6.5 buffer at RT.	107
Figure 42: Plot of ln A vs t for complex 123 in DMSO at RT.	107
Figure 43: Changes to the electronic absorption spectrum of 30 μM <i>cis</i> -[Ru(bpy) ₂ (119) ₂](PF ₆) ₂ (123) in a 1% DMSO aqueous solution upon irradiation (λ _{irr} > 395 nm) at t _{irr} = 0, 2, 3, 4, 5, 6, and 7 min; inset: 0, 1 min.....	108

Figure 44: IC ₅₀ curves for 119 (red) and 123 (with irradiation, blue, and without, black) against the cysteine protease papain.	110
Figure 45: IC ₅₀ curve for inhibition of cathepsin B activity with 119 (red), 123 “light” (yellow), and 123 “dark” (blue).....	122
Figure 46: IC ₅₀ curve for inhibition of cathepsin K activity with 119 (red), 123 “light” (yellow), and 123 “dark” (blue).....	124
Figure 47: IC ₅₀ curve for inhibition of cathepsin L activity with 119 (red), 123 “light” (yellow), and 123 “dark” (blue).....	125
Figure 48: IC ₅₀ curve for inhibition of cathepsin B activity from DU145 lysates with 119 (red), 123 “light” (yellow), and 123 “dark” (blue).....	127
Figure 49: IC ₅₀ curve for inhibition of cathepsin B activity from hBMSC lysates with 119 (red), 123 “light” (yellow), and 123 “dark” (blue).....	128
Figure 50: Cathepsin K inhibitor chosen for the second generation Ru-caged complex with literature reported IC ₅₀ and K _i values	130
Figure 51: Δ - <i>cis</i> -[Ru(bpy) ₂ (124) ₂]Cl ₂ and Λ - <i>cis</i> -[Ru(bpy) ₂ (124) ₂]Cl ₂	132
Figure 52: Changes to the electronic absorption spectrum of 52 μ M <i>cis</i> -[Ru(bpy) ₂ (124) ₂]Cl ₂ (126) in a 1% DMSO aqueous solution upon irradiation ($\lambda_{\text{irr}} > 395$ nm) at t _{irr} = 0, 3, 4, 5, 6, 7, 8, 10 and 15 min; inset: 0, 1 and 2 min	134
Figure 53: IC ₅₀ curves for inhibitor 124 (red, “dark”; green, “light”) and <i>cis</i> -[Ru(bpy) ₂ (124) ₂]Cl ₂ (126) (black, “dark”; blue, “light”) against isolated cathepsin K.....	136
Figure 54: Confocal microscopy images of mouse bone marrow macrophages cells treated with 250 nM complex 126 plus CA074 (1 μ M) for measuring specific Cat K activity, with or without irradiation, plus controls.....	139
Figure 55: Quantitative analysis of cathepsin K inhibition by <i>cis</i> -[Ru(bpy) ₂ (124) ₂]Cl ₂ (126) in live bone marrow macrophages (BMMs) under the dark and light conditions.....	140
Figure 56: BMM cell viability 24 hours after treatment with various concentrations of 126 or <i>cis</i> -[Ru ^{II} (bpy) ₂ (MeCN) ₂]Cl ₂ assayed using the MTT assay	142
Figure 57: PC3 cell viability 72 hours after treatment with various concentrations of 126 or <i>cis</i> -[Ru ^{II} (bpy) ₂ (MeCN) ₂]Cl ₂ assayed using the MTT assay	142

LIST OF TABLES

Table 1: <i>O</i> -Alkylation of protected serine derivatives in a homogenous solution.....	38
Table 2: <i>O</i> -Alkylation of protected serine derivatives in a heterogeneous solution using PTC..	39
Table 3: Hydrogenation of the <i>O</i> -alkylation product 66c	40
Table 4: Standard Solid Phase Peptide Synthesis (0.1 mmol scale)	52
Table 5: Reactions on the side chain (0.1 mmol scale).....	53
Table 6: Optimization of the asymmetric alkylation conditions with the cumyl ester 88	65
Table 7: Scope of the asymmetric alkylation reaction with the cumyl ester 88	66
Table 8: IC ₅₀ values (μM) for 119 and 123 (with and without irradiation) against isolated human cathepsins B, L and K with ratios under light vs. dark conditions	112
Table 9: IC ₅₀ values (μM) for 119 and 123 (with and without irradiation) against cathepsin B in human cell lysates with ratios under light vs. dark conditions	113

LIST OF ABBREVIATIONS

AA: amino acid

Ac₂O: acetic anhydride

BOC: *tert*-butoxycarbonyl

CALI: chromophore-assisted light inactivation

Cbz: Carboxybenzyl

DCC: N,N'-dicyclohexylcarbodiimide

DIPEA: diisopropylethylamine

DMF: dimethylformamide

EDC·HCl: N-(3-dimethylaminopropyl)-N'-ethylcarbodiimide

ee: enantiomeric excess

Et₂O: diethyl ether

EtOAc: ethyl acetate

EtOH: ethanol

Fmoc: N-(9-fluorenylmethoxycarbonyl)

GSH: glutathione

H-Gly-OBn: glycine benzyl ester

HOBt: N-hydroxybenzotriazole

KIE: kinetic isotope effect

LHRH: luteinizing hormone-releasing hormone

MeCN: acetonitrile

NBS: N-bromosuccinimide

PDT: photodynamic therapy

PPh₃: triphenylphosphine

PTC: phase transfer catalysis

ROS: reactive oxygen species

SPPS: solid phase synthesis

TBAB: tetrabutylammonium bromide

TBAF: tetrabutylammonium fluoride

TBAS: tetrabutylammonium sulfate

TBS-Cl: tert-butyldimethylsilyl chloride

TEA: triethylamine

TEBAC: benzyltriethylammonium chloride

TFA: trifluoroacetic acid

THF: tetrahydrofuran

TsCl: tosyl chloride

Vitride: sodium bis(2-methoxyethoxy)aluminum hydride solution

Part I : Methodologies for attaching polypyridyl ligands into amino acid side chains

Chapter 1. Introduction

One of the biggest challenges encountered by medicinal chemists is to gain specificity to avoid off-target side effects. Ideally the drug should only target the organism or organ affected by the condition. Many potential solutions have been proposed by numerous researchers working in the field, but a final answer has still not been found. One interesting and elegant method consists of attaching the potential drug molecule to a vector molecule which provides specificity for a class of tissues, cells or organs. Vectors are usually (bio)molecules such as nutrients for cells (sugars, amino acids, etc.), cofactors (Vitamin B₁₂), antibodies or others.¹

Although metals have been used as medicines for the last 4500 years, it's only the serendipitous discovery of a few metal-based drugs in the late 20th century such as Auranofin or cisplatin² that triggered a rational design of drugs based on metals. In early examples, researchers have exploited these early discoveries to design second generation drugs. Advances in inorganic chemistry, ligand synthesis and biochemistry have enabled the construction of novel metal based drugs for alternative targets such as thiol-containing proteins, redox processes, reactive oxygen species (ROS)³ and others.

In an effort to combine those two ideas and mimic nature's use of metalloproteins, bioinorganic chemists developed metal-peptide conjugates and explored them as potential medicinal agents, catalysts and in *de novo* proteins.^{4,6} They found numerous applications as

radiopharmaceuticals⁷⁻⁹, imaging agents,¹⁰⁻¹² anticancer or antibacterial agents¹ or DNA/protein inactivating agents.¹³⁻¹⁵

In spite of a great interest in attaching metals or metal ligands to peptides, there is a lack of methods that would enable an easy construction of ligands based on nitrogen-containing heterocycles attached to peptides. Previous studies present ways to append 2 or 3 atom donor ligands to peptides¹⁶⁻¹⁹ but methodologies using polydentate ligands beyond 3 are scarce.²⁰ The Kodanko group recently showed the use of polydentate non-heme ligands and the corresponding iron or cobalt complexes as agents that can cleave or oxidize amino acids,^{21, 22} have anticancer properties through carbon monoxide release,²³ inhibit the purified 20S proteasome²⁴ or mimic glutathionylcobalamin (GSCbl).²⁵ Tethering those complexes to peptides with the aim of specific delivery should first improve their activity and second enable a more in depth study of their modes of action. We sought to develop a divergent strategy for attaching such polypyridyl ligands to peptides through amino acid side chains through the synthesis of novel unnatural amino acids and applying them using solid phase synthesis (SPPS) in order to build their corresponding metal complexes. The divergency of the methodology would consist in introducing the ligand diversity as late as possible.

My contributions while in the Kodanko group towards the synthesis of those novel unnatural amino acids and their application through SPPS to accessing novel metal-peptide conjugates will be discussed in the first part of this dissertation. The first chapter will give a brief introduction on the different possibilities of building metal peptide conjugates and their applications, ferryl complexes and solid phase synthesis. Methodologies giving access to unnatural amino acids will be discussed with a special emphasis on enantioselective alkylation of benzophenone imine. The second chapter will present the conjoint development, with fellow

coworkers from the Kodanko group, Dr. Nitinkumar Jabre and M. Sc. Selma Ulku, of a novel divergent strategy for the synthesis of peptide polypyridyl ligand conjugates and its applications to SPPS. The third chapter will present the development of an optimal substrate for the enantioselective benzophenone glycine imine alkylation reaction enabling the use of acid sensitive substrates. The final chapter will present the conclusions of this first part of the dissertation, state the achievements and their importance and present future goals.

I.1.A. Peptide ligand conjugates

This section will give a brief overview of the different possibilities for attaching metal ligands to peptides. A more in depth description can be found in Dr. Nitinkumar Jabre's dissertation entitled: "Synthesis of peptide-ligand conjugates and their applications".²⁶

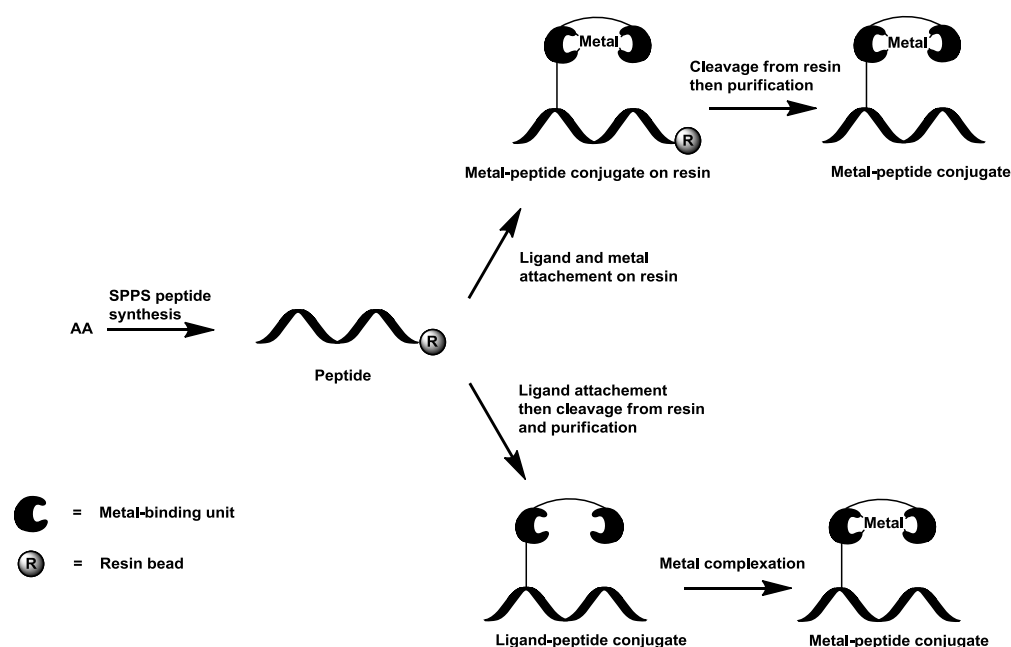


Figure 1: Strategies for attaching metals to peptides by SPPS

In principle there are two different strategies for attaching a metal to a peptide chain. The metal could either be covalently attached while the peptide is being built by SPPS or after

cleavage from resin and purification. The first strategy has the advantages of the synthesis being completed on resin and should in theory require less purification efforts. It has the inconvenience that the metal-peptide conjugate must survive the conditions used to cleave the peptide from resin.¹ For this reason we have chosen to focus on the second strategy only. The ligand peptide conjugate will be first synthesized in solution or by SPPS, purified and characterized before the metal complex is formed (Figure 1). Many different modes for the attachment of the metal ligand to the peptide can be imagined. The reactivities of the functional groups on both the C-, and N-termini can be used to covalently attach metal ligands to the peptide. Using a similar approach the ligands can be incorporated in the backbone as well. Other functional groups that can be found on some of the side-chains from the natural amino acids (lysine, glutamic and aspartic acid, tyrosine, phenylalanine) have been used to tether ligands through the side chain. Finally unnatural amino acids already having ligands attached to them, or having functional groups that can be used towards this goal can be synthesized (Figure 2).

In the next two sections, details about tethering ligands through the side-chains of natural amino acids and methodologies for the synthesis of novel unnatural amino acids will be given. We have chosen these two modes as the most pertinent because they enable the most flexibility in which position within the peptide the metal complex will be placed. For all the other modes of attachment please refer to Dr. Jabre's dissertation entitled "Synthesis of peptide-ligand conjugates and their applications".²⁶

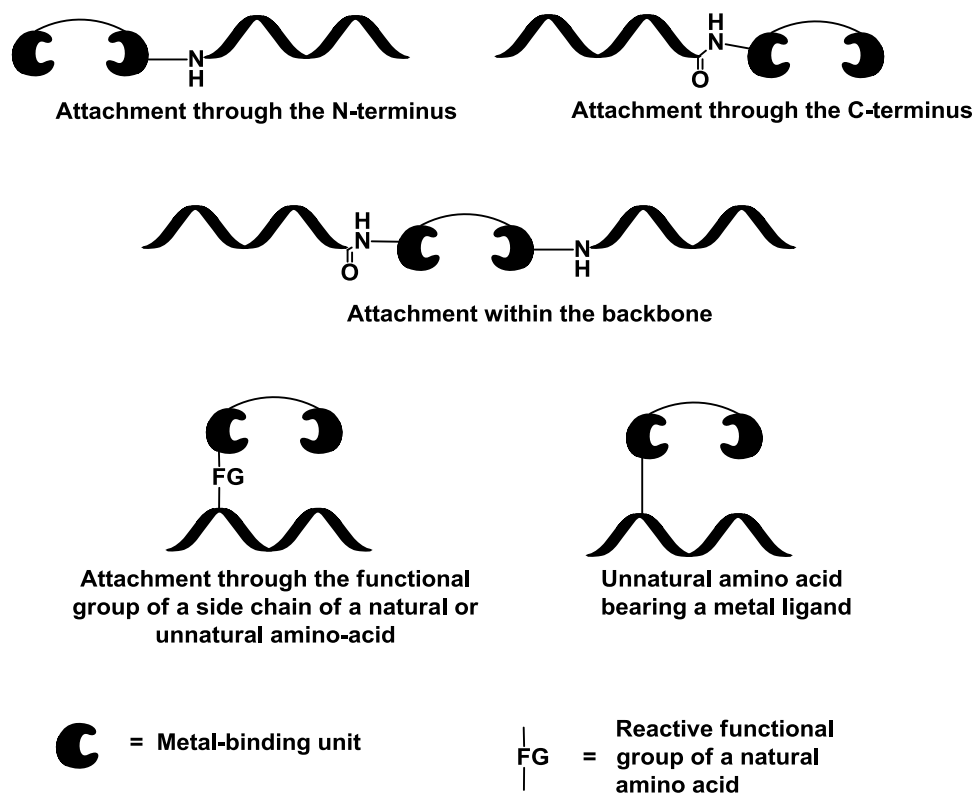


Figure 2: Different modes of attachment of metal ligands to peptides

I.1.A.a. Ligand attachment through amino acid side chains

Among the twenty natural amino acids, lysine's primary amine has been the most used side chain functional group to attach ligands to amino acids. The amino group can participate in reductive aminations, alkylation reactions giving the corresponding secondary or tertiary amines, amide bond formations, or can be transformed into the corresponding azide functionality to be further conjugated through "click" chemistry.

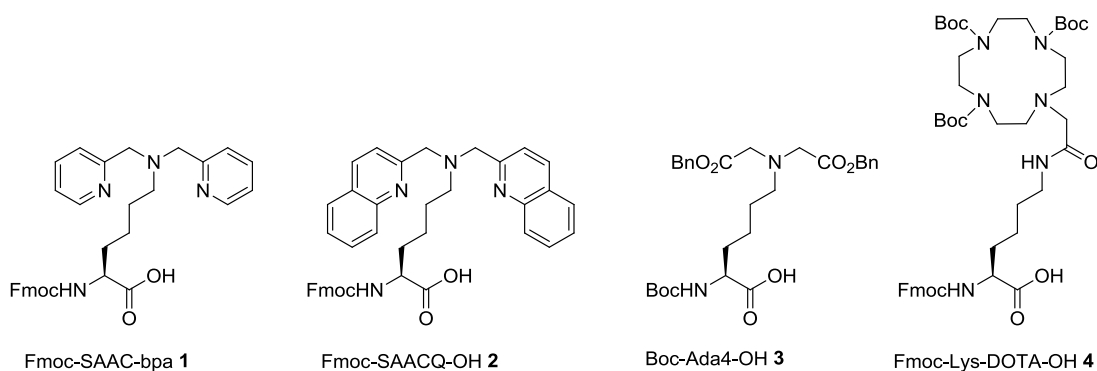


Figure 3: Examples of amino acids bearing metal ligands prepared from lysine

The Vaillant group prepared the single amino acid chelates (SAAC) containing bpa (2,2-bis(pyridylmethyl)amine) (**1**)^{27, 28} or bqa (2,2-bis(quinoleylmethyl)amine) (**2**)^{7, 29} using the reductive amination reaction between Fmoc-protected lysine and 2-pyridinecarboxaldehyde or quinoline-2-aldehyde, followed by reduction with a borohydride (Figure 3).

Aminodiacetic acid residues can be introduced into peptides by direct *N*-alkylation of lysine with benzyl-2-bromoacetate to give Boc-Ada₄-OH (**3**) according to the work of the Hopkins group.³⁰ Other amino acids bearing the same aminodiacetic acid motif could be prepared in a similar fashion if unnatural amino acids resembling lysine, but with shorter linkers (1-3 carbons) between the backbone and the amino functionality, were used (Figure 3).

Lysine can also participate in amide bond formation reactions. The Sherry group explored this reactivity to prepare Fmoc-Lysine-DOTA-OH (**4**). Bromoacetyl bromide was used to make the amide bond, and the resulting bromide was displaced with triprotected DO3A-(tBu₃) (Figure 3).³¹

Although lysine has been the most used natural amino acid to attach ligands to peptides, other amino acids such as glutamic and aspartic acids, tyrosine and phenylalanine have also been used. The Hovinen group used glutamic acid to attach a lanthanide (III) chelate through a peptide

bond formation reaction to make unnatural amino acid (**5**).³² In a very similar fashion, p-Aminoobenzyl-EDTA has been attached to aspartic acid by the Rana group (**6**) (Figure 4).³³

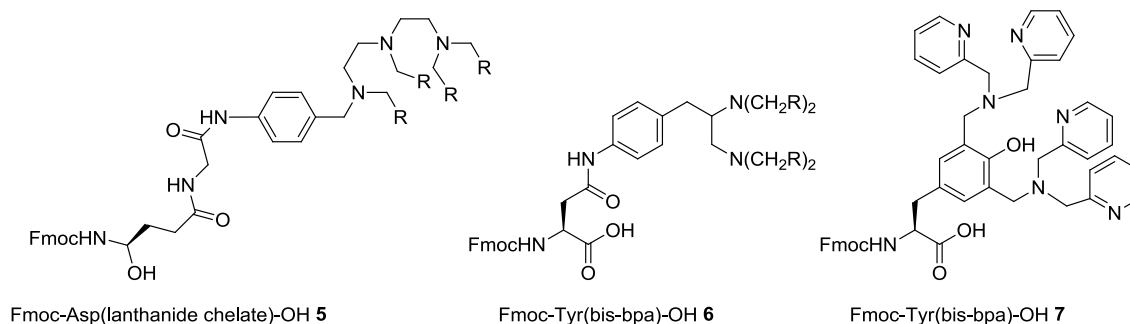


Figure 4: Examples of amino acids bearing metal ligands prepared from natural amino acids

The Smith group used tyrosine to attach two bpa (2,2-bis(pyridylmethyl)amine) units in a very short and clever way. The iminium ion, resulting from the Mannich reaction between dipicolylamine and paraformaldehyde, was reacted with tyrosine following an electrophilic aromatic substitution reaction to give zinc (II) chelator (**7**) (Figure 4).³⁴

I.1.A.b. Preparation of metal chelating unnatural amino acids

A different approach consists of preparing unnatural amino acids which bear metal-binding units directly attached to the peptide backbone. Most of the amino acids prepared this way have been incorporated into peptides using Fmoc based SPPS. Reactive functional groups are usually protected using acid sensitive protecting groups that are cleaved under the acid-mediated cleavage from resin.

The Imperiali group explored the Zn^{II} affinity of different bipyridine or phenanthroline containing alanine derivatives synthesized by asymmetric alkylation of benzophenone glycine imine. Molecules **8-12**^{17-19, 35} showed different metal binding affinities depending on the bipyridine moiety. Other bidentate or tridentate ligands featuring pyridoxal coenzyme (**13**)¹⁶ or quinoxaline³⁶ have also been prepared using the same synthetic method (Figure 5).

The Scrimin group used electrophilic serine β -lactone derivatives to directly attach the triazacyclononane (tacn) group to the β -carbon of alanine (**16**).^{37, 38} A different approach has been used by the Diederichsen group to attach the same tacn unit. “Click” chemistry has been employed to form a triazole linker by reacting Fmoc protected propargylglycine and an azide containing tacn unit (**17**).³⁹ The Yu group used the basicity of cyclen to N-alkylate bromo-homoserine to give cyclen containing amino acid **18** that could be easily coupled to other peptides (Figure 5).⁴⁰

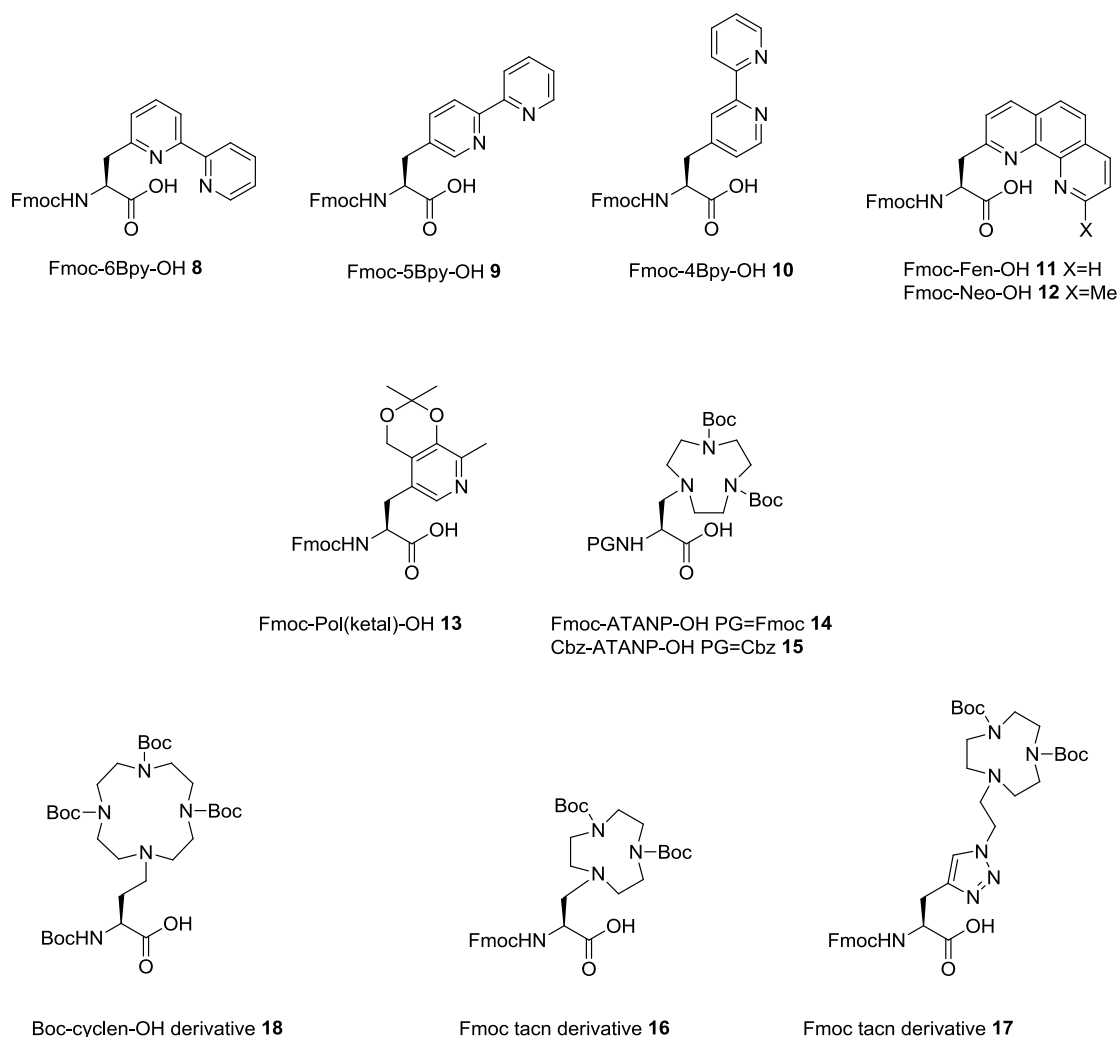


Figure 5: Examples of unnatural amino acids bearing metal ligands attached to the backbone

I.1.B. Biomedical applications of peptide ligand conjugates

Peptide metal ligand conjugates have found various applications in different areas such as biomedical chemistry and biology, catalysis of chemical and biological reactions and *de novo* synthesis of metallopeptides. The focus of this section will be on applications related to the biomedical field with a particular emphasis on peptide-based radiopharmaceuticals and imaging agents as well as therapeutic agents (inactivation of biomolecules, anticancer or antibacterial activity).

Receptor binding peptides have become an attractive target for vectoring metal-based radioimaging agents and therapeutic agents. Conjugation of the metal based “warheads” to specific peptides that can bind overexpressed receptors in cancer cells has opened new possibilities for targeted radiotherapy and cancer treatment.^{1, 9, 10, 41} Some of the most common peptide vectors are somatostatin, bombesin, gastrin, neurotensin and LHRH (luteinizing hormone-releasing hormone). In 1994, a specific example of a peptide based radioimaging agent has been authorized by the FDA for cancer diagnosis (¹¹¹In-DTPA-octreotide or OctreoScan®) and became a “golden standard” in the field (Figure 6). The development of new radiolabelling techniques and chemical modifications of the peptide vectors to gain more specificity, avoid short half lives (due to peptidase degradation), and enhance pharmacokinetics were the main researched areas. They gave rise to many new agents that have been tested in clinical trials, and for some, approved by the FDA. A few examples will be presented in the next paragraph.

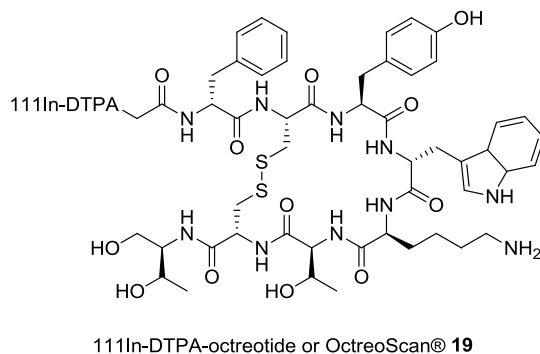


Figure 6: ¹¹¹In-DTPA-octreotide or OctreoScan®: the first FDA approved radiolabelled peptide for cancer imaging

The foundation of peptide-based radiolabelling agents lies in the identification of a molecular receptor (target) that is overexpressed on the surface of cancer cells and that is a target of an agonist peptide. The latter peptide is synthetically modified to improve its stability to peptidases and pharmacokinetics in a way that the binding affinity to the receptor is preserved.

The radiometal is covalently attached to the peptide using a metal-binding ligand and a spacer. Many aspects need to be optimized for the peptide-based radiolabelling agent to be successful such as accumulation in target and non target cells, *in vivo* stability, clearance, toxicology, etc. A few examples of peptide receptors expressed in human tumors^{1, 9, 10, 41} are listed below:

- Somatostatin: expressed in neuroendocrine tumors, melanomas, breast, brain and small lung cancers
- Bombesin: expressed in prostate, breast, pancreas and colorectal cancers
- Gastrin: expressed in thyroid cancer and stromal ovarian cancers
- LHRH: (luteinizing hormone-releasing hormone) expressed in prostate, breast and ovarian carcinomas

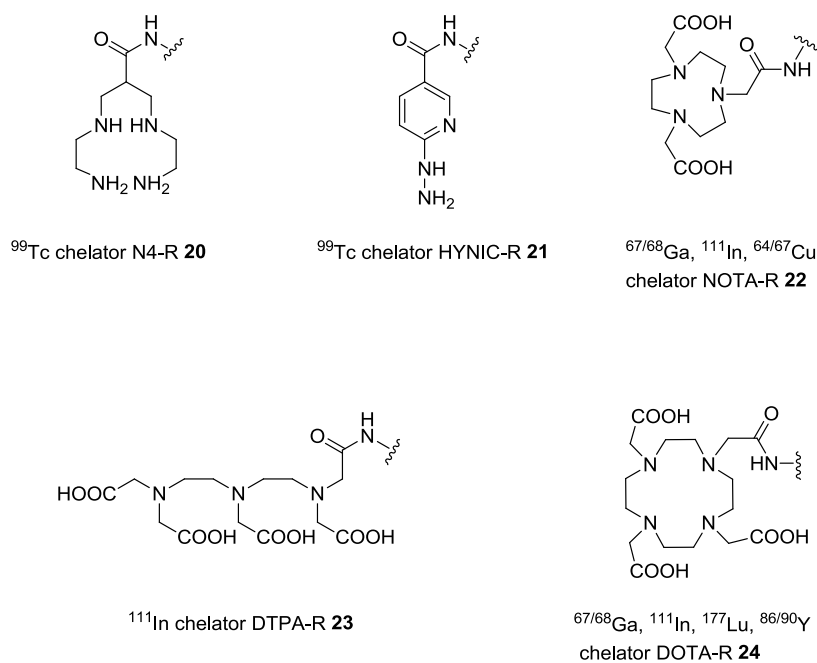


Figure 7: Commonly used radiometal chelators

The choice of the metal chelator and the radiometal itself depends on many factors and many metal-ligand partners are being used. The nature of the decay of the radiometal will

determine the imaging technique that can be used. The half life of the radiometal and the ease and cost of its preparation are also extremely important factors.

Some of the metals used are: ^{99}Tc (γ emission, no α or β radiation, low cost and easy access), ^{111}In (γ emission, longer half life, suitable for delayed imaging, high cost), ^{64}Cu (β emissions, can be used for both imaging and radiotherapy, high cost), $^{66/67/68}\text{Ga}$ (suitable for γ scintigraphy and PET imaging, high cost but excellent physical properties). Because of its low cost and ease of preparation, ^{99}Tc is used in 80% of cases in clinical applications. Representative examples of the most commonly used chelators and how they can be attached to the peptide are shown in Figure 7.

In the same manner, metal based “warheads” can be conjugated to peptides in order to inactivate biomolecules. The Shally⁴² group has attached known and clinically used antiproliferative metal complexes cisplatin [cis-diamminedichloroplatinum(II)] and transbis(salicylaldoximato)copper(II) to LHRH peptides through a D-Lysine linker and showed an increase of cytotoxic activity inhibition of [^3H]thymidine incorporation in human prostate cells ranging up to 73%.

In a different approach the Kodadek group has attached a singlet oxygen generating Ru(II)(tris-bipyridyl)²⁺ complex to a highly selective VEGF (vascular endothelial growth factor) peptoid antagonist GU40C.⁴³ Upon irradiation the CALI (chromophore-assisted light inactivation) reagent was up to 1000 times more active at inhibiting the activity of the VEGF receptor than compared to the same reagent left in the dark. In summary, the metal complex was used in this case to mask (and trigger using light) the action of the antagonist peptoid GU40C (Figure 8).

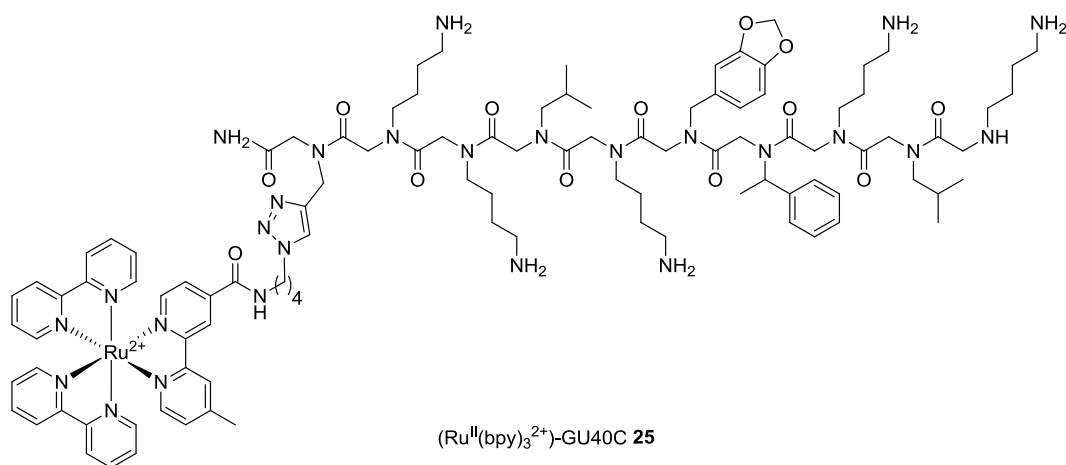


Figure 8: VEGF antagonist (Ru^{II}(bpy)₃²⁺)-GU40C metal peptoid conjugate

Numerous other examples of peptide metal conjugates, where both the peptide and metal can play different roles have been synthesized. This type of conjugation became popular in the recent years with the development of solid phase chemistry that enables quick and easy synthesis of the peptides. The development of inorganic and bioinorganic complexes as well as the discovery and further understanding of the overexpression of peptide receptors on different type of cells including cancer cells have also contributed to the popularity of this strategy.

The Kodanko group has been interested in the study of peptide ferryl conjugates. Studies to understand the oxidative reactions between ferryls, amino acids and peptides have been undertaken, as well as the potential use of those conjugates in a therapeutic way through oxidative protein inactivation. Ferryl chemistry will be discussed in the next section.

I.1.C. Ferryl chemistry

Nature uses different oxygen activating metalloenzymes to selectively oxidize different substrates. Some of them use iron as the central red/ox unit. The most studied, known and understood iron containing enzymes are heme-iron cytochrome P-450, which uses a protoporphyrin to bind Fe(II)⁴⁴ and non-heme iron enzyme methane monooxygenase (MMO).⁴⁵

Since the discovery of Fe(IV) complexes as active species in biological systems, many research groups have been trying to model them and prepare synthetic equivalents. Most research has focused on two different families of ligand structures, namely heme based structures as in the cytochrome P-450 or non-heme ligands. Non-heme ligands that can support iron-oxo species have mainly N-donor ligand frameworks consisting of tertiary amines, pyridines or cyclams. The first full characterization of a synthetic ferryl came in 2003⁴⁶ and five crystal structures have been reported since. The subject has been extensively covered in the literature and thorough reviews by Que^{47, 48} and Nam⁴⁹ have been published. Former graduate students from the Kodanko laboratory, Dr. Ahmed Abouelatta⁵⁰ and Dr. Ashley Campanali⁵¹ have discussed ferryl chemistry in their PhD dissertations, and for these reasons the description here will only briefly introduce the main aspects of non-heme iron-oxo chemistry.

In 2000 the Wieghardt group used oxone to oxidize $[\text{Fe}^{\text{III}}(\text{cyclam-acetato})(\text{CF}_3\text{SO}_3)]^{2+}$ at -80°C and characterized the product by Mössbauer spectroscopy.⁵² Three years later the Que group obtained a crystal structure of the ferryl complex $[\text{Fe}^{\text{IV}}(\text{O})(\text{TMC})(\text{MeCN})]^{2+}$. Many more complexes have been synthesized and characterized since then, and the usual synthetic strategy consist in reacting Fe(II) complexes with oxidants such as peracids,^{46, 53-55} PhIO,⁵⁶ KHSO_5 ,⁵⁷ ozone,⁵⁸ NaOCl ⁵⁹ or others. The oxidation of the iron center proceeds through a two-electron process for single oxygen donors or through a homolytic cleavage of an O-O bond for two oxygen donors such as hydroperoxide.⁶⁰

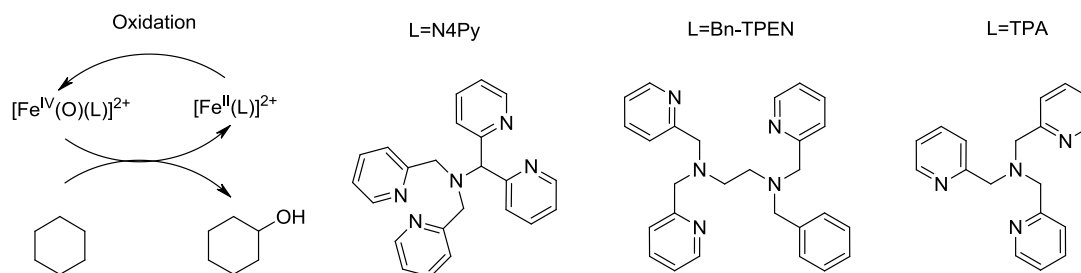


Figure 9: The oxidation chemistry of ferryl complexes

The Fe-O bond has characteristics of a double bond with a length of around 1.64 Å. The chemistry of ferryl complexes includes redox reactions and C-H activation. As noted before, most ferryls are obtained by oxidation from the corresponding Fe^{II} complexes. Once formed, the ferryls are prone to oxidizing numerous functional groups. In early studies, ferryls were used to oxidize functional groups that are prone to oxidation including phosphines,⁴⁶ alkenes,⁵³ or sulfides.⁶¹ An impressive result demonstrated that N4Py and Bn-TPEN derived ferryl complexes are able to oxidize C-H bonds (both activated and non-activated) with bond energies between 81 and 99 kcal/mol.⁶²

The Kodanko group has been interested in exploring the reactivity of ferryl groups with biologically relevant species. In a first study, the ferryl complex $[\text{Fe}^{\text{IV}}(\text{O})(\text{N4Py})]^{2+}$ was reacted with all 20 natural amino acids (protected as the Ac-AA-NHtBu). It was shown that different oxidation patterns exist depending on the nature of the amino acid submitted to the reaction with the ferryl.^{21, 22} Complex and rigorous kinetic and mechanistic studies have also shown a very broad array of reactivities with rate constants for the most reactive amino acid (cysteine) being 28,000 times higher than the one of the unreactive amino acids. Five amino acids (Gly, Met, Trp, Tyr and Cys, in increasing reactivity order respectively) were substantially more reactive than the other 15 and all reacted with different KIEs (kinetic isotope effect) and mechanisms.^{21, 22}

In a subsequent study, the intramolecular reaction of a ferryl complex within a peptide-ferryl conjugate was studied.⁶³ The results showed that reactivity is controlled by a remote benzyl ester that is situated 11 atoms away from the metal center.

Further studies with other biologically relevant systems have shown that N4Py derived ferryl complexes can oxidize glutathione (GSH) to its dimer form GSSG (the disulfide dimer).⁶⁴ Serine proteases, trypsin and chymotrypsin, can be inactivated by ferryl complexes of N4Py having a pendant guanidinium group. The inactivation occurs by oxidation of the side chain and not oxidative cleavage of the backbone.⁶⁵

Further investigations of both ferrous and ferryl complexes reactivities with short peptides and proteins were undertaken during my time in the Kodanko laboratory. The use of those complexes as potential inhibitory agents when tethered to vector peptides has also been studied by members of the Kodanko group. All these studies require efficient ways of attaching polypyridyl ligands to peptides. A new strategy developed with fellow students from the Kodanko laboratory, Dr. Jabre and M.Sc Ulku will be described in Chapter 2 of this thesis. The next sections will describe the use of solid phase synthesis for the preparation of peptides and synthetic strategies used to build new, unnatural amino acids.

I.1.D. Solid phase chemistry/peptide synthesis

The idea of solid phase synthesis came from the Merrifield laboratory in the early 1960s.⁶⁶ The process was based on the use of a polymeric resin bead cross linked to a growing chain of the peptide (through synthetic steps). The use of excess reagents (monomers, coupling reagents and deprotection cocktails, same as in a classical solution phase sequence) had the aim to force reactions to completion. The excess material could potentially be removed by simple

filtration leaving the growing peptide attached to the insoluble bead in the reaction flask. The whole process was based on 3 requirements:

- The polymeric support for the synthesis had to be inert to the conditions used to both building the peptide and the final cleavage from the resin
- A strategy of orthogonal protection and deprotection of the reactive amino acid functional groups had to ensure the ability to easily build the peptide and reduce the number of manipulations. Reactive side chains needed to be protected in a way that their reactivity was only uncovered during the final cleavage from resin or through an additional and final step (for example hydrogenolysis).
- The growing peptide needed to be attached to the resin bead in a way that a final reaction would cleave the final product from the bead and enable its isolation.

The first published example of a successful peptide synthesis using SPPS came from the Merrifield laboratory in 1963.⁶⁶ A Cbz protected amino acid (free C-terminus) was attached to the polystyrene resin bead through an ester bond. The Cbz protecting group was selectively removed using an HBr/HOAc mixture unveiling a reactive amino group. The latter could be reacted with a second Cbz protected amino acid using DCC coupling conditions. The Cbz group could be once again removed using the same HBr/HOAc cocktail and the sequence of reactions repeated until the desired peptide was fully constructed. The unreacted reagents were filtered off between reactions, leaving the insoluble resin bead in the flask. The final peptide was liberated from the resin by NaOH saponification of the first ester bond (Figure 10). Changes to the initial sequence were made by the Merrifield group to make the method more robust and enable better deprotection yields and selectivity by replacing the Cbz protecting group by a *tert*-butoxycarbonyl group (BOC) and the nitropolystyrene bead

by a 2% crosslinked polystyrene. Those efforts enabled the group to disclose the successful synthesis of bovine insulin in 1966⁶⁷

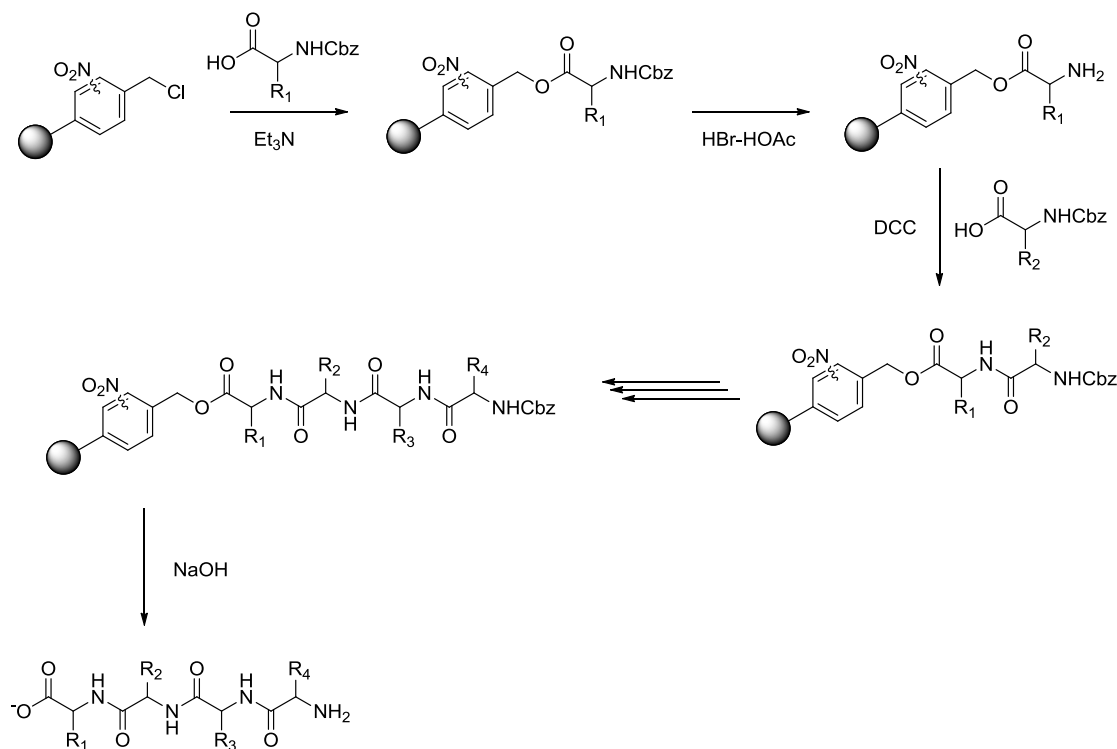


Figure 10: Merrifield's first solid phase synthesis sequence of a tetrapeptide

Despite the synthetic successes of these early solid phase syntheses, the community was very skeptical on the potential use of the method. In 1973 Max Brenner described the discovery of SPPS with the following words: *“The invention of the solid-phase method looked like an ingenious trick to overcome some of the unpleasant features of the classical methods. As we know today, the ingenuity of the trick remains, but only a large investment of heavy real effort will eventually, if ever, work it into a real progress over the classical approach.”*⁶⁸ A “large investment of heavy effort” made solid phase synthesis one of the most, if not the most, robust methodology to build not only peptides but also DNA, RNA and others and was recognized by a Nobel Prize for Merrifield in 1984.⁶⁹

Since its invention, SPPS has evolved and all parameters have been modified and optimized starting from the resin beads, the use of different linkers,⁷⁰ protecting groups and subsequent deprotecting cocktails as well as coupling agents. Automated systems are common synthetic laboratory equipment all over the world. All aspects have been thoroughly reviewed and only the main aspects relevant to the work presented in Chapters 2 and 3 of this dissertation will be explained in the following paragraphs.

One of the disadvantages of the BOC strategy is the use of either HF or TFA for the final cleavage step. HF is highly toxic and can react with standard glassware equipment (etching) so special equipment needs to be used. To circumvent those issues a different strategy, namely Fmoc SPPS can be adapted (Figure 11). In this case the amino acids are protected with the Fmoc protecting group that can be easily removed using a 20-50% secondary amine solution (such as piperidine) or DBU. The drawbacks of this method are higher aggregation of longer peptide compared to the BOC strategy, and racemization of Cys containing peptides.

PAM resin was introduced to circumvent losses of larger peptides from the Merrifield resin during the TFA mediated BOC deprotection.⁷¹ It offers better stability to TFA but also requires harsher conditions for the final cleavage often requiring the use of HF.

Wang resin, introduced in 1973 by the Wang group, has become the most used resin for the Fmoc SPPS. The linker attached to the polystyrene bead is a 4-hydroxybenzyl alcohol group through a phenyl ether bond.⁷² The peptide can be cleaved through acid-assisted ether bond cleavage (usually a TFA mixture with scavengers) to give the corresponding carboxylic acid product.

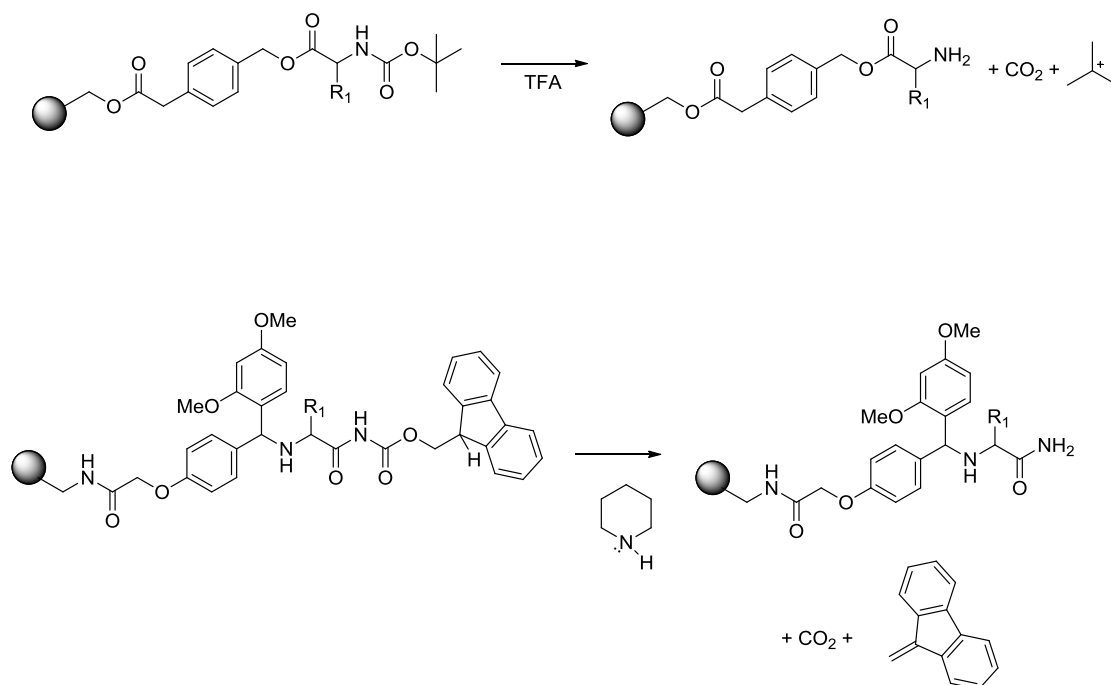


Figure 11: Boc and Fmoc deprotection

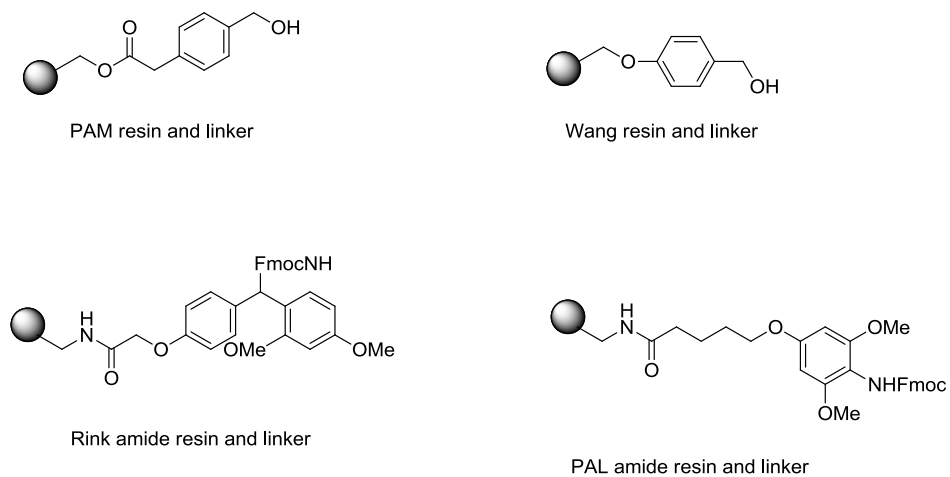


Figure 12: Commonly used resins and linkers in SPPS

If a C-terminal peptide amide is desired, the Rink amide⁷³ or PAL resin can be used. Similar to the Wang resin, the peptide is linked to the polystyrene bead through a phenyl ether linker that can be cleaved under TFA conditions.

Many other resins offering either a wide variety of cleavage conditions, such as the trityl and 2-chlorotryl resins⁷⁴ (acetic acid mediated cleavage), HMBA⁷⁵ (hydroxymethyl benzoic acid linked resin) (base mediated cleavage) or the preparation of specific terminal groups such as the DHP resin⁷⁶ (for the preparation of alcohols) or the Weinreb aminomethyl resin to prepare terminal aldehydes⁷⁷ have also been developed.

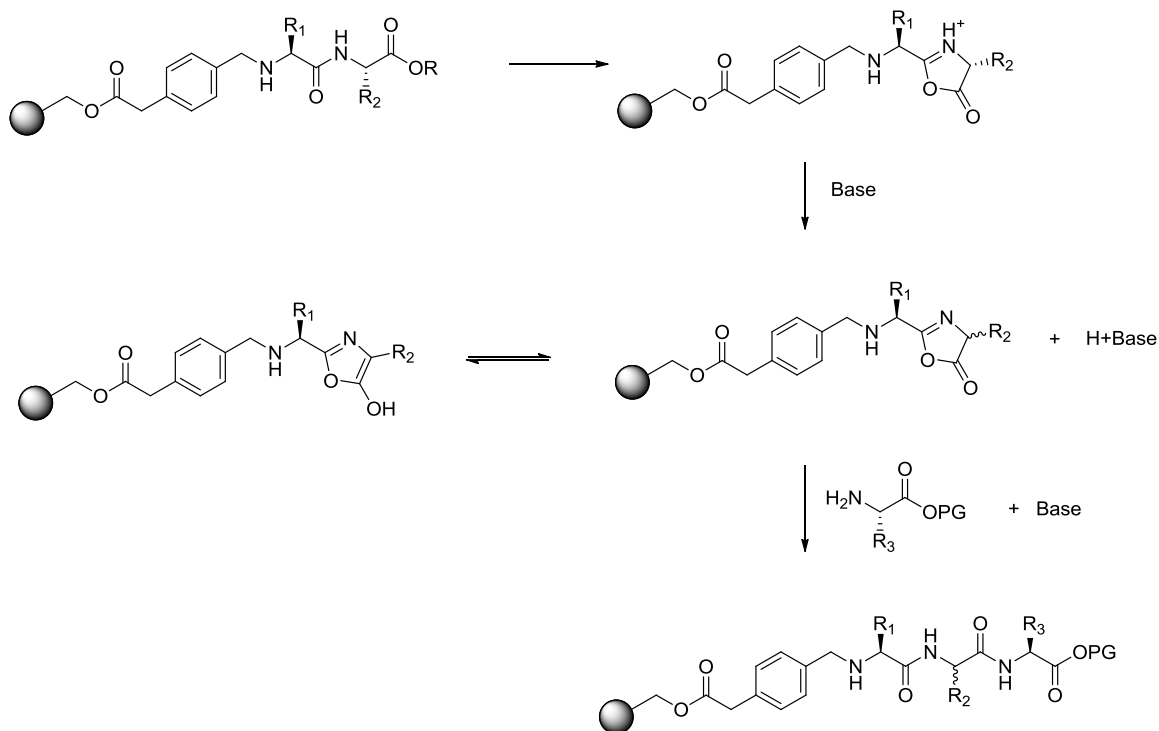


Figure 13: Formation of an intermediate oxazolone that epimerizes the R_2 α -carbon geometry while building a peptide from the N-terminus (example on PEG resin)

The coupling step has also seen a number of optimizations (known also from standard solution phase synthesis). As in all peptide synthesis, peptides are built from C-to N-terminus using SPPS. Building a peptide in the opposite direction presents a risk of epimerization of the α -carbon. Amides are indeed known for closing on an activated ester to form a five membered oxazolone where chirality is lost. When building a peptide from the C-terminus, the N-terminus

of a new peptide is protected as a carbamate (Fmoc, or Boc), and carbamates are known for not cyclizing in a similar fashion (Figure 13, Figure 14).

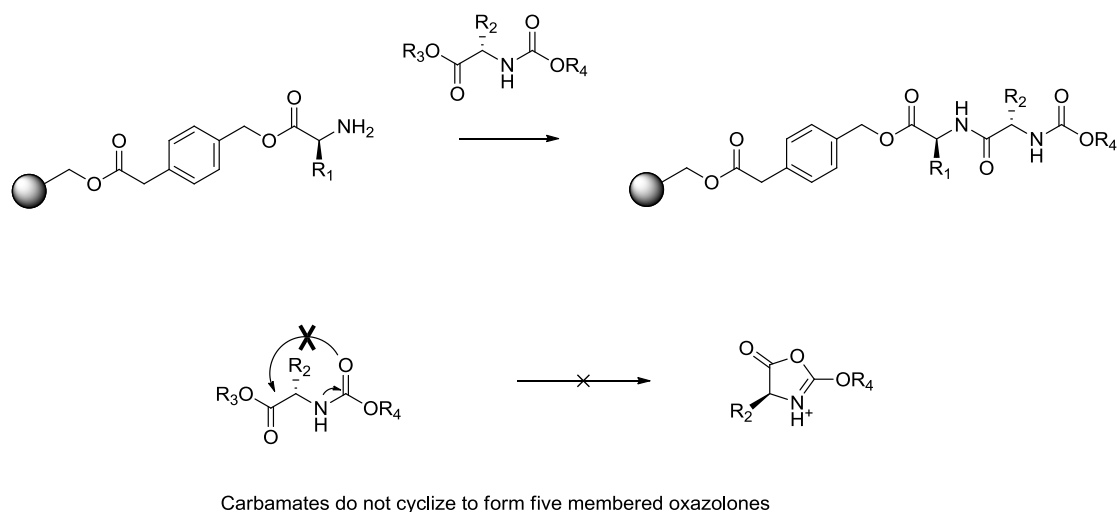


Figure 14: Absence of formation of an intermediate oxazolone while peptide is built from the C-terminus (use of carbamate protection) (example on PEG resin)

The other potential risk for epimerization comes from a slow reacting amino acid in the peptide bond formation reaction. Upon activation of the C-terminus as an active-ester, an intermediate ketene can be formed by deprotonation of the α -carbon leading to epimerization. The ketene is still reactive in the peptide bond forming reaction, leading to an epimerized peptide. This problem is recurrent with carbodiimide activated esters (and DCC in particular). To circumvent this problem, HOBt (1-hydroxybenzotriazole) can be added in stoichiometric fashion. HOBt reacts with the activated ester to give a new ester. The latter is still reactive in the peptide bond formation reaction but does not lead to ketene formation.

Modern coupling phosphonium-based reagents like BOP (Benzotriazol-1-yloxy)tris(dimethylamino)phosphonium hexafluorophosphate) or aminium-based such as HBTU (O-(Benzotriazol-1-yl)-N,N,N',N'-tetramethyluroniumhexafluorophosphate) or HATU have OBt incorporated in them as a leaving group leading to the formation of the HOBt ester in situ, thus

facilitating synthesis. Many other coupling reagents have been developed for special, difficult to make, peptide bonds (Figure 15).

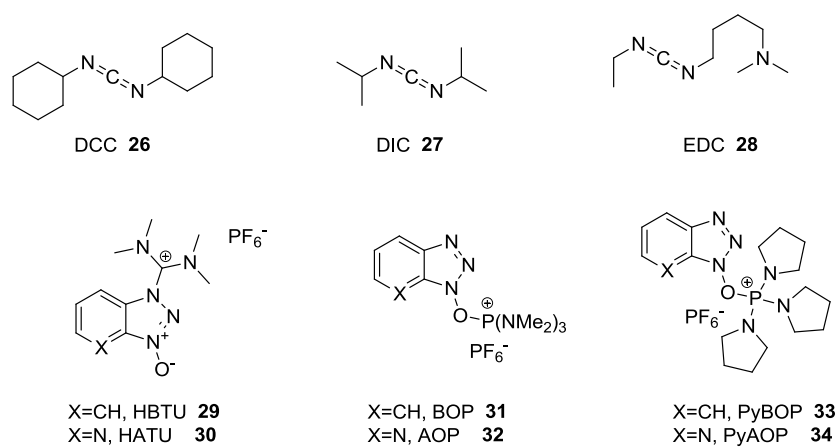


Figure 15: Commonly used peptide coupling agents

In order to use SPPS for the construction of metal peptide conjugates, new unnatural amino acids need to be prepared. The following section presents synthetic methods to prepare such amino acids.

I.1.E. Unnatural amino acid synthesis strategies

The α -amino acids (AAs) are one of the most important chiral building blocks for both medicinal and synthetic chemists. Methods for the isolation of enantiomerically enriched α -amino acids have evolved over the years. The high demand for new unnatural amino acids has motivated synthetic chemists to discover new methodologies for the construction of α -AAs, marking a switch from the classical methods. Historically, α -AAs were either isolated from natural sources or resolved either chemically or enzymatically. The last 20 years have seen an emergence of catalytic asymmetric syntheses of α -AAs. The next sections will present some of the methodologies in each of the approaches used to synthesize α -AAs with a special emphasis

on enantioselective alkylations of glycine derivatives. More specific information can be found in the numerous review articles devoted to the subject.⁷⁸⁻⁸²

Two main approaches are available for the enantioselective construction of an α -AA. The first one is the asymmetric introduction of the α -hydrogen. The main types of reactions that belong to this group of transformations are enantioselective hydrogenations of α - β carbon-carbon double bonds and the analogous hydrogenation (or hydride addition) of nitrogen-carbon bonds.⁸³ All the other strategies, aim at introducing one of the constituents of an amino acid, namely an α -amino group, or the α -side chain or the carboxy group (Figure 16).⁸⁰ Only a few examples will be given to illustrate each strategy as hundreds of methods, catalyst and ligands exist for each transformation (Figure 16). A more in depth description of the asymmetric alkylation of glycine imines using quaternary ammonium salts will be given in the following section.

Asymmetric hydrogenation is one of the most employed and researched catalytic transformations in organic chemistry. Since the work on the synthesis of L-Dopa by Knowles⁸⁴ and early efforts by Noyori and Kagan (recognized by the Nobel Prize in 2001 for Knowles and Noyori), numerous applications have emerged including the synthesis of α -AAs. Both monodentate and bidentate ligands can induce high levels of enantioselectivity using mostly Rh and Ir complexes.

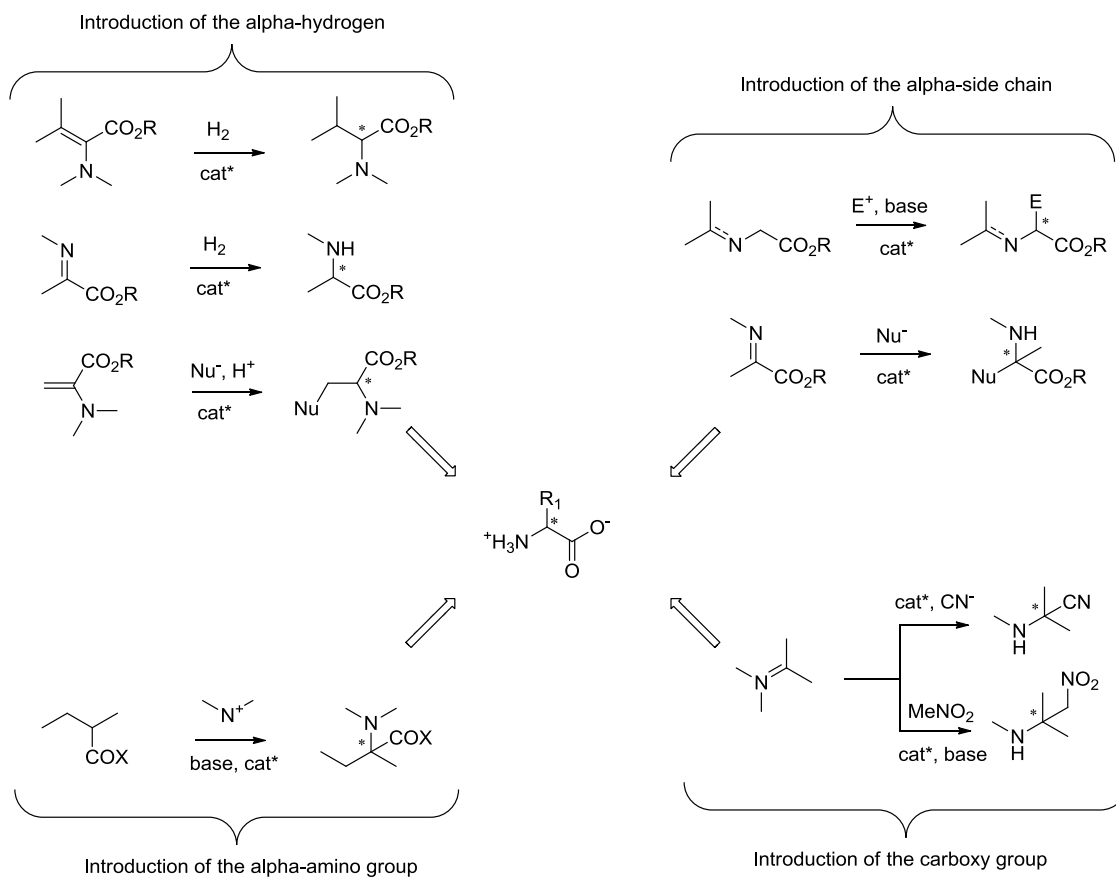


Figure 16: Different approaches to build α -AAs⁸⁰

Rhodium complexes with different families of monodentate ligands including phosphines, phosphonium salts, phosphonites, aminophosphonites, phosphoramidites and phosphites systematically induce levels of ee (enantiomeric excess) higher than 90% in the asymmetric reduction of α - β -dehydro α -AAs **35**.⁸⁵⁻⁸⁹ Examples of some of these ligands are shown in Figure 17.

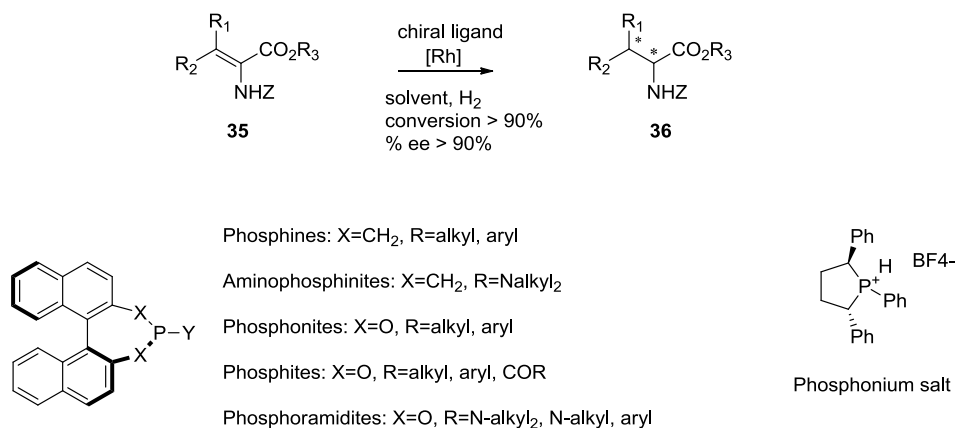


Figure 17: Asymmetric hydrogenation of α - β -dehydro α -AAs with Rh complexes

Analogous bidentate ligand-Rh complexes have been found to be even more efficient than monodentate systems, enabling lower levels of ligand to be used (catalytic turnover often as high as 10,000). Interestingly, bidentate phosphines are also great ligands for the asymmetric hydrogenation of α - β carbon-nitrogen double bonds as in α -imines **37**⁹⁰ or hydrazones **39**⁹¹ (Figure 18).

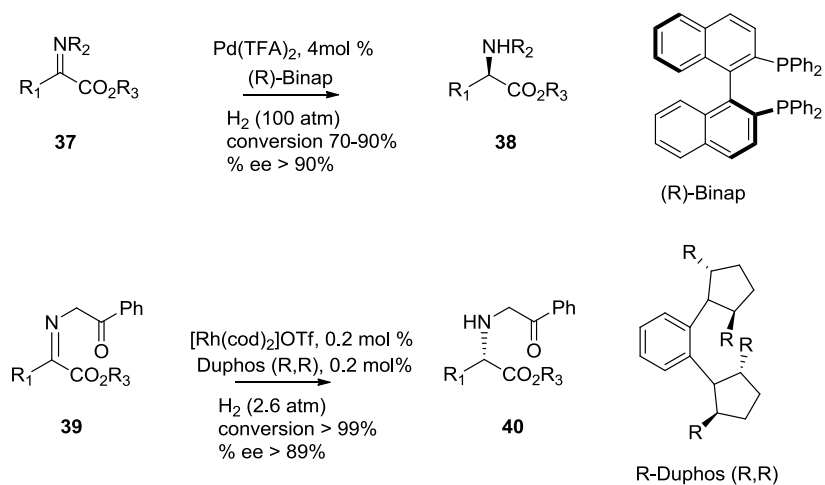


Figure 18: Asymmetric hydrogenation of α - β carbon-nitrogen double bonds with bidentate phosphine ligand-metal complexes

The Strecker reaction is one of the oldest amino acid synthesis methods, where an aldehyde or ketone is reacted with potassium cyanide in the presence of ammonium chloride to

give an amino acid after hydrolysis. Although discovered in 1850, the reaction was only a source of racemic α -AAs until recent development of its asymmetric catalytic analogue in the 1990s. Asymmetric Strecker type reactions can be catalyzed by both metal and organocatalysts. The Vilaivan group has shown that the catalytic addition of TMSCN to imine **41** in the presence of a titanium complex gives the product with good yields and up to 90% ee (Figure 19).⁹²

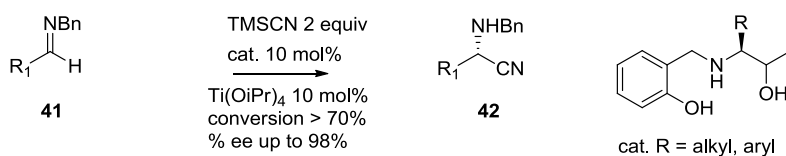


Figure 19: Strecker type asymmetric α -AA synthesis

In a similar fashion, aldimines such as tosylimines derived from aliphatic aldehydes can undergo a cyanide addition catalyzed by quaternary ammonium iodides to give the corresponding products in good yields and excellent enantioselectivities (% ee > 98%).⁹³

The introduction of the α -side chain to glycine analogues is one of the most versatile methods of building α -AAs. Most methodologies use phase transfer catalysis to alkylate glycine imine derivatives. The next section will present the historical discovery of this type of reactions and give a perspective on this very robust method.

I.1.F. Enantioselective alkylation of glycine imine derivatives

I.1.F.a. Strategies

Phase transfer catalysts (PTCs) are ionic compounds that ease the migration of molecules between the aqueous and organic phase in a biphasic solution. They are known to highly accelerate the rate of reaction of heterogeneous reactions.

The high acidity of α -hydrogens of α -aminoacid ester imines **43** enables easy access to highly nucleophilic enolate derivatives **44** *in situ*. PTCs permit a controlled delivery of the enolate into the electrophile-containing phase, offering many advantages. Reactions are usually more selective due to controlled delivery. Nucleophiles are often more reactive due to higher charge separation of the phase transfer catalyst-nucleophile ion pairs. A wide array of solvents is allowed, giving easy solutions for the isolation and recovery of products and catalysts. The catalysts are often organic quaternary ammonium salts which facilitate reactions compared to water-and air-sensitive transition metal catalysts. All these points make asymmetric phase transfer catalysis a very attractive methodology that has seen increasing attention and widespread applications. Numerous review papers describe the different aspects of the subject.^{82, 94-97}

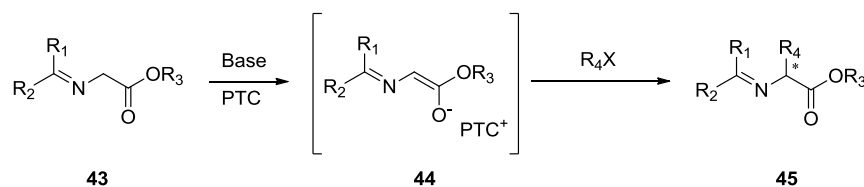


Figure 20: Phase transfer catalysis of α -aminoacid ester imines

The next section will describe some of the optimization work dedicated to substrate and catalysts for the phase transfer catalysis of glycine imines. Other applications are included in previous review articles and will not be discussed.^{87, 99-102}

I.1.F.b. Substrate and catalyst optimization

O'Donnell was the first to report the use of chiral PTC for the asymmetric alkylation of glycine imine esters in 1989.⁹⁸ The catalyst used was an N-benzyl ammonium salt derived from the natural alkaloid *Cinchonine*. Low to moderate levels of enantioselectivity were obtained ranging from 42% to 66% ee in favor of the (R) enantiomer. Interestingly, the (S) enantiomer

could be obtained if a stereoisomer and pseudo-enantiomer of the catalyst derived from *Cinchonidine* was used, with the same levels of enantioselectivity. The optimized conditions used a *tert*-butyl ester benzophenone imine as the substrate, a 50% NaOH/CH₂Cl₂ solvent system and high stirring for 24 hours at RT (Figure 21).

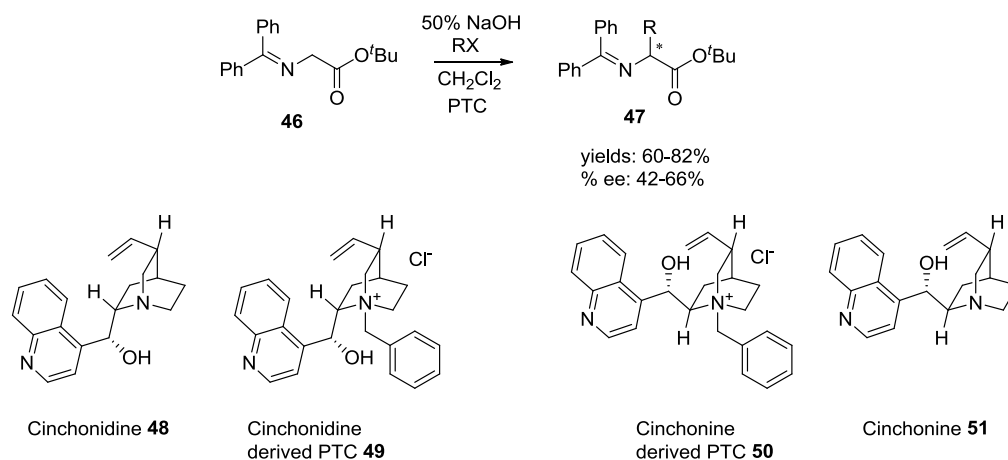


Figure 21: First example of *Cinchona* derived PTC of glycine imines by O'Donnell

A major breakthrough for this subject was registered almost at the same time (submitted within a week) from two independent labs in 1997. The Corey group hypothesis stated that increased steric hindrance on the bridgedhead nitrogen atom should increase the shielding of three of the four quadrant phases of the pseudo tetrahedron, thus enabling a closer ion-pair contact of the catalyst with the substrate and higher levels of enantioselectivity. To prove their hypothesis the Corey group built a new catalyst using a 9-anthracenylmethyl group to construct a *Cinchonidine* derived quaternary ammonium salt. The secondary alcohol was also transformed into an allyl ether. The alkylation reaction using O'Donnell's substrate with solid CsOH gave good yields and excellent levels of enantioselectivity (92-99% ee).^{99, 100} The Lygo group conducted a very similar analysis, and prepared the analogous catalyst with the exception of leaving the free alcohol (which is believed to get alkylated during the reaction and does not seem

to have an influence on the levels of ee). Their levels of enantioselectivity were slightly lower than that of Corey, but the reactions were conducted at RT (Figure 22).¹⁰¹

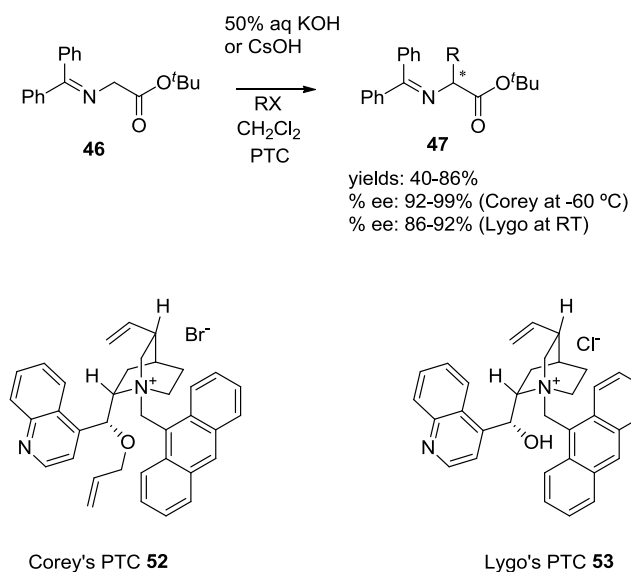


Figure 22: Optimized cinchonidinium PTC for the asymmetric alkylation of glycine imines

Since the simultaneous discovery of this new catalyst by Corey and Lygo, most optimizations have focused on the nature of the catalyst. The most interesting modifications have been the use of organic bases such as the Schwesinger BTTP or BEMP showing no loss of % ee in homogenous catalysis¹⁰² and the attachment of the catalyst to different type of SPPS resins^{103, 104} to enable the synthesis of amino acids using that technology or higher order oligomers^{105, 106} (dimers and trimers of the *Cinchona* catalyst) that could improve the levels of enantioselectivity.

Only minimal attention has been given to substrate optimization. The original O'Donnell paper mentions that benzyl protected ester gives only 28% ee compared to 66% when the *tert*-butyl protected ester imine is used. In 2003, the Lygo group presented a short study on the influence of the size of the ester protecting group. Surprisingly, the ethyl group could induce levels of ee between 73% and 87% compared to 79% for the benzyl ester and 63% for the benzhydryl ester.¹⁰⁷ Nonetheless, the *tert*-butyl ester protected benzophenone imine is the only

substrate to date to consistently induce high levels of enantioselectivity with the *Cinchona* derived catalysts.

Spiro type C_2 -symmetric quaternary salts derived from (R)-or (S)-Binol are the other family of PTCs that have been successfully developed for the alkylation of glycine imines. Their synthesis is more difficult as they are purely synthetic (compared to derivatives of the *Cinchona* family natural alkaloids), which also enabled a huge variety of analogues and room for optimization. The levels of enantioselectivity induction are comparable or even higher than with the *Cinchona* derived PTCs. Examples of such catalysts are given in Figure 23.^{87, 99-102}

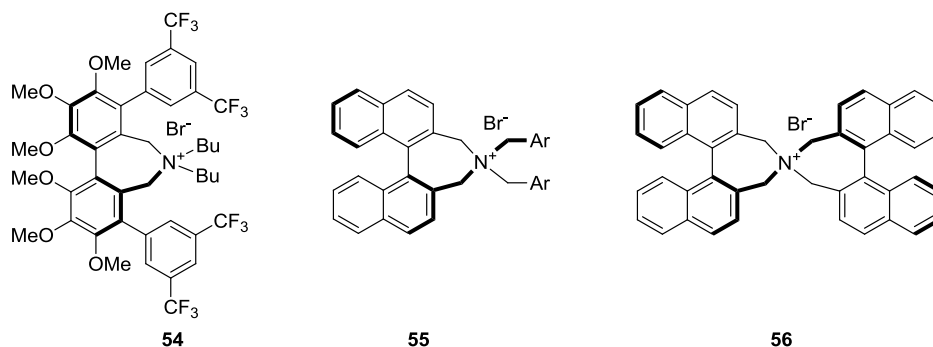


Figure 23: C_2 -symmetric quaternary salts derived from (R)-or (S)-Binol

I.1.G. Thesis statement (Part I)

The use of peptides as vectors for therapeutic agents is a very efficient and elegant way of gaining specificity. Concurrently metal complexes are finding more and more medicinal applications as both imaging and therapeutic agents. It seemed natural to combine those two areas and build metal peptide conjugates, and research in this field has been recently dynamic. Despite these facts, there is a lack of efficient and divergent strategies to build such peptide metal conjugates. A great improvement for the fast synthesis and evaluation of such species would be to develop a SPPS “friendly” and divergent method that would enable both modularity

on where within the peptide to attach the metal binding unit and also vary its structure. Ideally, the structural diversity would be introduced late in the synthetic sequence and from a common precursor, limiting the number of reactions for each compound.

The goals for this first part of this dissertation were first to develop a SPPS friendly, divergent methodology for the attachment of non-heme polypyridyl ligands to peptides through a novel unnatural amino acid. Solution phase methodologies and unnatural amino acids suitable for the construction of such metal-peptide conjugates have been synthesized previously in the Kodanko group in standard solution phase chemistry.⁶³ The translation from solution phase to SPPS prior to my investigations had been unsuccessful.

The second goal was to develop a new and optimized substrate for the asymmetric, phase transfer catalyzed alkylation reaction of benzophenone imine. The current methodology suffers from the fact that the only substrate to date to consistently induce high levels of enantioselectivity with the *Cinchona* derived catalysts is the *tert*-butyl ester benzophenone imine. With the first goal in mind, namely the use of Fmoc SPPS for the construction of metal peptide conjugates it becomes clear that large amounts of Fmoc unnatural amino acids would be needed. Amino acids for Fmoc SPPS with their side chains protected with acid-labile protecting groups (that are disclosed during the final acid mediated cleavage from resin) are not easily synthesized (or require extra protecting group manipulation steps) using the phase transfer *Cinchona* catalyzed alkylation of glycine benzophenone imine, because the *tert*-butyl ester deprotection (acid mediated) also removes the side chain protecting groups. There is a clear need for a substrate having an orthogonal protecting group with the side chain's protecting group that would induce high levels of enantioselectivity.

Strategies to complete each of the goals, as well as all relevant experimental data, will be discussed in the next two chapters. Conclusions and future directions will be presented at the end of this Part I of the dissertation.

Chapter 2. Novel, divergent strategy for the synthesis of peptide polypyridyl ligand conjugates and its applications to SPSS

I.2.A. Background and project design

The Kodanko group demonstrated that ferryl complexes derived from N4Py can cleave peptide backbones and oxidize side chains when reacted with single, protected amino acids.^{21, 22} With the aim of studying ferryl complexes attached to peptides, a divergent strategy has been developed and applied to the construction of a short peptide incorporating polypyridyl ligands. The work of Dr. Jabre has shown that the pyridyl ring being a core element of numerous non-heme polypyridyl ligands, a pyridylmethyl containing unnatural amino acid is a perfect anchor for a divergent synthesis of such peptide-ferryl conjugates. The clever design of the Fmoc-HPA(OTBS)-OH unnatural amino acid (HPA: 2-hydroxymethyl-5-pyridyl alanine) enabled a quick synthesis of a ferryl containing dipeptide Ac-HPA(Fe^{IV}(O)(N₃Py))-Gly-OBn in solution phase (Figure 24) (for the synthesis of Fmoc-HPA(OTBS)-OH, please refer to Chapter 3, Scheme 9).⁶³ The decomposition of the oxo species was shown to be controlled by the ester moiety located 11 atoms away from the iron center.

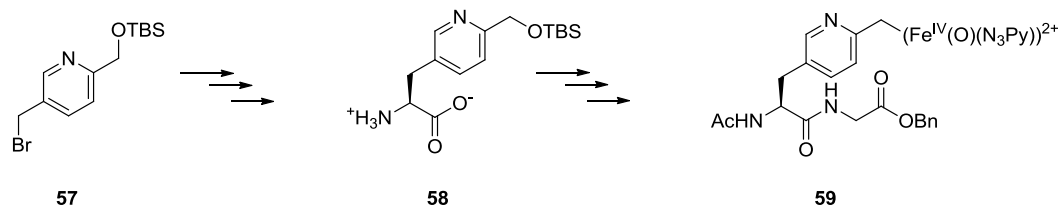


Figure 24: Design of the HPA(OTBS) unnatural amino acid leading to the synthesis of dipeptide Ac-HPA(Fe^{IV}(O)(N₃Py))-Gly-OBn

In order to broaden the investigation of the stability of peptide ferryl conjugates, two new unnatural amino acids have been designed. S. Ulku, a colleague from the Kodanko laboratory, envisioned an analogous unnatural amino acid to HPA, but having a three hydrocarbon linker between the backbone and the pyridyl moiety, namely HPN ((2-**h**ydroxymethyl-5-**p**yridyl **n**orvaline) (for the synthesis of Fmoc-HPN(OTBS)-OH, please refer to Chapter 3, Scheme 10). To ease the synthesis of the third unnatural amino acid, we sought a synthesis that would start from a natural amino acid, with the hope of not having to build a new chiral center. We hypothesized that serine could be the starting amino acid leading to unnatural amino acid HPMA ((2-**h**ydroxymethyl-5-**p**yridyl **m**ethoxy)-3-**a**lanine) (Figure 25).

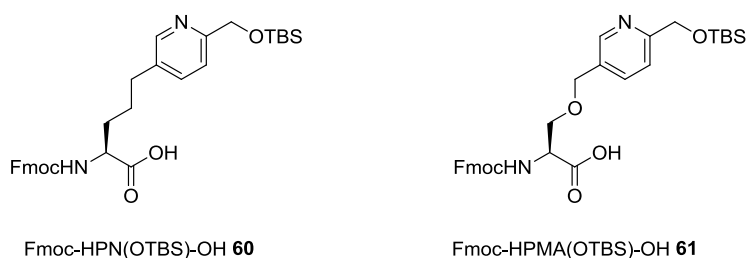


Figure 25: Design of the second generation unnatural amino acids HPN and HPMA

Most importantly, the full potential of this methodology could only be obtained if the synthesis of peptide ferryl conjugates could be adapted to SPPS with a more combinatorial and divergent approach (Figure 26). N. Jabre demonstrated that polypyridyl ligands and corresponding ferryl conjugates could be synthesized using the HPA unnatural amino acid in solution phase but the transition to SPPS had to be established.

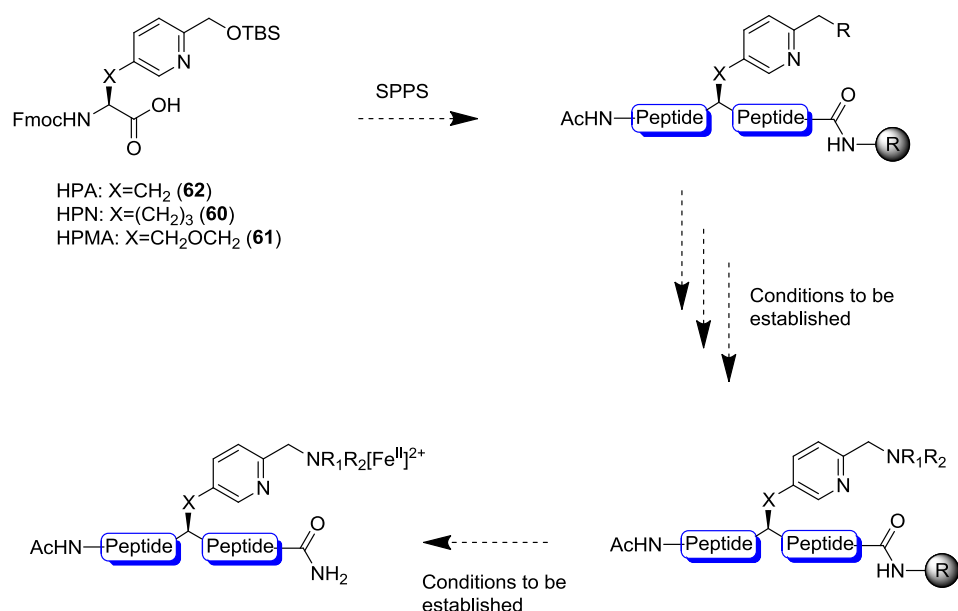
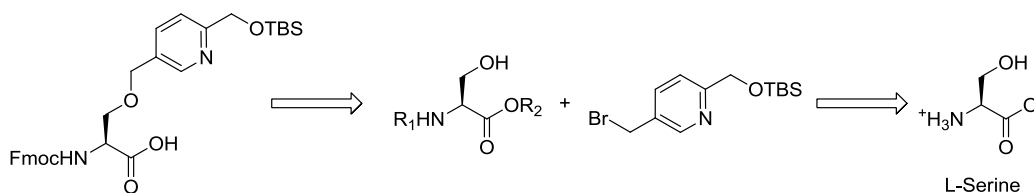


Figure 26: Solid phase, divergent and combinatorial, synthesis of peptide-ferryl conjugates

I.2.B. Results and discussion

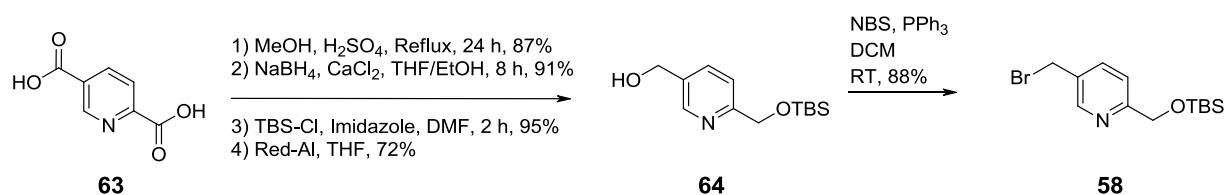
I.2.B.a. Fmoc-HPMA-OH

The new HPMA ((2-hydroxymethyl-5-pyridyl methoxy)-3-alanine) amino acid has been designed so that the chirality of the α -center could be inherited from commercially available and enantiomerically enriched L-serine. This presents a great advantage compared to the synthesis of HPA and HPN, in which the geometry is introduced using a chiral catalyst (results do not exceed 92% ee and the catalyst needs to be synthesized). Scheme 1 presents the retrosynthetic approach towards HPMA that uses L-serine as a starting material. The key step in that sequence is the *O*-alkylation of a serine derivative with 2,5-dibromo-substituted pyridine derivative to give TBS protected HPMA.



Scheme 1: Retrosynthetic approach to HPMA using L-serine as a starting material

The synthesis of the 2,5-dibromo-substituted pyridine derivative starting with pyridine-2,5-dicarboxylic acid **63** has been developed by N. Jabre in our laboratory and was used without any changes (Scheme 2).



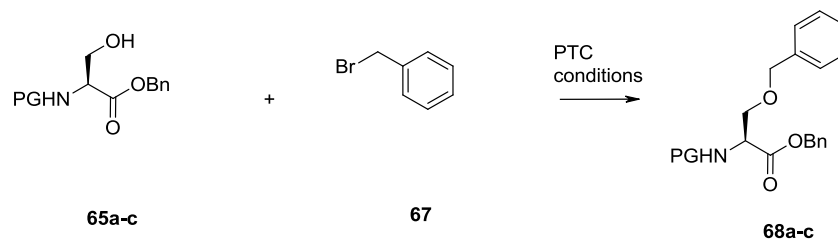
Scheme 2: Synthesis of the 2,5-substituted pyridine derivatives

Methods where the serine derivative plays the nucleophilic role were the first methods of choice because the *O*-alkylation of benzyl bromide or its derivatives with the serine-derived alkoxide is described in the literature.^{108, 109} The only drawback of this approach is that **58** decomposes within a day so it has to be prepared and used immediately in the alkylation trials.

The standard procedure to alkylate the β -alcohol of serine uses two equivalents of NaH to make the alkoxide dianion, which is quenched with an electrophile such as benzyl bromide. Following this procedure, the serine dianion alkoxide was quenched with **58** but only gave decomposition products (Scheme 3, Table 1).

A screening of different temperatures, number of equivalents, bases and solvents produced only decomposition products or starting materials. We hypothesize that either the

4, Table 2, entries 1-3, 4). The optimized conditions, where an excess of concentrated aqueous NaOH (at least 5 equiv, 40% NaOH; 20% NaOH gave lower yields), vigorous stirring (1000 rpm), and either DCM or benzene associated with TBAB or TEBAC gave yields between 49 and 66%. Specific literature on PTC also confirmed that the amount of base, vigorous stirring as well as the trityl protecting group¹¹² are key in this type of reaction.¹¹³⁻¹¹⁵



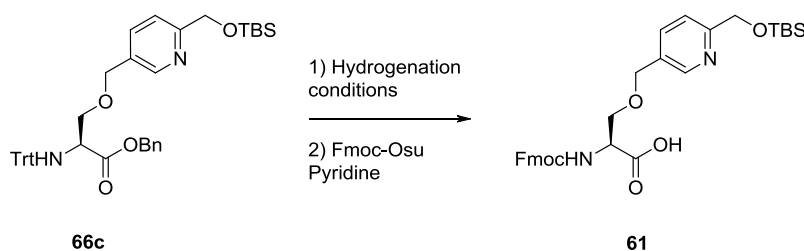
Scheme 4: Serine as the nucleophilic partner in PTC alkylation trials

Entry	65a-c	base	catalyst	solvent	conditions	yield
1	65a PG=Boc	K ₂ CO ₃ 1 equiv	TBAB 10%	Toluene	RT, 24 h	No reaction
2	65b PG=Cbz	KOH 1.5 equiv	Aliquat 336	DCM	RT, 24 h	No reaction
3		CsOH 1 equiv	TBAS	DCM	RT, 24 h	No reaction
4	65c PG=Trt	10 equiv NaOH 40%	TBAB	DCM	RT, 24 h	26%
5		10 equiv NaOH 40%	TBAB	Benzene	RT, 24 h	66%
6		10 equiv NaOH 40%	TEBAC	DCM	RT, 24 h	40%
7		10 equiv NaOH 40%	TEBAC	Benzene	RT, 24 h	49%

Table 2: O-Alkylation of protected serine derivatives in a heterogeneous solution using PTC

The conditions found using benzyl bromide were then tested with **58** as the electrophilic partner with both TBAB and TEBAC as catalysts and 40% aqueous NaOH associated with either DCM or benzene. The combination of TBAB and benzene gave the best results (**66c** isolated with a 66% yield on a multigram scale).

With the alkylation adduct in hand, Fmoc-HPMA(OTBS)-OH was in sight, just protecting group manipulations away. Our plan was to remove both protecting groups at the same time and telescope that reaction with Fmoc re-protection. Two choices were available, acid-mediated trityl and benzyl ester removal (probably requiring fairly harsh conditions that would also certainly remove the TBS group) or hydrogenolysis. We decided that the latter would be a better option.



Scheme 5: Hydrogenation of the *O*-alkylation product **66c** and subsequent Fmoc protection

Entry	catalyst	solvent	conditions	yield
1	Pd/C 10%w/w	EtOH	NH ₄ +HCO ₂ 15 equiv	slow partial reduction
2	Pd/C 10% w/w	MeOH	H ₂ gas 1.0 atm	partial reduction
3	Pd/C 10% w/w	MeOH	H ₂ gas 2.5 atm	partial reduction
4	Pd/C 10% w/w	EtOH	H ₂ gas 1.0 atm	partial reduction
5	Pd/C 10% w/w	EtOAc	H ₂ gas 1.0 atm	slow partial reduction
6	Pd(OAc) ₂ 10% w/w	MeOH	H ₂ gas 1.0 atm	reaction completed after 24 h
7	Pd(OH) ₂ 5% w/w	MeOH	H ₂ gas 1.0 atm	reaction completed after 4 h

Table 3: Hydrogenation of the *O*-alkylation product **66c**

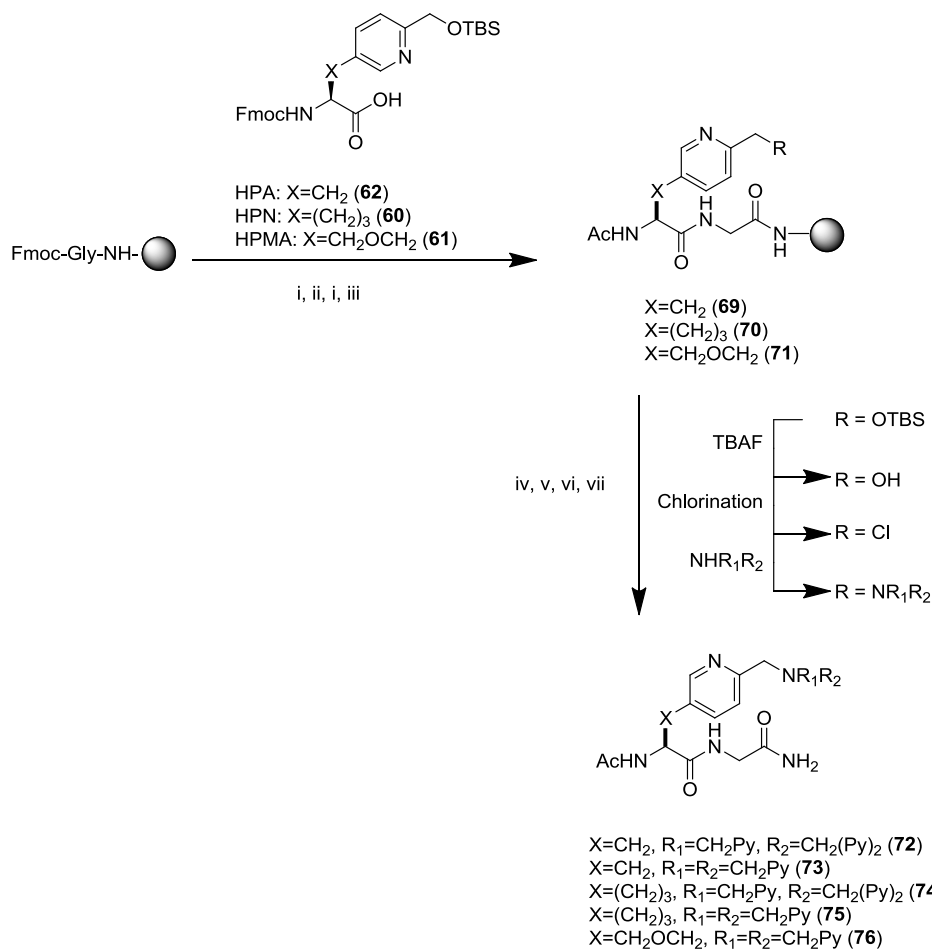
Pd/C was the first catalyst screened associated with either hydrogen gas or ammonium formate as hydrogen donors.¹¹⁶⁻¹¹⁸ None of the conditions using Pd/C (with different solvents and different hydrogen pressures) gave complete removal of the trityl protecting group (Scheme 5,

Table 3, Entries 1-5). Other catalysts were screened and Pd(OH)₂ was found to be suitable for this transformation at 10% w/w loading, H₂ at atmospheric pressure and methanol as solvent (Scheme 5, Table 3, Entries 6-7). The catalyst loading could be lowered to 5% w/w on a multigram scale, giving 99% yields after catalyst filtration and solvent removal.

Purification of the free amino acid was not attempted due to the polarity of the unprotected HPMA amino acid. Triphenylmethane being the only byproduct (toluene was removed under reduced pressure) the crude material was subjected to an Fmoc protection reaction with pyridine acting as a base and solvent to give Fmoc-HPMA(OTBS)-OH **61** in an acceptable yield (55% isolated yield after chromatography over the 2 steps, Scheme 5).

I.2.B.b. Applications to SPPS

The Kodanko laboratory had previously tried to incorporate N4Py onto peptides under SPPS conditions with Wang resins without success. It was decided to switch the type of resin in favor of the Rink amide resin. This resin affords a terminal amide after cleavage that should be more compatible with the different nitrogen based ligands and their synthesis. The Rink amide resin has been then applied to the synthesis of different peptides with all three synthetic amino acids developed by our laboratory (HPA, HPN and HPMA).



Conditions: i) 20% piperidine, RT, 20 min (2 cycles), ii) Fmoc-AA-OH, HBTU, *i*-Pr₂EtN, DMF, RT, 3–4 h, iii) Ac₂O, *i*-Pr₂EtN, DMF, RT, 1 h
 iv) TBAF, AcOH, THF, RT, 1 h (2 cycles), v) LiCl, TsCl, *i*-Pr₂EtN, CH₃CN, RT, 6 h, vi) NHR₁R₂, *i*-Pr₂EtN, CH₃CN, NaI, 55 °C, 24 h
 vii) TFA:H₂O (9:1), RT, 1h.

Scheme 6: Construction of polypyridyl ligand-peptide conjugates by SPPS on Rink amide resin

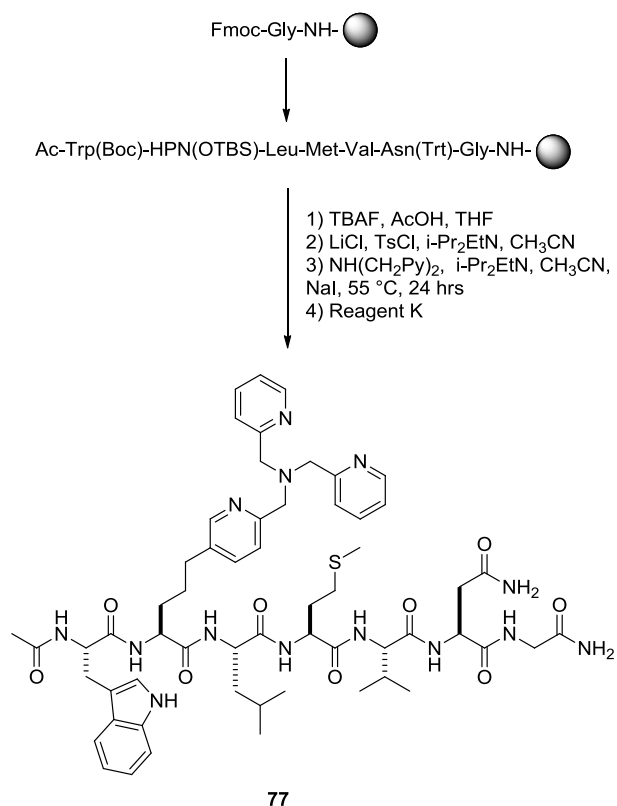
The synthesis started with Fmoc-protected glycine Rink resin (the initial glycine can be loaded manually as well). After Fmoc deprotection under standard 20% piperidine conditions, coupling with all three unnatural Fmoc protected synthetic amino acids **60–62** was achieved. After a second Fmoc deprotection the free amine was acetylated to give acetylated dipeptides **69–71** on resin. TBS deprotection and chlorination reactions had been previously developed on SPPS with the Wang resin by our laboratory and were applied here. Desilylation occurred smoothly under TBAF/acetic acid conditions and a same second cycle was performed to ensure complete deprotection. The resulting alcohols were chlorinated under LiCl/TsCl conditions. The

efficiency of this step was checked by deprotection of a minimal amount of product from resin and assessed by NMR. The *N*-alkylation reactions with the desired secondary amines were performed in a classical manner on resin. After 24 hours the beads were transferred back to the SPPS reactor to wash out the unreacted starting materials before a final TFA/H₂O deprotection. The final products were purified on HPLC under basic conditions (0.01% NH₄OH) (Scheme 6).

N-alkylation leading to both TPA and N₄Py containing conjugates were investigated. The introduction of TPA was successful with all three unnatural amino acids leading to dipeptides Ac-HPA/HPN/HPMA(N₂Py)-Gly-NH₂ **73**, **75** and **76**. The crude purities after final cleavage were greater than 80% giving the final products in pure form after HPLC purification. The introduction of N₄Py was successful on HPA- and HPN-containing dipeptides giving dipeptides Ac-HPA/HPN/(N₃Py)-Gly-NH₂ **72** and **74**. The HPMA containing dipeptide was not compatible with N₄Py, despite trying numerous conditions. Nonetheless, the proof of concept for this SPPS divergent methodology for the construction of peptide ligand conjugates was achieved (Scheme 6). S. Ulku has expanded this methodology for building conjugates with multiple binding units (structures not shown).¹¹⁹

To expand the scope of this methodology, and check functional group compatibility with the *N*-alkylation and resin cleavage conditions, the heptapeptide Ac-Trp-HPN(N₂Py)-Leu-Met-Val-Asn-Gly-NH₂ **77** was prepared. First, the pentapeptide Fmoc-Leu-Met-Val-Asn(Trt)-Gly bound to Rink resin was synthesized on an automated peptide synthesizer. The beads were then transferred into a SPPS reactor, the Fmoc group was removed manually, and coupling with Fmoc-HPN(OTBS)-OH was performed. A full cycle of coupling with Fmoc-Trp(BOC)-OH completed the building phase of the peptide before the installation of the TPA ligand. The same

conditions as for compounds **72-76** were used, and TPA was incorporated to give compound **77** (Scheme 7).



Scheme 7: Construction of heptapeptide **77** by SPPS

I.2.C. Conclusion

A new unnatural amino acid has been synthesized. Its synthesis can be easily scaled up to furnish multigram quantities of Fmoc-HPMA-OH. A crucial *O*-alkylation reaction under phase transfer conditions had to be used in order to take advantage of the chirality inherited from L-serine. Although the introduction of N4Py is problematic into peptide conjugates containing HPMA, other smaller ligands like TPA have been introduced successfully.

Finally, this divergent methodology has been successfully transferred onto SPPS that greatly accelerates the synthesis of new peptide conjugates. The possibility of using SPPS for the

construction of peptide ligand conjugates with the possibility of placing one or more metal ligands within the peptide, at any desirable position, should enable the synthesis of a wide array of new peptide-metal ligand conjugates. Moreover, the ligand diversity is introduced in the last step of the sequence (other than the cleavage from resin) making this methodology highly divergent. The robustness of this methodology has been demonstrated with the construction of the TPA containing heptapeptide **77**. The use of this methodology for the construction of biologically active agents is also being explored in the Kodanko laboratory.

The work presented in this chapter was published in the *Journal of Organic Chemistry*: Jabre, N. D., Respondek, T., Ulku, S., Korostelova N., Kodanko, J. J. "A Divergent Strategy for Attaching Polypyridyl Ligands to Peptides", *J. Org. Chem.*, **2010**, 75(3), 650-659.¹²⁰

I.2.D. Experimental section

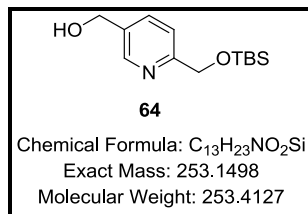
I.2.D.a. General considerations

All reagents were purchased from commercial suppliers and used as received. NMR spectra were recorded on a Varian FT-NMR Mercury-300, 400 or 500 MHz Spectrometer. Low-resolution mass spectra were recorded on a Waters ZQ2000 single quadrupole mass spectrometer using an electrospray ionization source, while high-resolution mass spectra were recorded on a Waters-Micromass LCT Premier XE time of flight mass spectrometer. IR spectra were recorded on a Nicolet FT-IR spectrophotometer. Optical rotations were obtained by using a PERKIN-ELMER 241-MC Polarimeter. HPLC was performed on an Agilent 1200 preparative purification system equipped with a multi-wavelength detector. Column purifications were performed using silica gel flash chromatography unless mentioned otherwise. All reactions were performed under

ambient atmosphere unless otherwise noted. Anaerobic reactions were performed in Schlenk tubes. All NMR spectra and chromatographs can be found in the Appendix section.

I.2.D.b. Experimental procedures and tabulated characterization data

(6-((tert-butyldimethylsilyloxy)methyl)pyridin-3-yl)methanol (**64**):



To a solution of pyridine-2,5-dicarboxylic acid (20.0 g, 0.12 mmol) in 120 ml of CH₃OH (31.25 equiv) was slowly added H₂SO₄ (40.0 ml, 0.75 mmol, 6.25 equiv). The solution was temporarily placed in an ice bath to control the exotherm. After completing the addition the resulting solution was heated to reflux for 24 h. The crude was worked up by slow addition of 50 ml of water (the solution is placed in an ice bath to control the exotherm and Na₂CO₃ is added to get a pH~9-10 (need to control the speed of addition and avoid emulsion, some additional water addition is needed)). The basic aqueous solution is extracted with CHCl₃ (3×250 mL). The organic layers are combined, dried over Na₂SO₄ and concentrated to give **dimethylpyridine-2,5-dicarboxylate** as a white to yellow solid (19.9 g, 83% isolated yield): ¹HNMR (CDCl₃ δ 7.27) : δ 9.31 (d, 1H, J=1.62Hz), 8.44-8.47 (dd, 1H, J₁=8.11Hz, J₂=1.62Hz), 8.20-8.23 (d, 1H, J=8.11Hz), 4.04 (s, 3H).

Dimethylpyridine-2,5-dicarboxylate (1.00 g, 5.12 mmol, 1.0 equiv) was dissolved in dry THF/EtOH (45 ml, 1/2) under Argon. CaCl₂ (2.27 g, 20.50 mmol, 4.0 equiv) is added and the solution cooled down to 0°C. NaBH₄ (485 mg, 12.8 mmol, 2.5 equiv) is added in small portions and the resulting solution is stirred at 0 °C for 6-8 h. After completion of the reaction (as judged

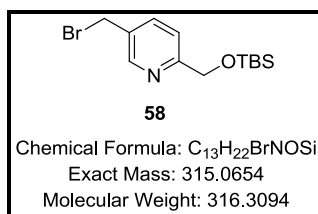
by TLC), 60 ml of water are added drop wise. The resulting solution is extracted with CHCl_3 (3×60 mL). The organic layers are combined, dried over Na_2SO_4 and concentrated to give **methyl-6-(hydroxymethyl)nicotinate** as a white to yellow oil (0.78 g, 93% isolated yield): $^1\text{H NMR}$ (CDCl_3 δ 7.27) : δ 9.15 (d, 1H, $J=1.62\text{Hz}$), 8.28-8.30 (dd, 1H, $J_1=8.11\text{Hz}$, $J_2=1.62\text{Hz}$), 7.37-7.39 (d, 1H, $J=8.11\text{Hz}$), 4.83 (s, 2H), 3.96 (s, 3H)

To a solution of **methyl-6-(hydroxymethyl)nicotinate** (0.778 g, 4.65 mmol, 1.0 equiv) in 10 mL of DMF was added imidazole (477 mg, 7.0 mmol, 1.4 equiv) and TBS-Cl (771 mg, 5.12 mmol, 1.1 equiv) at RT. The resulting solution was stirred for 2 h. After completion of the reaction (as judged by TLC), 25 mL of water are added drop wise. The resulting solution is extracted with EtOAc (3×25 mL). The organic layers are combined, dried over Na_2SO_4 to give **methyl-6-((tert-butyldimethylsilyloxy)methyl)nicotinate** as a white to yellow oil (1.248g, 95% isolated yield): $^1\text{H NMR}$ (CDCl_3 δ 7.27) : δ 9.10-9.11 (d, 1H, $J=2.43\text{Hz}$), 8.30-8.32 (dd, 1H, $J_1=8.11\text{Hz}$, $J_2=2.43\text{Hz}$), 7.60-7.62 (d, 1H, $J=8.11\text{Hz}$), 4.88 (s, 2H), 3.94 (s, 3H), 0.96 (s, 9H), 0.13 (s, 6H)

A mixture of **methyl-6-((tert-butyldimethylsilyloxy)methyl)nicotinate** (5.00 g, 17.8 mmol) and dry THF (125 mL) was cooled to 0 °C under a nitrogen atmosphere. A solution of $\text{NaAlH}_2(\text{OCH}_2\text{CH}_2\text{OMe})$ in toluene (65% w/w) (12.7 mL, 40.8 mmol) was added dropwise over 30 min, resulting in an orange solution. The solution was maintained at 0 °C for 1.5 h. After consumption of the starting material, as judged by TLC analysis, the reaction mixture was quenched by dropwise addition of MeOH (4.5 mL) followed by addition of a 0.1M NaOH solution (10 mL). The reaction mixture was combined with H_2O (200 mL) and the aqueous layer was extracted with EtOAc (3×75 mL). The combined organic layer was dried over anhydrous Na_2SO_4 and concentrated to give a yellow viscous oil which upon crystallization from cold

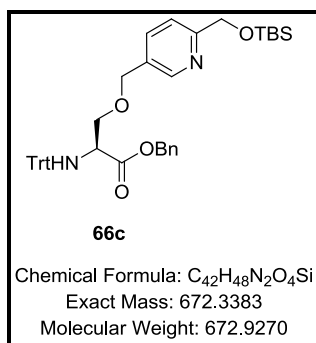
hexanes (10 mL) furnished **64** as a white crystalline solid (3.50 g, 78%): mp = 50-51 °C; ^1H NMR (400 MHz, CDCl_3) δ 8.34 (brs, 1H), 7.69 (d, $J = 8.1$ Hz, 1H), 7.46 (d, $J = 8.1$ Hz, 1H), 4.76 (s, 2H), 4.64 (s, 2H), 3.57 (b, 1H), 0.91 (s, 9H), 0.07 (s, 6H); ^{13}C NMR (100 MHz, CDCl_3) δ 160.4, 147.2, 135.8, 134.7, 119.9, 65.7, 62.2, 25.9, 18.3, -5.4; IR (thin film) 3211 (b), 2953, 2927, 2856, 1604, 1573, 1491, 1458, 1399, 1377, 1358, 1341, 1255, 1102, 1060, 1031, 1006, 860, 839, 776, 670, 647 cm^{-1} ; LRMS (ESMS) calculated for $\text{C}_{13}\text{H}_{24}\text{NO}_2\text{Si}$ ($\text{M}+\text{H}$) $^+$ 254, found: 254.

5-(bromomethyl)-2-((tert-butyldimethylsilyloxy)methyl)pyridine (58):



To a solution of (6-((tert-butyldimethylsilyloxy)methyl)pyridin-3-yl)methanol **64** (1013 mg, 4.0 mmol, 1.0 equiv) in 20 ml of CH_2Cl_2 dried over molecular sieves under Argon at RT were added NBS (783 mg, 4.4 mmol, 1.1 equiv) and PPh_3 (1.15 g, 4.4 mmol, 1.1 equiv). The reaction was stirred at RT for 90 min. After completion of the reaction (as judged by TLC), CH_2Cl_2 is removed on Rotavap and the crude is purified by flash chromatography (9/1 to 8/2 hexanes/EtOAc) and **58** was obtained as a white oil (1.12 g, 88% isolated yield). The product decomposes within a day (turns pinkish and then purple): ^1H NMR (CDCl_3 δ 7.27): δ 8.52-8.53 (d, 1H, $J=2.44\text{Hz}$), 7.74-7.77 (dd, 1H, $J_1=7.94\text{Hz}$, $J_2=2.44\text{Hz}$), 7.51-7.53 (d, 1H, $J=7.94\text{Hz}$) 4.84 (s, 2H), 4.49 (s, 2H), 0.97 (s, 9H), 0.13 (s, 6H); ^{13}C NMR (CDCl_3 δ 77.00): δ 161.62148.70, 137.22, 131.67, 119.98, 65.85, 29.80, 25.88, 18.34, -5.41; LRMS (ESMS): calculated for $\text{C}_{13}\text{H}_{22}\text{BrNOSi}$ ($\text{M}+\text{H}$) $^+$: 317, found: 317 ($\text{M}+\text{H}$) $^+$

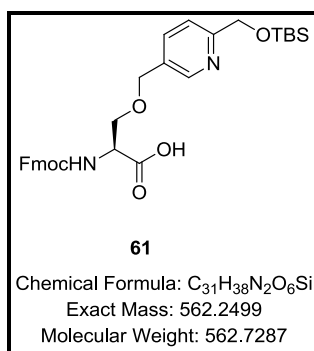
(S)-benzyl 3-(((6-((2,3,3-trimethylbutan-2-yloxy)methyl)pyridin-3-yl)methoxy)-2-(tritylamino)propanoate (66c):



To a solution of 5-(bromomethyl)-2-((tert-butyldimethylsilyloxy)methyl)pyridine **58** (95 mg, 0.3 mmol, 1.0 equiv) in 1 mL of benzene at RT were added (S)-benzyl 3-hydroxy-2-(tritylamino)propanoate **65c** (131 mg, 0.3 mmol, 1.0 equiv) in 1.0 mL of benzene. To the resulting solution were added TBAB (97 mg, 0.3 mmol, 1.0 equiv) and 10 equiv of 40% NaOH (300 mg, 3.0 mmol, 10 equiv). The reaction was stirred at 1000 rpm for 24 h. After completion of the reaction (as judged by TLC,), 2 mL of water were added and the resulting solution was extracted with EtOAc (3×5 mL). The organic layers were combined, dried over Na₂SO₄ and concentrated. The resulting crude was purified by flash chromatography (9/1 to 8/2 hexanes/EtOAc) and **66c** was obtained as a white oil (118 mg, 59% isolated yield): ¹HNMR (MeOD δ 3.31) : δ 8.30 (d, 1H, J=1.62Hz), 7.59-7.62 (dd, 1H, J₁=8.11Hz, J₂=1.62Hz), 7.45-7.46 (m, 7H), 7.13-7.23 (m, 14H), 4.78 (s, 2H), 4.72-4.76 (d, 1H, J=12.97Hz), 4.50-4.53 (d, 1H, J=12.97Hz), 4.38-4.46 (d, 2H, 7.30), 3.68-3.71 (dd, 1H J₁=8.92Hz, J₂=4.05Hz), 0.96 (s, 9H), 0.12 (s, 6H), 3.47-3.56 (m, 2H); ¹³CNMR (MeOD δ 48.94) : δ 175.19, 161.57, 154.08, 148.65, 147.39, 138.45, 137.20, 134.07, 130.05, 129.55, 129.30, 129.25, 129.09, 127.80, 121.72, 75.54, 73.88, 71.28, 67.81, 66.65, 57.99, 26.54, 19.35, -5.08; IR (KBr): 3061, 3032, 2955, 2928, 2887, 2854, 1734, 1601, 1489, 1471, 1456, 1448, 1371, 1362, 1254, 1182, 1174, 1128, 1101, 837, 777,

746, 706 cm^{-1} ; LRMS (ESI): calculated for $\text{C}_{42}\text{H}_{48}\text{N}_2\text{O}_4\text{Si}$ ($\text{M}+\text{H}$) $^+$: 673, found: 673($\text{M}+\text{H}$) $^+$, 695 ($\text{M}+\text{Na}$) $^+$

(S)-2-(((9H-fluoren-9-yl)methoxy)carbonylamino)-3-(((6-((tert-butyldimethylsilyloxy)methyl)pyridin-3-yl)methoxy)propanoic acid (61):



A mixture of compound **66c** (2.10 g, 3.12 mmol), $\text{Pd}(\text{OH})_2/\text{C}$ (525 mg, 5% w/w) and MeOH (210 mL) was stirred at RT under H_2 (1 atm) for 12 h. The reaction mixture was filtered through a celite bed to remove Pd/C and the filtrate was concentrated to give a colorless solid. A mixture of the latter colorless solid (100 mg, 0.17 mmol), FmocOSu (69 mg, 0.21 mmol) and pyridine (2.8 mL) was maintained at RT for 12 h. The reaction mixture was concentrated to obtain the crude product. The crude product was dissolved in water (10 mL) and acidified with 5% aqueous citric acid (pH= 5-6). The aqueous layer was extracted with CH_2Cl_2 (3×30 mL). The combined organic layer was dried over anhydrous Na_2SO_4 and concentrated to obtain the crude product. The resulting crude was purified by silica gel chromatography (0% to 10% MeOH: CH_2Cl_2) to obtain **61** as a colorless amorphous solid (53 mg, 55%): ^1H NMR (400 MHz, CD_3OD) δ 8.40 (s, 1H), 7.79 (d, J = 8.1 Hz, 1H), 7.76 (d, J = 7.3 Hz, 2H), 7.63 (dd, J = 6.9, 3.2 Hz, 2H), 7.47 (d, J = 8.1 Hz, 1H), 7.36 (t, J = 7.3 Hz, 2H), 7.26 (t, J = 6.9 Hz, 2H), 4.75 (s, 2H), 7.58-7.51 (m, 2H), 4.38 (dd, J = 10.5, 7.3 Hz, 2H), 4.31-4.23 (m, 2H), 4.18 (t, J = 6.5 Hz, 1H), 3.91-3.79 (m, 2H), 0.93 (s, 9H), 0.10 (s, 6H); ^{13}C NMR (100 MHz CD_3OD) δ 175.7, 160.2,

157.2, 147.4, 144.2, 144.1, 141.4, 137.2, 127.6, 127.0, 125.1, 125.0, 120.4, 119.8, 70.9, 70.0, 66.8, 65.3, 47.2, 25.2, 18.0, -6.5; IR (thin film) 3340 (b) 2953, 2856, 1716, 1606, 1506, 1450, 1253, 1105, 910, 839, 779, 759, 738 cm^{-1} ; $[\alpha] = +11.3^\circ$ ($c = 0.97$, MeOH); HRMS (ESMS) calculated for $\text{C}_{31}\text{H}_{37}\text{N}_2\text{O}_6\text{SiNa}_2$ ($\text{M-H}+2\text{Na}$)⁺, 607.2216, found: 607.2209.

Solid phase peptide synthesis general considerations:

All peptides were synthesized on a 0.12-0.40 mmol scale by solid phase peptide synthesis methods using N^α-9-fluorenylmethoxy-carbonyl (Fmoc) amino acids with HBTU-activated ester chemistry in a Peptide Synthesis Vessel (ChemGlass CG-1860). Burrell Model 75 Wrist Action Lab Shaker was used for shaking the reaction mixture. Commercially available starting materials and reagents were purchased from ChemPep.Inc., AnaSpec.Inc. and Chem Impex.

Solid phase peptide synthesis procedures:

Fmoc-Gly-Rink Amide MBHA Resin (0.32 mmol/g) or Rink Amide MBHA Resin (0.75 mmol/g) was used to afford C-terminal amides. Typical protocols for coupling a residue involved 1-4 h coupling cycles with 3-4 equiv of amino acid. However, for the unnatural amino acids **HPA**, **HPN** and **HPMA** only 2 equiv were used. Activated esters were formed *in situ* using HBTU and *i*-Pr₂EtN in DMF. After coupling, Fmoc deprotection as well as washing steps, solutions were filtered manually through a CG-1860 Peptide Synthesis Vessel. The Fmoc deprotection was performed using 20% Piperidine/DMF with three cycles 10-20 min each. After constructing the desired length of a peptide chain, the *N*-terminal was acetylated using acetic anhydride (50 equiv) and *i*-Pr₂EtN (50 equiv) in DMF for 2 h. After each reaction step, the resin was washed with DMF, *i*-Pr₂EtN and CH₂Cl₂. Kaiser test was used to monitor the coupling reactions and deprotection of the Fmoc-group. Standard SPPS steps were summarized in Table 4.

Operation	Reagent	Vol	Time
Fmoc deprotection	20% Piperidine/DMF	7 mL	3 × 15 min
Drain and wash	DMF	4 mL	2 min
	IPA	4 mL	
	CH ₂ Cl ₂	4 mL	
Coupling with Gly or Ala	Fmoc-AA-OH (0.3 mmol) HBTU (0.3 mmol) <i>i</i> -Pr ₂ EtN (0.3 mmol)	2 mL DMF	1-2 h
Coupling with HPN, HPA or HPMA	Fmoc-AA-OH (0.2 mmol) HBTU (0.2 mmol) <i>i</i> -Pr ₂ EtN (0.2 mmol)	1.5 mL DMF	3-4 h
Capping	Ac ₂ O (5 mmol) <i>i</i> -Pr ₂ EtN (5 mmol)	2.5 mL DMF	1 h

Table 4: Standard Solid Phase Peptide Synthesis (0.1 mmol scale)

General Procedure for Chlorination:

Cleavage of the silyloxyether group of compounds **69-71** were performed by shaking a mixture of the corresponding intermediate with acetic acid (1 equiv) and TBAF (4 equiv) in THF at RT for 1 h. The cleavage procedure was repeated to ensure complete cleavage of the silyloxyether group. After applying the standard washing procedure, resin was dried under vacuum. A mixture of the dried resin, flame dried LiCl (50 equiv), MeCN and *i*-Pr₂EtN (15 equiv) was purged under nitrogen atmosphere for 5-10 min and TsCl (10 equiv) was added. The reaction mixture was shaken at RT for 6 h. The color of the resin changed from pale yellow to red. At least one water washing was included in the standard washing protocol. Finally, the resin was dried under vacuum. At this point, % conversion to the chloride can be checked by cleaving a small amount of the peptide from the resin using TFA/H₂O (95:5) and analyzing the crude

peptide by ^1H NMR and ESMS. In some cases, it was necessary to resubject the resin-bound peptide to the chlorination conditions (LiCl, TsCl, *i*-Pr₂EtN) to observe complete conversion to the chloride.

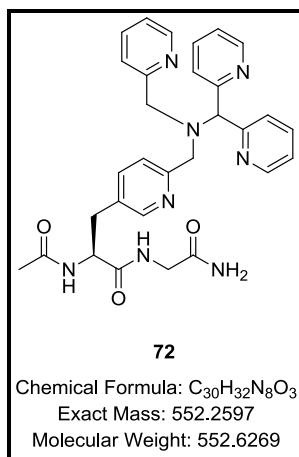
General Procedure for *N*-Alkylation:

A mixture of the resin containing the chlorinated adduct, MeCN, *i*-Pr₂EtN (12 equiv), sodium iodide (0.2 equiv) and the corresponding secondary amine (10 equiv) was heated at 55 °C for 24 h. The reaction mixture was washed using the standard washing procedure and the peptides were cleaved from the resin by treatment with TFA/H₂O (95:5) for 2 h. In the case of compound **77**, Reagent K was used for cleavage of the peptide from the resin. The resin was filtered, washed with TFA, and the combined filtrate was concentrated to 1-2 mL and stirred with ether/hexanes. The supernatant was decanted and remaining residue was purified by preparative HPLC.

Operation	Reagent	Vol	Time	Temperature
TBS- Cleavage	TBAF (1M in THF, 0.4 mmol) AcOH (0.1 mmol)	4 mL THF	2 × 1 h	RT
Chlorination	LiCl (5 mmol) TsCl (1 mmol) <i>i</i> -Pr ₂ EtN (1.5 mmol)	4 mL CH ₃ CN	1 × 6 h	RT
<i>N</i>-Alkylation	NaI (0.02 mmol) R ¹ R ² NH (1 mmol) <i>i</i> -Pr ₂ EtN (1.2 mmol)	2 mL CH ₃ CN	1 × 12-24 h	55 °C

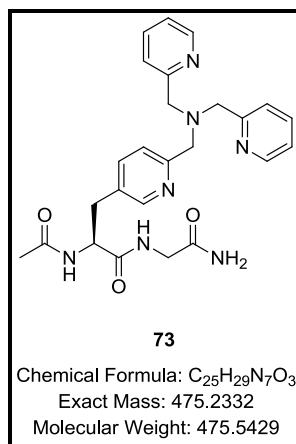
Table 5: Reactions on the side chain (0.1 mmol scale)

2-acetamido-N-(2-amino-2-oxoethyl)-3-(6-(((dipyridin-2-ylmethyl)(pyridin-2-ylmethyl)amino)methyl)pyridin-3-yl)propanamide (72).



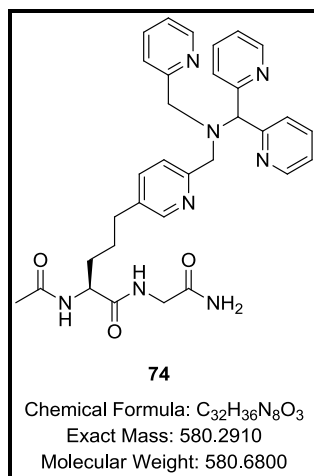
The crude product was purified by preparative HPLC. HPLC column: Phenomenex LUNA C18 (2) 100 Å 250 × 21.2 mm; Mobile phase: 0.01% aq NH₄OH and MeOH; Flow rate = 20 mL/min; Gradient elution 0-4 min 5-20% MeOH in aq NH₄OH, 4-25min 20-95% MeOH in aq NH₄OH, RT = 16.3 min. ¹H NMR (400 MHz, CD₃OD) δ 8.47 (d, J = 4.9 Hz, 2H), 8.37 (d, J = 4.9 Hz, 1H), 8.27 (d, J = 1.6 Hz, 1H), 7.83-7.73 (m, 5H), 7.73-7.68 (m, 1H), 7.68-7.61 (m, 2H), 7.31-7.26 (m, 2H), 7.25-7.20 (m, 1H), 5.32 (s, 1H), 4.50 (dd, J = 8.9, 6.5 Hz, 1H), 3.95 (s, 2H), 3.90 (s, 2H), 3.86 (d, J = 17.0 Hz, 1H), 3.69 (d, J = 17.0 Hz, 1H), 3.14 (dd, J = 14.2, 6.1 Hz, 1H), 2.91 (dd, J = 13.8, 8.9 Hz, 1H), 1.91 (s, 3H); ¹³C NMR (100 MHz CD₃OD) δ 172.9, 172.5, 172.4, 159.6, 159.3, 157.7, 148.9, 148.7, 148.3, 137.9, 137.3, 137.2, 131.9, 124.5, 123.5, 123.2, 122.8, 122.4, 72.8, 57.2, 56.9, 54.9, 41.9, 34.0, 21.2; IR (KBr) 3431, 2918, 2850, 1662, 1594, 1571, 1541, 1471, 1435, 1293, 1092, 1004, 770, 692, 561, 459 cm⁻¹; HRMS (ESMS) calculated for C₃₀H₃₂N₈O₃Na (M+Na)⁺: 575.2495, found: 575.2501

2-acetamido-N-(2-amino-2-oxoethyl)-3-(6-((bis(pyridin-2-ylmethyl)amino)-methyl)pyridin-3-yl)propanamide (73).



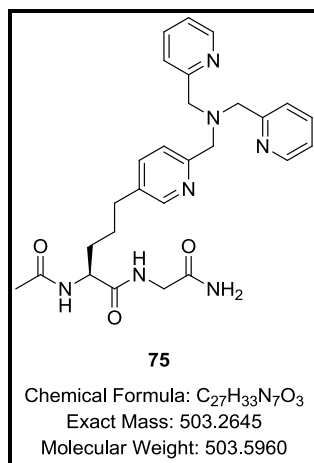
The crude product was purified by preparative HPLC. HPLC column: Phenomenex LUNA C18 (2) 100 Å 250 × 21.2 mm; Mobile phase: 0.01% aq NH₄OH and MeOH; Flow rate = 20 mL/min; Gradient elution 0-4 min 5-20% MeOH in aq NH₄OH, 4-25 min 20-75% MeOH in aq NH₄OH, RT = 19.8 min. ¹H NMR (400 MHz, CD₃OD) δ 8.34 (d, J = 4.9 Hz, 2H), 8.32 (d, J = 2.4 Hz, 1H), 7.79 (td, J = 7.7, 1.6 Hz, 2H), 7.71 (dd, J = 8.1, 1.6 Hz, 1H), 7.66 (d, J = 8.1 Hz, 2H), 7.61 (d, J = 8.1 Hz, 1H), 7.28 (dd, J = 6.5, 4.9 Hz, 2H), 4.53 (dd, J = 8.9, 6.5 Hz, 1H), 3.86 (d, J = 17.0 Hz, 1H), 3.83 (s, 4H), 3.82 (s, 2H), 3.69 (d, J = 16.2 Hz, 1H), 3.16 (dd J = 14.2, 6.1 Hz, 1H), 2.93 (dd, J = 14.6, 8.9 Hz, 1H), 1.90 (s, 3H); ¹³C NMR (100 MHz, CD₃OD) δ 172.9, 172.4, 172.3, 158.6, 157.0, 148.9, 148.3, 138.3, 137.6, 132.4, 123.8, 123.4, 122.8, 59.7, 59.5, 54.8, 41.9, 34.1, 21.2; IR (KBr) 3435, 2927, 2850, 1669, 1595, 1570, 1541, 1436, 1374, 1294, 1203, 1129, 1050, 1003, 836, 768, 600 cm⁻¹; HRMS (ESMS) calculated for C₂₅H₂₉N₇O₃Na (M+Na)⁺: 498.2230, found: 498.2229

(S)-2-acetamido-N-(2-amino-2-oxoethyl)-5-(6-(((dipyridin-2-ylmethyl)(pyridin-2-ylmethyl)amino)methyl)pyridin-3-yl)pentanamide (74).



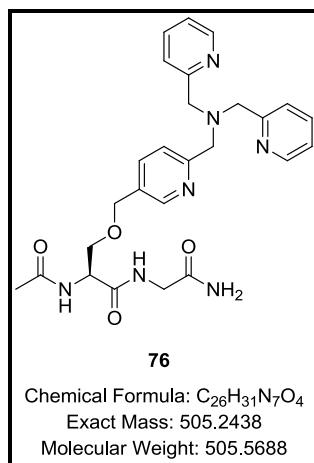
The crude product was purified by preparative HPLC. HPLC column: Phenomenex LUNA C18 (2) 100 Å 250 × 21.2 mm; Mobile phase: 0.01% aq NH₄OH and MeOH; Flow rate = 20 mL/min; Gradient elution 0-4 min 5-20% MeOH in aq NH₄OH, 4-25 min 20-95% MeOH in aq NH₄OH, RT = 16.7 min. ¹H NMR (400 MHz, CD₃OD) δ 8.47 (d, J = 4.9 Hz, 2H), 8.35 (d, J = 4.9 Hz, 1H), 8.20 (s, 1H), 7.82-7.73 (m, 4H), 7.72 (dd, J = 7.3, 1.6 Hz, 1H), 7.70-7.66 (m, 1H), 7.62-7.55 (m, 2H), 7.31-7.25 (m, 2H), 7.23-7.18 (m, 1H), 5.32 (s, 1H), 4.23 (dd, J = 7.3, 5.7 Hz, 1H), 3.95 (s, 2H), 3.93 (s, 2H), 3.88 (d, J = 17.0 Hz, 1H), 3.76 (d, J = 17.0 Hz, 1H), 2.62 (dd, J = 7.3, 5.7 Hz, 2H), 1.99 (s, 3H), 1.87-1.70 (m, 1H), 1.75-1.60 (m, 3H); ¹³C NMR (100 MHz CD₃OD) δ 173.7, 173.1, 172.7, 159.7, 159.4, 156.7, 137.3, 137.2, 136.3, 124.4, 123.5, 123.3, 122.8, 122.4, 73.1, 57.4, 57.2, 54.1, 42.0, 31.8, 30.9, 27.3, 21.2; IR (KBr) 3435, 2924, 2852, 1659, 1594, 1571, 1541, 1471, 1435, 1384, 1088, 1003, 773, 693, 459 cm⁻¹; [α] = +2.5° (c = 0.60, MeOH); HRMS (ESMS) calculated for C₃₂H₃₆N₈O₃Na (M+Na)⁺: 603.2808, found: 603.2810

(S)-2-acetamido-N-(2-amino-2-oxoethyl)-5-(6-((bis(pyridin-2-ylmethyl)amino)-methyl)pyridin-3-yl)pentanamide (75).



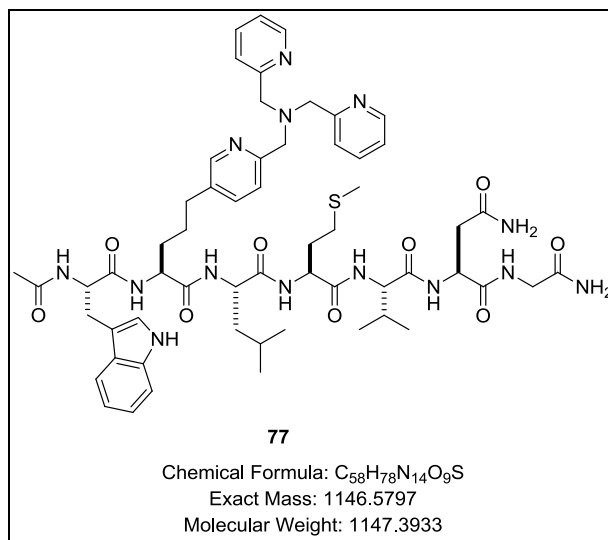
The crude product was purified by preparative HPLC. HPLC column: Phenomenex LUNA C18 (2) 100 Å 250 × 21.2 mm; Mobile phase: 0.01% aq NH₄OH and MeOH; Flow rate = 20 mL/min; Gradient elution 0-4 min 5-20% MeOH in aq NH₄OH, 4-25 min 20-75% MeOH in aq NH₄OH, RT = 21.5 min. ¹H NMR (400 MHz, CD₃OD) δ 8.42 (d, J = 4.9 Hz, 2H), 8.28 (s, 1H), 7.78 (td, J = 7.5, 2.0 Hz, 2H), 7.66 (d, J = 8.1 Hz, 2H), 7.62 (d, J = 2.4 Hz, 1H), 7.56 (d, J = 8.1 Hz, 1H), 7.27 (t, J = 6.5 Hz, 2H), 4.24 (t, J = 6.5 Hz, 1H), 3.87 (d, J = 17.0 Hz, 1H), 3.84 (s, 4H), 3.82 (s, 2H), 3.76 (d, J = 17.0 Hz, 1H), 2.65 (t, J = 6.5 Hz, 2H), 1.98 (s, 3H), 1.87-1.77 (m, 1H), 1.75-1.62 (m, 3H); ¹³C NMR (100 MHz, CD₃OD) δ 173.7, 173.1, 172.7, 158.9, 156.4, 148.3, 148.2, 137.5, 136.6, 123.7, 123.4, 122.7, 60.0, 59.7, 54.1, 42.0, 31.8, 30.9, 27.2, 21.2; IR (KBr) 3439, 2925, 2851, 1660, 1595, 1570, 1541, 1436, 1374, 1311, 1258, 1124, 1051, 1003, 768, 603 cm⁻¹; [α] = +3.0° (c = 0.75, MeOH); HRMS (ESMS) calculated for C₂₇H₃₃N₇O₃Na (M+Na)⁺: 526.2543, found: 526.2552

(S)-2-acetamido-N-(2-amino-2-oxoethyl)-3-(((6-((bis(pyridin-2-ylmethyl)amino)-methyl)pyridin-3-yl)methoxy)propanamide (76)



The crude product was purified by preparative HPLC. HPLC column: Phenomenex LUNA C18 (2) 100 Å 250 × 21.2 mm; Mobile phase: 0.01% aq NH₄OH and MeOH; Flow rate = 20 mL/min; Gradient elution 0-4 min 5-20% MeOH in aq NH₄OH, 4-25 min 20-75% MeOH in aq NH₄OH, RT = 19.3 min. ¹H NMR (400 MHz, CD₃OD) δ 8.44 (d, J = 4.9 Hz, 2H), 8.42 (d, J = 1.6 Hz, 1H), 7.83-7.76 (m, 3H), 7.69-7.64 (m, 3H), 7.30-7.25 (m, 3H), 4.62-4.54 (m, 2H), 4.51 (t, J = 5.3 Hz, 1H), 3.89-3.79 (m, 8H), 3.82 (dd, 3.74 (J = 9.7, 5.7 Hz, 1H), 3.74 (dd, J = 9.7, 4.9 Hz, 1H), 2.02 (s, 3H); ¹³C NMR (100 MHz CD₃OD) δ 173.0, 172.8, 171.5, 158.8, 158.4, 148.3, 147.8, 137.5, 137.0, 132.8, 123.7, 123.4, 122.7, 70.2, 69.6, 59.7, 54.3, 42.1, 21.3; IR (KBr) 3440 (b), 2919, 2849, 1678, 1541, 1435, 1384, 1204, 1181, 1122, 837, 800, 773, 722, 693, 467; [α] = +4.5° (c= 0.37, MeOH); HRMS (ESMS) calculated for C₂₆H₃₁N₇O₄Na (M+Na)⁺: 528.2335, found: 528.2332

Heptapeptide Ac-Trp-HPN(N₂Py)-Leu-Met-Val-Asn-Gly-NH₂ (77):

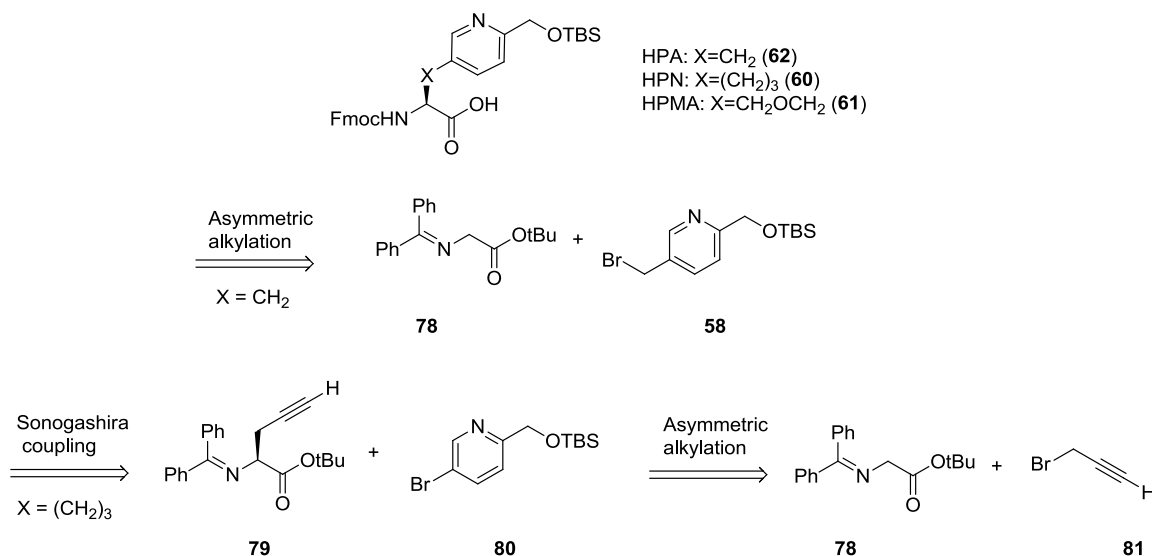


The crude product was purified by preparative HPLC. HPLC column: Phenomenex LUNA C18 (2) 100 Å 250 × 21.2 mm; Mobile phase: 0.01% aq NH₄OH and MeOH; Flow rate = 20 mL/min; Gradient elution 0-25 min 50-95% MeOH in aq NH₄OH, RT = 22.4 min. See Appendix for NMR spectrum. HRMS (ESMS) calculated for C₅₈H₇₈N₁₄O₉Na (M+Na)⁺: 1169.5695, found: 1169.5750.

Chapter 3. Development of an “optimal substrate” for the enantioselective alkylation of benzophenone imine

I.3.A. Background and project design

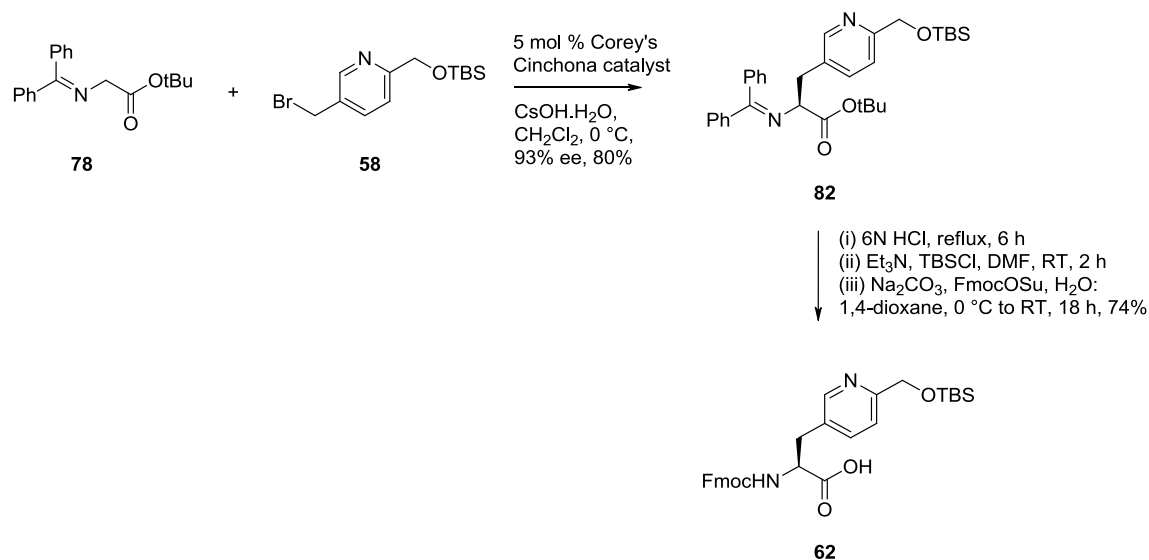
The divergent methodology for the incorporation of polypyridyl ligands into peptides developed and presented in the previous chapter is based on the use of unnatural amino acids bearing a pyridine moiety as an anchoring group. Three unnatural amino acids had been designed by the Kodanko group (the synthesis of the HPMA unnatural amino acid was presented in Chapter 2, Scheme 4 and Scheme 5) whereas the syntheses of HPA and HPN had been developed by fellow group members N. Jabre and S. Ulku. In these two latter syntheses an asymmetric alkylation of a benzophenone glycine imine derivative was the key step (Scheme 8).



Scheme 8: Retrosynthetic analysis of HPA and HPN unnatural amino acids

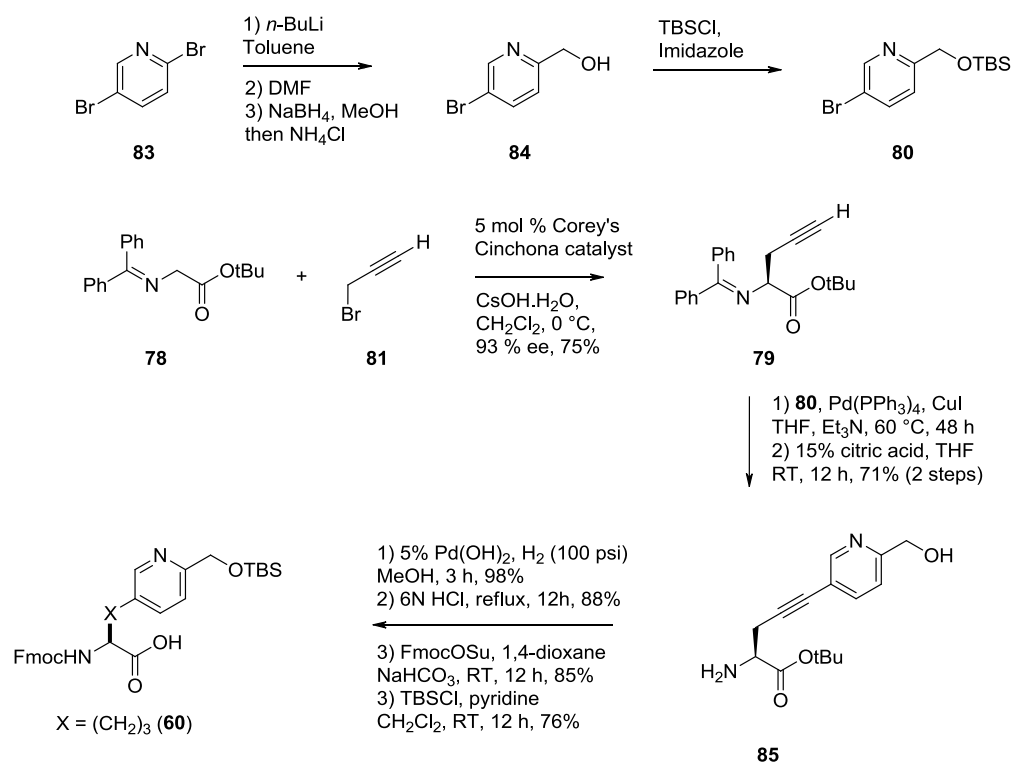
N. Jabre’s synthesis of HPA started with the phase transfer catalyzed alkylation of benzophenone glycine imine **78** with partner **58**. Because the *Cinchona* derived catalysts used to

catalyze the former alkylation reaction require the *tert*-butyl ester protecting group for the C-terminus in order to achieve high ee levels (enantiomeric excess), a 6 N HCl hydrolysis had to be used to remove the latter protecting group. Those harsh conditions were also responsible for the removal of the TBS group that had to be reintroduced leading to Fmoc-HPA(OTBS)-OH after Fmoc protection (Scheme 9).



Scheme 9: N. Jabre's synthesis of Fmoc-HPA(OTBS)-OH **62**

Similarly, S. Ulku's synthesis of HPN utilized the analogous phase transfer catalyzed alkylation reaction of benzophenone glycine imine **78** with partner **81**. Once again, protecting groups were removed under acid mediated hydrolysis conditions. After Sonogashira coupling between partners **79** and **80**, the imine was cleaved using citric acid. After hydrogenation of the alkyne moiety, the *tert*-butyl ester was removed under 6 N HCl hydrolysis conditions, resulting in the need to reintroduce the TBS group, finally leading to Fmoc-HPN(OTBS)-OH after Fmoc protection (Scheme 10).



Scheme 10: S. Ulku's synthesis of Fmoc-HPN(OTBS)-OH **60**

Those two first generation syntheses, although granting access to needed unnatural amino acids HPA and HPN, are not atom economical or well suited for multigram quantities because of the numerous protecting group manipulation steps.

On a larger perspective, the *Cinchona* catalyzed alkylation of glycine imine is one of the most used methodologies for the synthesis of enantiomerically enriched amino acids but is not compatible with acid sensitive substrates due to the fact that it requires the use of the *tert*-butyl ester as the protecting group for the C-terminus (or requires extra protecting group manipulation steps as in the examples explained above). The *tert*-butyl ester forces the use of harsh acidic conditions in the deprotection step. Newer classes of catalysts based on biphenyl or binaphthyl motifs^{121, 122} enable high levels of enantioselectivity with a variety of glycine C-terminal protecting groups. Their main drawback is a difficult multistep synthesis. In the view of Fmoc-

based SPPS, where acid-labile protecting groups are typically used for the protection of reactive side chains, new methods needed to be developed.

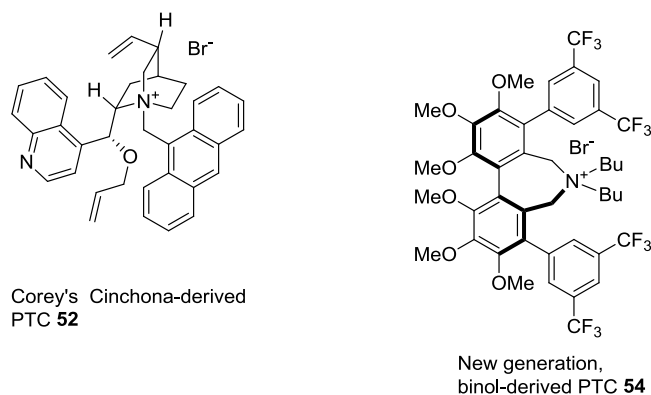


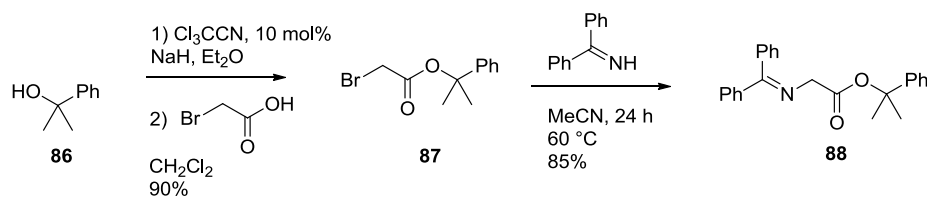
Figure 27: Examples of phase transfer catalysts used in the alkylation of glycine benzophenone imine reaction

To solve this problem we decided to pursue a substrate for the asymmetric alkylation of benzophenone glycine imine that leads to high ee and is orthogonal to acid-labile protecting groups. We hypothesized that the cumyl ester protected glycine imine would have enough steric hindrance on the C-terminus to maintain high levels of enantioselectivity and be removable under mild conditions by hydrolysis.¹²³

I.3.B. Results and discussion

I.3.B.a. Synthesis of cumyl ester protected benzophenone imine

Our initial retrosynthetic plan for the synthesis of the cumyl ester benzophenone imine started with Fmoc-protected glycine that was esterified with 2-phenyl-2-propanol. The plan then envisioned a transamination with diphenyl ketimine after Fmoc removal. The direct esterification of Fmoc protected glycine with DCC and DMAP proceeded in 38% yield.¹²⁴ Such a low yield in the first step of our synthesis was unacceptable, so a trichloacetimidate intermediate was proposed to access the cumyl ester (Scheme 11).^{125, 126}



Scheme 11: Synthesis of cumyl ester protected benzophenone imine

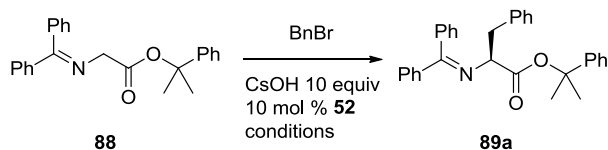
The synthesis started with the NaH catalyzed preparation of the trichloroacetimidate derived from 2-phenyl-2-propanol **86**. The reaction proceeded cleanly and the trichloroacetimidate could be stored on a multigram scale in cyclohexanes for two months.^{125, 126} Upon exposure to bromoacetic acid, ester **87** was obtained with a 90% yield over two steps after chromatography. Alkylation of **87** with diphenyl ketimine¹²⁷ afforded compound **88** in 85% yield after purification on silica gel.¹²⁸

Our proposed substrate for the enantioselective alkylation of benzophenone imine could be accessed in three steps and 77% overall yield from commercially available 2-phenyl-2-propanol. With **88** in hand, the exploration of the alkylation reaction and resulting enantioselectivities obtained with the use of **52** as the catalyst could be started. It was decided to optimize the conditions using benzyl bromide.

I.3.B.b. Enantioselective alkylation conditions optimization

The enantioselective alkylation of **88** was optimized with benzyl bromide. In DCM or mixtures of toluene and DCM, the reaction proceeded cleanly with average yields (48-67 %) and good levels of ee (87-91%) with CsOH as the base at low temperatures ($-50\text{ }^\circ\text{C}$ to $-78\text{ }^\circ\text{C}$). Changing the solvent system to toluene/chloroform (7:3) raised the ee to 94% (all ee were determined by chiral HPLC by comparison with the racemic product). We also observed that benzyl bromide was not completely consumed at the end of the reaction, due probably to a slight

instability of the imine moiety in **88**. Raising the number of equivalents of **88** to 1.4 enabled higher yields (86% based on benzyl bromide) (Scheme 12, Table 6).



Scheme 12: Optimization of the asymmetric alkylation conditions with the cumyl ester **88**

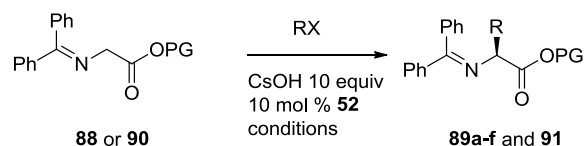
Entry	Equiv of 88	Solvent	Temp (°C)	yield (%)	ee %
1	1.0	CH ₂ Cl ₂	-50	67	87
2	1.0	CH ₂ Cl ₂	-78	52	91
3	1.0	Toluene/CH ₂ Cl ₂ (7:3)	-78	48	90
4	1.0	Toluene/CHCl ₃ (7:3)	-50	62	94
5	1.0	Toluene/CHCl ₃ (7:3)	-78	42	89
6	1.4	Toluene/CHCl ₃ (7:3)	-50	86	94

Table 6: Optimization of the asymmetric alkylation conditions with the cumyl ester **88**

I.3.B.c. Reaction scope

Having found optimized conditions for the enantioselective alkylation of **88**, the reaction scope was investigated. Before screening electrophiles, it was decided to run a control experiment to ensure that high levels of enantioselectivity with the new substrate are not solely due to optimized reaction conditions but rather to the nature of the substrate. To prove our hypothesis, benzyl protected glycine benzophenone imine was used in the alkylation reaction with **58** under the same optimized conditions which provided an ee of only 80%. The analogous reaction between **88** and **58** provided the product with 94% ee. This proved that the new cumyl protected substrate, and not the optimized conditions, are the reason for the high levels of ee. At that point the use of different electrophiles, varying in size and electronic nature (sp^3 , sp^2 and sp hybridized) was investigated. Levels of ee were high in all cases. EtI (Table 7, entry 4, 85% ee),

was the only example showing levels of ee lower than 90%. Good yields and excellent enantioselectivities were obtained with all other electrophiles (Table 7, yields ranging from 56 to 91% and ee from 91 to 94%).



Scheme 13: Scope of the asymmetric alkylation reaction with the cumyl ester **88**

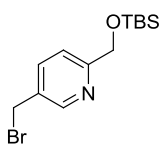
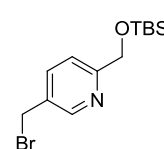
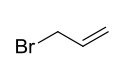
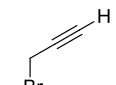
Entry	PG	RX	Product	yield (%)	ee %
1	OBn (90)		91	70	80
2	OCumyl (88)		89b	79	94
3	OCumyl	MeI	89c	56	92
4	OCumyl	EtI	89d	77	85
5	OCumyl		89e	85	91
6	OCumyl		89f	91	92

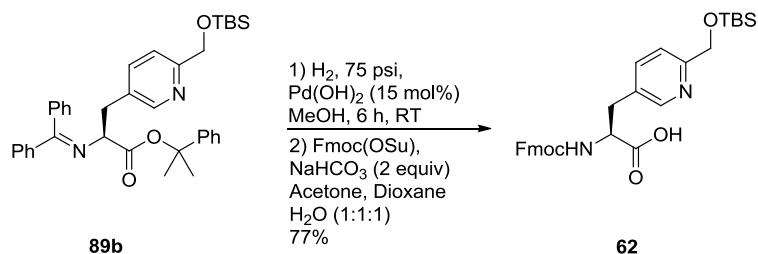
Table 7: Scope of the asymmetric alkylation reaction with the cumyl ester **88**

Finally, during the initial development of the HPA amino acid, N. Jabre showed that the alkylation of the *tert*-butyl ester protected glycine with **58** gives the corresponding product with 80% yield and 93% ee. No loss in yield or enantioselectivity is observed with the new method (Table 7, entry 2).⁶³

The results presented above were very promising, as no loss of ee was observed between the new method and the methods previously developed by Corey, Lygo and others. The potential novelty associated with the use of the cumyl ester protected glycine imine versus the established *tert*-butyl ester consists in the compatibility of the acid-labile side chain protecting groups such as a TBS group with the deprotection reaction conditions. To demonstrate this potential, conditions for a global deprotection of both the C and N-termini that would not cleave the latter protecting groups needed to be found. Compound **89b** was a perfect substrate to investigate those reaction conditions.

I.3.B.d. Hydrogenolysis of **89b** and synthesis of Fmoc-HPA-OH **62**

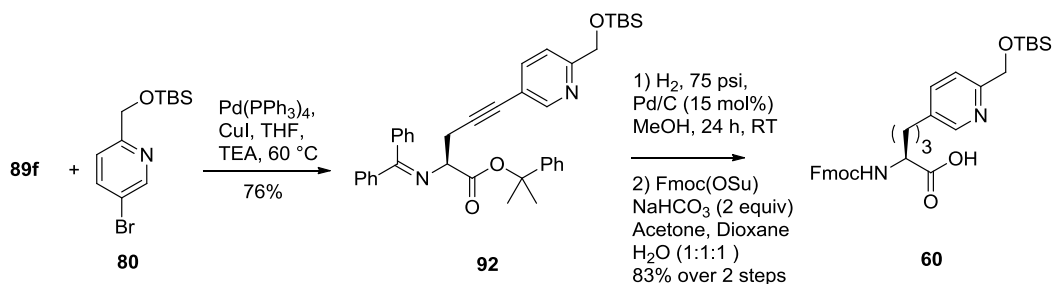
To complete the synthesis of HPA from **89b** a global deprotection of both protecting groups needed to be performed first before the Fmoc protecting group would be installed on the N-terminus. After optimization we found that hydrogenolysis of substrate **89b** using H₂ (75 psi) and Pd(OH)₂/C as the catalyst afforded the C- and N-deprotected unnatural amino acid HPN. The mixture also contained diphenylmethane, a benzophenone imine byproduct, and isopropyl benzene. After filtration of the catalyst and evaporation, the crude mixture was subjected to standard Fmoc protection conditions with Fmoc(OSu) and 5% NaHCO₃ in a dioxane-acetone-water mixture. Fmoc-HPA-OH **62** was obtained in 77% yield after purification by chromatography (Scheme 14). This result presents a great improvement compared to our initial method, which required two additional steps: acidic hydrolysis of the *tert*-butyl ester, and reprotection of the pyridine moiety with the TBS group. Gratified by those findings, the preparation of Fmoc-HPN-OH **60** from **89f** was investigated.



Scheme 14: Synthesis of Fmoc-HPA-OH **62** from product **89b**

I.3.B.e. Synthesis of Fmoc-HPN-OH **60**

To complete the improvements of this new methodology we needed to show that **89f** could be taken forward and coupled with the suitable partner **88** under Sonogashira conditions, and then perform a global hydrogenolysis and reduction of the alkyne functionality. The Sonogashira coupling of **89f** and **88** proceeded cleanly to give **92** in 76% yield. To our delight, **92** could be fully reduced within 24 hours with H₂ (75 psi) and Pd/C to the unprotected unnatural amino acid HPN, diphenylmethane and isopropyl benzene. Under similar conditions as for the synthesis of **62**, Fmoc-HPN-OH (**60**) was obtained in a 83% yield over the 2 steps (Scheme 15). This result is a great improvement compared with the first synthesis of HPN developed in our laboratory. The sequence described in Scheme 15 previously took six steps (Scheme 10), three of which were protecting group manipulations.



Scheme 15: Synthesis of Fmoc-HPN-OH **60** from **89f**

The syntheses of unnatural amino acids **60** and **62** demonstrate the utility of this new methodology. The pyridine moiety in unnatural amino acids HPA and HPN is protected with a TBS group. Previous syntheses were based on the enantioselective alkylation of *tert*-butyl ester-protected glycine imine forcing harsh deprotection conditions and loss of the TBS group that had to be reintroduced in separate steps. The use of the cumyl ester-protected glycine imine enables the use of hydrogenolysis for the deprotection step, leaving the TBS group in place. Acid-labile side chain protecting groups are thus now compatible with the enantioselective alkylation reactions using the *Cinchona* catalysts.

I.3.C. Conclusion

We have developed a novel substrate for a classical reaction that enables quick access to a variety of unnatural amino acids. Our method presents an important advantage: electrophiles bearing acid-labile protecting groups can be now used, which was not the case previously. We expect this method to facilitate the synthesis of Fmoc protected unnatural amino acids in the community.

The results presented in the Chapter were published in *Organic Letters*: Respondek T., Cueny E., Kodanko J. J, "Cumyl Ester as the C-Terminal Protecting Group in the

Enantioselective Alkylation of Glycine Benzophenone Imine" *Org. Lett.*, **2012**, 14 (1), pp 150–153).¹²⁹

From a more general perspective, the results presented in this part of this dissertation describe a novel approach to building peptide-ligand conjugates. The strategy was designed to accelerate the synthesis of full libraries of peptides where the sequence and nature of the ligand can be easily modified. It uses the combinatorial approach to build a plethora of molecules for testing their properties as metal complexes or biologically active molecules through the use of SPPS. The utility of this strategy is based on the use of unnatural amino acids having a TBS protected pyridylmethyl moiety that is used for anchoring a diversity of ligands once the desired peptide has been constructed. The TBS group and the subsequent ligand attachment are chemically compatible with standard Fmoc SPPS synthesis.

Recognizing that our initial syntheses of unnatural amino acids were not compatible with acid-labile protecting groups (the TBS group in this precise example) we have reexamined one of the most used methods in the literature for the synthesis of enantiomerically enriched amino acids and synthesized an “optimal” substrate for the *Cinchona* catalyzed phase transfer alkylation of glycine benzophenone imine. The new cumyl ester-protected benzophenone glycine imine offers the same levels of enantiomeric excess compared to the original studies with very mild deprotection conditions, now compatible with acid-labile protecting groups. The conjoined use of this methodology with the divergent synthesis of peptide-ligand conjugates gives a very straightforward access to a multitude of new molecules in a very efficient manner. We believe that the strategies described above will facilitate the study of metal-peptide conjugates as potential active molecules with new properties inherited from both the metal complexes and peptides.

The Kodanko group is actively interested in studying the use of metal complexes as potential warheads for biological targets. Metal-peptide conjugates offer a new range of opportunities in the areas of directing those metal warheads to site specific areas or through the use of caging strategies. The methodologies described in this part of the dissertation contribute to the synthesis and evaluation of novel, potentially biologically active molecules. Their syntheses and evaluation are underway in our laboratory

I.3.D. Experimental section

I.3.D.a. General considerations

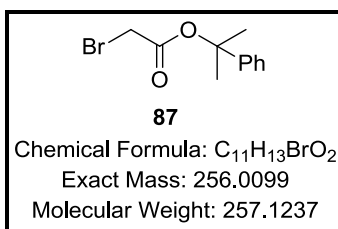
All reagents were purchased from commercial suppliers and used as received. NMR spectra were recorded on a Varian FT-NMR Mercury-300, 400 or 500 MHz Spectrometer. Low-resolution mass spectra were recorded on a Waters ZQ2000 single quadrupole mass spectrometer using an electrospray ionization source, while high-resolution mass spectra were recorded on a Waters-Micromass LCT Premier XE time of flight mass spectrometer. IR spectra were recorded on a Nicolet FT-IR spectrophotometer. Optical rotations were obtained by using a PERKIN-ELMER 241-MC Polarimeter. HPLC was performed on an Agilent 1200 Preparative Purification System equipped with a multi-wavelength detector. Column purifications were performed using silica gel flash chromatography unless mentioned otherwise. All reactions were performed under ambient atmosphere unless otherwise noted. Anaerobic reactions were performed in Schlenk tubes.

Compounds **90**¹³⁰, **52**⁹⁹, **80**¹³¹ and benzophenone imine¹²⁷ used in this report were synthesized according to previously reported literature procedures. All reactions were performed under ambient atmosphere unless otherwise noted. Anaerobic reactions were performed in Schlenk

tubes. These reactions were deoxygenated by performing five vacuum-backfill cycles with Ar and were run under a constant purge of Ar. For anaerobic reactions, Et₃N, Hunig's base and CH₃CN were distilled over CaH₂. All NMR spectra and chromatographs used to determine the ee can be found in the Appendix section.

I.3.D.b. Experimental procedures and tabulated characterization data

2-phenylpropan-2-yl 2-bromoacetate (87).

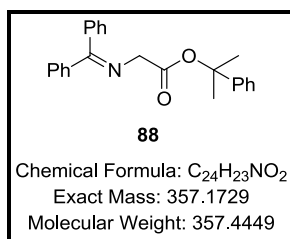


Sodium hydride (60% in oil, 180 mg 4.50 mmol) was suspended in anhydrous ether (4.50 mL) and a solution of 2-phenyl-2-propanol in ether (6.50 mL) was added dropwise with stirring, under an Ar atmosphere. After 20 min the solids have dissolved and the solution was cooled down to 0°C. Trichloroacetonitrile (6.82 g, 47.2 mmol) was then added dropwise over 15 min and the reaction mixture was allowed to warm up to RT over 60 min. The reaction mixture was concentrated to a syrup and pentane (4.50 ml) was added. The resulting solution was filtered on a Buchner filtration set-up and washed with pentane (2×4.50 mL). The filtrate was evaporated to give the crude imidate that was used as is without further purification. The imidate was stored at -20°C as solutions in cyclohexanes (1.00 mmol/1.00 mL) for periods up to 2 months.^{125, 126}

The imidates in cyclohexanes (3.00 mL, 3.00 mmol) were added to bromoacetic acid (417 mg, 3.00 mmol) in dry CH₂Cl₂ under Ar at RT and the resulting solution stirred for 12 h. The trichloroacetamide was filtered off on a Buchner set-up and washed with CH₂Cl₂. The solvent was evaporated to give a solidifying crude mixture that was purified by flash chromatography on

silica (5 to 10% EtOAc in hexanes) to afford the product **87** as an oil (696 mg, 2.71 mmol, 90%): ^1H NMR (400 MHz, CDCl_3) δ 7.44-7.32 (m, 4H), 7.32-7.25 (m, 1H), 3.80 (s, 2H), 1.82 (s, 6H); ^{13}C NMR (100 MHz, CDCl_3) δ 165.8, 145.1, 128.6, 127.6, 124.5, 84.1, 28.6, 27.5; IR (thin film) 3089, 3061, 3028, 2982, 2935, 2875, 1737, 1603, 1584, 1496, 1468, 1449, 1420, 1384, 1367, 1285, 1202, 1178, 1139, 1100, 1077, 1030, 960, 938, 909, 827, 764, 699 cm^{-1} ; HRMS (ESMS) calculated for $\text{C}_{11}\text{H}_{13}\text{BrO}_2\text{Na}$ 278.9997 ($\text{M}+\text{Na}$) $^+$, found : 279.0003.

2-phenylpropan-2-yl 2-((diphenylmethylene)amino)acetate (88).



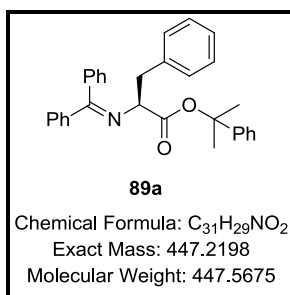
To a solution of 2-phenylpropan-2-yl 2-bromoacetate **87** (5.80 g, 22.6 mmol) in anhydrous CH_3CN (23 mL), DIPEA (3.93 mL, 22.56 mmol) and benzophenone imine¹²⁷ (4.09 g, 22.6 mmol) were added under an Ar atmosphere. The resulting solution was stirred for 24 h at RT. After the reaction completion (followed by TLC) the crude was filtered through a cotton plug, dissolved with 75 mL of CH_2Cl_2 and 50 mL of 5% NaHCO_3 in H_2O . The organic layer was separated and the aqueous layer extracted with 2×50 mL CH_2Cl_2 . The organic layers were combined, dried over Na_2SO_4 , filtered and evaporated. The crude was purified by flash chromatography on silica basified with 1% TEA (1% TEA in 4 to 9% EtOAc/hexanes) to give product **88** as an oil (6.87g, 19.2 mmol, 85%): ^1H NMR (400 MHz, CDCl_3) δ 7.71-7.66 (m, 2H), 7.50-7.45 (m, 3H), 7.43-7.31 (m, 7H), 7.29-7.33 (m, 1H), 7.20-7.15 (m, 2H), 4.26 (s, 2H), 1.82 (s, 6H); ^{13}C NMR (100 MHz, CDCl_3) δ 172.0, 169.3, 145.9, 139.6, 136.3, 130.7, 130.3, 129.1, 129.0, 128.9, 128.5, 128.3, 128.0, 127.3, 124.6, 82.5, 56.6, 28.9; IR (thin film) 3058, 3026, 2980,

2929, 1744, 1659, 1625, 1598, 1577, 1495, 1446, 1383, 1343, 1315, 1274, 1193, 1137, 1102, 1076, 1029, 1000, 940, 907, 838, 764, 696 cm^{-1} ; HRMS (ESMS) calculated for $\text{C}_{24}\text{H}_{24}\text{NO}_2$ 358.1807 ($\text{M}+\text{H}$)⁺, found : 358.1807.

General procedure for the asymmetric alkylation of glycine benzophenone imine **88:**

To a solution of 2-phenylpropan-2-yl 2-((diphenylmethylene)amino)acetate **88** (150 mg, 0.42 mmol) in Toluene/ CHCl_3 (7/3, 1.05 mL) in a Schlenk flask was added the catalyst **52** (18.2 mg, 0.03 mmol) and the resulting solution cooled down to $-55\text{ }^\circ\text{C}$. The electrophile (0.30 mmol) was then added at $-55\text{ }^\circ\text{C}$ and the resulting solution stirred for 3 min. $\text{CsOH}\cdot\text{H}_2\text{O}$ was then added in one portion (504 mg, 3.00 mmol) at $-55\text{ }^\circ\text{C}$ and the resulting solution turned rapidly yellow and was stirred at $-55\text{ }^\circ\text{C}$ for 12-24 h. The completion of the reaction was followed by TLC. The crude was then dissolved in 10 mL of H_2O and 20 mL of anhydrous ether. The organic layer was washed with H_2O ($2\times 10\text{ mL}$). The combined aqueous layers were then extracted with anhydrous ether ($3\times 15\text{ mL}$). All organic layers were combined, dried over Na_2SO_4 and evaporated. The crude was purified by flash chromatography on silica basified with 1% TEA (1% TEA in 4 to 9% EtOAc/hexanes) to give the alkylation product **89a-f** as an oil.

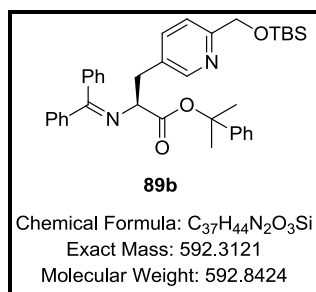
(S)-2-phenylpropan-2-yl 2-((diphenylmethylene)amino)-3-phenylpropanoate (89a**):**



89a was obtained as a yellow oil (115 mg, 0.257 mmol, 86 %): ^1H NMR (400 MHz, CDCl_3) δ 7.70-7.64 (m, 2H), 7.47-7.17 (m, 14H), 7.16-7.09 (m, 2H), 6.71-6.55 (d, $J = 5.7$, Hz,

2H), 4.29-4.22 (dd, $J = 8.9, 4.1$ Hz, 1H), 3.38-3.20 (m, 2H), 1.85 (s, 3H), 1.80 (s, 3H); ^{13}C NMR (100 MHz, CDCl_3) δ 170.5, 170.3, 145.9, 139.7, 138.6, 136.5, 130.5, 130.2, 129.0, 128.5, 128.5, 128.4, 128.4, 128.3, 127.9, 127.3, 126.5, 124.6, 82.7, 68.2, 39.6, 29.2, 28.6; IR (thin film) 3083, 3060, 3027, 2979, 2927, 2853, 1741, 1623, 1597, 1576, 1495, 1446, 1382, 1365, 1315, 1272, 1247, 1200, 1180, 1137, 1101, 1076, 1029, 1000, 975, 909, 841, 779, 762, 696, 637 cm^{-1} ; $[\alpha] = -48.9^\circ$ ($c = 0.922$, CHCl_3); HRMS (ESMS) calculated for $\text{C}_{31}\text{H}_{30}\text{NO}_2$ 448.2277 ($\text{M}+\text{H}$) $^+$, found : 448.2266. The enantiomeric excess was determined using HPLC on a Chiralcel OD-H column (250 \times 4.6 mm ID) for the racemic and enantioenriched substrates under isocratic conditions (100:2 Hexanes-Isopropanol) with a flowrate of 1.0 ml/min. Retention times: 6.98 min and 8.10 min. Enantiomeric excess: 94%.

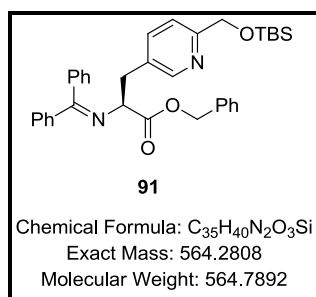
(S)-2-phenylpropan-2-yl 3-(6-(((tert-butyldimethylsilyl)oxy)methyl)pyridin-3-yl)-2-((diphenylmethylene)amino)propanoate (89b):



89b was obtained as a yellow oil (140 mg, 0.237 mmol, 79 %): ^1H NMR (400 MHz, CDCl_3) δ 8.23 (d, $J = 1.6$ Hz, 1H), 7.64-7.58 (m, 2H), 7.44-7.20 (m, 13H), 6.74-6.60 (d, $J = 7.3$ Hz, 2H), 4.21-4.17 (dd, $J = 8.9, 4.1$ Hz, 1H), 3.28-3.12 (m, 2H), 1.79 (s, 3H), 1.75 (s, 3H), 0.94 (s, 9H), 0.10 (s, 6H); ^{13}C NMR (100 MHz, CDCl_3) δ 171.2, 169.9, 159.5, 150.0, 145.7, 139.3, 138.3, 136.3, 132.0, 130.6, 129.0, 128.8, 128.6, 128.5, 128.3, 127.7, 127.3, 124.5, 119.7, 82.9, 67.5, 66.2, 36.4, 29.2, 28.5, 26.2, 18.6, -5.1; IR (thin film) 3445 (broad), 3062, 2954, 2928, 2855,

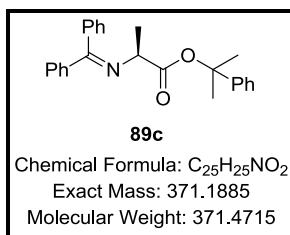
1741, 1622, 1600, 1574, 1488, 1471, 1463, 1447, 1396, 1383, 1366, 1314, 1253, 1199, 1136, 1102, 1077, 1030, 1006, 838, 778, 763, 697, 667 cm^{-1} ; $[\alpha] = -30.0^\circ$ ($c = 0.3$, CHCl_3); HRMS (ESMS) calculated for $\text{C}_{37}\text{H}_{45}\text{N}_2\text{O}_3\text{Si}$ 593.3199 ($\text{M}+\text{H}^+$), found : 593.3201. The enantiomeric excess was determined using HPLC on a Chiralcel OD-H column (250×4.6 mm ID) for the racemic and enantioenriched substrates under isocratic conditions (100:2 Hexanes-Isopropanol) with a flowrate of 1.0 ml/min. Retention times: 7.21 min and 11.21 min. Enantiomeric excess: 94%.

(S)-benzyl 3-(6-(((tert-butyldimethylsilyl)oxy)methyl)pyridin-3-yl)-2-((diphenylmethylene)amino)propanoate (91):



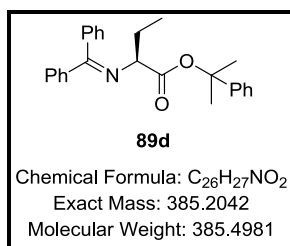
The enantiomeric excess was determined using HPLC on a Chiralcel OD-H column (250×4.6 mm ID) for the racemic and enantioenriched substrates under isocratic conditions (100:1 Hexanes-Isopropanol) with a flowrate of 1.0 ml/min. Retention times: 12.31 min and 16.94 min. Enantiomeric excess: 80%.

(S)-2-phenylpropan-2-yl 2-((diphenylmethylene)amino)propanoate (89c):



89c was obtained as a yellow oil (62 mg, 0.17 mmol, 56 %): ¹H NMR (400 MHz, CDCl₃) δ 7.70-7.64 (m, 2H), 7.49-7.44 (m, 3H), 7.44-7.21 (m, 8H), 7.21-7.15 (m, 2H), 4.14-4.12 (q, *J* = 6.5 Hz, 1H), 1.79 (s, 3H), 1.75 (s, 3H), 1.44 (d, *J* = 6.5 Hz, 3H); ¹³C NMR (100 MHz, CDCl₃) δ 171.4, 169.7, 146.0, 139.8, 136.7, 130.5, 129.0, 128.8, 128.4, 128.3, 128.0, 127.2, 124.5, 82.3, 61.5, 29.1, 28.6; 19.2; IR (thin film) 3059, 3026, 2980, 2932, 2870, 1743, 1661, 1623, 1598, 1577, 1495, 1446, 1382, 1366, 1315, 1273, 1198, 1140, 1121, 1102, 1076, 1030, 1001, 951, 909, 841, 780, 764, 697 cm⁻¹; [α] = -35.8° (c = 1.025, CH₂Cl₂); HRMS (ESMS) calculated for C₂₅H₂₆NO₂ 372.1964 (M+H)⁺, found : 372.1957. The enantiomeric excess was determined using HPLC on a Chiralcel OD-H column (250 × 4.6 mm ID) for the racemic and enantioenriched substrates under isocratic conditions (500:1 Hexanes-Isopropanol) with a flowrate of 1.0 ml/min. Retention times: 11.10 min and 12.02 min. Enantiomeric excess: 92%.

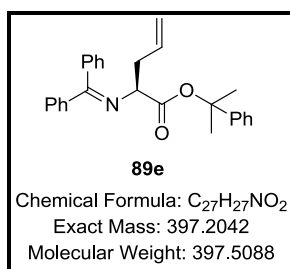
(S)-2-phenylpropan-2-yl 2-((diphenylmethylene)amino)butanoate (89d):



89d was obtained as a yellow oil (89 mg, 0.23 mmol, 77 %): ¹H NMR (400 MHz, CDCl₃) δ 7.72-7.65 (m, 2H), 7.49-7.42 (m, 3H), 7.42-7.20 (m, 8H), 7.20-7.12 (m, 2H), 3.99-3.92 (dd, *J* = 8.1, 4.9 Hz, 1H), 2.06-1.87 (m, 2H), 1.80 (s, 3H), 1.76 (s, 3H), 0.89 (t, *J* = 7.3 Hz, 3H); ¹³C

NMR (100 MHz, CDCl₃) δ 170.9, 170.3, 146.0, 139.9, 136.9, 130.4, 130.3, 129.0, 128.7, 128.6, 128.4, 128.3, 128.1, 127.1, 124.6, 82.3, 67.6, 29.1, 28.6; 26.9; 10.9; IR (thin film) 3060, 3027, 2976, 2932, 2874, 1739, 1660, 1623, 1598, 1577, 1496, 1447, 1383, 1366, 1316, 1276, 1198, 1139, 1102, 1076, 1030, 1000, 941, 919, 838, 780, 763, 698, 638 cm⁻¹; $[\alpha] = -56.2^\circ$ (c = 1.6, CHCl₃); HRMS (ESMS) calculated for C₂₆H₂₈NO₂ 386.2120 (M+H)⁺, found : 386.2121. The enantiomeric excess was determined using HPLC on a Chiralcel OD-H column (250 × 4.6 mm ID) for the racemic and enantioenriched substrates under isocratic conditions (100:1 Hexanes-Isopropanol) with a flowrate of 1.0 ml/min. Retention times: 10.10 min and 11.66 min. Enantiomeric excess: 85%.

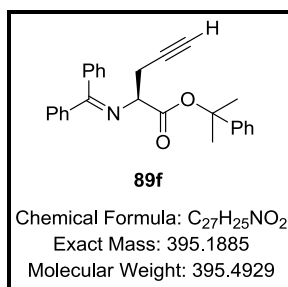
(S)-2-phenylpropan-2-yl 2-((diphenylmethylene)amino)pent-4-enoate (89e) :



89e was obtained as a yellow oil (101 mg, 0.254 mmol, 85 %): ¹H NMR (400 MHz, CDCl₃) δ 7.70-7.64 (m, 2H), 7.47-7.43 (m, 3H), 7.43-7.21 (m, 8H), 7.20-7.13 (m, 2H), 5.80-5.67 (m, 1H), 5.13-5.01 (m, 2H), 4.14-4.09 (dd, *J* = 7.3, 2.4 Hz, 1H), 2.78-2.62 (m, 2H), 1.80 (s, 3H), 1.75 (s, 3H); ¹³C NMR (100 MHz, CDCl₃) δ 170.5, 170.3, 145.9, 139.8, 136.8, 134.9, 130.5, 129.0, 128.8, 128.7, 128.4, 128.3, 128.2, 127.2, 124.6, 117.7, 82.5, 66.1, 38.1, 29.2, 28.5; IR (thin film) 3061, 3025, 2980, 2928, 1741, 1623, 1598, 1576, 1495, 1446, 1414, 1383, 1365, 1314, 1271, 1245, 1194, 1137, 1102, 1076, 1030, 1000, 915, 839, 780, 763, 697, 651 cm⁻¹; $[\alpha] = -7.6^\circ$ (c = 1.84, CHCl₃); HRMS (ESMS) calculated for C₂₇H₂₈NO₂ 398.2120 (M+H)⁺, found : 398.2116. The enantiomeric excess was determined using HPLC on a Chiralcel OD-H column

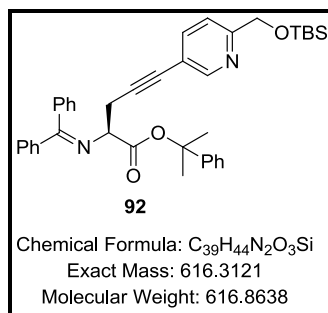
(250 × 4.6 mm ID) for the racemic and enantioenriched substrates under isocratic conditions (500:1.5 Hexanes-Isopropanol) with a flowrate of 1.0 ml/min. Retention times: 10.58 min and 12.06 min. Enantiomeric excess: 91%.

(S)-2-phenylpropan-2-yl 2-((diphenylmethylene)amino)pent-4-ynoate (89f) :



89f was obtained as a yellow oil (108 mg, 0.274 mmol, 91 %): ¹H NMR (400 MHz, CDCl₃) δ 7.73-7.68 (m, 2H), 7.50-7.44 (m, 3H), 7.44-7.21 (m, 10H), 4.31-4.25 (dd, *J* = 8.1, 4.9 Hz, 1H), 2.91-2.75 (m, 2H), 1.98 (t, *J* = 2.4 Hz, 1H), 1.80 (s, 3H), 1.76 (s, 3H); ¹³C NMR (100 MHz, CDCl₃) δ 171.8, 169.0, 145.6, 139.7, 136.4, 130.7, 129.2, 128.9, 128.7, 128.5, 128.3, 127.3, 124.6, 83.1, 81.5, 65.0, 29.1, 28.5; 23.4; IR (thin film) 3293, 3059, 3026, 2980, 2924, 2854, 1740, 1659, 1623, 1598, 1577, 1496, 1447, 1383, 1366, 1316, 1276, 1196, 1138, 1102, 1076, 1030, 1000, 942, 919, 838, 781, 764, 698, 638 cm⁻¹; [α] = -75.4° (c = 1.0, CH₂Cl₂); HRMS (ESMS) calculated for C₂₇H₂₆NO₂ 396.1964 (M+H)⁺, found : 396.1971. The enantiomeric excess was determined using HPLC on a Chiralcel OD-H column (250 × 4.6 mm ID) for the racemic and enantioenriched substrates under isocratic conditions (100:1 Hexanes-Isopropanol) with a flowrate of 0.6 ml/min. Retention times: 13.62 min and 15.25 min. Enantiomeric excess: 92%.

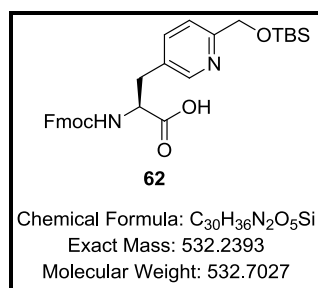
(S)-2-phenylpropan-2-yl 5-(6-(((tert-butyl)dimethylsilyl)oxy)methyl)pyridin-3-yl)-2-((diphenylmethylene)amino)pent-4-ynoate (92) :



To a solution of, (S)-2-phenylpropan-2-yl 2-((diphenylmethylene)amino)pent-4-ynoate (99.0 mg, 0.25 mmol) **89f** in anhydrous THF (3 mL) in a pressure flask under Ar were added 5-bromo-2-((tert-butyldimethylsilyloxy)methyl)pyridine **80** (83.0 mg, 0.28 mmol), Pd(PPh₃)₄ (29.0 mg, 0.03 mmol), CuI (7.00 mg, 0.04 mmol) and Et₃N (350 μL, 2.50 mmol). The solution turned quickly brown-black and was heated to 60 °C for 36 h. The completion of the reaction was monitored by TLC. After completion of the reaction, the crude was extracted with CH₂Cl₂ (3×10 mL, addition of 15 mL of 5% NaHCO₃ in H₂O). The organic layers were collected, dried over Na₂SO₄ and evaporated. The crude was purified by flash chromatography on silica basified with 1% TEA (1% TEA in 4% EtOAc/hexanes) to give the coupling product **92** as a yellow oil (117 mg, 0.19 mmol, 76%): ¹H NMR (400 MHz, CDCl₃) δ 8.47 (d, *J* = 2.4 Hz, 1H), 7.74-7.67 (m, 2H), 7.63 (dd, *J* = 8.1, 2.4 Hz, 1H) 7.47-7.39 (m, 5H), 7.39-7.31 (m, 4H), 7.31-7.20 (m, 5H), 4.81 (s, 2H), 4.39-4.34 (dd, *J* = 8.1, 4.9 Hz, 1H), 3.14-2.98 (m, 2H), 1.82 (s, 3H), 1.78 (s, 3H), 0.96 (s, 9H), 0.12 (s, 6H); ¹³C NMR (100 MHz, CDCl₃) δ 171.9, 169.1, 160.4, 151.4, 145.6, 139.7, 139.4, 136.4, 130.7, 129.2, 129.0, 128.7, 128.5, 128.4, 128.3, 127.3, 124.5, 119.5, 118.9, 90.1, 83.1, 79.4, 66.2, 65.2, 29.1, 28.6, 26.2, 18.6, -5.1; IR (thin film) 3449 (broad), 3060, 3026, 2953, 2929, 2885, 2856, 1742, 1624, 1595, 1576, 1556, 1485, 1471, 1463, 1447, 1418, 1376, 1366, 1314, 1258, 1215, 1188, 1136, 1102, 1077, 1029, 1006, 987, 967, 908, 839, 779, 763, 697,

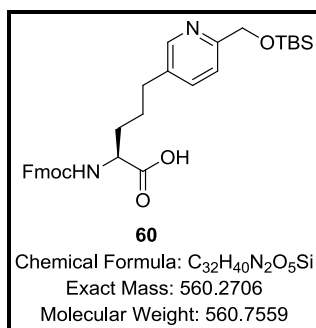
640 cm^{-1} ; $[\alpha] = -23.5^\circ$ ($c = 1.18$, CHCl_3); HRMS (ESMS) calculated for $\text{C}_{39}\text{H}_{45}\text{N}_2\text{O}_3\text{Si}$ 617.3199 ($\text{M}+\text{H}^+$), found : 617.3180.

(S)-2-((((9H-fluoren-9-yl)methoxy)carbonylamino)-3-(6-((tert-butyl)dimethylsilyl)oxy)methyl)pyridin-3-yl)propanoic acid (62).



From compound 89b: A mixture of (S)-2-phenylpropan-2-yl 3-(6-((((tert-butyl)dimethylsilyl)oxy)methyl)pyridin-3-yl)-2-((diphenylmethylene)amino)propanoate (**89b**) (88.0 mg, 0.15 mmol), $\text{Pd}(\text{OH})_2/\text{C}$ (13.0 mg, 15% w/w) and MeOH (2.6 mL) was stirred at RT under H_2 (75 psi) for 12 h. The reaction mixture was filtered through a celite bed or HPLC filter to remove Pd/C and the filtrate was concentrated to give the deprotected amino acid (60 mg) as a colorless to white solid. An NMR was taken to ensure the completion of the hydrogenolysis step. The solid was then dissolved in a 1:1 mixture of H_2O and acetone (2.00 mL), NaHCO_3 (25.0 mg, 0.295 mmol) and Fmoc-OSu (54.8 mg, 0.16 mmol) in dioxane (1.00 mL) were added and the resulting solution was stirred at RT for 16 h. After completion of the reaction (monitored by TLC), the pH of the reaction was brought to pH~4-5 with 10% citric acid in H_2O and extracted with EtOAc (5×10 mL). The organic layers were collected, dried over Na_2SO_4 and evaporated. The crude was purified by flash chromatography on silica (1 to 10% CH_3OH in CH_2Cl_2) to give **62** as an amorphous solid. The NMR and optical rotation were matching with the literature data.¹²⁰

((S)-2-phenylpropan-2-yl 5-(6-(((tert-butyldimethylsilyl)oxy)methyl)pyridin-3-yl)-2-((diphenylmethylene)amino)pentanoate (60).



From compound 92: A mixture of ((S)-2-phenylpropan-2-yl 5-(6-(((tert-butyldimethylsilyl)oxy)methyl)pyridin-3-yl)-2-((diphenylmethylene)amino)pent-4-ynoate (**92**) (100 mg, 0.16 mmol), Pd/C black (15 mg, 15% w/w) and MeOH (2.85 mL) was stirred at RT under H₂ (75 psi) for 36 h. The reaction mixture was filtered through a celite bed or HPLC filter to remove Pd/C and the filtrate was concentrated to give the deprotected amino acid (69 mg) as a colorless to white solid. An NMR was taken to ensure the completion of the hydrogenolysis step. The solid was then dissolved in a 1:1 mixture of H₂O and acetone (2.20 mL), NaHCO₃ (27.0 mg, 0.32 mmol) and Fmoc-OSu (60.3 mg, 0.18 mmol) in dioxane (1.10 mL) were added and the resulting solution was stirred at RT for 16 h. After completion of the reaction (monitored by TLC), the pH of the reaction was brought to pH~4-5 with 10% citric acid in H₂O and extracted with EtOAc (5×10 mL). The organic layers were collected, dried over Na₂SO₄ and evaporated. The crude was purified by flash chromatography on silica (1 to 10% CH₃OH in CH₂CL₂) to give **60** as an amorphous solid. The NMR and optical rotation were matching with the literature data.¹²⁰

Part II : Synthesis and biological evaluation of novel light activated cysteine proteases inhibitors caged by $\text{Ru}^{\text{II}}(\text{bpy})_2$

Chapter 1. Introduction:

II.1.A. Proteases

Proteolytic enzymes or proteases are enzymes that facilitate protein degradation by hydrolysis of the peptide bond. More than 500 different proteases have been identified in the human body to date, and they can be classified between six different categories, namely, serine, threonine, cysteine, aspartic, glutamic and metallo proteases.^{132, 133} They are believed to be the intracellular turnover police¹³⁴ controlling such processes as cell death and proliferation, DNA replication, tissue remodeling etc. Because of the complex role that proteases are involved in, the signaling pathways are extremely complicated and disrupting those cascades can create serious safety issues.¹³⁵

Protease dysregulation leads to serious disease states and has been linked to many conditions. Insufficient proteolysis, due to a lack of activation, is often a result of genetic anomalies or caused by pathogens.^{136, 137} On the other hand, upregulation of proteolytic activity has been closely related to cardiovascular, neurodegenerative, inflammatory and cancer diseases. Inhibition of upregulated proteases involved in such states became a popular therapeutic strategy, making proteases a viable target.¹³⁸ Because of the complexity in the signaling pathways, the

necessity for not disturbing the tightly regulated proteolytic activity in healthy cells, and the resemblance between many proteases, achieving inhibitor selectivity has been one of the main areas of research leading to successful developments of drug molecules¹³⁹ as well as clinical failures.^{140, 141}

Research in the area of proteases and their inactivation has been extremely abundant and nearly 10,000 papers are published every year on the subject.¹⁴² Thus, only a modest introduction, directly related to the projects described in this dissertation will be presented.

II.1.B. Cysteine cathepsins and cancer

Cathepsins are a family of cysteine proteases expressed in humans, animals and plants belonging to the papain subfamily.¹³³ Most of the 11 cathepsins expressed in humans are endopeptidases and found in lysosomes.¹⁴³ For a long time, cathepsins were believed to be only involved in protein turnover, however they have been found to be associated with particular physiological processes such as brain and skin development¹⁴⁴ and bone resorption.¹⁴⁵ Cathepsin activity is highly regulated in healthy cells, and many safety mechanisms to avoid dysregulation exist. More and more data has directly implied the causal role of cathepsin upregulation in cancer where the natural “safety mechanisms” are overridden. Moreover, dyslocalization of cathepsin activity to the extracellular milieu has also been reported in cancer cells.¹⁴⁶ Recent, excellent review articles have summarized the overall role of cathepsin upregulation in cancer in general and tumor growth, invasion, angiogenesis and metastasis in particular, and thus will not be further discussed here.¹⁴⁶⁻¹⁵⁰

Cathepsin K is a lysosomal cysteine protease that is mostly expressed in osteoclasts¹⁵¹ and responsible for collagen I degradation.¹⁵² Recent publications from the Podgorski laboratory link cathepsin K activity to bone marrow metastases from prostate and breast cancers.¹⁵³

Cathepsin K has been shown to process the protein SPARC implicated in bone metastasis and inflammation.^{154, 155}

More recently, cathepsin K levels in bone marrow macrophages (BMM) have been linked to tumor progression in bone.¹⁵⁶ Cathepsin K inhibitors have been known for a few years now to have beneficial effects on patients with breast cancer and bone metastases. The selective cathepsin K inhibitor drug odanacatib has been shown to reduce bone resorption.¹⁵⁷ Taken all together, these data suggest that cathepsin K inhibition is a viable therapeutic target for metastatic bone disease and related conditions.¹⁵⁸

II.1.C. Cysteine cathepsin inhibitors

Three different classes of small molecule cathepsin inhibitors have so far demonstrated efficacy *in vivo*. All react with the enzymes's free thiol in the active site, but epoxysuccinyl-based and vinyl sulfone inhibitors react in an irreversible fashion whereas nitrile-based inhibitors are reversible inhibitors. Epoxysuccinyl-based inhibitor E64 was stopped in phase III clinical trials because of suboptimal results.¹⁵⁹ Vinyl sulfone inhibitor K11777 is being clinically tested for Chagas disease.¹⁶⁰ Finally, multiple nitrile-based inhibitors are in development. Clinical phase III trials of odanacatib were recently closed early with “a favorable benefit-risk profile” and a new study is scheduled for next year.¹⁵⁷ Excellent review papers summarize the efforts by both academia and industry to develop new potent cysteine cathepsin inhibitors.^{134, 159, 161-163}

II.1.D. Metals as therapeutic or biologically relevant agents

Since the discovery of cisplatin by Rosenberg in the 1960's, inorganic complexes have gathered a more important role as therapeutic agents in medicine.¹⁶⁴ As of now, more than 50% of cancer treatments involve some use of cisplatin.¹⁶⁵ Other complexes of platinum, ruthenium

and gold have entered clinical trials.¹⁶⁶ New designs use metals and light to gain spatial and temporal control over the delivery of drugs through the use of photodynamic therapy, CALI (chromophore-assisted laser inactivation) and caging strategies. The next sections will provide some insight into the use of ruthenium complexes in the latter mentioned approaches.

II.1.D.a. Platinum anticancer drugs

Although cisplatin ([cis-diamminedichloro platinum(II)]) **93** was first synthesized and characterized more than 150 years ago¹⁶⁷, its anticancer properties were not discovered until the 1960s by Rosenberg, while using platinum electrodes with ammonium chloride to study *Escherichia coli* growth.¹⁶⁸ Cisplatin was subsequently identified as a platinum complex that inhibits sarcoma 180 and leukemia L1210 cells in mice¹⁶⁹ and approved by the FDA as an anticancer drug in 1978. The full mechanism of action is still not completely understood although it is clear that one main mode of action is caused by binding of cisplatin to DNA, provoking 1,2-intrastrand crosslinks at d(GpG) sites further blocking replication.¹⁷⁰ Because of severe side effects associated with treatments using cisplatin¹⁷¹ and intrinsic/acquired resistance, new platinum, gold and ruthenium anticancer have been synthesized, entered clinical trials or have been approved by the FDA.^{172, 173} (Figure 28 shows FDA approved platinum anticancer agents)

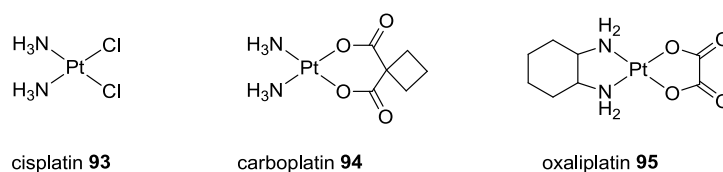


Figure 28: FDA approved platinum complexes for cancer treatment

Drug resistance is cell-line dependent, usually increases with time and is not fully understood. Some of the causes are related to reduced accumulation, increased deactivation by

natural cell detoxification operations mediated by glutathione or repair of platinum DNA adducts. Related ruthenium complexes have been thought to be less toxic and capable of overcoming usual drug resistance pathways.¹⁷⁴

II.1.D.b. Ruthenium anticancer drugs

The research area of ruthenium complexes with potential anticancer activities has been extremely active. Many excellent review articles describe the history of the development of these complexes as well as the analogies and differences compared to related platinum complexes and challenges for finding actual drug molecules.¹⁷³⁻¹⁷⁹ Only a few major examples will be described here.

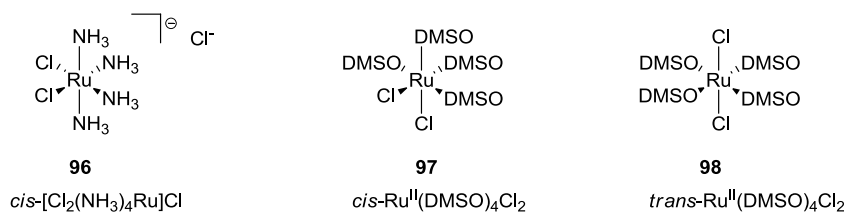


Figure 29: Early Ru based complexes with anticancer activity

Early designs were clearly mimicking known platinum-based drugs as in complex **96**,^{180, 181} but quickly new hypotheses emerged. Scientists believed that ruthenium was a better metal anchor to build potential drugs around because three oxidation states could be easily accessible under physiological conditions (from Ru(II) to Ru(IV)). Moreover, the octahedral geometry is usually preferred for these complexes, offering more geometrical possibilities and opening the door for more SAR type studies. To improve water solubility compared to **96**, *cis*- and *trans*-Ru(DMSO)₄X₄ (with X = Cl or Br) were synthesized,¹⁸² and surprisingly showed that the *trans* isomer was 20 times more cytotoxic than the *cis* isomer, implying that the DNA binding of Ru

complexes was either not following the same mechanism as for Pt complexes or a different mode of action was responsible for the cytotoxicity.¹⁸³

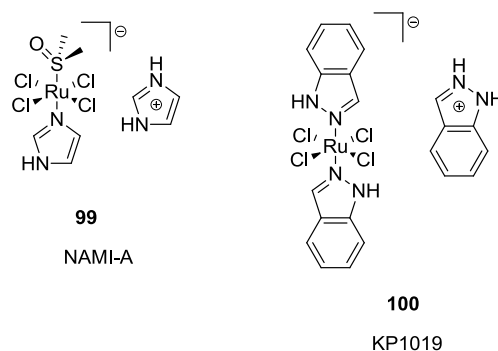


Figure 30: Ru complexes being investigated in clinical trials

One of the early hypotheses, namely the “activation by reduction”^{180, 181} led to the development of the only two ruthenium based anticancer agents that have entered clinical trials, namely NAMI-A by the Sava group and KP1019 by the Keppler group. The theory was based on the fact that the environment of cancer cells is mostly hypoxic and pH levels are lower because cancer cells divide rapidly to form masses with poor blood circulation and thus force glycolysis over the Krebs’ cycle. Taken together, these conditions should be favorable to reduce Ru(III) complexes into Ru(II) complexes, giving the possibility to administer less toxic Ru(III) prodrugs that would predominately become active in the tumor cell environment by reduction. Although the theory could be verified in simplified *in vitro* setups, it has not been validated *in vivo*. Nonetheless, NAMI-A¹⁸⁴ and KP1019¹⁸⁵ have successfully advanced through phase I clinical trials. Interestingly, these two molecules show different types of cytotoxicity even though they are closely related. NAMI-A shows selectivity towards lung metastases,¹⁸⁶ whereas KP1019 shows activity towards cisplatin-resistant human colon carcinoma cell lines¹⁸⁷ which seems to be contradicting the “activation by reduction theory”. A new study aimed at explaining those results has shown the ability of certain Ru complexes to mimic Fe complexes and bind to transferrin,¹⁸⁸

thus facilitating the transport of the molecules into cells.¹⁸⁹⁻¹⁹¹ Interactions with other biologically relevant molecules including proteins could also contribute to the toxicities of these complexes. NAMI-A has, for example, been recently shown to accumulate on RNA *in vitro* and *in cellulo*.¹⁹²

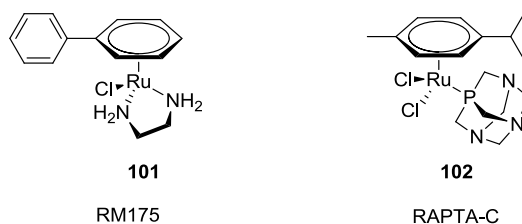


Figure 31: Examples of Ru-arene complexes with anticancer activity

A different family of Ru complexes showing similar selectivity for metastases is the ruthenium-arene family (also called “piano-stool” complexes). Ethylenediamine piano complexes such as RM175 have similar aquation rates and cytotoxicities to Pt(II) complexes.¹⁹³⁻¹⁹⁵ The RAPTA-C complex was the first molecule from this family that has shown interesting cytotoxicity and is still used as a standard for the evaluation of new entities in this family of potential anticancer agents. A number of 1,3,5-triaza-7-phosphaadamantane (PTA) containing RAPTA complexes have been synthesized and tested.^{193, 196} Early studies have shown that the interaction between the aquated ruthenium complex with DNA could be the main mode of action of the drug, but lately new interactions such as inhibition of thioredoxin reductase and cathepsin B¹⁹⁷ (in the lower micromolar range) suggest a DNA independent mode of action.

Polypyridyl ruthenium complexes have been known for a long time to bind to DNA in a site specific fashion depending on the geometry (chirality) of the complex. Barton has shown that Ru(phen)₂Cl₂ binds covalently and selectively to DNA with substantial differences in binding between the Δ and the Λ isomers.^{198, 199} The latter result clearly demonstrated the

possibility of binding to DNA leading to new complexes also having toxic effects. Brabec has shown that *mer*-[Ru(terpy)Cl₃] (terpy = terpyridine) had particularly high cytotoxic effects in murine and human tumor cell lines compared to related [Ru(terpy)(bpy)Cl]Cl and *cis*-[Ru(bpy)₂Cl₂] complexes.²⁰⁰ The study also supported that the mechanism involved DNA interstand cross-linking. Intercalation of metal complexes with DNA has been thoroughly reviewed and will not be discussed further.²⁰¹

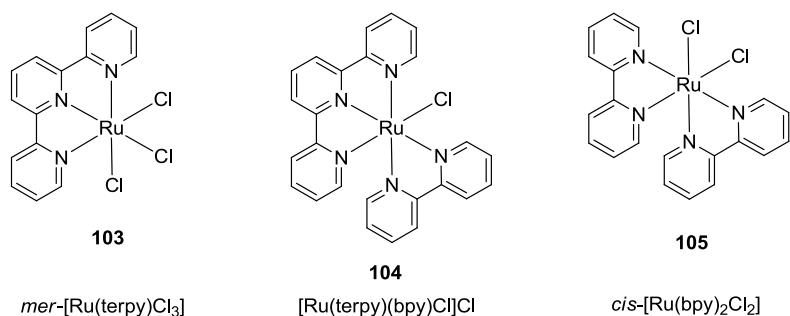


Figure 32: Examples of Ru-polypyridyl complexes mimicking cisplatin

New classes of polypyridyl ruthenium complexes that lack labile groups (such as Cl, H₂O or DMSO) have also been shown to have cytotoxic effects comparable to cisplatin. Although, DNA interactions are still believed to be the principal mode of action of those complexes, intercalation instead of covalent cross linking is postulated as the key type of interaction.²⁰²

The Schatzschneider group showed that *cis*-[Ru(bpy)₂(4,5,9,16-tetraazadibenzoA[a,c]naphthacene)] **106** presents low micromolar IC₅₀ values against HT-29 and MCF-7 cancer cell lines and levels of cellular uptakes suggesting a cell adhesion mediated mode of action.²⁰³ The Liang group has shown various spectrographic data suggesting that the related Ru(II) complex, [Ru(phen)₂PMIP]²⁺ (PMIP=2-(4-methylphenyl)imidazo[4,5-f]1,10-phenanthroline) (**107**) binds to both transfer RNA and calf thymus DNA suggesting intercalation as the mode of action.²⁰⁴ More recently, the Hall group presented the first ever crystal structure

showing a Λ -[Ru(1,4,5,8-tetraazaphenanthrene)₂(dipyridophenazine)]²⁺ complex **108** bound to duplex DNA resulting in kinking of the double helix due to dppz ligand intercalation. Previous studies on the same molecule also suggest a possible semi-intercalation of the TAP ligand, but it is not yet clear if both modes of interaction are happening at the same time.²⁰⁵⁻²⁰⁷

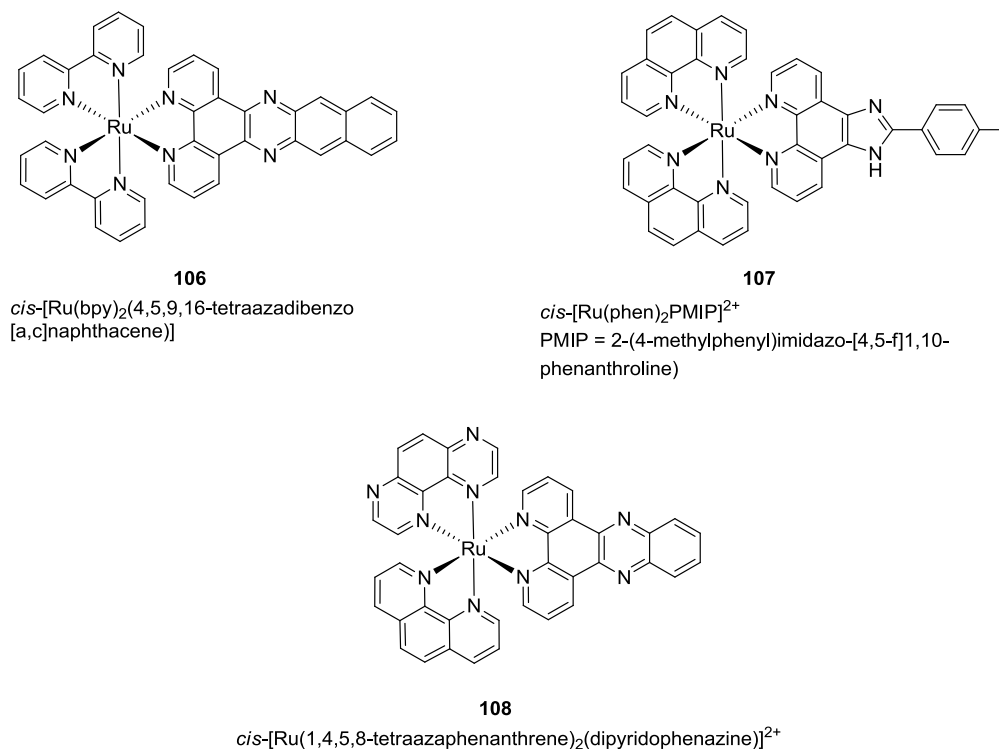


Figure 33: New classes of polypyridyl ruthenium complexes that lack labile ligands

Other classes of Ru complexes such as Ru-polyaminocarboxylate complexes²⁰⁸ or Ru-arylazopyridine complexes²⁰⁹ also show interesting cytotoxic effects in cancer cell lines but will not be discussed here. It should be made very clear that this research area is still very much in progress, mostly because the modes of action of the different classes of complexes are not well understood, thus making rational development of new candidates difficult.

II.1.E. Kinetic and spatial control over drug delivery

An interesting characteristic of certain Ru complexes is their photoreactivity and photodissociation under exposure to light. Ru complexes such as $\text{Ru}(\text{bpy})_3^{2+}$ generate singlet oxygen upon irradiation with visible light²¹⁰⁻²¹⁵ and thus constitute viable candidates as a new class of inorganic photosensitizers for photodynamic therapy (PDT).²¹⁶ Octahedral Ru complexes with distorted geometries decompose upon exposure to light with wavelengths corresponding to their metal to ligand charge transfer energies by ligand dissociation.^{217, 218} These characteristics make Ru complexes interesting scaffolds for either PDT or caging strategies in order to gain spatial control over the delivery of the biologically active agent.

II.1.E.a. Photodynamic therapy (PDT) and chromophore-assisted laser inactivation (CALI) strategies

Classic PDT strategies use organic photosensitizers to generate reactive oxygen species (ROS) to inactivate targets in the vicinity of the sensitizer upon exposition to light (often administered using lasers).²¹⁹ Two major reaction pathways include the direct reaction with the substrate through radical formation, or generation of highly reactive singlet oxygen.²²⁰ PDT is now a clinically tested and approved therapy for various diseases. Classical approaches based on macrocycles such as porphyrins²²¹⁻²²³ will not be discussed here, as they do not relate directly to the work presented in this dissertation, but recent examples where Ru complexes have been used will be described in the following section.

Chromophore-assisted laser inactivation (CALI) of proteins is a direct application of PDT to study biological functions of proteins through their specific inactivation. CALI is based on a target specific antibody labeled with a photosensitizer. After binding to the target and activation

upon exposure to light using a laser, the target protein is inactivated through oxidative processes. Initial CALI strategies used organic sensitizers such as malachite green or fluorescein.²²⁴ Recent developments include more efficient organic photosensitizers such as EGFP or KillerRed.²²⁵⁻²²⁷

The Kodadek group has recently described the use of Ru complexes as photosensitizers for CALI.²²⁸ HaloTag ligands (HT) of the commercially available haloalkane dehalogenase HaloTag protein (HTP) were covalently attached to either $[\text{Ru}(\text{bpy})_3]^{2+}$ or fluorescein (**109** and **110** respectively). The Ru based CALI agent was found to be more than ten times effective at inactivating the target protein compared to fluorescein after a 30 min irradiation. Those results were attributed to the more efficient quantum yield for the generation of triplet oxygen by $[\text{Ru}(\text{bpy})_3]^{2+}$ compared to fluorescein demonstrating the potential for $[\text{Ru}(\text{bpy})_3]^{2+}$ to be used as a CALI photosensitizer.^{214, 229}

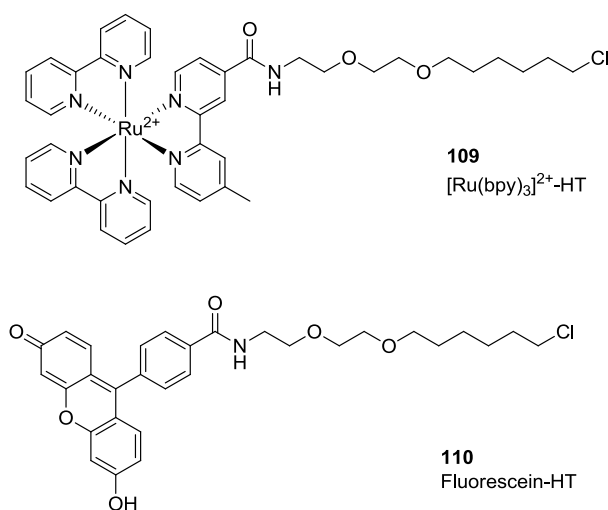


Figure 34: $[\text{Ru}(\text{bpy})_3]^{2+}$ used as a CALI photosensitizer

An impressive application of this strategy was recently disclosed by the Kodadek group. Singlet oxygen generating $[\text{Ru}(\text{bpy})_3]^{2+}$ complex was attached to a highly selective VEGF (vascular endothelial growth factor) peptoid antagonist GU40C of the VEGF receptor 2

(VEGFR2).⁴³ Upon irradiation the CALI reagent was up to 1000 times more active at inhibiting the activity of VEGFR2 compared to the same reagent left in the dark.

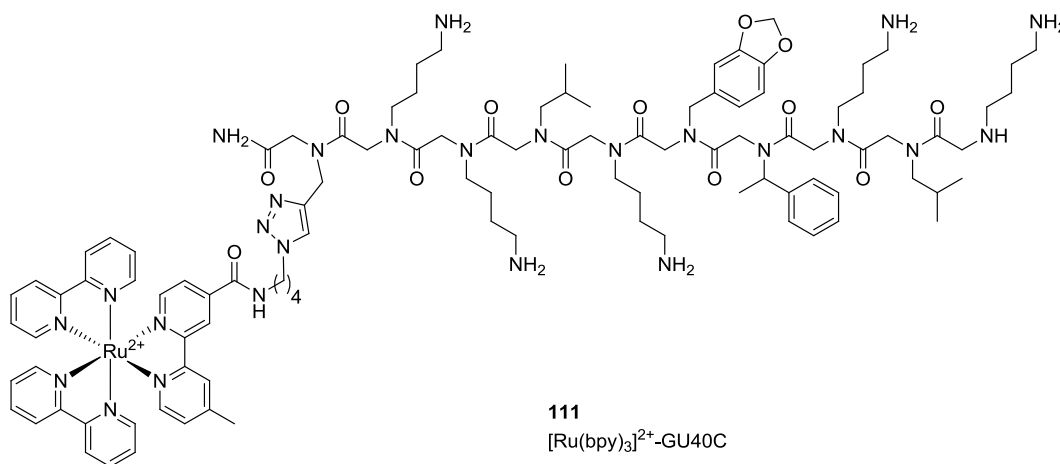


Figure 35: [Ru(bpy)₃]²⁺-GU40C CALI agent

II.1.E.b. Caging strategies using Ru complexes

The photophysical and photochemical properties of Ru and Rh complexes have been known and used as DNA probes for years. One of the most studied examples is [Ru(phen)₂(dppz)]²⁺, a molecule that is naturally luminescent in organic solvents but does not luminesce if its ligands participate in H-bonding, for example in water. Upon intercalation, the molecule's luminescence is restored, as molecules of water are unable to H-bond with the ligand that is "surrounded" by the DNA duplex.^{230, 231} The corresponding Rh complex has also been shown to initiate strand scission upon irradiation through abstraction of a hydrogen atom from the adjacent deoxyribose ring (as in PDT).¹⁶⁶

The possibility of photoactivating covalent binding of Ru complexes with DNA using light was first shown by the Turro group. *cis*-[Ru(bpy)₂(NH₃)₂]²⁺ was effectively photodissociated upon irradiation with light wavelengths between 350 and 400 nm and the resulting aqua complex bound to DNA. Interestingly, the related *cis*-

$[\text{Ru}(\text{bpy})_2(\text{ethylenediamine})]^{2+}$ complex did not undergo photodissociation.²³² Similarly, *cis*- $[\text{Ru}(\text{bpy})_2(5\text{CNU})_2]^{2+}$ (5CNU = 5-cyanouracil) could be photolyzed with even greater efficiencies. The resulting aqua complex was shown to bind to DNA in a fashion similar to cisplatin (Figure 36).²³³

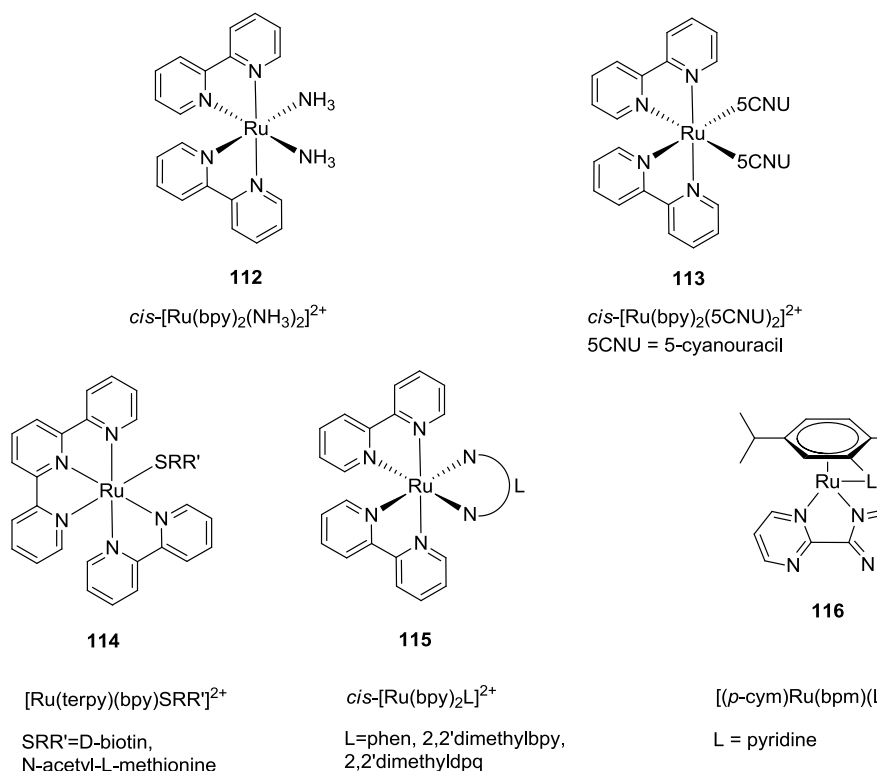


Figure 36: Ru complexes used as cages: prodrugs of Ru based, cisplatin like anticancer agents

The Bonnet group prepared $[\text{Ru}(\text{terpy})(\text{bpy})(\text{SRR}')]^{2+}$ (with SRR' being either N-acetyl-L-methionine or D-biotin), and showed that the thioester could be photoreleased giving the aqua adduct that is known to be biologically active.²³⁴ An impressive result came from the Glazer group, where a series of $[\text{Ru}(\text{bpy})_2\text{L}]^{2+}$ complexes were synthesized (with L being phen, 2,2'-dimethylbpy, 2,2'-dimethyldpq) (Figure 36) and irradiated with visible light, generating molecules that have cytotoxicities comparable to cisplatin after irradiation. The same complexes are 100 times less active in the dark and they do not undergo photodissociation.^{235, 236}

The Sadler group has also recently shown the photoactivation of Ru(II) arene complexes using the same strategy. $[(p\text{-cym})\text{Ru}(\text{bpm})(\text{py})][\text{PF}_6]_2$ was photodissociated to the corresponding aqua complex using white light (400-600 nm), and the latter complex bound 9-ethylguanine (9-EtG) to form $[(p\text{-cym})\text{Ru}(\text{bpm})(\text{py})][9\text{-EtG}]^{2+}$ when photolysis was performed in the presence of one equivalent of 9-EtG, demonstrating potential anticancer activity through DNA binding.²³⁷ In a subsequent publication, the Sadler and Brabec groups have screened multiple piano-stool Ru complexes of the type $[(\eta^6\text{-arene})\text{Ru}(\text{N},\text{N}')(\text{L})]^{2+}$ for their photodissociative abilities and anticancer activities. Low micromolar IC_{50} values against A2780 human ovarian cancer cells were shown upon irradiation with light with several of those complexes.²³⁸

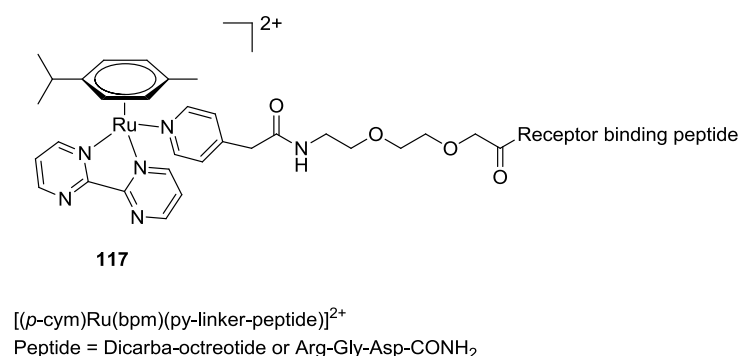


Figure 37: Double directing strategy of a potential anticancer Ru complex $[(p\text{-cym})\text{Ru}(\text{bpm})(\text{py}\text{-linker-peptide})]^{2+}$

A unique approach consisting of a double directing-caging strategy was also recently disclosed by the Sadler group. In addition to the caging strategy described above, the Sadler group attached a receptor binding peptide to the photolabile ligand of $[(p\text{-cym})\text{Ru}(\text{bpm})(\text{py})][\text{PF}_6]_2$ in order to direct the agent towards overexpressed peptide receptors present on tumor cells. This strategy is described in the Chapter I.1.B. of this dissertation. The authors decided to use either the Arg-Gly-Asp (RGD) sequence as a vector of tumor endothelial cells²³⁹ or octreotide, a somatostatin binding peptide.²⁴⁰⁻²⁴² For both complexes,

photodissociation gave the same aqua complex as with complex **116** described above. Complex **117** bound to DNA model substrate 9-EtG as well as two guanidines in DNA sequences $5'$ dCATGGCT and $5'$ dAGCCATG showing potential anticancer activity.²⁴³

The Ru based caging strategy has been effectively used by others over the last 10 years to study neurotransmitters. The Etchenique group has attached diverse amines and neurotransmitters to $[\text{Ru}(\text{bpy})_2\text{L}_2]$ (with L = neurotransmitters) namely tryptamine, tyramine, serotonin, butylamine, 4-aminopyridine and GABA, and shown the ability of the complexes to photodissociate upon irradiation with visible light and stimulate neuron response^{244, 245} The same group has also shown that a two photon uncaging was possible using wavelengths at the limit of the visible-IR range.²⁴⁶ Moreover, the replacement of one of the amine ligands with triphenylphosphine resulted in an increased quantum yield.²⁴⁷

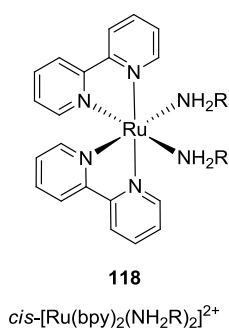


Figure 38: Ru based caging of amine based neurotransmitters

Finally, a completely different approach for spatially controlled delivery of biologically relevant molecules has been demonstrated by the Mascharak group over the last years. Ruthenium-nitrosyl complexes efficiently photorelease NO in the visible range. A recent review by Mascharak describes the development of this class of complexes and further details will not be described here.²⁴⁸

It is clear from the examples described above that Ru is a great anchor for the caging strategy, offering the possibility of spatially and temporarily controlling the delivery of a biologically active agent. The mechanistic details describing the photodissociation of such Ru complexes are described below.

II.1.F. Photodissociation of $[\text{Ru}(\text{bpy})_2(\text{X})_2](\text{Y})_2$ complexes

The photochemical and photophysical properties of $\text{Ru}(\text{bpy})_3^{2+}$ have been recognized for decades, and the complex has been successfully used as a sensitizer for years.²⁴⁹ Studies originating in the 1970s suggested that the original photochemistry and photodissociation of the complex could be mechanistically explained by a thermally accessible ^3MC (metal centered, $^3\text{d-d}^*$ ligand field) state under kinetic equilibrium with a $^3\text{MLCT}$ (metal to ligand charge transfer) state. The $^3\text{MLCT}$ state is accessible from the $^1\text{MLCT}$ state by intersystem crossing.^{217, 250} This mechanistic picture has been extended to $[\text{Ru}(\text{bpy})_2(\text{X})_2]^{2+}$ complexes.²¹⁸ The much higher photostability of $\text{Ru}(\text{bpy})_3^{2+}$ compared to $[\text{Ru}(\text{bpy})_2(\text{X})_2]^{2+}$ complexes has been attributed to efficient ring reclosures.²¹⁷ The general role for metal centered (MC) excited states is now well understood and accepted as one of the key components in the design of complexes with photooptical properties.²⁵¹

The recent interest in $[\text{Ru}(\text{bpy})_2(\text{X})_2]^{2+}$ complexes as possible cages for neurotransmitters, potential anticancer DNA bonding agents or inhibitors and the advances in ultrafast transient absorption spectroscopy²⁵² and time resolved X-ray techniques have enabled a better depiction of the molecular structures characteristic of the different excited states.²⁵³ The Turro group recently disclosed the study of the photodecomposition of $[\text{Ru}(\text{bpy})_2(\text{MeCN})_2]^{2+}$ in H_2O showing that ligand exchange generating $[\text{Ru}(\text{bpy})_2(\text{MeCN})(\text{L})]^{2+}$ proceeds through the formation of $[\text{Ru}(\text{bpy})_2(\text{MeCN})(\text{H}_2\text{O})]^{2+}$ as the pentacoordinate intermediate

$[\text{Ru}(\text{bpy})_2(\text{MeCN})]^{2+}$ is too short-lived to permit bimolecular reactions.²⁵⁴ The recent work from the Lamberti group using OTA (optical transient absorption) and XTA (X-ray transient absorption) spectroscopy techniques gives more insight into the geometries of the different excited states that were postulated earlier by DFT calculations.²⁵⁵ This work shows that the geometry of the $^3\text{MLCT}$ state of $\text{cis}-[\text{Ru}(\text{bpy})_2(\text{py})]^{2+}$ is close to the ground state geometry. Elongation of the dissociating Ru-N(py) bond and simultaneous shortening of the *trans*-Ru-N(bpy) bond characterize the $^3\text{MLCT}$ whereas the ^3MC state shows completely distorted Ru-N(py) bonds.²⁵⁶

II.1.G. Thesis statement (Part II)

Side effects due to drug off-target reactivity are very common and there is a clear need to develop strategies to either direct therapeutic agents towards specific sites or selectively activate them in the desired areas of the body. Recent developments in ruthenium chemistry offer new possibilities for establishing a caging strategy for a controlled delivery of inhibitors. We sought to use the $\text{cis}-[\text{Ru}(\text{bpy})_2(\text{L})_2]^{2+}$ complex as a platform to deliver nitrile-based inhibitors in a spatially controlled fashion. This strategy has been recently demonstrated to cage neurotransmitters and ligands such as MeCN that could be photodissociated upon irradiation with visible light. Inspired by these reports, we hypothesized that nitrile-based small molecule cathepsin inhibitors could be covalently bound to $\text{Ru}(\text{bpy})_2$ and released using light.

The first goal for this second part of the dissertation was to demonstrate the possibility of attaching nitrile-based inhibitors to $\text{Ru}(\text{bpy})_2$ to form $\text{cis}-[\text{Ru}(\text{bpy})_2(\text{L})_2]^{2+}$ complexes, with L being the nitrile-based inhibitors. The metal complexes were fully characterized and the stability in the dark and photorelease of the ligands assessed upon synthetic success. Upon completion of the first goal, the study of inhibitory properties of the caged inhibitors was undertaken. As a

starting point the inhibition of isolated cysteine proteases such as papain and different cathepsins was surveyed. Inhibition experiments under conditions in the dark and after photorelease were performed and “dark/light” ratios determined. To prove the compatibility of *cis*-[Ru(bpy)₂(L)₂]²⁺ complexes to cage and photorelease inhibitors in biological media, studies on living cells were undertaken. Finally, the viability of cells after treatment with ruthenium complexes such as *cis*-[Ru(bpy)₂(L)₂]²⁺ were measured with the hope to demonstrate the lack of toxicity inherent with the metal center adducts. Strategies to complete each of the goals as well as all relevant experimental data are discussed in the next two chapters. Conclusions and future directions are presented at the end of this Part II of this dissertation.

Chapter 2. Synthesis and biological testing of the first nitrile containing cysteine protease inhibitor caged by $\text{Ru}^{\text{II}}(\text{bpy})_2$ and activated by light

II.2.A. Background and project design

The Kodanko group has been interested in developing methodologies for using metal complexes as potential biological "warheads", as explained in the first part of this dissertation. We have disclosed ways of attaching metal ligands to vector peptides with the goal of gaining specificity. Recently, we started investigating a different approach using metal complexes to gain control over the delivery of biologically active molecules. In this new approach we envisioned the use of metal complexes, not as warheads, but rather as a protecting group or cage of the inhibitors, that would be able to release the therapeutics with the use of light. As presented in Part II Chapter 1, similar strategies were employed to either release neurotransmitters or Ru based anticancer agents. We hypothesized that we could use the same *cis*- $[\text{Ru}^{\text{II}}(\text{bpy})_2(\text{L})_2]$ metal complex to cage nitrile-based inhibitors.

One of the main sources of toxicity when delivering a drug is off-target reactivity. To contribute to the discussion addressing spatial and temporal drug delivery that would minimize off-target reactivity, we set out to build a metal-based construct where known inhibitors would be covalently bound to the metal center. The success of this approach would be reached if the metal complex was chemically inert in a biological media in the dark so that it does not decompose and does not react with the targeted enzyme and, at the same time, could photorelease the caged inhibitor upon irradiation with light in a site specific manner. The use of

light to activate compounds was demonstrated with the development of PDT and is a clinically proven methodology.²¹⁶ With the advances made in this area, it is now possible to reach almost any area in the body with light upon the use of lasers and fiber optics.²⁵⁷

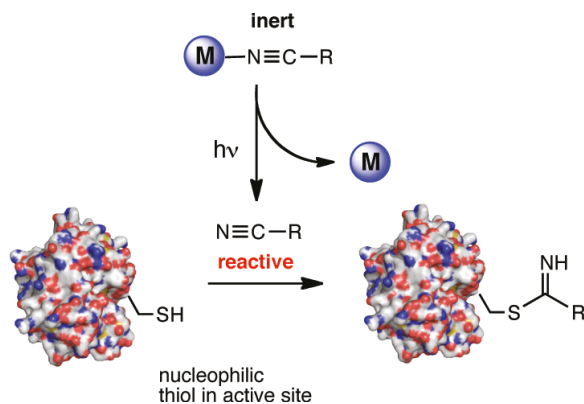


Figure 39: Light activated release of nitrile containing cysteine proteases

We postulated the possibility of caging peptidomimetic nitrile containing cysteine proteases inhibitors with $Ru^{II}(bpy)_2$ complexes. We indeed realized that $[Ru^{II}(bpy)_2(MeCN)_2]^{2+}$ is a stable complex in aqueous solutions in the dark. Upon exposure to light (> 400 nm), the complex will quickly release two molecules of MeCN and $[Ru^{II}(bpy)_2(H_2O)_2]^{2+}$.²⁵⁴ We imagined that upon replacement of the MeCN ligands by peptidomimetic nitrile containing cysteine protease inhibitors (examples are in Phase III clinical studies), we could potentially cage the inhibitors and release them upon irradiation with light. Caging bioactive molecules and being able to release them with light could be a novel way of gaining kinetic and spatial control over their activity that has never been demonstrated. We chose cysteine proteases as they are associated with various medical conditions and cancer in particular. A specific family of cysteine proteases, namely cathepsins B, K and S has been proposed as a promising target for metastatic bone disease (see Part II.1.B. for more details).

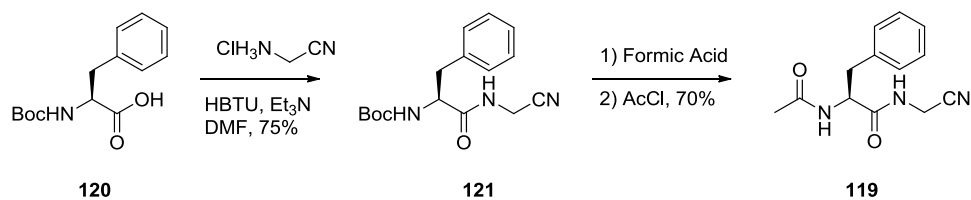
Many medicinal groups, in academia and industry, have isolated numerous potent and specific nitrile-based peptidomimetic cathepsin inhibitors.^{134, 159, 161-163} In our initial studies, we have deliberately chosen simple nitrile-based inhibitors that might not be as potent as more complex, SAR developed molecules, to show a proof of concept. The next sections describe the synthesis of both the organic cathepsin inhibitors and the Ru based cage inhibitors. We disclose the metal complexes characterization as well as their stability in the dark and ability to photorelease the nitrile inhibitors upon irradiation with light. In the following chapters, a series of biological studies on isolated enzymes, *in vitro* and *in cellulo* is also presented.

II.2.B. Results and discussion

II.2.B.a. Synthesis of nitrile cathepsin inhibitor **119**

As explained above, the first generation Ru-nitrile inhibitor cages were designed as a proof of concept with a very simple to synthesize nitrile inhibitor N-acetyl-L-phenylalanyl-glycine-nitrile (Ac-Phe-Gly- ψ [C \equiv N] **119**). We chose **119** because of its chemical simplicity and ease of synthesis, but also its promising inhibitory activity against both the plant enzyme papain and mammalian cathepsins B, K, L and S.^{258, 259}

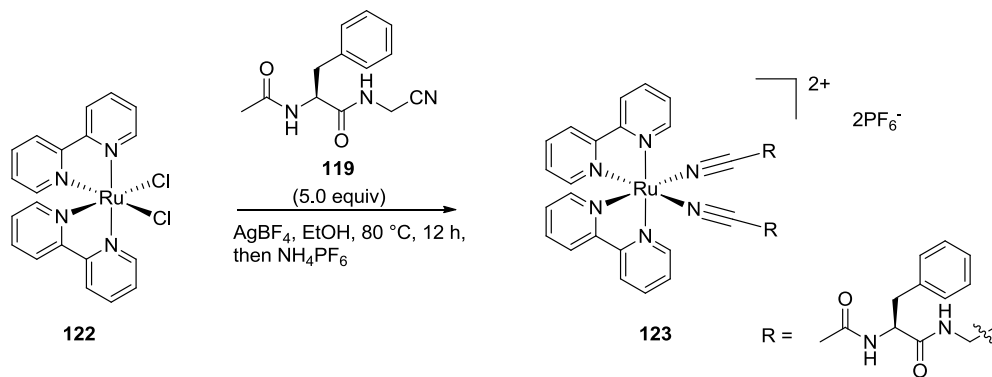
The synthesis was straightforward and began with commercially available Boc-protected L-phenylalanine **120** that was coupled with glycine amino nitrile under HBTU conditions to give the coupled product **121** in a 75% isolated yield. The Boc protecting group could be removed with formic acid and the resulting N-terminus was acetylated with acetyl chloride to give the nitrile inhibitor **119** with a 70% isolated yield over two steps (Scheme 16).



Scheme 16: Synthesis of nitrile inhibitor Ac-Phe-Gly- ψ [C \equiv N] **119**

II.2.B.b. Synthesis of *cis*-[Ru(bpy)₂(**119**)₂](PF₆)₂

With **119** in hand, a method for covalently bonding the latter nitrile to Ru^{II}(bpy)₂ had to be devised. The Turro group from the Department of Chemistry at the Ohio State University has demonstrated the use of Ru^{II}(bpy)₂ as a potential anticancer agent that could be photoreleased from diverse complexes such as [Ru^{II}(bpy)₂(L)₂]²⁺. We decided to use the Turro group's expertise in this domain, and started a collaborative effort to synthesize and study Ru-caged nitrile inhibitors. A successful synthesis was designed after multiple discussions and trials.



Scheme 17: Synthesis of *cis*-[Ru^{II}(bpy)₂(**119**)₂]²⁺

When Ru^{II}(bpy)₂Cl₂ was reacted with five equivalents of **119** along with two equivalents of AgBF₄ in EtOH in the dark, a bright orange solution was observed. After filtration, concentration and precipitation from acetone, the NMR of the crude material was consistent with the formation of the desired complex and excess **119**. The excess of **119** was removed by extraction with EtOAc. The complex was then precipitated with a saturated aqueous solution of

NH_4PF_6 . The analytically pure complex was obtained by slow recrystallization in a cold acetone/DCM mixture.

II.2.B.c. Characterization of *cis*-[Ru(bpy)₂(**119**)₂](PF₆)₂

The complex **123** was obtained as a racemic mixture of both Λ and Δ diastereoisomers. This was expected because the starting material *cis*-Ru^{II}(bpy)₂Cl₂ **122** was a mixture of Λ and Δ stereoisomers, and ligand **119** is chiral and enantioenriched (synthesized from enantioenriched L-phenylalanine with the (S) configuration). The ¹H NMR spectrum confirmed the presence of two diastereoisomers, as two distinct peaks, corresponding to the acetyl groups for each of the diastereoisomers. It is important to note that both **119** ligands on each of the diastereoisomer are equivalent by C₂ symmetry. The methylene hydrogens adjacent to the nitrile functional group were shifted by ~ 0.5 ppm between the free ligand and when bonded to the Ru center.

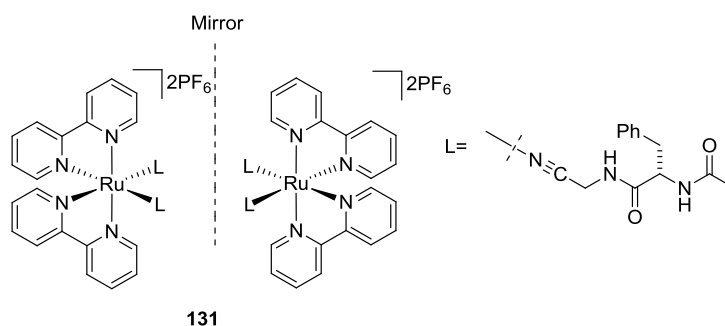


Figure 40: Δ -*cis*-[Ru(bpy)₂(**119**)₂](PF₆)₂ and Λ -*cis*-[Ru(bpy)₂(**119**)₂](PF₆)₂

The IR spectrum for **119** shows the characteristic resonance for CN functional groups at $\nu_{\text{CN}} = 2250 \text{ cm}^{-1}$. The latter resonance is shifted in complex **123** by 30 cm^{-1} to 2280 cm^{-1} consistent with the nitrile binding to the Ru center.²⁶⁰ The UV-Vis spectrum of **123** shows a very similar set of electronic absorptions compared to related complexes with a λ_{max} at 281 nm ($\epsilon = 60,000 \text{ M}^{-1}\text{cm}^{-1}$) and 414 nm ($\epsilon = 10,700 \text{ M}^{-1}\text{cm}^{-1}$).²⁶¹ The identity of the complex was also

confirmed by high resolution mass spectrometry showing a prominent peak at $m/z = 452.1366$ and a Ru isotope pattern consistent with the dication $[\text{Ru}(\text{bpy})_2(\mathbf{119})_2]^{2+}$ was observed. Elemental analysis was consistent with $[\text{Ru}(\text{bpy})_2(\mathbf{119})_2](\text{PF}_6)_2 \cdot 2\text{H}_2\text{O}$. With the identity of the caged Ru-complex confirmed we started investigating the stability of the complex in the dark and the photorelease of the nitrile inhibitors.

II.2.B.d. Stability in the dark and release using light

Solutions of **123** (25 μM) in pure DMSO or 0.1 M phosphate buffer pH 6.5 (0.5% DMSO) were monitored for decomposition by UV-vis spectroscopy at RT by following absorbance at 414 nm. First-order rate constants for decomposition of **123** were calculated using slopes of $\ln A_{414}$ vs time graphs. Rate constants were determined to be $2.3 \times 10^{-7} \text{ s}^{-1}$ (0.1 M phosphate buffer pH 6.5, Figure 41) and $2.8 \times 10^{-7} \text{ s}^{-1}$ (DMSO, Figure 42). These values correspond to half-lives $t_{1/2}$ of 35 and 29 days, respectively.

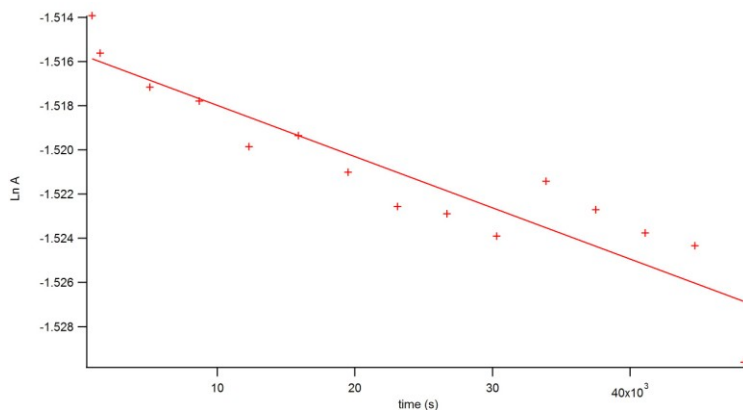


Figure 41: Plot of $\ln A$ vs t for complex **123** in 0.1M phosphate pH 6.5 buffer at RT.

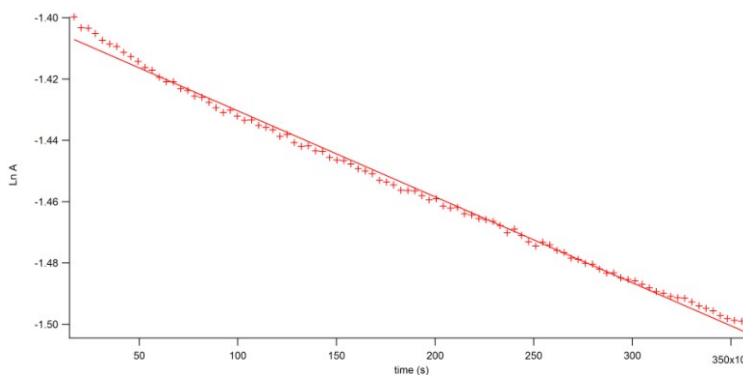


Figure 42: Plot of $\ln A$ vs t for complex **123** in DMSO at RT.

Steady-state photolysis experiments were conducted by the Turro group at the Ohio State University. The electronic absorption at 414 nm corresponding to the metal to ligand charge transfer (MLCT) absorption of the Ru cage **123**, was followed by UV-Vis spectroscopy. Upon irradiation, the decrease of the intensity of the absorption at 414 nm was associated with the advent of absorption at 444 nm within 1 min of irradiation (Figure 43). This new peak is hypothesized to correspond to the Ru→bpy MLCT absorption of the mono-aqua complex, *cis*-[Ru(bpy)₂(**119**)(H₂O)]²⁺. With subsequent irradiation between one and ten minutes, the peak at 444 nm gradually disappears but a new absorption can be spotted at 490 nm with no additional change upon irradiation for more than 10 min. The peak at 490 nm ($\epsilon = 9,300 \text{ M}^{-1}\text{cm}^{-1}$) is

attributed to $cis-[Ru(bpy)_2(H_2O)_2]^{2+}$ according to similar photorelease data from other studies.^{218,}

261

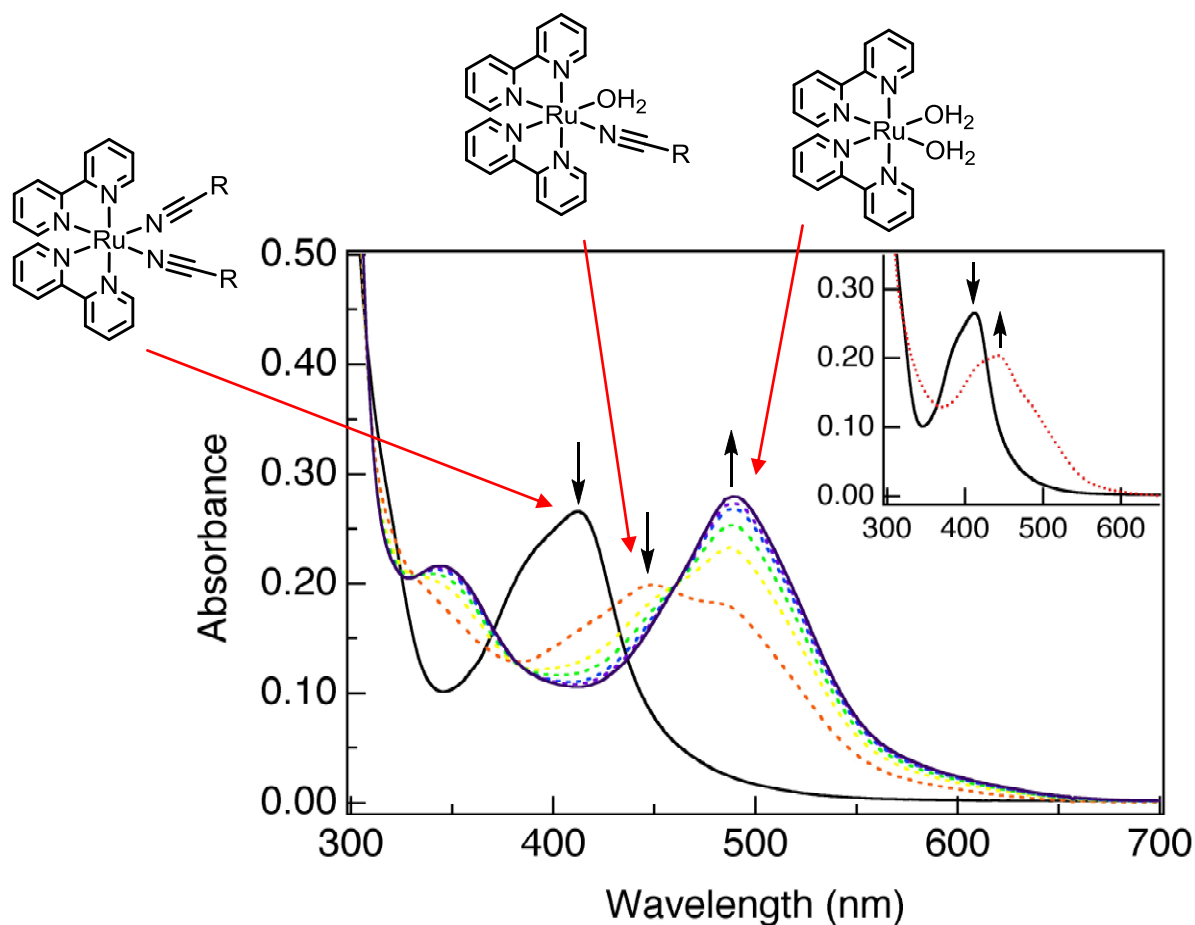


Figure 43: Changes to the electronic absorption spectrum of 30 μ M $cis-[Ru(bpy)_2(\mathbf{119})_2](PF_6)_2$ (**123**) in a 1% DMSO aqueous solution upon irradiation ($\lambda_{irr} > 395$ nm) at $t_{irr} = 0, 2, 3, 4, 5, 6,$ and 7 min; inset: 0, 1 min

The quantum yield for the disappearance of the reactant $cis-[Ru(bpy)_2(\mathbf{119})_2]^{2+}$ (R) to form the mono-aqua intermediate (I), $\Phi_{R \rightarrow I}$, was measured at early reaction times to be 0.080(4), whereas that determined for the formation of the product $cis-[Ru(bpy)_2(H_2O)_2]^{2+}$ (P) from the $cis-[Ru(bpy)_2(\text{peptide})_2]^{2+}$ starting material, $\Phi_{R \rightarrow P}$, was 0.00091(7). From these values, the quantum yield of the second step of the reaction, $\Phi_{I \rightarrow P}$, can be calculated to be 0.011(1). The overall photoaquation quantum yield, $\Phi_{R \rightarrow P}$, is significantly smaller than that reported for $cis-$

$[\text{Ru}(\text{bpy})_2(\text{CH}_3\text{CN})_2]\text{Cl}_2$, 0.21 ($\lambda_{\text{irr}} = 400 \text{ nm}$),²⁵⁴ but similar to that measured for the formation of the mono-aqua species, $\Phi_{\text{R} \rightarrow \text{I}}$, upon irradiation of *cis*- $[\text{Ru}(\text{bpy})_2(5\text{cnu})_2]\text{Cl}_2$, 0.16²³³ (see Part II.2.D.b. for more details).

The results shown above complete the initial requirements for a potential Ru-based cage of nitrile peptidomimetic cysteine protease inhibitors. The complex demonstrates excellent stability in aqueous solutions in the dark, and very fast release of both inhibitors upon irradiation with visible light. The complex **123** was then tested in different biological assays to determine if the caging strategy can be effectively used to inhibit different families of enzymes.

II.2.B.e. Biological evaluation of nitrile containing cysteine protease inhibitor caged by $\text{Ru}^{\text{II}}(\text{bpy})_2$ against papain

The inhibition studies with papain were carried out following a modified procedure by Gütschow.²⁵⁸ Enzyme activity was determined with the chromogenic substrate BAPNA (Z-Phe-Arg-NHNp, $\text{N}\alpha$ -Benzoyl-L-arginine-4-nitroanilide hydrochloride) and is expressed as a percentage, with 100% equal to activity in the absence of inhibitor. Photolysis was conducted for 10 min (with gentle shaking of the plate every 2-3 min) using a 250 W tungsten halogen lamp (Osram Xenophot HLX) powered by a 24 V power supply. The irradiation wavelength was selected by placing a bandpass filter (395 nm cutoff) between the lamp and the sample, along with a 10 cm water cell to absorb infrared light. Different concentrations of the inhibitor **119** alone and Ru inhibitor **123** were plated in wells on a 96 well plate in sextuplets (a series of triplicates on the right and left side of the plate). Half of the plate was covered with aluminum foil to keep one series of triplicates in the dark while the other series was irradiated following the set-up described above.

The IC_{50} for the cysteine protease inhibitor **119** was determined to be 638 nM against 650 nM papain (red trace, Figure 44). In the dark, the complex **123** has an IC_{50} of 9.5 μ M (black trace, Figure 44). A 32 fold enhancement of activity was noticed for the complex **123** after a 10 min exposure to light (>395 nm) to give an IC_{50} of 295 nM (blue trace, Figure 44). It is also important to notice, that those values suggest that two equivalents of **119** have been released upon irradiation (as expected from the photolability studies).

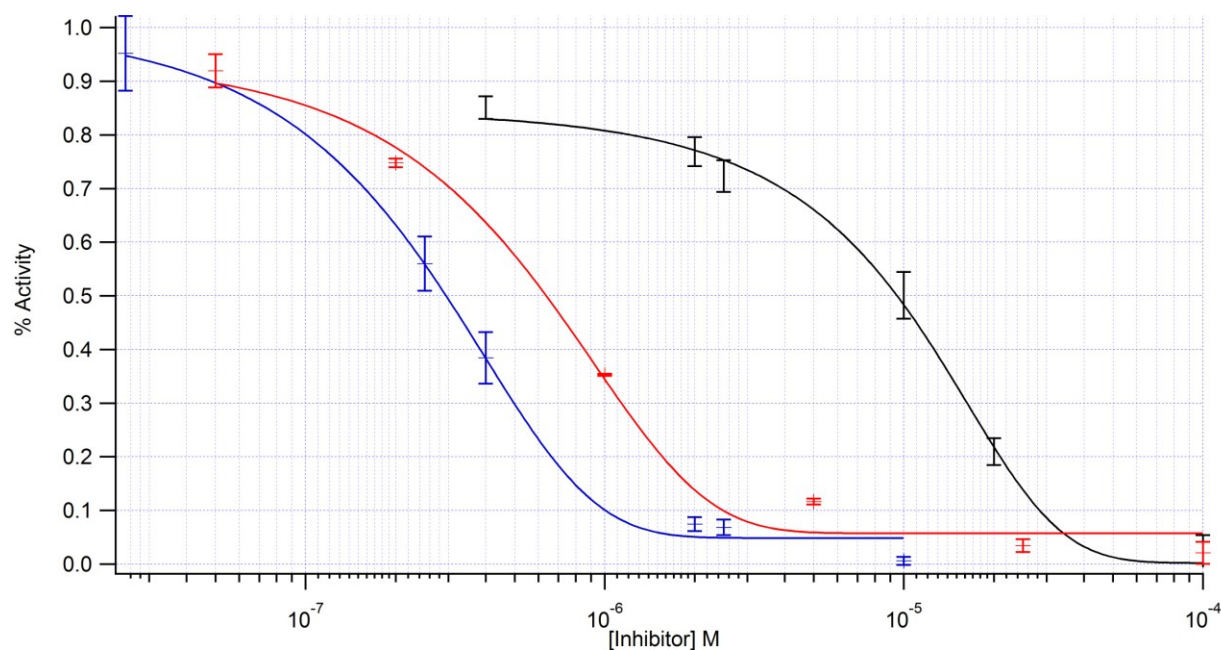


Figure 44: IC_{50} curves for **119** (red) and **123** (with irradiation, blue, and without, black) against the cysteine protease papain.

These results suggest that we have effectively caged the nitrile-based inhibitor **119** with $Ru^{II}(bpy)_2$. To explain the inhibition of papain with **123** in the dark, we postulate that either low amounts of **119** were released during the different manipulations (all studies were conducted in the dark, but some amount of light in the room was obviously necessary for the manipulations to be conducted without error) or **123** acts a weak inhibitor of the enzyme by nonbonding interaction of either the $Ru^{II}(bpy)_2$ moiety or the caged peptide. Control experiments using *cis*-

$[\text{Ru}^{\text{II}}(\text{bpy})_2(\text{MeCN})_2](\text{PF}_6)_2$ with or without light did not show any inhibition below 500 μM suggesting that *cis*- $[\text{Ru}^{\text{II}}(\text{bpy})_2(\text{H}_2\text{O})_2]^{2+}$ or any other byproduct of the photorelease are not responsible for the inhibition. Inhibition by reactive oxygen species such as $^1\text{O}_2$ are also very unlikely because of the very short lifetime of the excited state of the Ru complex²⁵⁴ and same levels of inhibition in the control experiments with $[\text{Ru}^{\text{II}}(\text{bpy})_2(\text{MeCN})_2](\text{PF}_6)_2$ in the dark and upon irradiation.

These exciting results motivated us to conduct more inhibition studies with enzymes expressed in human cells. To help us with the studies we started a collaboration with the Podgorski group from the Pharmacology department at Wayne State University that specializes in the work with different cathepsins and cathepsin K in particular.

II.2.B.f. Biological evaluation of nitrile containing cysteine protease inhibitor caged by $\text{Ru}^{\text{II}}(\text{bpy})_2$ against isolated human cathepsins

Inhibition studies with isolated human enzymes were conducted in a very similar fashion to the papain inhibition studies. Enzyme activity was determined with the fluorogenic substrates Z-Arg-Arg-AMC (cathepsin B), Z-Phe-Arg-AMC (cathepsin K) and Z-Gly-Pro-Arg-AMC (cathepsin L) and is expressed as a percentage, with 100% equal to activity in the absence of inhibitor. Photolysis was conducted for 10 min (with gentle shaking of the plate every 2-3 min) (see Part II.2.D.c. for more details).

Inhibitor **119** was a much weaker inhibitor of human cathepsins B, K and L than papain, but in all cases we noticed significant enhancement of activity upon irradiation of **123** with visible light when compared to **123** left in the dark (Table 8). The data also suggest, once again, that two equivalents of the nitrile inhibitor are released from every Ru complex consistent with

the photolability studies. To further extend our studies we decided to examine the inhibition of cathepsin B expressed in a series of human cell lysates

compound	119	123 (dark)	123 (light)	dark/light ratio
	IC ₅₀			
human cathepsin				
B	133	892	63	14.2
K	12	176	5.4	32.6
L	72	225	40	5.6

Table 8: IC₅₀ values (μM) for **119** and **123** (with and without irradiation) against isolated human cathepsins B, L and K with ratios under light vs. dark conditions

II.2.B.g. Biological evaluation of nitrile containing cysteine protease inhibitor caged by Ru^{II}(bpy)₂ against cathepsins B in cancer cell lysates

Cancer cell lines that are known for overexpressing diverse proteolytic enzymes and cathepsin B in particular were chosen to conduct this study. DU145 prostate carcinoma cells metastatic to the brain²⁶² have been shown to exhibit increased cathepsin B activity,²⁶³ whereas primary human bone marrow stromal cells (hBMSC) have been demonstrated to modulate the progression of cancer in bone through cathepsin activity.¹⁵³ In both cases, the levels of expressed cathepsin B were much higher than that of cathepsin K and L so we have chosen to study the inhibition of cathepsin B with the use of its specific fluorogenic substrate Z-Arg-Arg-AMC. The studies followed the same setup as explained previously, with enzyme activity expressed as a percentage, with 100% equal to activity in the absence of inhibitor. The photolysis was conducted for 10 min (with gentle shaking of the plate every 2-3 min) (see see Part II.2.D.c. for more details).

Similar to the results presented in the previous section, the inhibitor **119** was not a very potent inhibitor of cathepsin B, but **123** showed a significant increase (between 6.6 and 8 times

more potent) in potency after irradiation, and once again suggests that two equivalents of **119** were released from every Ru complex demonstrating the utility of the caging strategy.

compound	119	123 (dark)	123 (light)	dark/light ratio
	IC ₅₀			
lysate				
DU145	182	658	82	8.0
hBMSC	183	580	88	6.6

Table 9: IC₅₀ values (μM) for **119** and **123** (with and without irradiation) against cathepsin B in human cell lysates with ratios under light vs. dark conditions

II.2.C. Conclusions and further directions

The results presented in this chapter describe a very efficient way of caging nitrile based cathepsin inhibitors and activating them within minutes upon exposure to visible light. This is the first example of such a strategy. We believe that this methodology should help us to achieve kinetic and spatial control over protease activity.

The Ru complex *cis*-[Ru^{II}(bpy)₂(**119**)₂]²⁺ shows excellent stability in aqueous solutions in the dark (with half lives in the order of ~ 30 days), and the ability to release two equivalents of **119** upon irradiation with visible light within ten minutes. Inhibition studies with papain and human cathepsins B, K and L have shown significant enhancement of the inhibitory activity associated with the nitrile based inhibitor, ranging from 5.6 to 33 times upon irradiation with visible light. This strategy has also been tested with the inhibition of cathepsin B expressed in lysates of cancer cells. We are planning to synthesize new Ru complexes caging more potent inhibitors and show that the strategy can be applied to control the activity of proteases in live cells.

The results presented in this chapter have been published in the *Journal of the American Chemical Society* with fellow collaborators Robert Garner and Claudia Turro from the Ohio State University and Mackenzie Herroon and Izabela Podgorski from the Pharmacology Department at the Medical School, Wayne State University (Respondek T., Garner R. N., Herroon M. K., Podgorski I., Turro C., Kodanko J. J. "Light Activation of a Cysteine Protease Inhibitor: Caging of a Peptidomimetic Nitrile with Ru^{II}(bpy)₂" *J. Am. Chem. Soc.*, **2011**, 133(43), 17164-17167).²⁶⁴

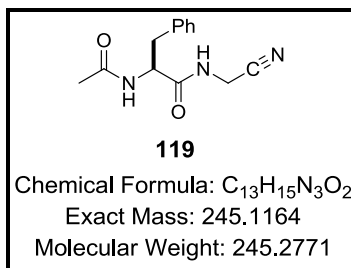
II.2.D. Experimental section

II.2.D.a. General considerations

All reagents were purchased from commercial suppliers and used as received. NMR spectra were recorded on a Varian FT-NMR Mercury-400 Spectrometer. Mass spectra were recorded on a Time-of-Flight Micromass LCT Premier XE Spectrometer. IR spectra were recorded on a Perkin Elmer Spectrum 2000 FT-IR Spectrometer. Enzymatic assays were conducted on a Tecan Infinite M200 or Tecan SPECTRAFluor Plus microplate reader. UV-vis spectra were recorded on a Varian Cary 50 spectrophotometer. Time-dependent UV-Vis spectra were recorded on a Varian Cary 50 spectrophotometer. The photolysis experiments were conducted using a 250 W Tungsten Halogen lamp (Osram Xenophot HLX) powered by a 24 V power source. The irradiation wavelength was selected by placing a bandpass filter (395 nm cutoff) between the lamp and the sample, along with a 10 cm water cell to absorb infrared light. All reactions were performed under ambient atmosphere unless otherwise noted. Anaerobic reactions were performed by purging the reaction solutions with Ar or N₂. All NMR, IR and mass spectra be found in the Appendix section.

II.2.D.b. Experimental procedures and tabulated characterization data

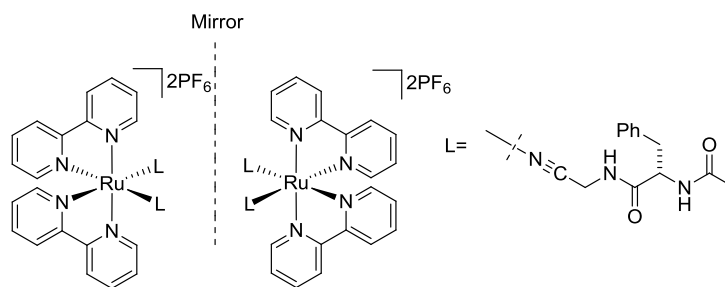
(S)-2-acetamido-N-(cyanomethyl)-3-phenylpropanamide (**119**).



Compound **119** was prepared by modification of published procedures.^{258, 265} Boc-Phe-OH (20.0 mmol, 5.31 g) in dry DMF (110 mL) was treated with HBTU (24.0 mmol, 9.10 g), aminoacetonitrile hydrochloride (24.0 mmol, 2.22 g) and Et₃N (48.0 mmol, 6.76 mL). The solution was stirred for 16 h. The crude reaction solution was combined with CH₂Cl₂ (150 mL) and the organic layer was washed with 0.1 M HCl (2 x 50 mL), sat. aqueous NaHCO₃ (2 x 50 mL) and brine (2 x 50 mL). The organic layer was dried (Na₂SO₄), filtered and concentrated. The crude product was analyzed by ¹H NMR spectroscopy (> 90% purity) and was used without further purification. The crude solid was dissolved in formic acid (100 mL) and maintained for 16 h. Excess formic acid was removed under reduced pressure and the resulting yellowish oil dissolved in H₂O (100 mL), basified with sat. NaHCO₃ and extracted with EtOAc (3 x 100 mL). The organic layer was dried (Na₂SO₄), filtered and concentrated. The resulting solid was treated with CH₂Cl₂ (100 mL), Et₃N (48.0 mmol, 6.75 mL) and acetic anhydride (24.0 mmol, 2.27 mL) and the solution was stirred for 12 h. The resulting slurry was partitioned between EtOAc (100 mL) and 0.1 M HCl (100 mL). The aqueous layer was extracted with EtOAc (3 x 100 mL). The organic layers were combined, dried (Na₂SO₄), filtered and concentrated. The crude product was recrystallized from hot EtOAc to give **119** as a white powder (2.42 g, 9.81 mmol, 49% over the 3 steps): ¹H NMR (400 MHz, DMSO-d₆) δ: 8.71 (t, *J* = 5.7 Hz, NH), 8.22 (d, *J* = 8.1 Hz, NH),

7.21 (m, 5H), 4.44 (dd, $J = 13.0, 4.9$ Hz, 1H), 4.10 (d, $J = 5.7$ Hz 2H), 2.97 (dd, $J = 13.8, 4.9$ Hz, 1H), 2.73 (dd, $J = 13.9, 9.7$ Hz, 1H), 1.75 (s, 3H); $[\alpha]_D^{20} + 6.4$ ($c = 0.5$, MeOH); ^{13}C NMR (100 MHz, DMSO- d_6) δ : 172.75, 169.93, 138.39, 129.74, 128.80, 127.04, 118.14, 54.50, 38.01, 27.74, 23.11; IR ν_{max} (cm^{-1}): 3302, 3066, 3033, 2978, 2937, 2346, 2251, 1956, 1661, 1639, 1606, 1542, 1496, 1455, 1431, 1416, 1372, 1343, 1320, 1298, 1281, 1239, 1193, 1106, 1071, 1037, 966, 914, 893, 791, 747, 731, 702, 618, 600, 565, 519, 472; HRMS (ESMS) calculated for $\text{C}_{13}\text{H}_{15}\text{N}_3\text{O}_2\text{Na}$ $[\text{M}+\text{Na}]^+$: 268.1062, found: 268.1072.

Δ -*cis*-[Ru(bpy) $_2$ (119**) $_2$](PF $_6$) $_2$ ·2H $_2$ O and Λ -*cis*-[Ru(bpy) $_2$ (**119**) $_2$](PF $_6$) $_2$ ·2H $_2$ O (**123**):**



123

Chemical Formula: $\text{C}_{46}\text{H}_{46}\text{F}_{12}\text{N}_{10}\text{O}_4\text{P}_2\text{Ru}$

Exact Mass: 1194.2031

Molecular Weight: 1193.9204

A sealable tube was charged with *cis*-Ru(bpy) $_2$ Cl $_2$ (0.20 mmol 97 mg), AgBF $_4$ (0.80 mmol, 156 mg) and (*S*)-2-acetamido-N-(cyanomethyl)-3-phenylpropanamide (**119**) (1.00 mmol, 245 mg) and freshly distilled EtOH (40 mL). The resulting solution was sealed under inert atmosphere in a glove box, wrapped in aluminum foil and heated to 80°C for 12 h, during which it turned from dark violet to bright orange. After cooling the crude solution to rt, the reaction mixture was placed in the freezer at -20 °C for 16 h. The reaction mixture was filtered through celite to remove precipitated silver salts and the filter cake was washed with cold EtOH. The solvents were removed under reduced pressure, resulting in the formation of a yellow solid. The

resulting yellow solid was dissolved in acetone (3 mL), layered with Et₂O (15 mL) and placed in the freezer at -20 °C for 16 h. The yellow solid was isolated by filtration and washed with cold Et₂O. The resulting solid was dissolved in H₂O (25 mL) and the aqueous layer was extracted with EtOAc (3 x 20 mL) and MTBE (1 x 20 mL). The aqueous layer was treated with a saturated aqueous solution of NH₄PF₆ (5 mL), resulting in the formation of an orange precipitate that was isolated by centrifugation. The precipitate was washed with cold CH₂Cl₂, then dissolved in a mixture of CH₂Cl₂ and acetone (10:1). After storing this solution for 2 days at -20 °C the complex **123** precipitated and was obtained as a microcrystalline bright yellow-orange solid (45 mg, 37 μmol, 19% yield): mp = 110 °C (decomp); ¹H NMR (400 MHz, acetone-d₆) δ: 9.55 (d, *J* = 5.7 Hz, 1H), 9.51 (d, *J* = 4.9 Hz, 1H), 8.81 (d, *J* = 8.1 Hz, 2H), 8.68 (d, *J* = 8.1 Hz, 2H), 8.43 (t, *J* = 8.1 Hz, 2H, NH), 8.20 (t, *J* = 5.7 Hz, NH), 8.11 (dt, *J* = 7.7, 1.6 Hz, 2H), 8.03 (t, *J* = 6.5 Hz, 2H), 7.87 (d, *J* = 5.7 Hz, 2H), 7.80 (d, *J* = 7.3 Hz, NH), 7.60 (d, *J* = 7.3 Hz, NH), 7.45 (d, *J* = 6.1 Hz, 2H), 7.23 (m, 10H), 4.56 (m, 5H), 4.32 (m, 1H), 3.12 (dd, *J* = 9.72, 4.9 Hz, 1H), 3.09 (dd, *J* = 9.3, 5.3 Hz, 1H), 2.93 (dd, *J* = 13.8, 7.3 Hz, 1H), 2.91 (dd, *J* = 13.8, 6.5 Hz, 1H), 1.89 (s, 3H), 1.85 (s, 3H); IR (KBr) ν_{max} (cm⁻¹): 3635, 3415, 3297, 3062, 3031, 2930, 2346, 2289, 1665, 1605, 1524, 1467, 1448, 1427, 1375, 1342, 1314, 1275, 1243, 1193, 1161, 1125, 1071, 1031, 961, 839, 766, 741, 731, 702, 663, 648, 558, 488; HRMS (ESMS) calculated for C₄₆H₄₆N₁₀O₄Ru [M]²⁺: 452.1380, found: 452.1366; Anal. Calcd for C₄₆H₅₀F₁₂N₁₀O₆P₂Ru ([Ru(bpy)₂(**1**)₂](PF₆)₂·2H₂O): C, 44.92; H, 4.10; N, 11.39. Found: C, 44.79; H, 3.91; N, 11.33.

General Considerations for the Time Dependent UV-Vis spectra:

Time dependent UV-Vis spectra were recorded on a Varian Cary 50 spectrophotometer. The photolysis experiments were conducted using a 250 W Tungsten Halogen lamp (Osram Xenophot HLX) powered by a 24 V power source. The irradiation wavelength was selected by

placing a bandpass filter (395 nm cutoff) between the lamp and the sample, along with a 10 cm water cell to absorb infrared light.

Stability of 123 in 0.1M phosphate buffer pH 6.5 (0.5% DMSO)

A 25 μM solution of **123** in 0.1 M phosphate buffer pH 6.5 (0.5% DMSO) was placed in a cell, and UV-Vis spectra recorded for 6 h (the cell was shaken to help diffusion). Ln A was plotted vs. time and fitted to give a first order reaction rate $r = 2.32\text{e-}7\text{s}^{-1}$. The half life corresponding to this rate was approximately 34.5 days ($t_{1/2} = 0.693/r$).

Stability of 123 in DMSO

A 25 μM solution of **123** in DMSO was placed in a cell, and UV-Vis spectra recorded for 100 h (the cell was shaken to help diffusion). Ln A was plotted vs. time and fitted to give a first order reaction rate $r = 2.80\text{e-}7\text{s}^{-1}$. The half life corresponding to this rate was approximately 28.6 days ($t_{1/2} = 0.693/r$).

Quantum yield and time dependent UV-vis spectra upon irradiation of 123:

Steady-state photolysis experiments for quantum yield determination were conducted using a 150 W Xe arc lamp in a PTI housing (Milliarc Compact Lamp Housing) powered by an LPS-220 power supply (PTI) with an LPS-221 igniter (PTI) as a source. The irradiation wavelength was selected by placing long-pass colored glass filters (Melles Griot) or bandpass filters (Newport) between the lamp and the sample, along with a 10 cm water cell to absorb infrared light. Electronic absorption spectra were collected on a diode array spectrometer (HP 8453) with HP 8453 Win System software.

Quantum yields were measured relative to ferrioxalate using a standard procedure²⁶⁶. The quantum yield of reactant (R) to intermediate (I), $\Phi_{R \rightarrow I}$, was determined by monitoring the decrease in the MLCT absorption of the reactant at 414 nm up to 5% of the reaction. The

quantum yield of reactant (R) to product (P), $\Phi_{R \rightarrow P}$, was determined by monitoring the increase in the absorption of the latter with maximum at 490 nm. The quantum yield of intermediate (I) to product (P), $\Phi_{I \rightarrow P}$, was calculated using the equation $\Phi_{R \rightarrow P} = \Phi_{R \rightarrow I} \cdot \Phi_{I \rightarrow P}$.

The electronic absorption spectrum of *cis*-[Ru(bpy)₂(**119**)₂](PF₆)₂ exhibits ligand-centered (LC) bpy $\pi\pi^*$ and Ru→bpy metal-to-ligand charge transfer (MLCT) absorption peaks at 281 nm ($\epsilon = 54\,430\text{ M}^{-1}\text{ cm}^{-1}$) and 414 nm ($8\,760\text{ M}^{-1}\text{ cm}^{-1}$), respectively, in a 1% DMSO aqueous solution. Similar transition energies and intensities have been reported for the related complexes *cis*-[Ru(bpy)₂(CH₃CN)₂](PF₆)₆ and *cis*-[Ru(bpy)₂(5cnu)₂]Cl₂ (5cnu = 5-cyanouracil). The former exhibits absorption maxima at 283 nm ($\epsilon = 52\,500\text{ M}^{-1}\text{ cm}^{-1}$) and 425 nm ($\epsilon = 8\,590\text{ M}^{-1}\text{ cm}^{-1}$) in CH₃CN²⁶⁷ and at 427 nm ($\epsilon = 8\,900\text{ M}^{-1}\text{ cm}^{-1}$) in water,²⁶¹ and for the latter maxima were reported at 284 nm ($\epsilon = 48\,300\text{ M}^{-1}\text{ cm}^{-1}$) and 410 nm ($\epsilon = 7\,800\text{ M}^{-1}\text{ cm}^{-1}$) in H₂O.²³³

The changes in the electronic absorption spectrum of a 1% DMSO aqueous solution of 30 μM *cis*-[Ru(bpy)₂(**119**)₂](PF₆)₂ upon irradiation with visible light ($\lambda_{\text{irr}} > 395\text{ nm}$) were used to monitor the progress of the photochemical reaction, as shown in Figure 43. A decrease in the MLCT absorption of the reactant at 414 is observed with a concomitant appearance of a new peak at 444 nm within 1 min of irradiation (Figure 43). This peak is attributed to the Ru→bpy MLCT absorption of the mono-aqua complex, *cis*-[Ru(bpy)₂(**119**)(H₂O)]²⁺. With continued irradiation the absorption at 444 nm decreases with an increase in the intensity of the peak at 490 nm ($\epsilon = 9\,300\text{ M}^{-1}\text{ cm}^{-1}$) known to correspond to *cis*-[Ru(bpy)₂(H₂O)₂]²⁺.²⁶⁸ The photochemistry discussed here is similar to that of numerous related complexes,²⁶⁹⁻²⁷¹ including *cis*-[Ru(bpy)₂(CH₃CN)₂]²⁺ and *cis*-[Ru(bpy)₂(5cnu)₂]²⁺.^{218, 233, 261} The quantum yield for the disappearance of the reactant *cis*-[Ru(bpy)₂(**119**)₂]²⁺ (R) to form the mono-aqua intermediate (I),

$\Phi_{R \rightarrow I}$, was measured at early reaction times to be 0.080(4), whereas that determined for the formation of the product $cis\text{-}[\text{Ru}(\text{bpy})_2(\text{H}_2\text{O})_2]^{2+}$ (P) from the $cis\text{-}[\text{Ru}(\text{bpy})_2(\text{peptide})_2]^{2+}$ starting material, $\Phi_{R \rightarrow P}$, was 0.00091(7). From these values, the quantum yield of the second step of the reaction, $\Phi_{I \rightarrow P}$, can be calculated to be 0.011(1). The overall photoaquation quantum yield, $\Phi_{R \rightarrow P}$, is significantly smaller than that reported for $cis\text{-}[\text{Ru}(\text{bpy})_2(\text{CH}_3\text{CN})_2]\text{Cl}_2$, 0.21 ($\lambda_{\text{irr}} = 400$ nm),²⁵⁴ but similar to that measured for the formation of the mono-aqua species, $\Phi_{R \rightarrow I}$, upon irradiation of $cis\text{-}[\text{Ru}(\text{bpy})_2(5\text{cnu})_2]\text{Cl}_2$, 0.16(4).²³³

II.2.D.c. Enzyme Inhibition Studies

Papain Inhibition Studies:

The inhibition studies with papain were carried out following a modified procedure by Gütschow.²⁵⁸ Enzyme activity was determined with the chromogenic substrate BAPNA (Z-Phe-Arg-NHNp) and is expressed as a percentage, with 100% equal to activity in the absence of inhibitor. A 0.25 mM papain stock solution was prepared in 0.1 mM HCl and kept frozen. For each experiment, the stock solution was diluted 250 times and activated for 45 min at 25 °C with a 0.1 M phosphate pH 6.5, 15 mM DTT and 2.5 mM EDTA buffer solution. A 10.0 mM solution of BAPNA in DMSO was prepared daily and plated (final concentration 1.0 mM). The inhibitor was plated as a 1% DMSO solution in the assay buffer. All 3 experiments in triplicates (**119**, **123** in the dark, and **123** photolyzed) were plated on the same 96 well plate. The wells containing **119** and **123** “dark” were carefully wrapped in aluminum foil and the plate exposed to visible light. The photolysis was conducted for 10 min (with gentle shaking of the plate every 2-3 min) using a 250 W tungsten halogen lamp (Osram Xenophot HLX) powered by a 24 V power supply. The irradiation wavelength was selected by placing a bandpass filter (395 nm cutoff) between the lamp and the sample, along with a 10 cm water cell to absorb infrared light. After photolysis, the

reaction was initiated by addition of 65 μL of enzyme (final volume 100 μL , final enzyme concentration 0.65 μM). The absorbance changes due to the hydrolysis product p-nitroaniline (pNA) were measured at 405 nm every 2 min for 14 min (8 measures) at 25 $^{\circ}\text{C}$.

Cathepsin Inhibition Studies:

Cathepsin enzyme activity was determined from kinetic measurements performed by fluorometric detection of the hydrolysis product AMC at 37 $^{\circ}\text{C}$ every 2 min for 14 min (8 measures). The excitation and emission wavelengths were 360 and 485 nm respectively. Selective fluorescent substrate Z-Arg-Arg-AMC for cathepsin B, Z-Phe-Arg-AMC for cathepsin L, and Z-Gly-Pro-Arg-AMC for cathepsin K were used at a final concentration of 100 μM (all obtained from Bachem). Enzyme activities are expressed as a percentage, with 100% equal to activity in the absence of inhibitor.

Cathepsin B:

Purified cathepsin B (human liver) was obtained from Enzo Life Sci and a 5 μM stock solution was prepared in 50 mM sodium acetate, pH 5.0, 1 mM EDTA and kept at -80 $^{\circ}\text{C}$. For each experiment the stock solution was diluted 625 times and activated for 15 min at 37 $^{\circ}\text{C}$ with a 400 mM sodium acetate, pH 6.0, 4 mM EDTA, 8 mM DTT assay buffer solution. The inhibitor was prepared as a 1% DMSO solution in the activated enzyme buffer solution and plated (50 μL). All 3 experiments in triplicates (**119**, **123** in the dark, and **123** photolyzed) were plated on the same 96 well plate. The wells containing **119** and **123** “dark” were carefully wrapped in aluminum foil and the plate was exposed to visible light. The photolysis was conducted for 10 min (with gentle shaking of the plate every 2-3 min) using a 250 W tungsten halogen lamp (Osram Xenophot HLX) powered by a 24 V power supply. The irradiation wavelength was selected by placing a bandpass filter (395 nm cutoff) between the lamp and the sample, along

with a 10 cm water cell to absorb infrared light. After photolysis, the reaction was initiated by addition of 50 μL of 200 μM Z-Arg-Arg-AMC solution in the assay buffer (final volume 100 μL , final enzyme concentration 4 nM). Cathepsin enzyme activity was determined from kinetic measurements performed by fluorometric detection of the hydrolysis product AMC at 37 $^{\circ}\text{C}$ every 2 min for 14 min (8 measures) and MAX RFU slope values used for plotting.

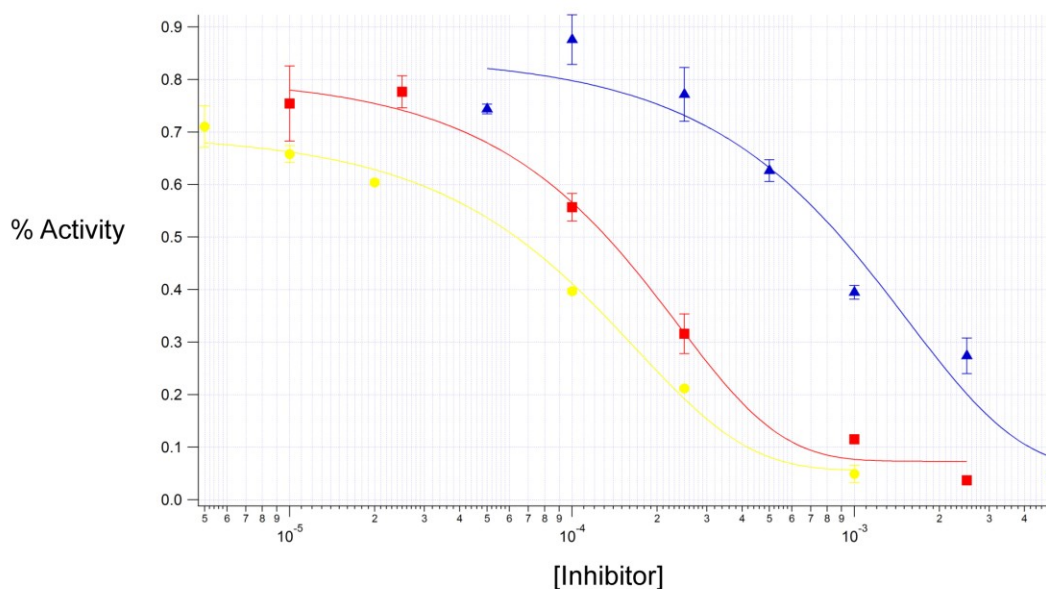


Figure 45: IC₅₀ curve for inhibition of cathepsin B activity with **119** (red), **123** “light” (yellow), and **123** “dark” (blue)

Cathepsin K:

Recombinant cathepsin K (human) was obtained from Enzo Life Sci as a 880 nM stock solution in 50 mM sodium acetate, pH 5.5, 50 mM NaCl, 0.5 mM EDTA and 5 mM DTT and kept at -80 $^{\circ}\text{C}$. For each experiment the stock solution was diluted 44 times and activated for 15 min at 37 $^{\circ}\text{C}$ with a 400 mM sodium acetate, pH 5.5, 4 mM EDTA, 8 mM DTT assay buffer solution. The inhibitor was prepared as a 1% DMSO solution in the activated enzyme buffer solution and plated (50 μL). All 3 experiments in triplicates (**119**, **123** in the dark, and **123**

photolyzed) were plated on the same 96 well plate. The wells containing **119** and **123** “dark” were carefully wrapped in aluminum foil and the plate exposed to visible light. The photolysis was conducted for 10 min (with gentle shaking of the plate every 2-3 min) using a 250 W tungsten halogen lamp (Osram Xenophot HLX) powered by a 24 V power supply. The irradiation wavelength was selected by placing a bandpass filter (395 nm cutoff) between the lamp and the sample, along with a 10 cm water cell to absorb infrared light. After photolysis, the reaction was initiated by addition of 50 μL of 200 μM Z-Gly-Pro-Arg-AMC solution in the assay buffer (final volume 100 μL , final enzyme concentration 10 nM). Cathepsin enzyme activity was determined from kinetic measurements performed by fluorometric detection of the hydrolysis product AMC at 37 °C every 2 min for 14 min (8 measures) and MAX RFU slope values used for plotting.

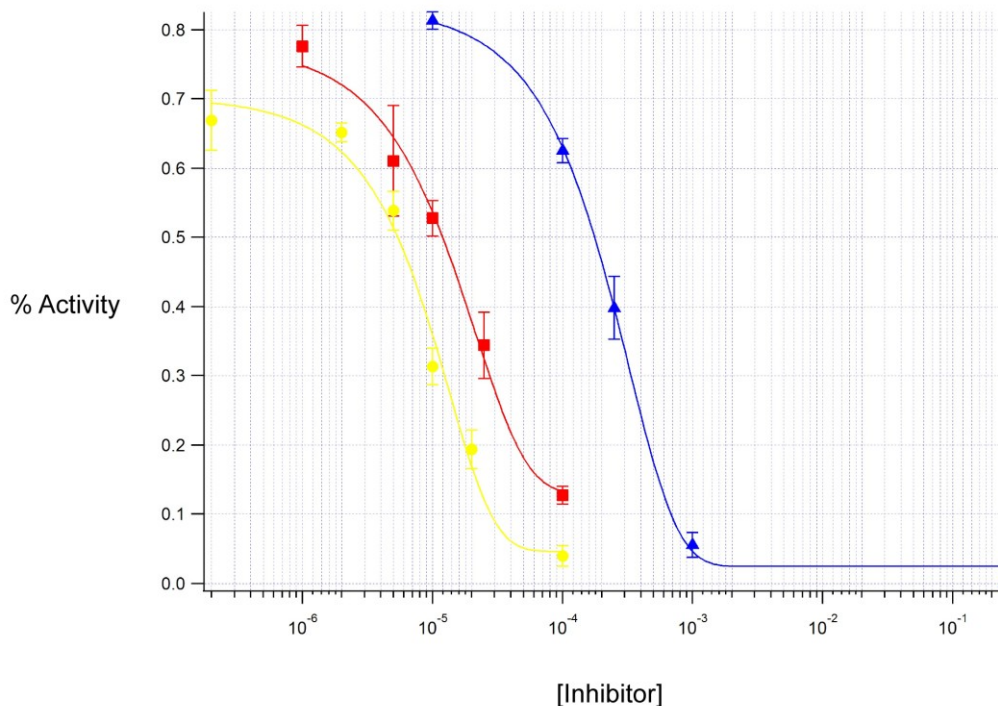


Figure 46: IC₅₀ curve for inhibition of cathepsin K activity with **119** (red), **123** “light” (yellow), and **123** “dark” (blue)

Cathepsin L:

Cathepsin L was obtained from Sigma as a 10 μ M stock solution in 20 mM malonate, pH 5.5, 1 mM EDTA, 400 mM NaCl and kept at -80 $^{\circ}$ C. For each experiment the stock solution was diluted 500 times and activated for 15 min at 25 $^{\circ}$ C with a 400 mM sodium acetate, pH 5.5, 4 mM EDTA, 8 mM DTT assay buffer solution. The inhibitor was prepared as a 1% DMSO solution in the activated enzyme buffer solution and plated (50 μ L). All 3 experiments in triplicates (**119**, **123** in the dark, and **123** photolyzed) were plated on the same 96 well plate. The wells containing **119** and **123** “dark” were carefully wrapped in aluminum foil and the plate exposed to visible light. The photolysis was conducted for 10 min (with gentle shaking of the plate every 2-3 min) using a 250 W tungsten halogen lamp (Osram Xenophot HLX) powered by

a 24 V power supply. The irradiation wavelength was selected by placing a bandpass filter (395 nm cutoff) between the lamp and the sample, along with a 10 cm water cell to absorb infrared light. After photolysis, the reaction was initiated by addition of 50 μL of 200 μM Z-Phe-Arg-AMC solution in the assay buffer (final volume 100 μL , final enzyme concentration 10 nM). Cathepsin enzyme activity was determined from kinetic measurements performed by fluorometric detection of the hydrolysis product AMC at 37 $^{\circ}\text{C}$ every 2 min for 14 min (8 measures) and MAX RFU slope values used for plotting.

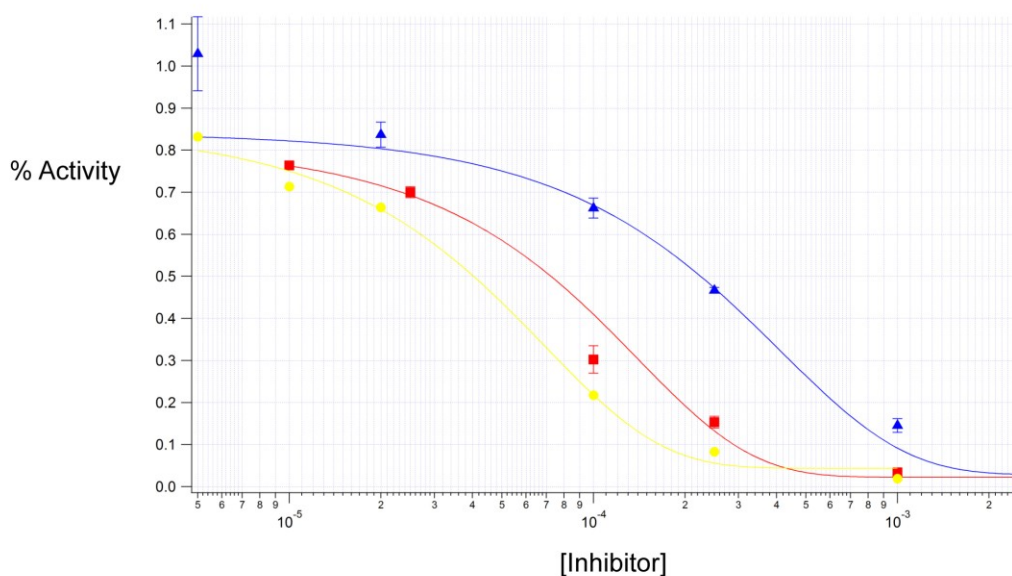


Figure 47: IC_{50} curve for inhibition of cathepsin L activity with **119** (red), **123** “light” (yellow), and **123** “dark” (blue)

Inhibition Studies in Human Cell Lysates

DU145 lysates: DU145 cells were purchased from American Type Culture Collection (ATCC; Manassas, VA) and were cultured in Dulbecco’s modified Eagle’s medium (DMEM) (Sigma; St. Louis, MO) supplemented with 10% fetal bovine serum (FBS) (Invitrogen; Carlsbad, TCA) according to ATCC guidelines. Cells were maintained in a 37 $^{\circ}\text{C}$ humidified incubator ventilated with 5% CO_2 . Lysates were obtained by culturing cells to roughly 80% confluency on

uncoated 100-mm² tissue culture dishes. Cells were then washed with phosphate-buffered saline (PBS), scraped and collected in 250 mM sucrose, 25 mM MES, 1 mM EDTA, pH 6.5, and 0.1% Triton X-100 (SME). Cells were lysed by gentle sonication followed by passing through a 26-gauge needle. For each experiment the lysates in SME were diluted 8 times with assay buffer solution containing 400 mM sodium acetate, pH 5.5, 4 mM EDTA, and 8 mM DTT. The inhibitor was prepared as a 1% DMSO solution in the activated lysates buffer solution and plated (50 μ L). All 3 experiments in triplicates (**119**, **123** in the dark, and **123** photolyzed) were plated on the same 96 well plate. The wells containing **119** and **123** “dark” were carefully wrapped in aluminum foil and the plate exposed to visible light. The photolysis was conducted for 10 min (with gentle shaking of the plate every 2-3 min) using a 250 W tungsten halogen lamp (Osram Xenophot HLX) powered by a 24 V power supply. The irradiation wavelength was selected by placing a bandpass filter (395 nm cutoff) between the lamp and the sample, along with a 10 cm water cell to absorb infrared light. After photolysis, the reaction was initiated by addition of 50 μ L of 200 μ M Z-Arg-Arg-AMC solution in the assay buffer (final volume 100 μ L). Cathepsin enzyme activity was determined from kinetic measurements performed by fluorometric detection of the hydrolysis product AMC at 37 °C every 2 min for 14 min (8 measures) and MAX slope values used for plotting.

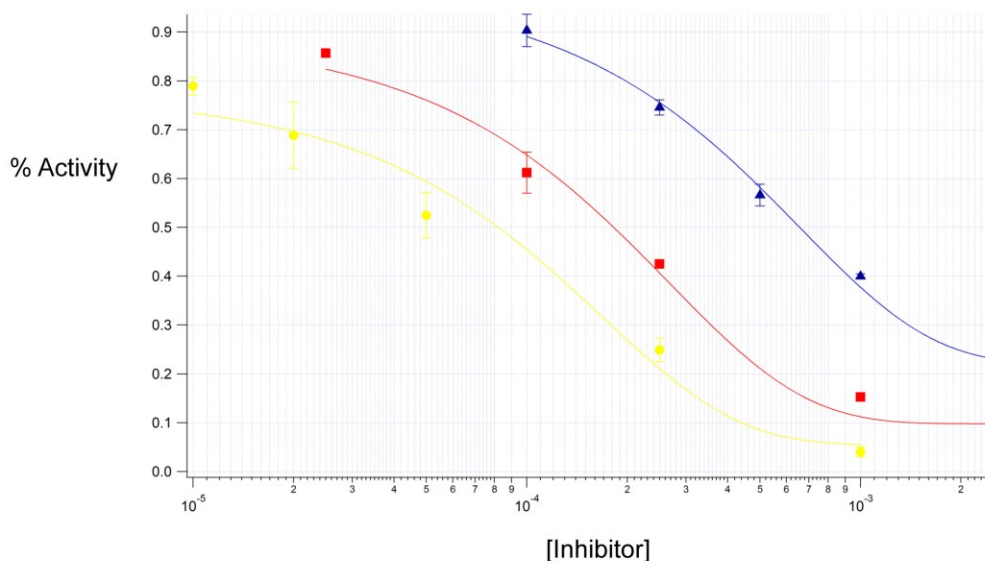


Figure 48: IC₅₀ curve for inhibition of cathepsin B activity from DU145 lysates with **119** (red), **123** “light” (yellow), and **123** “dark” (blue)

Human Bone Marrow Stromal Cell (hBMSC) lysates. Human bone marrow stromal cells (hBMSC) were derived from human male fetal femurs as previously described.¹⁵³ Cells were cultured in DMEM supplemented with 10% FBS, and maintained in a 37°C humidified incubator ventilated with 5% CO₂. Lysates were obtained by culturing cells to roughly 80% confluency on uncoated 100-mm² tissue culture dishes. Cells were then washed with phosphate-buffered saline (PBS), scraped and collected in 250 mM sucrose, 25 mM MES, 1 mM EDTA, pH 6.5, and 0.1% Triton X-100 (SME). Cells were then lysed by sonication and by passing through a 26-gauge needle. For each experiment the lysates in SME were diluted 8 times with assay buffer containing 400 mM sodium acetate, pH 5.5, 4 mM EDTA, and 8 mM DTT. The inhibitor was prepared as a 1% DMSO solution in the activated lysates buffer solution and plated (50 μL). All 3 experiments in triplicates (**119**, **123** in the dark, and **123** photolyzed) were plated on the same 96 well plate. The wells containing **119** and **123** “dark” were carefully wrapped in aluminum foil and the plate exposed to visible light. The photolysis was conducted for 10 min (with gentle

shaking of the plate every 2-3 min) using a 250 W tungsten halogen lamp (Osram Xenophot HLX) powered by a 24 V power supply. The irradiation wavelength was selected by placing a bandpass filter (395 nm cutoff) between the lamp and the sample, along with a 10 cm water cell to absorb infrared light. After photolysis, the reaction was initiated by addition of 50 μL of 200 μM Z-Arg-Arg-AMC solution in the assay buffer (final volume 100 μL). Cathepsin enzyme activity was determined from kinetic measurements performed by fluorometric detection of the hydrolysis product AMC at 37 $^{\circ}\text{C}$ every 2 min for 14 min (8 measures) and MAX slope values used for plotting.

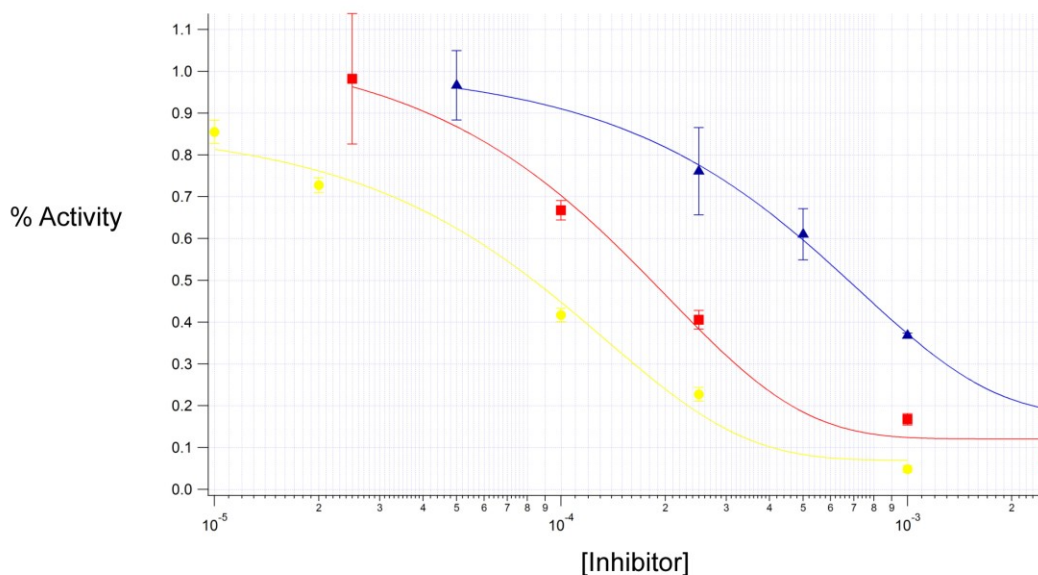


Figure 49: IC_{50} curve for inhibition of cathepsin B activity from hBMSC lysates with **119** (red), **123** “light” (yellow), and **123** “dark” (blue)

Chapter 3. Synthesis and biological testing of a second generation nitrile containing cathepsin K inhibitor caged by $\text{Ru}^{\text{II}}(\text{bpy})_2$ and live cell assays

II.3.A. Background and project design

The collaborative effort between the Kodanko, Podgorski and Turro group leading to the first example of a caged nitrile-based protease inhibitor was disclosed in the previous chapter. In this “proof of concept” approach we have effectively neutralized the reactivity of a small nitrile-based inhibitor towards a free thiol by covalently attaching it to a Ru center. The design of the complex also enabled us to photorelease two equivalents of the inhibitor upon irradiation with visible light for ten minutes.²⁶⁴ To extend the study of this new class of Ru cages we sought to build a new complex caging a more potent inhibitor for cathepsin K.

We chose to target cathepsin K as more and more evidence suggests that cathepsin K activity in bone marrow macrophages is associated with aberrant proteolysis in prostate cancer metastases.¹⁵³ The choice for the new inhibitor was motivated by several factors. The inhibitor used in our initial study²⁶⁴ (Chapter II.2.B.) was only a modest inhibitor of cathepsin K with literature data suggesting a $K_i = 7.5 \mu\text{M}$ ²⁵⁸ and our own studies showing an $\text{IC}_{50} = 12 \mu\text{M}$; the use of a more potent inhibitor in this second generation Ru cage was the natural step forward. One of the goals of this new series of studies was to demonstrate that our strategy could be used to survey protease activity in living cells. The desired inhibitor would preferentially have structural similarities to avoid changing too many parameters compared to the initial work. Our choice was directed towards inhibitor Cbz-Leu-Gly- $\psi[\text{C}\equiv\text{N}]$ **124** that could be easily synthesized from Cbz protected L-leucine and shows two hundred times more inhibitory activity compared to **119**.²⁷²

Moreover, **124** has been previously used to inhibit cathepsin K in live cell assays.²⁷³ The synthesis, characterization, stability in the dark and upon exposure to light, enzymatic assays on isolated cathepsin K and *in cellulo* assays as well as cytotoxicity studies of this new Ru-caged nitrile-based cathepsin K inhibitor will be presented in the next sections.

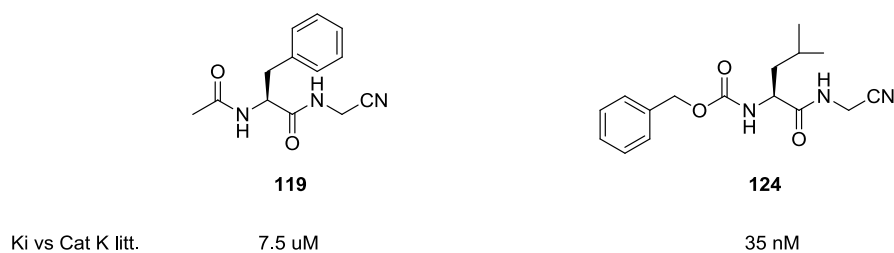
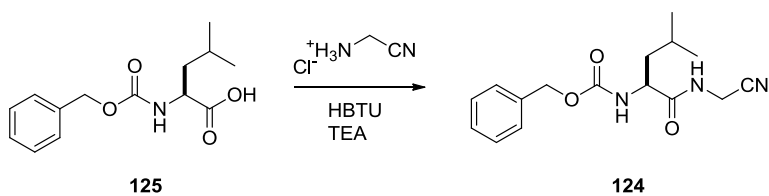


Figure 50: Cathepsin K inhibitor chosen for the second generation Ru-caged complex with literature reported IC_{50} and K_i values

II.3.B. Results and discussion

II.3.B.a. Synthesis of nitrile cathepsin K inhibitor **124**

The synthesis of **124** is even more straightforward than that of **119**. Commercially available (or accessible in one step from L-leucine) Cbz-protected L-leucine **125** was coupled with glycine amino nitrile under HBTU conditions to give the coupled product **124** in a 45 % isolated yield over two steps from free L-leucine.

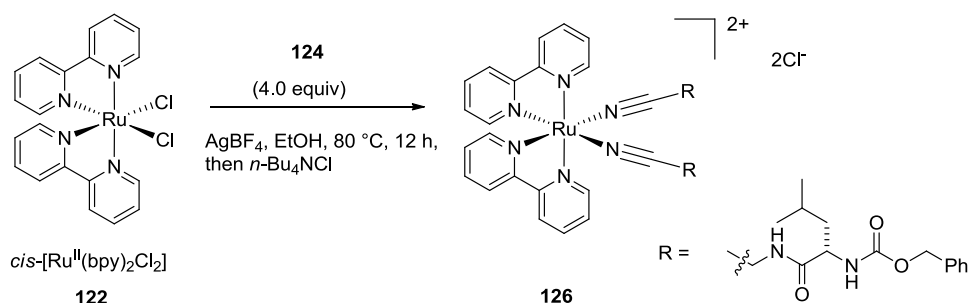


Scheme 18: Synthesis of cathepsin K nitrile inhibitor Cbz-Leu-Gly- ψ [C \equiv N] **124**

II.3.B.b. Synthesis of *cis*-[Ru(bpy)₂(**124**)₂]Cl₂

With the nitrile inhibitor in hand, the method developed in the initial work (presented in the previous chapter) was applied to the synthesis of this new Ru complex. When *cis*-Ru^{II}(bpy)₂Cl₂ was reacted with four equivalents of **124** along with three equivalents of AgBF₄ in EtOH in the dark (prepared under N₂ atmosphere in a glove box), a quick formation of a dark purple-black solution was observed that turned bright orange upon heating to reflux for six hours (kept rigorously in the dark). After filtration and concentration, the ¹H NMR spectrum of the crude product indicated clean formation of the final complex and no other Ru-based side products. The crude complex was dissolved in EtOAc saturated with *n*-Bu₄NCl and upon cooling to -20 °C an oily orange residue was obtained. Several washings with cold Et₂O and toluene were effective to remove excess *n*-Bu₄NCl and the final complex was precipitated in analytically pure form with cold acetone/Et₂O.^a

^a The same complex was resynthesized and isolated in a different manner by Raj Sharma, a colleague from the Kodanko group, since this work had been completed. A better purity of the complex was obtained leading to better “dark/light” ratios. Investigations to explain the differences in the results are in progress.



Scheme 19: Synthesis of cis -[Ru^{II}(bpy)₂(**124**)₂]Cl₂

II.3.B.c. Characterization of cis -[Ru^{II}(bpy)₂(**124**)₂]Cl₂

Similarly to the previously described complex **123**, cis -[Ru^{II}(bpy)₂(**124**)₂]Cl₂ (**126**) was obtained as a racemic mixture of both Λ and Δ diastereoisomers. The ¹H NMR confirmed this observation, and two distinct peaks corresponding to amide protons for each of the diastereoisomers were split (see tabulation in experimental section and appendix).

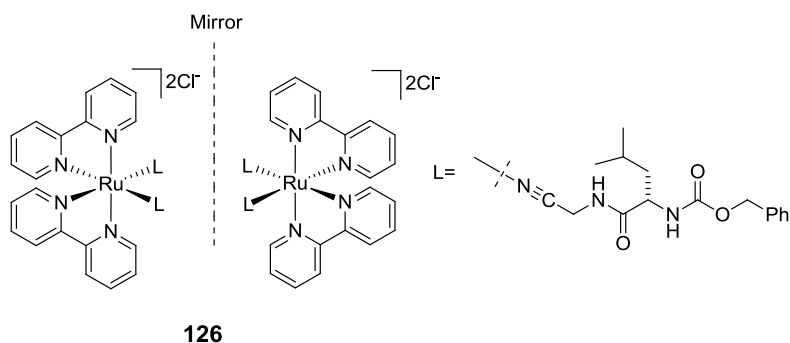


Figure 51: Δ - cis -[Ru(bpy)₂(**124**)₂]Cl₂ and Λ - cis -[Ru(bpy)₂(**124**)₂]Cl₂

The IR spectrum for **126** shows the characteristic resonance for the CN functional group at $\nu_{CN} = 2258 \text{ cm}^{-1}$. This resonance is shifted in the complex **126** by 16 cm^{-1} to 2274 cm^{-1} consistent with the nitrile binding to the Ru center.²⁶⁰ The UV-Vis spectrum of **126** shows a very similar set of electronic absorptions compared to related complexes such as cis -[Ru^{II}(bpy)₂(MeCN)₂]²⁺ and cis -[Ru^{II}(bpy)₂(**119**)₂]²⁺ with a λ_{max} at 281 nm ($\epsilon = 55,600 \text{ M}^{-1}\text{cm}^{-1}$) and 412 nm ($\epsilon = 9,600 \text{ M}^{-1}\text{cm}^{-1}$). Elemental analysis was also consistent with

[Ru(bpy)₂(**124**)₂]Cl₂·3.5H₂O. With the identity of the caged Ru-complex confirmed we started investigating the stability of the complex in the dark and the photorelease of the nitrile inhibitors.

II.3.B.d. Stability in the dark and release using light

Solutions of **126** (50 μM) in 0.1 M phosphate buffer pH 6.5 (0.5% DMSO) or 400 mM sodium acetate, pH 5.5, 4 mM EDTA, 8 mM DTT buffer solution (cathepsin K activity assay) (0.5% DMSO) were monitored for decomposition by UV-Vis spectroscopy at RT by following the absorbance at 412 nm. First-order rate constants for the decomposition of **126** were calculated using slopes of ln A₄₁₂ vs time graphs. Rate constants were determined to be 1.0x10⁻⁶ s⁻¹ (0.1 M phosphate buffer pH 6.5) and 2.1x10⁻⁶ s⁻¹ (cathepsin K activity assay buffer). These values correspond to half-lives t_{1/2} of ~ 8 and 3.8 days, respectively.

Steady-state photolysis experiments were conducted by the Turro group at the Ohio State University. The electronic absorption at 412 nm corresponding to the metal to ligand charge transfer (MLCT) absorption of the Ru complex **126** at 412 nm was followed by UV-Vis spectroscopy. Upon irradiation, the decrease of the intensity of the absorption at 414 nm was associated with the advent of an absorption ~ 450 nm within 2-3 minutes of irradiation. This new peak is hypothesized to correspond to the Ru→bpy MLCT absorption of the mono-aqua complex, *cis*-[Ru(bpy)₂(**124**)(H₂O)]²⁺. With subsequent irradiation up to 15 minutes, the peak ~ 450 nm gradually disappears but a new absorption can be spotted at 486 nm with no additional change upon irradiation for more than 15 minutes. The peak at 486 nm (ε = 9,600 M⁻¹cm⁻¹) is attributed to *cis*-[Ru(bpy)₂(H₂O)₂]²⁺ according to similar photorelease data from other studies.^{218,}

²⁶¹ The quantum yield of intermediate (I) to product (P), Φ_{I→P}, was calculated using the equation Φ_{R→P} = Φ_{R→I} · Φ_{I→P}. The quantum yield for the conversion of the reactant (R) **126** to the intermediate (I) *cis*-[Ru(bpy)₂(**124**)(H₂O)]²⁺ (Φ_{R→I}) and to the product (P) *cis*-

$[\text{Ru}(\text{bpy})_2(\text{H}_2\text{O})_2]^{2+}$ ($\Phi\text{R}\rightarrow\text{P}$) were determined, as previously described for *cis*- $[\text{Ru}(\text{bpy})_2(\mathbf{119})_2](\text{PF}_6)_2$, to be 0.050(6) and 0.0067(4), respectively ($\lambda_{\text{irr}} = 400$ nm). These values are significantly lower than those reported for the photoaquation of the related complex *cis*- $[\text{Ru}(\text{bpy})_2(\text{MeCN})_2]^{2+}$ ²⁵⁴ but are similar to those measured for *cis*- $[\text{Ru}(\text{bpy})_2(\mathbf{119})_2](\text{PF}_6)_2$ (see II.3.D.b. for more details).

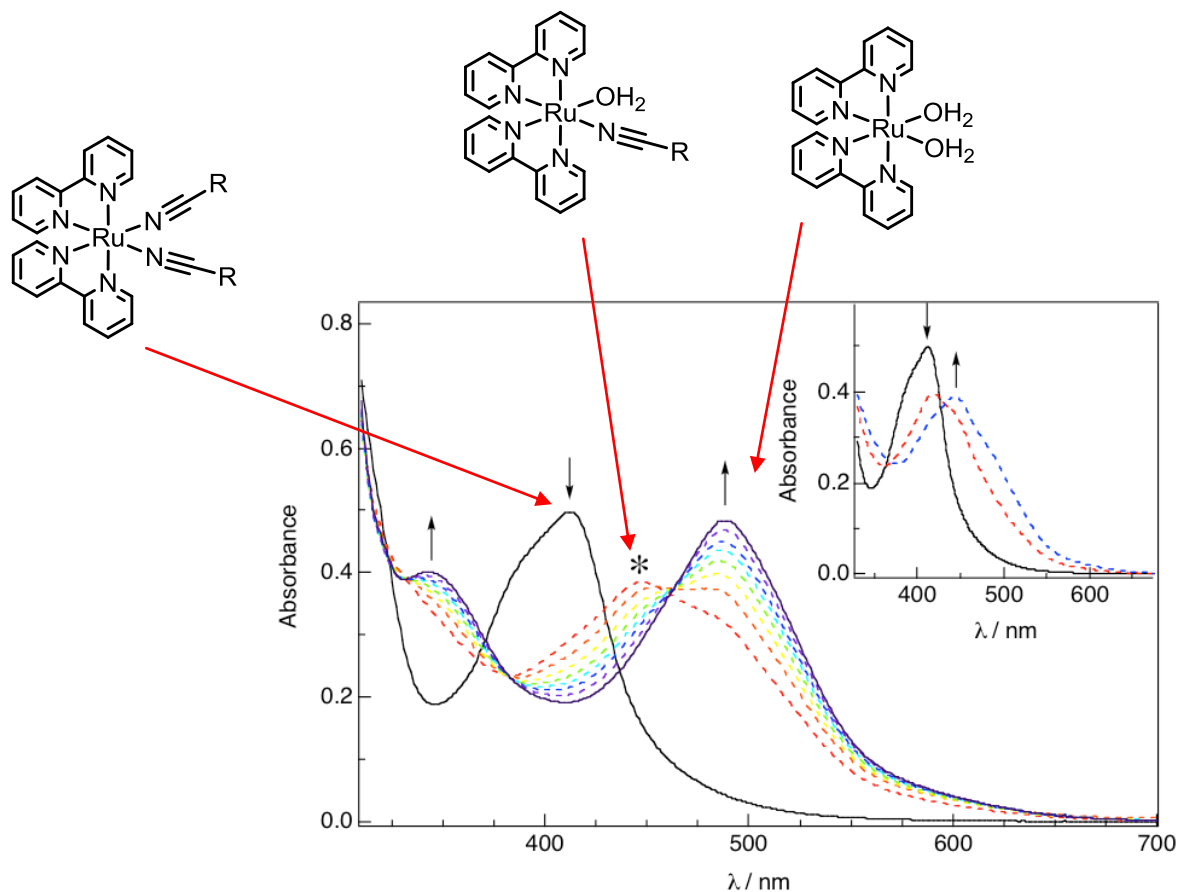


Figure 52: Changes to the electronic absorption spectrum of 52 μM *cis*- $[\text{Ru}(\text{bpy})_2(\mathbf{124})_2]\text{Cl}_2$ (**126**) in a 1% DMSO aqueous solution upon irradiation ($\lambda_{\text{irr}} > 395$ nm) at $t_{\text{irr}} = 0, 3, 4, 5, 6, 7, 8, 10$ and 15 min; inset: 0, 1 and 2 min

The results shown above complete the initial requirements for a potential Ru-based cage of a nitrile-based cathepsin K inhibitor. The complex **126** has similar stability properties in aqueous solutions to complex **123** in the dark, and dissociates upon irradiation with light under

similar conditions (15 minute irradiation is needed versus ten minutes for complex **123**). The complex **126** was then tested as an inhibitor of cathepsin K activity on the isolated enzyme and in living cells.

II.3.B.e. Biological evaluation of a nitrile containing cathepsin K inhibitor **124** caged by Ru^{II}(bpy)₂ (**126**) against isolated human cathepsin K

Inhibition studies with isolated human cathepsin K were conducted according to the procedures described in the previous chapter.²⁶⁴ Enzyme activity was determined with the fluorogenic substrates Z-Phe-Arg-AMC and is expressed as a percentage, with 100% equal to activity in the absence of inhibitor. Photolysis was conducted for 15 min (with gentle shaking of the plate every 2-3 min) using a 250 W tungsten halogen lamp (Osram Xenophot HLX) powered by a 24 V power supply. The irradiation wavelength was selected by placing a bandpass filter (395 nm cutoff) between the lamp and the sample, along with a 10 cm water cell to absorb infrared light. Different concentrations of the inhibitor **124** alone and Ru complex **126** were plated on a 96 well plate in sextuplets (a series of triplicates on the right and left side of the plate). Half of the plate was covered with aluminum foil to keep one series of triplicates in the dark while the other series was irradiated following the set-up described above.

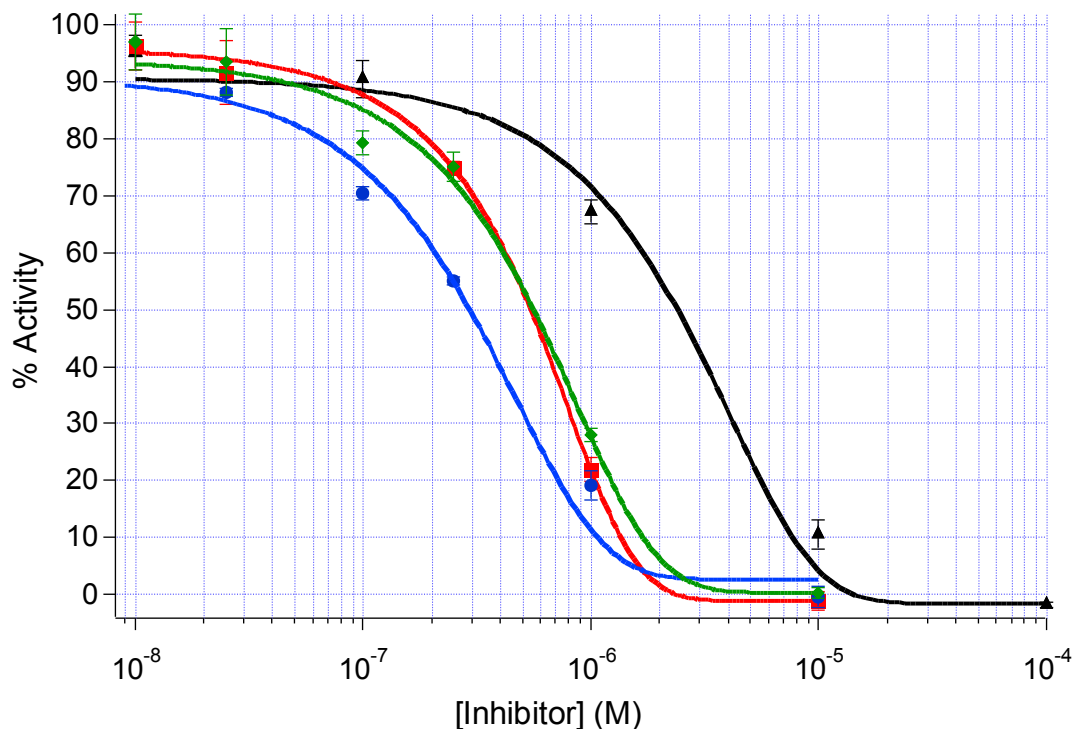


Figure 53: IC₅₀ curves for inhibitor **124** (red, “dark”; green, “light”) and *cis*-[Ru(bpy)₂(**124**)₂]Cl₂ (**126**) (black, “dark”; blue, “light”) against isolated cathepsin K.

Inhibitor **124** was a much more potent inhibitor of human cathepsin K showing an IC₅₀ value of 550 nM compared to 12 μM for **119**. This value was in accordance with the literature data giving a K_i = 35 nM that can be converted to IC₅₀ values using a web based tool.²⁷⁴ Significant enhancement of inhibitory activity upon irradiation of **126** with visible light was noted once again with IC₅₀ values of 290 nM and 2.4 μM for **126** after irradiation and in the dark respectively.^b We still hypothesize that the inhibition in the dark is probably due to either

^bThe same complex has been resynthesized and isolated in a different manner by Raj Sharma, a colleague from the Kodanko group, since this work has been completed. A better purity of the complex has been obtained leading to better “dark/light” ratios. Investigations to explain the differences in the results are in progress.

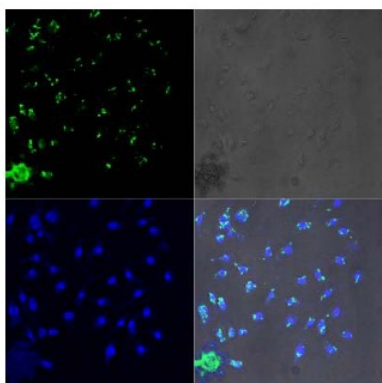
nonbonding interactions of *cis*-[Ru^{II}(bpy)₂(**124**)₂]²⁺ with the enzyme or small amounts of **124** released during the different manipulations. The latter results are in agreement with our previous studies, suggesting that two molecules of nitrile-based inhibitor are released from every molecule of the complex and that the new complex is overall a more potent inhibitor of cathepsin K (290 nM vs. 5.4 μM)²⁶⁴ that should be more suitable for live cell assays.

II.3.B.f. Biological evaluation of a nitrile containing cathepsin K inhibitor **124** caged by Ru^{II}(bpy)₂ (**126**) in live cells

To show the full potential of our caging strategy we were interested in the possibility of inhibiting cathepsin K activity in live cells. Bone macrophage cells (BMM) differentiated as pre-osteoclast were chosen as the target cells because they express high levels of cathepsin K and have been recently linked to inflammatory, osteolytic and tumor cell-driven events in bone-tumor microenvironments.¹⁵⁶ We chose an established live cell assay to monitor the activity of cathepsin K that combines the power of confocal microscopy²⁷⁵ with a modified substrate, namely Z-Gly-Pro-Arg-4-methoxy-β-naphthylamide (Z-Gly-Pro-Arg-4MβNA) that leads to 4-methoxy-β-naphthylamine.²⁷³ The latter is precipitated upon reaction with nitrosalicylaldehyde and can be detected and quantified by fluorescence measurements. Because cathepsin B is usually expressed in higher concentration than cathepsin K, the cells were treated with 1 μM epoxide-based cathepsin B specific inhibitor CA074 to ensure that only activity due to cathepsin K was assessed.

Cells were treated with four concentrations of **126** from 1 nM to 10 μM and 1 μM CA074 and incubated for 30 minutes. After a thorough wash, to remove all extracellular inhibitors, the cells were split in two and either irradiated with visible light for 15 minutes or kept in the dark. The cells were then treated with 1.0 mM Z-Gly-Pro-Arg-4MβNA and 0.5 mM

nitrosalicylaldehyde for 30 minutes and after a second wash, fixed with 1% formaldehyde. The activity was measured using a confocal laser scanning microscope (Zeiss LSM 510) and DAPI was used as the nuclear dye. Controls with cells treated with buffer only or *cis*- $[\text{Ru}^{\text{II}}(\text{bpy})_2(\text{MeCN})_2](\text{PF}_6)_2$ were examined in the same way. Activity was detected by a green coloration whereas the nuclei were colored in blue (DAPI). The upper left quadrant corresponds to the activity due to cathepsin K (green coloration), the lower left denotes the nuclei stained with DAPI (blue coloration), the lower right is the superposition of the two left quadrants and finally the upper right quadrant corresponds to the raw image (Figure 54).



A: Buffer "Light", CA074 (1 uM)

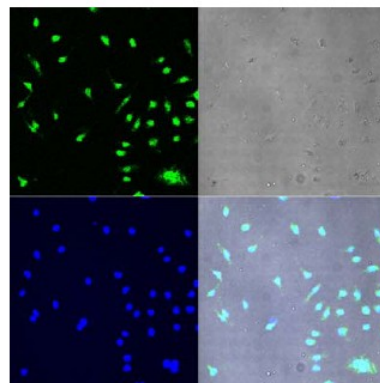
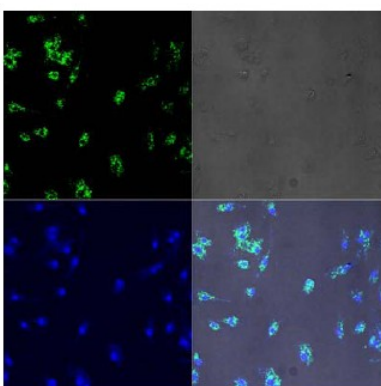
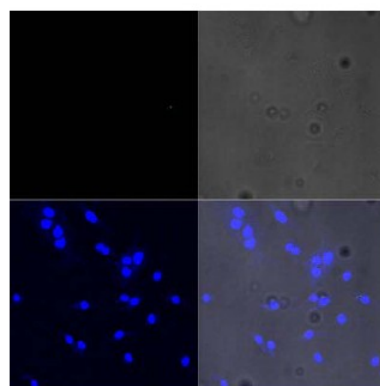
B: *cis*-[Ru^{II}(bpy)₂(MeCN)₂](PF₆)₂ "Light", CA074 (1 uM)C: **126** 250 nM "Dark", CA074 (1 uM)D: **126** 250 nM "Light", CA074 (1 uM)

Figure 54: Confocal microscopy images of mouse bone marrow macrophages cells treated with 250 nM complex **126** plus CA074 (1 μ M) for measuring specific Cat K activity, with or without irradiation, plus controls

To our delight, cells treated with 250 nM **126** and irradiated with light did not show any activity associated with cathepsin K whereas cells treated with the same concentration of inhibitor **126** and left in the dark showed activity levels comparable to cells treated with the buffer solution alone. Moreover, all activity for the cells left in the dark (green) was associated around the nuclei (blue) suggesting that the intracellular activity of cathepsin K could be knocked down using our light activated inhibitor **126**.

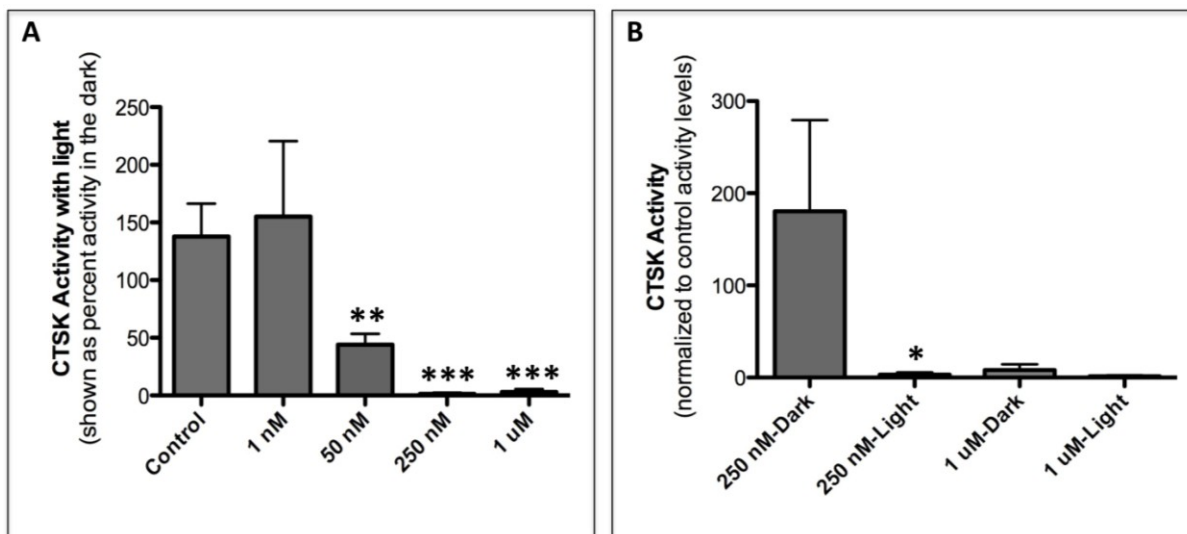


Figure 55: Quantitative analysis of cathepsin K inhibition by *cis*-[Ru(bpy)₂(**124**)₂]Cl₂ (**126**) in live bone marrow macrophages (BMMs) under the dark and light conditions

(All data were analyzed using Graph Prizm software and are shown as mean \pm S.D. * indicates $p = 0.08$; ** indicates $p = 0.02$; and *** indicates $p = 0.003$; p values < 0.05 are considered statistically significant. Results are representative of at least 3 experiments)

The fluorescence data was quantified to give a better assessment of the efficacy of **126** to inhibit the activity of cathepsin K. Four snapshots were taken per microscope plate (each corresponding to different conditions) and the images of control and complex **126**-treated BMMs (4 images/treatment) were analyzed using MetaMorph software. Integrated intensities of green fluorescence were normalized to the number of nuclei (DAPI). Graph **A** shows CTSK activity in BMMs in the absence (control) or presence of increasing concentrations of complex **126** after exposure to light (Figure 55). Integrated intensity/nuclei values were normalized to controls and expressed as percent activity in the dark. A dose-dependent inhibition of cathepsin K activity is observed with increasing concentrations of complex **126** and is completely abolished at 250 nM. Graph **B** shows cathepsin K activity in BMMs treated with 250 nM and 1 μ M complex concentrations of **126** under dark and light conditions. Data are shown as percent activity under control conditions. At 250 nM complex **126** completely inhibits cathepsin K activity with light

but not dark exposure. At 1 μM concentration, inhibition of cathepsin K is observed under both, light and dark conditions (Figure 55).

These data strongly suggest that light activation of the nitrile-based inhibitor **126** has been accomplished in a dose-dependent fashion. Cathepsin K activity can be thus controlled with light demonstrating the usefulness of this strategy to study the effects of activity/inhibition of activity of cathepsin K on different disease states in a spatially controlled fashion. Ideally this strategy could enable spatial knockdown of cathepsin K in selected cells/areas of living organisms. To further demonstrate the robustness of the $\text{Ru}^{\text{II}}(\text{bpy})_2$ cage strategy, we decided to investigate cell viability after treatment with our Ru complex **126**

II.3.B.g. Toxicity evaluation of a nitrile containing cathepsin K inhibitor **124** caged by $\text{Ru}^{\text{II}}(\text{bpy})_2$ (**126**)

As a final complement to this study, we were interested in gaining insight into the possible toxic effects of the ruthenium complexes on the cells under both light and dark conditions. The possible product of the photorelease, namely $\text{cis-}[\text{Ru}^{\text{II}}(\text{bpy})_2(\text{H}_2\text{O})_2]^{2+}$ is a potential anticancer agent, with a mode of action mimicking that of cisplatin by covalently bonding to DNA.^{232, 233, 235, 236} To address this question, it was decided to test the viability of the same BMM cells as the ones used in the previous live cell assay using the MTT (3-(4,5-dimethylthiazol-2-yl)-2,5-diphenyltetrazolium bromide, a yellow tetrazole) assay. Cells were treated with concentrations of **126** and $\text{cis-}[\text{Ru}^{\text{II}}(\text{bpy})_2(\text{MeCN})_2]\text{Cl}_2$ between 1 nM and 100 μM , incubated for 30 min, washed thoroughly and irradiated for 15 minutes or left in the dark (following the same procedure as in the live cell assay). Cell viability was assessed after 24 hours using the MTT assay, showing no cytotoxicity for any of the compounds at any concentration.

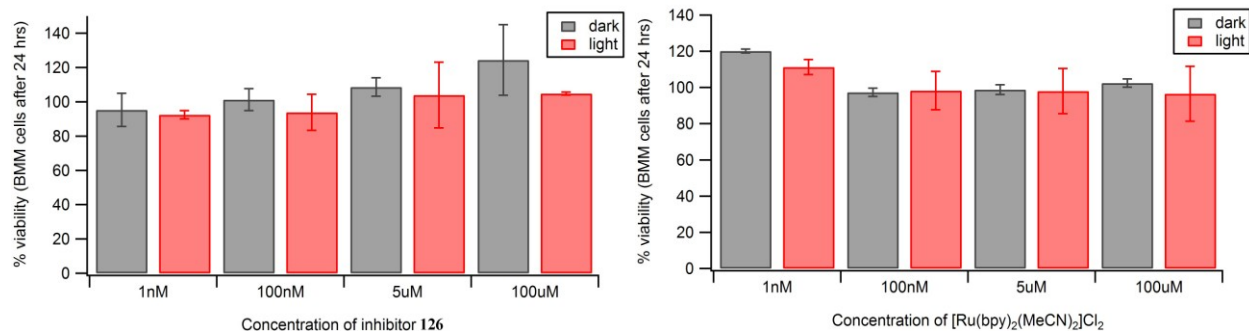


Figure 56: BMM cell viability 24 hours after treatment with various concentrations of **126** or $cis-[Ru^{II}(bpy)_2(MeCN)_2]Cl_2$ assayed using the MTT assay

Because growth inhibitory effects have been reported in the literature for certain Ru complexes with treatments extended to 72 hours,²⁰³ we repeated the latter study with PC3 cells (BMM cells were unfortunately not well suited for a prolonged study). Following the same protocol as described previously, PC3 cells were assessed for viability using the MTT assay after 72 hours and once again did not show any signs of cytotoxicity.

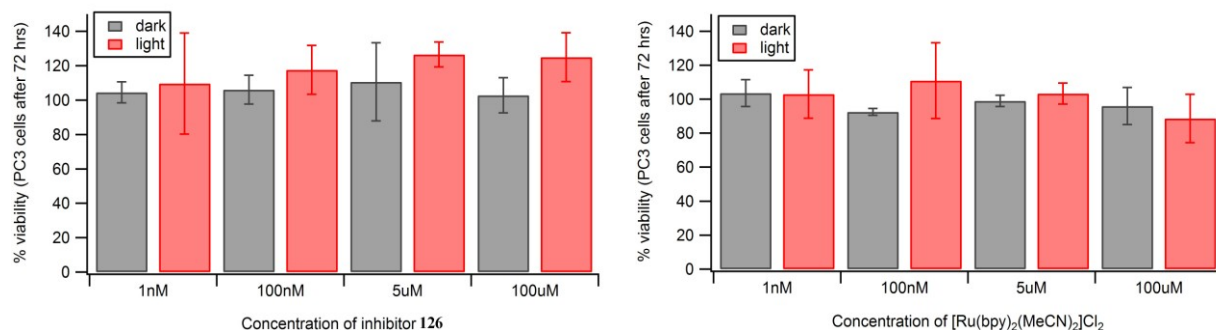


Figure 57: PC3 cell viability 72 hours after treatment with various concentrations of **126** or $cis-[Ru^{II}(bpy)_2(MeCN)_2]Cl_2$ assayed using the MTT assay

The lack of cytotoxicity underlines even more the potential of the Ru cage strategy. The cage does not seem to have any toxic side effects upon treatment with high micromolar concentrations of **126** or control Ru complex $cis-[Ru^{II}(bpy)_2(MeCN)_2]Cl_2$ and has been shown in the previous section to be effective at inhibiting the activity of cathepsin K in high nanomolar

concentrations. Further studies with extended treatment times might be required to completely rule out any toxic effects associated with the Ru^{II}(bpy)₂ cage.

Also, studies that could clarify the pharmacokinetics of Ru complexes such as **126** or *cis*-[Ru^{II}(bpy)₂(MeCN)₂]Cl₂ need to be designed. It is not clear if the Ru complexes penetrate the cell membranes. The effective inhibition of cathepsin K could be explained through at least two scenarios where either the Ru cage penetrates the cells, and then releases the nitrile-based inhibitors inside or only associates with cell membranes releasing the nitrile-based inhibitor outside of the cell, followed by inhibitor penetration. Because complexes like **126** are not luminescent at RT,²⁷⁶ we have not been able to determine the fate of the complexes so far. We have tried to investigate potential Ru accumulation in cells, that was analyzed by atomic absorption, but the low concentrations found did not provide conclusive results.²⁰³ Knowing the fate of the Ru complexes could bring more understanding to their potential toxic effects.

II.3.C. Conclusions and further directions

The results presented in this chapter describe an efficient way of caging nitrile based cathepsin inhibitors and activating them within minutes upon exposure to visible light. We have extended our initial studies on isolated enzymes to living cells. We demonstrated a dose-dependent inactivation of cathepsin K with our Ru complex **126** and the nitrile-based inhibitor **124** that is released upon irradiation with visible light at high nanomolar concentrations. Moreover, the Ru^{II}(bpy)₂ did not show any toxic effects with high micromolar concentrations highlighting the usefulness of this strategy to selectively inhibit targets with spatial and kinetic control. We believe this strategy can be an extremely useful tool to study aberrant proteolysis in cancer models as well as animal models. This successful study also opens a number of doors for new and challenging analyses as number of parameters need to be addressed and improved.

We chose to use a moderate inhibitor of cathepsin K in this study as cathepsin K has become a very alluring target for various disease states and bone tumor growth in particular. Cathepsin K is largely overexpressed in metastases to the bone from prostate²⁷⁷ and breast cancers²⁷⁸ and bone lesions from such metastases are very severe and often irreversible.²⁷⁹ The use of this caging strategy might be a very interesting tool in the study of the effects of cathepsin K inhibition in bone marrow macrophages and osteoclasts that have been demonstrated to highly overexpress cathepsin K.¹⁵³ Because proteases in general, and cathepsins in particular, are such an attractive therapeutic target, several families of very potent inhibitors have been designed by SAR studies. Molecules such as odanacatib¹⁵⁷ have successfully entered clinical trials offering a wide variety of potential nitrile-based inhibitors that can be used in our caging strategy. The variety of motifs already synthesized and tested by others might be a very helpful benefit to modulate the pharmacokinetics and pharmacodynamics of future complexes.

Families of targets other than cathepsins such as caspases are also effectively inhibited by nitrile-based inhibitors. We strongly believe that the strategy described here could be a general methodology to study protease inactivation in a light controlled fashion. To achieve this goal, further studies are in progress in the Kodanko, Podgorski and Turro laboratories. We are actively caging new, more potent inhibitors and trying to improve the dark/light activation ratios. The modulation of the bpy moieties should have a direct influence on the MLCT absorption band. We are hoping to improve the photodissociation quantum yields and shift the necessary irradiation wavelengths towards the near-IR wavelengths as light with longer wavelengths penetrates deeper within tissues and is less toxic. Finally, we are designing new complexes that could allow us to study their biological fate after cell treatment and photodissociation. Building

complexes that are luminescent at RT or using flow cytometry are some of the strategies that we have envisioned so far.

In conclusion, this part of the dissertation described the first metal based caging strategy for nitrile-based inhibitors. In our initial study, we built “proof of concept” Ru^{II}(bpy)₂ cages that effectively deliver and inhibit cysteine proteases upon delivery of nitrile-based inhibitors triggered by light. After fully characterizing the new complexes and their behavior in aqueous solutions in the dark and upon irradiation with visible light we have shown high dark/light inactivation ratios on isolated enzymes and have extended the applications to the inactivation of cathepsin K in living cells in the latest study. By showing that no toxic effects are associated with the use of Ru^{II}(bpy)₂ as a cage, further studies will be carried out to establish this methodology as a general method to study proteolysis in a spatially controlled fashion *in vivo*.

The results presented in this chapter will be published in due time (Respondek T., Sharma R., Garner R. N., Herroon M. K., Podgorski I., Turro C., Kodanko J. J.): “Targeting intracellular proteolysis with a light-activated cathepsin K inhibitor” *Manuscript in preparation*.

II.3.D. Experimental section

II.3.D.a. General considerations

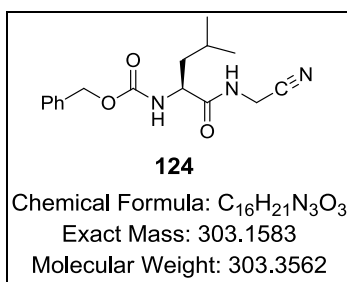
All reagents were purchased from commercial suppliers and used as received. NMR spectra were recorded on a Varian FT-NMR Mercury-400 Spectrometer. Mass spectra were recorded on a Waters ZQ2000 single quadrupole mass spectrometer using an electrospray ionization source. IR spectra were recorded on a Perkin Elmer Spectrum 2000 FT-IR Spectrometer. Enzymatic assays (CatK inhibition, MTT and Bradford) were conducted on a Tecan Infinite M200 or Tecan SPECTRAFluor Plus microplate reader. UV-vis spectra were

recorded on a Varian Cary 50 spectrophotometer. Time-dependent UV-Vis spectra were recorded on a Varian Cary 50 spectrophotometer. The photolysis experiments were conducted using a 250 W Tungsten Halogen lamp (Osram Xenophot HLX) powered by a 24 V power source. The irradiation wavelength was selected by placing a bandpass filter (395 nm cutoff) between the lamp and the sample, along with a 10 cm water cell to absorb infrared light. The confocal microscopy was performed with a Zeiss 510 Laser Scanning Microscope. All reactions were performed under ambient atmosphere unless otherwise noted. Anaerobic reactions were performed by purging the reaction solutions with Ar or N₂.

All NMR, IR and mass spectra can be found in the Appendix section.

II.3.D.b. Experimental procedures and tabulated characterization data

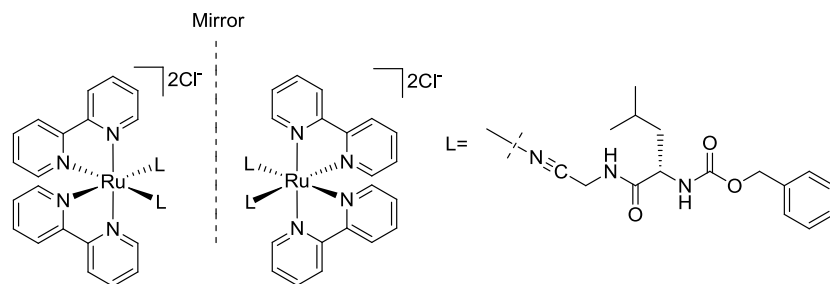
(S)-benzyl (1-((cyanomethyl)amino)-4-methyl-1-oxopentan-2-yl)carbamate (**124**).



124 was prepared by a modification of published procedures.^{258, 272} L-leucine (15.0 mmol, 1.97 g) was dissolved in 18.5 mL of 2.0 M NaOH and cooled to 0°C. Benzyl chloroformate (17.3 mmol, 2.46 mL) was added in small portions over 30 min and the resulting solution stirred at RT for 12 h. The crude reaction solution was then acidified with 6.0 N HCl and extracted with EtOAc (3 x 30 mL). The organic layers were combined, dried over Na₂SO₄, filtered and concentrated to give 3.82 g of a sticky white solid. The crude product Cbz-Leu-OH was analyzed by ¹H NMR spectroscopy (> 90% purity) and was used without further

purification. Crude Cbz-Leu-OH (7.00 mmol, 1.86 g) was dissolved in dry DMF (10.0 mL). Aminoacetonitrile HCl (8.40 mmol, 777 mg) was mixed with HBTU (8.4 mmol, 3.19 g) and Et₃N (16.8 mmol, 2.36 mL) and dissolved in dry DMF (30.0 mL). Both solutions were combined and the resulting solution stirred under N₂ for 16 h. The crude reaction solution was combined with CH₂Cl₂ (75 mL) and the organic layer was washed with 0.1 M HCl (2 x 30 mL), 1.0 M HCl (1 x 30 mL), sat. aqueous NaHCO₃ (2 x 30 mL) and brine (2 x 30 mL). The organic layer was dried over Na₂SO₄, filtered and concentrated. The crude product was recrystallized from hot EtOAc/Hexanes to give **124** as a white powder (950 mg, 45% from the first crop over the 2 steps). Mother liquors can be further recrystallized or purified by flash chromatography on silica. ¹H NMR (400MHz CD₂Cl₂-d₆ δ) 7.33 (m, 5H), 7.06 (br, s, NH, 1H), 5.39 (br, s, NH, 1H), 5.0 (Aq, 2H), 4.21 (br, s, 1H), 4.05 (d, *J* = 3.9 Hz, 2H), 1.63 (m, 2H), 1.52 (m, 1H), 0.91 (d, *J* = 6.4 Hz, 3H), 0.89 (d, *J* = 5.9 Hz, 3H); ¹³C NMR (100MHz CD₂Cl₂-d₆ δ) 172.68, 156.48, 136.22, 128.52, 128.21, 127.89, 116.07, 67.20, 40.66, 27.48, 24.62, 22.63, 21.48; [α]_D²⁰ – 33.9 (c 1.0, CH₂Cl₂); mp 125.5-127 °C; IR ν_{max} (thin film, cm⁻¹): 3306, 3065, 3036, 2958, 2872, 2258, 1693, 1673, 1531, 1537, 1469, 1455, 1411, 1388, 1369, 1342, 1261, 1238, 1172, 1121, 1043, 1028, 964, 909, 778, 739, 697; LRMS (ESMS) calculated for C₁₆H₂₂N₃O₃ [M+H]⁺: 304.2, found: 304.5.

Δ-cis-[Ru(bpy)₂(124)₂]Cl₂·3.5H₂O and Λ-cis-[Ru(bpy)₂(124)₂]Cl₂·3.5H₂O (126):



126

Chemical Formula: C₅₂H₅₈Cl₂N₁₀O₆Ru

Exact Mass: 1090.2961

Molecular Weight: 1091.0563

In the glove box, a shlenk flask was charged with *cis*-Ru(bpy)₂Cl₂ (0.1 mmol 48.4 mg), AgBF₄ (0.4 mmol 77.9 mg) and (S)-benzyl (1-((cyanomethyl)amino)-4-methyl-1-oxopentan-2-yl)carbamate (**124**) (0.6 mmol 91.0 mg) and 20.0 ml of freshly distilled EtOH. The resulting solution was wrapped in aluminum foil and heated to 80°C for 6 h during which it turned from dark violet to bright orange. After cooling the crude solution to RT, it was placed in the freezer at -20°C for 16 h. The precipitated silver salts were filtered off on celite and washed with cold EtOH. The solvents were removed under reduced pressure and an NMR taken to monitor the completion of the reaction and formation of Ru by-products. The resulting yellow solid was dissolved in ~2 ml of acetone and layered with ~10 ml of Et₂O and placed in the freezer at -20°C for 16 h. The solid was filtered off and washed with cold Et₂O. The resulting solid was dissolved in ~15 ml of EtOAc and extracted 3 times with 15 ml H₂O. The organic layer was then precipitated (oily residue) with 2 ml of sat. *n*-Bu₄NCl in EtOAc at -20°C. The oily residue was spun out and washed with cold EtOAc (3 times), and then cold Toluene (7 times). It was finally dissolved in a minimum amount of acetone and layered with Et₂O and placed -20°C for 16 h. The resulting solid was washed with Et₂O to give the title compound as an orange solid in analytically pure form (21.0 mg, 0.019 mmol, 19%): ¹H NMR (400MHz CD₂Cl₂-d₂ δ) 9.93 (s, br, 2H), 9.54 (d, *J* = 4.9 Hz, 1H), 9.51 (d, *J* = 4.9 Hz, 1H), 8.53 (d, *J* = 8.1 Hz, 1H), 8.45 (d, *J* =

8.1 Hz, 2H), 8.36 (d, $J = 8.1$ Hz, 1H), 8.15 (m, 2H), 8.02 (m, 2H), 7.93 (m, 2H), 7.54 (d, $J = 5.9$ Hz, 2H), 7.32 (m, 8H), 7.25 (m, 2H), 6.86 (d, $J = 9.7$ Hz, 1H, NH), 6.74 (d, $J = 8.1$ Hz, 1H, NH), 5.04 (m, 3H), 4.16 (d, $J = 12.2$, 1H), 4.28 (m, 6H), 1.08 (under the H₂O peak, m, 4H), 0.91 (m, 12H); IR (KBr) ν_{\max} (cm⁻¹): 3419, 3029, 2957, 2870, 2347, 2274, 1714, 1676, 1604, 1523, 1466, 1446, 1424, 1386, 1337, 1246, 1170, 1122, 1047, 917, 771, 731, 698, 670; LRMS (ESMS) calculated for C₅₂H₅₈N₁₀O₆Ru [M]²⁺: 510.2, found: 510.1; Anal. Calcd for C₅₂H₆₅Cl₂N₁₀O_{9.5}Ru ([Ru(bpy)₂(1)₂]Cl₂·3.5H₂O): C, 54.12; H, 5.68; N, 12.14. Found: C, 54.16; H, 5.46; N, 12.13.

General Considerations for the Time Dependent UV-Vis spectra:

Time dependent UV-Vis spectra were recorded on a Varian Cary 50 spectrophotometer. The photolysis experiments were conducted using a 250 W Tungsten Halogen lamp (Osram Xenophot HLX) powered by a 24 V power source. The irradiation wavelength was selected by placing a bandpass filter (395 nm cutoff) between the lamp and the sample, along with a 10 cm water cell to absorb infrared light.

Stability of 126 in 0.1M pH 6.5 phosphate buffer:

A 50 μ M solution of **126** in a 0.1M pH 6.5 phosphate buffer (1.0% DMSO) was placed in a cell, and UV-Vis spectra recorded for 12 h (the cell was shaken to help diffusion before the start of the experiment). Ln A was plotted vs. time and fitted to give a first order reaction rate $r = 0.00006026 \text{ min}^{-1}$. The half life corresponding to this rate was approximately 11500 min \sim 8.0 days ($t_{1/2} = -0.693/r$).

Stability of 126 in CatK assay buffer:

A 50 μ M solution of **126** in a 400 mM sodium acetate, pH 5.5, 4 mM EDTA, 8 mM DTT buffer solution (0.5% DMSO) was placed in a cell, and UV-Vis spectra recorded for 6 h (the cell was shaken to help diffusion). Ln A was plotted vs. time and fitted to give a first order reaction

rate $r = 0.00012802 \text{ min}^{-1}$. The half life corresponding to this rate was approximately 5413 min \sim 3.75 days ($t_{1/2} = 0.693/r$).

Quantum yield and time dependent UV-vis spectra upon irradiation of **126**:

Steady-state photolysis experiments for quantum yield determination were conducted using a 150 W Xe arc lamp in a PTI housing (Milliarc Compact Lamp Housing) powered by an LPS-220 power supply (PTI) with an LPS-221 igniter (PTI) as a source. The irradiation wavelength was selected by placing long-pass colored glass filters (Melles Griot) or bandpass filters (Newport) between the lamp and the sample, along with a 10 cm water cell to absorb infrared light. Electronic absorption spectra were collected on a diode array spectrometer (HP 8453) with HP 8453 Win System software.

Quantum yields were measured relative to ferrioxalate using a standard procedure.²⁶⁶ The quantum yield of reactant (R) to intermediate (I), $\Phi_{R \rightarrow I}$, was determined by monitoring the decrease in the MLCT absorption of the reactant at 414 nm up to 5% of the reaction. The quantum yield of reactant (R) to product (P), $\Phi_{R \rightarrow P}$, was determined by monitoring the increase in the absorption of the latter with maximum at 490 nm. The quantum yield of intermediate (I) to product (P), $\Phi_{I \rightarrow P}$, was calculated using the equation $\Phi_{R \rightarrow P} = \Phi_{R \rightarrow I} \cdot \Phi_{I \rightarrow P}$. The quantum yield for the conversion of the reactant (R) **126** to the intermediate (I) *cis*-[Ru(bpy)₂(**124**)(H₂O)]²⁺ ($\Phi_{R \rightarrow I}$) and to the product (P) *cis*-[Ru(bpy)₂(H₂O)₂]²⁺ ($\Phi_{R \rightarrow P}$) were determined, as previously described for *cis*-[Ru(bpy)₂(**119**)₂](PF₆)₂,²⁶⁴ to be 0.050(6) and 0.0067(4), respectively ($\lambda_{\text{irr}} = 400$ nm). These values are significantly lower than those reported for the photoaquation of the related complex *cis*-[Ru(bpy)₂(CH₃CN)₂]²⁺,²⁵⁴ but are similar to those measured for *cis*-[Ru(bpy)₂(**119**)₂](PF₆)₂.²⁶⁴

II.3.D.c. Cathepsin K inhibition studies

Cathepsin K inhibition studies.

Cathepsin enzyme activity was determined from kinetic measurements performed by fluorimetric detection of the hydrolysis product AMC at 37°C every 2 min for 14 min (8 measures). The excitation and emission wavelengths were 360 and 485 nm respectively. The selective fluorescent substrate Z-Phe-Arg-AMC was used at a final concentration of 100 µM (obtained from Bachem, Torrance, CA). Enzyme activities are expressed as a percentage, with 100% equal to activity in the absence of inhibitor. Recombinant cathepsin K (human) was obtained from Enzo Life Sciences (Farmingdale, NY). An 880 nM stock solution was prepared in 50 mM sodium acetate, pH 5.5, 50 mM NaCl, 0.5 mM EDTA and 5 mM DTT and kept at -80°C. For each experiment the stock solution was diluted 440 times and activated for 15 min at 37°C with a 400 mM sodium acetate, pH 5.5, 4 mM EDTA, 8 mM DTT assay buffer solution. The inhibitor was prepared as a 1% DMSO solution in the activated enzyme buffer solution and plated (Corning® 96 Well Flat Clear Bottom Black Polystyrene TC-Treated Microplates, 50 µL/well). Three experiments in triplicates (**124** or **126**, light or dark) were carried out on the same 96 well plate. The wells containing **124** and **126** “dark” were carefully wrapped in aluminum foil and the plate was exposed to visible light. The photolysis was conducted for 15 min (with gentle shaking of the plate every 2-3 min) using a 250 W tungsten halogen lamp (Osram Xenophot HLX) powered by a 24 V power supply. The irradiation wavelength was selected by placing a bandpass filter (395 nm cutoff) between the lamp and the sample, along with a 10 cm water cell to absorb infrared light. After photolysis, the reaction was initiated by addition of 50 µL of 200 µM Z-Phe-Arg-AMC solution in the assay buffer (final volume 100 µL, final enzyme concentration 1 nM). Cathepsin enzyme activity was determined from kinetic

measurements performed by fluorimetric detection of the hydrolysis product AMC at 37°C every 2 min for 14 min (8 measures) and MAX RFU slope values used for plotting

Cell Assays and Imaging.

The live cell cathepsin K activity staining assays were performed following a method described previously.²⁷⁵ Briefly, bone marrow macrophages (BMMs) were derived from FVBN mice as previously described.¹⁵⁶ BMMs were cultured in 24-well plates on acid-washed coverslips in MEM α media (Sigma) containing 10% fetal bovine serum (FBS), 10 ng/ml RANKL (R&D Systems), and 20 ng/ml MCSF (R&D Systems) to induce pre-osteoclast differentiation. After 48 hours, media containing fresh RANKL and MCSF was replenished and cells were cultured for additional 24 hours. On the day of experiment cells were incubated for 30 min at 37°C with 250 μ L of reaction buffer (0.2 M sodium acetate, pH 6.0, 0.1 mM EDTA and 0.125 mM BME) containing **124** or **126** (1- 1000 nM, +/- 1 μ M CA074, a cathepsin B inhibitor) in 1% DMSO. After 30 min, the cells were carefully washed with and left in PBS (phosphate buffered saline), the “dark” plate was wrapped in aluminum foil, whereas the “light” plate was exposed to visible light. The photolysis was conducted for 15 min (with gentle shaking of the plate every 2-3 min) using a 250 W tungsten halogen lamp (Osram Xenophot HLX) powered by a 24 V power supply, using bandpass and water filters, as described previously. The cells were washed with PBS, and treated with 250 μ L of substrate solution in reaction buffer consisting of 1.0 mM Z-Gly-Pro-Arg-4M β NA (cathepsin K substrate), and 1.0 mM nitrosalicylaldehyde (precipitating agent). The reaction was allowed to occur for 30 min at 37°C. Controls were incubated in the same manner but without substrate (with or without 1.0 μ M CA074). After 30 min, the cells were washed and fixed with 1% formaldehyde for 20 min minutes at RT. After being washed with PBS and distilled water, the coverslips were mounted on microscope slides

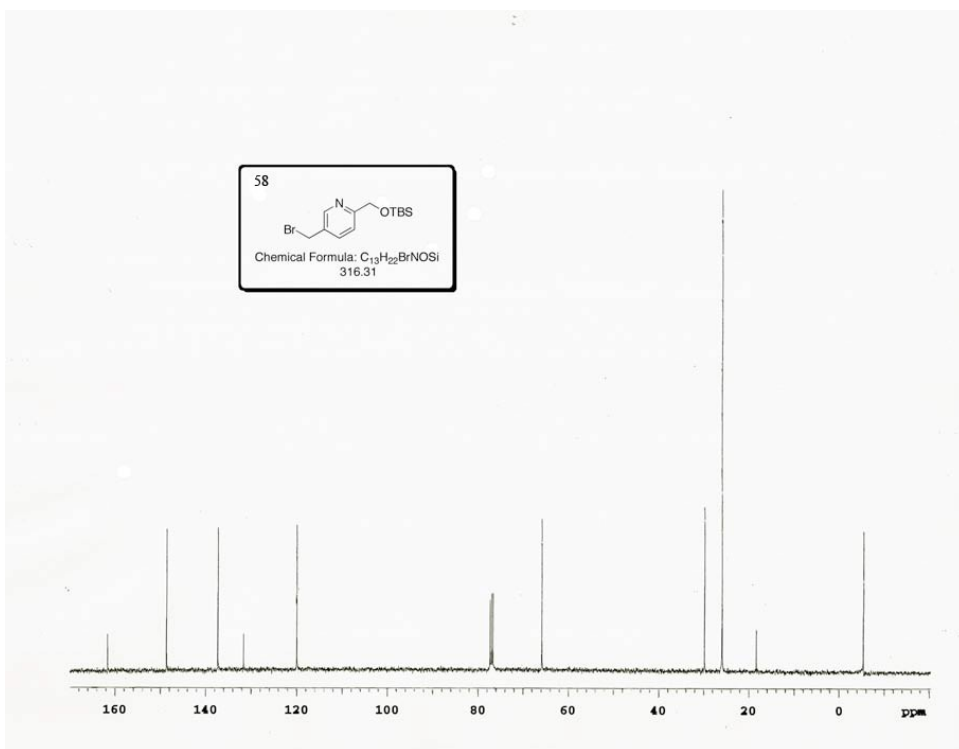
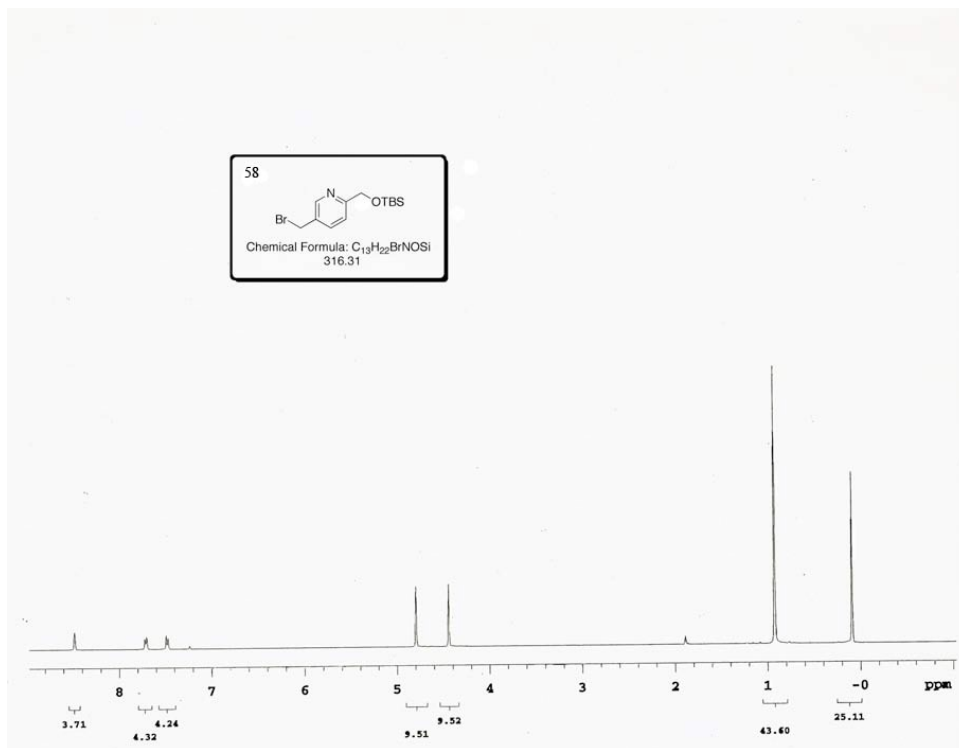
and viewed with a confocal laser scanning microscope (Zeiss LSM 510). DAPI was used as the nuclear dye. For quantitative studies, cells were fixed and images captured with Zeiss 510 laser confocal microscope using a 40x oil immersion lens. Images of control and complex 3-treated BMMs (4 images/treatment) were analyzed using MetaMorph software. Integrated intensities of green fluorescence were normalized to the number of nuclei (DAPI).

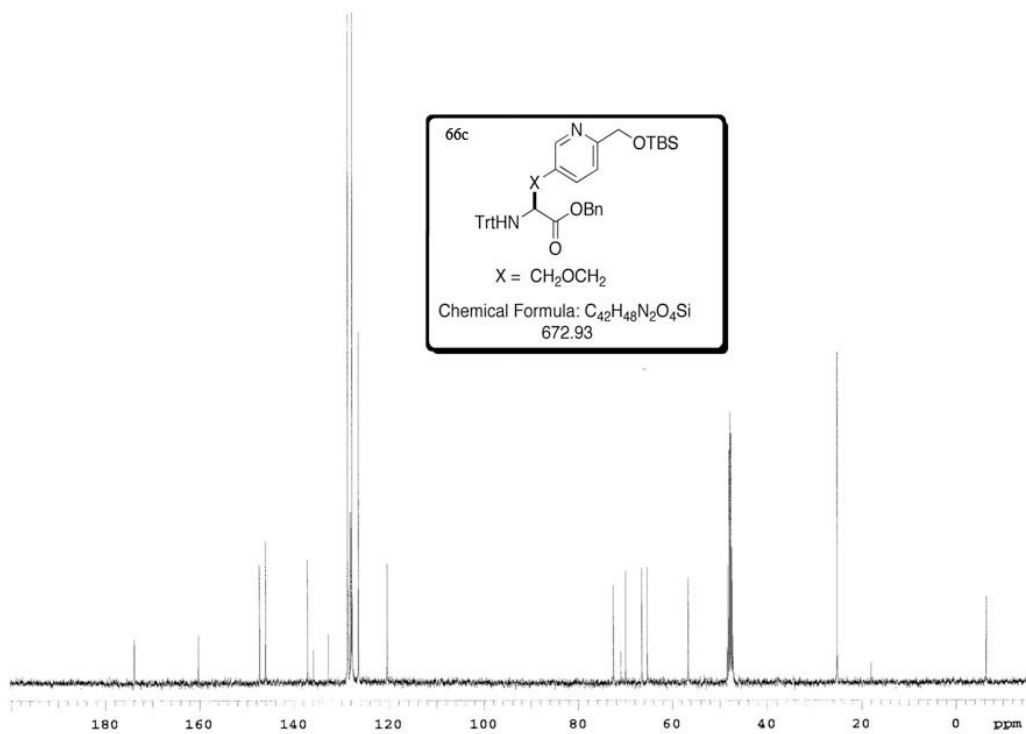
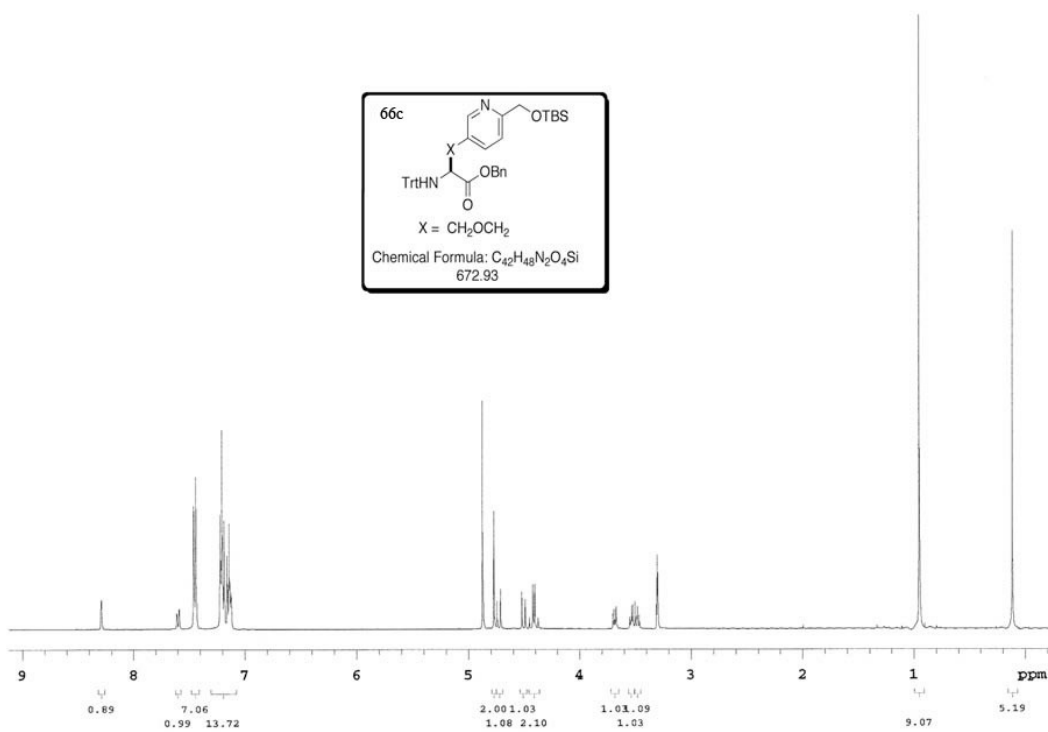
II.3.D.d. Cell Viability Determinations.

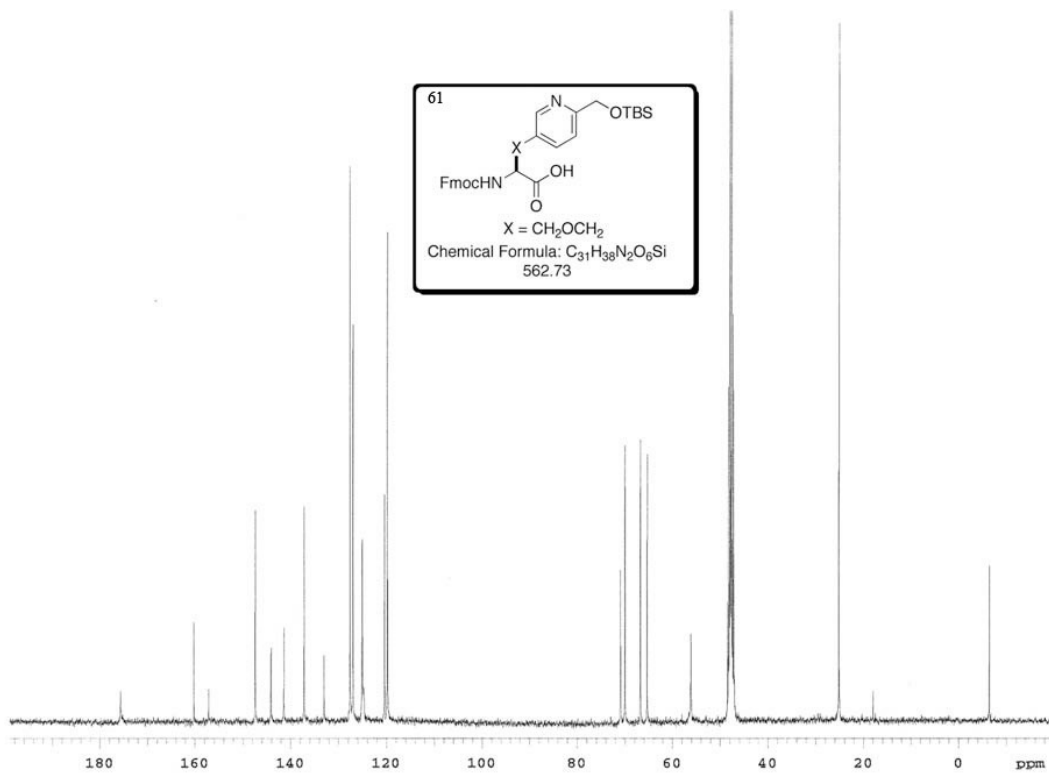
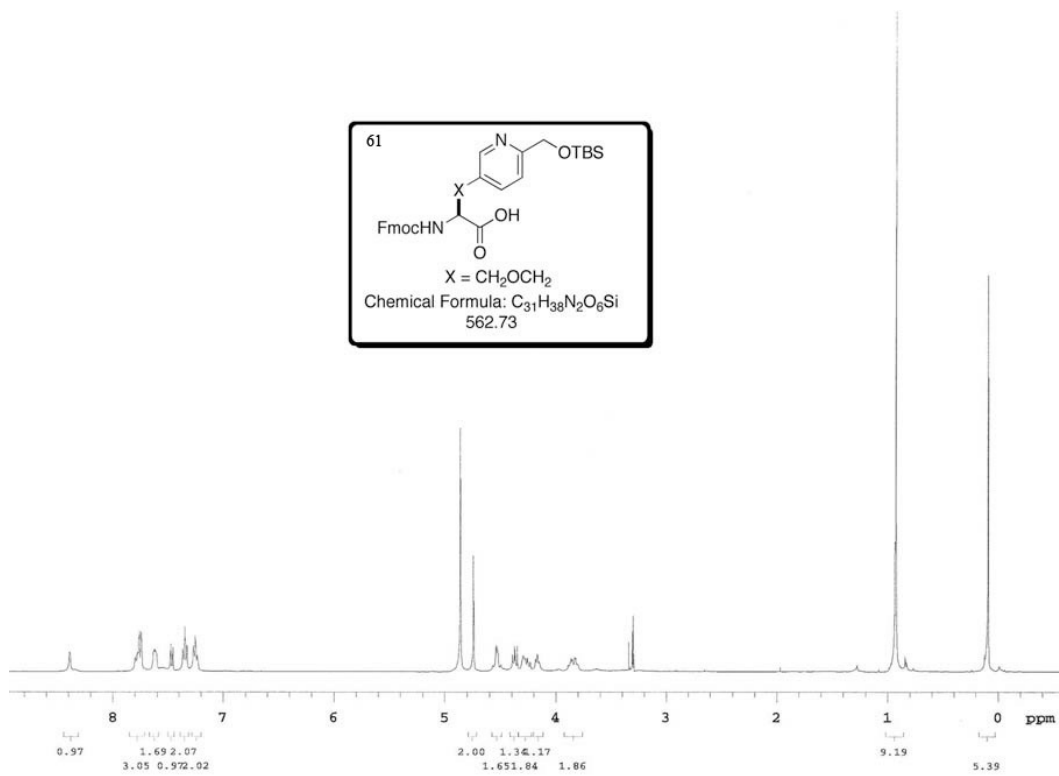
The cell viability of BMM and PC3 prostate carcinoma cells in the presence of **124**, **126** and *cis*-[Ru(bpy)₂(CH₃CN)₂]²⁺ was measured using the MTT assay according to the manufacturer's instructions (Invitrogen, Grand Island, NY). Briefly, the cells were grown in a 96 well plate for 48 h. After removing the media, the cells were treated with 50 μL solutions of **124**, **126** or *cis*-[Ru(bpy)₂(MeCN)₂]Cl₂ in the appropriate culture media and incubated for 30 min at 37°C. The media was then removed, and the cells were washed 3 times and left in PBS buffer. The "dark" plate was wrapped in aluminum foil while the "light" plate was exposed to visible light. The photolysis was conducted for 15 min (with gentle shaking of the plate every 2-3 min) using a 250 W tungsten halogen lamp (Osram Xenophot HLX) powered by a 24 V power supply, using bandpass and water filters, as described previously. The cells were washed 6 times with PBS buffer. New media was then added and the cells were incubated for 24 h or 72 h in the dark under a 5% CO₂ atmosphere and 37°C. After the incubation time, the media was removed and 100 μL of new media was added. 10 μL of a 12 mM MTT stock solution (5 mg of MTT dissolved in 1.0 mL of sterile PBS) was then added to each well. The cells were covered and incubated for 4 h. A negative control consisting of 10 μL of stock MTT solution added to 100 μL media in empty wells was also prepared. 85 μL was then removed from each well and was replaced by 50 μL of DMSO, and thoroughly mixed. Absorbance measurements at 540 nm were

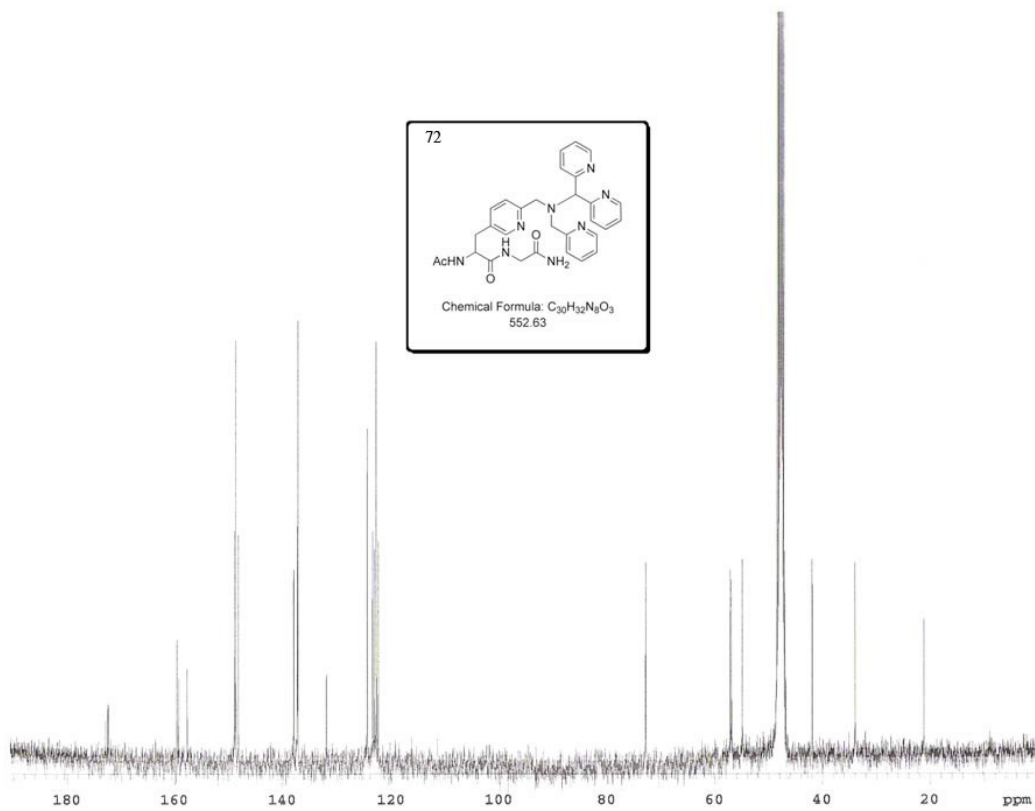
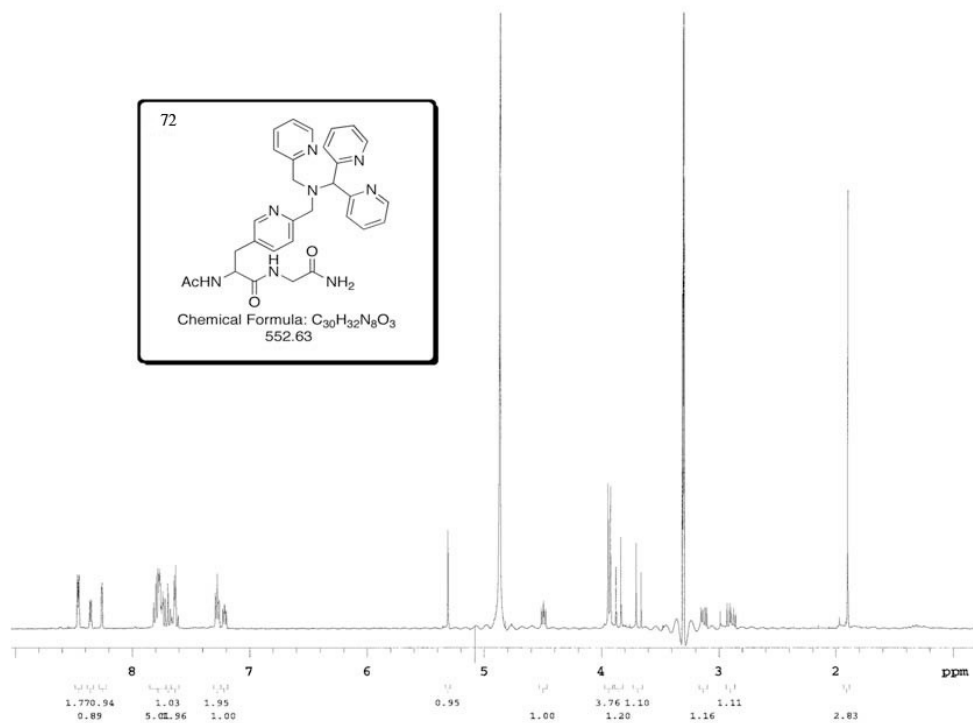
collected on a microplate reader. Cell viabilities were expressed as a percentage, with 100% equal to activity in the absence of any Ru complex.

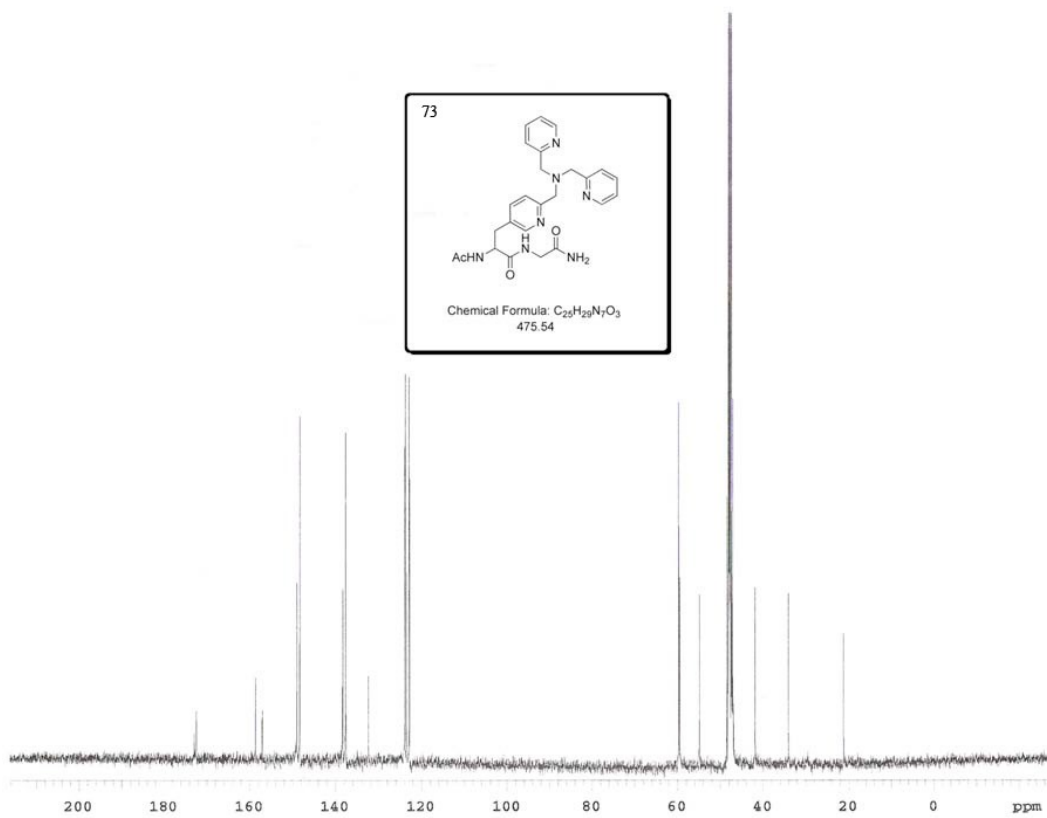
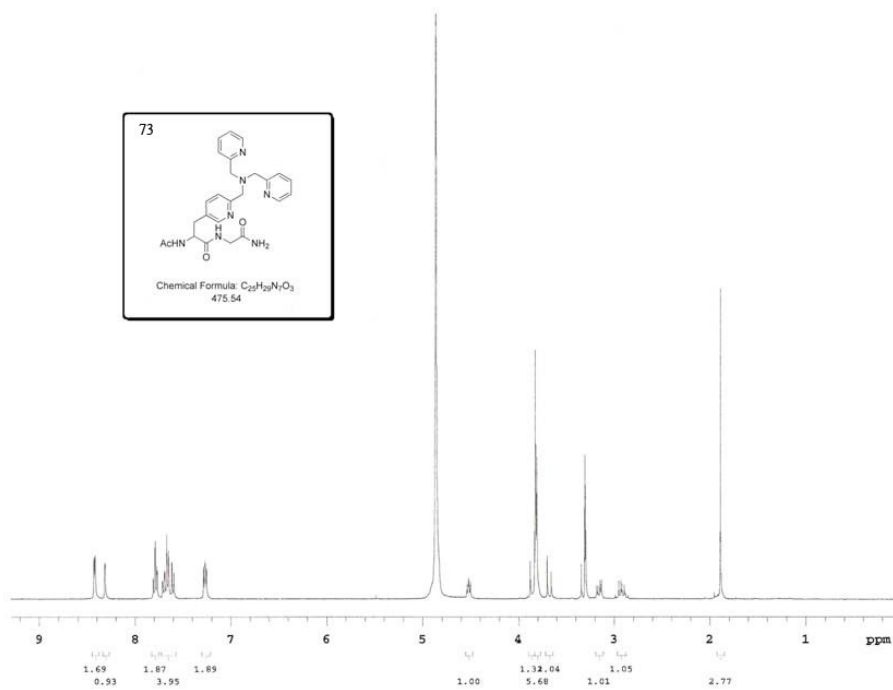
APPENDIX

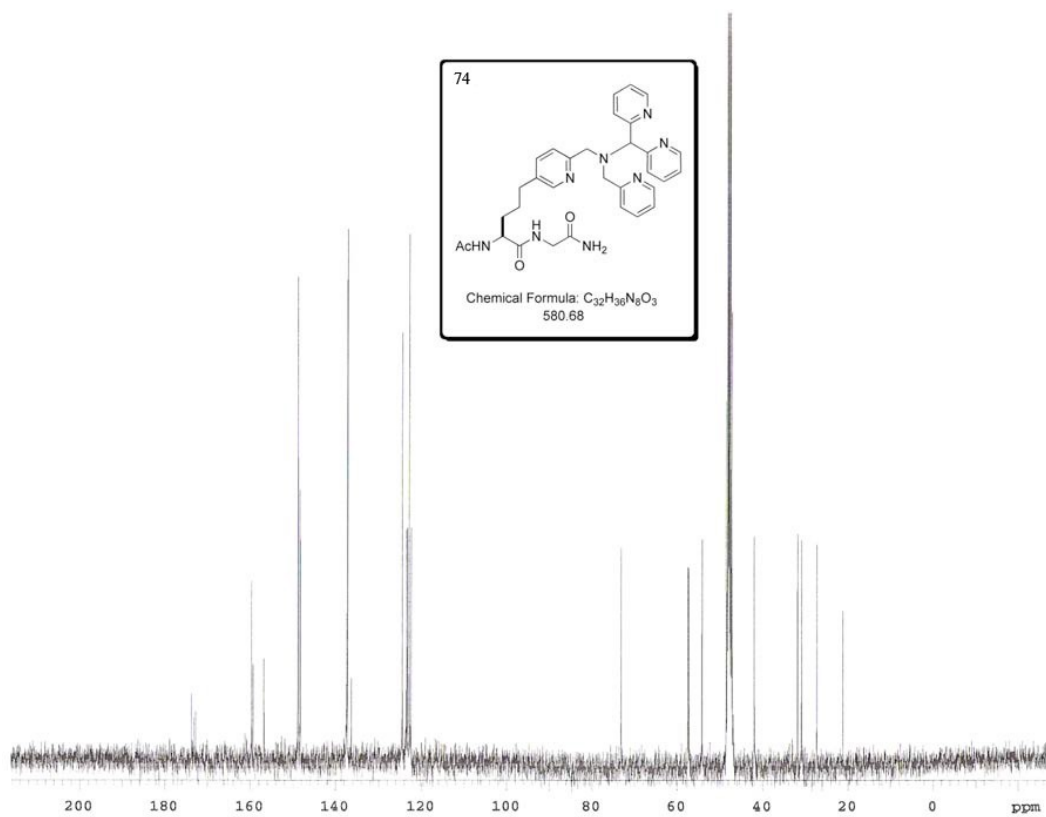
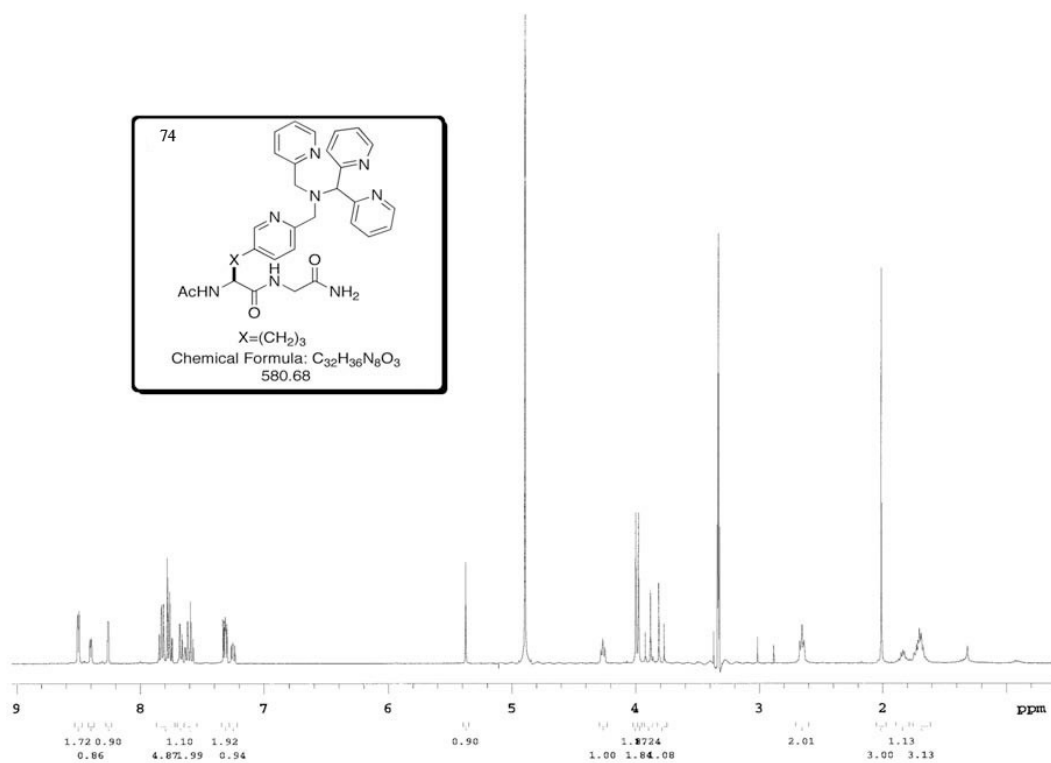


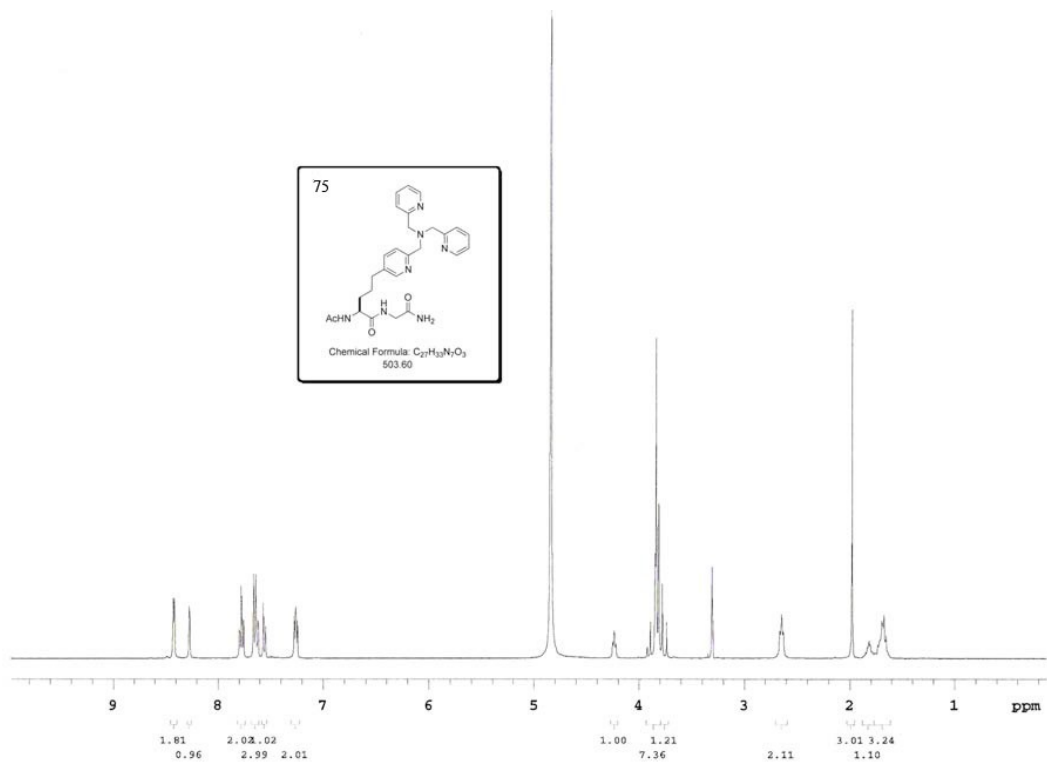
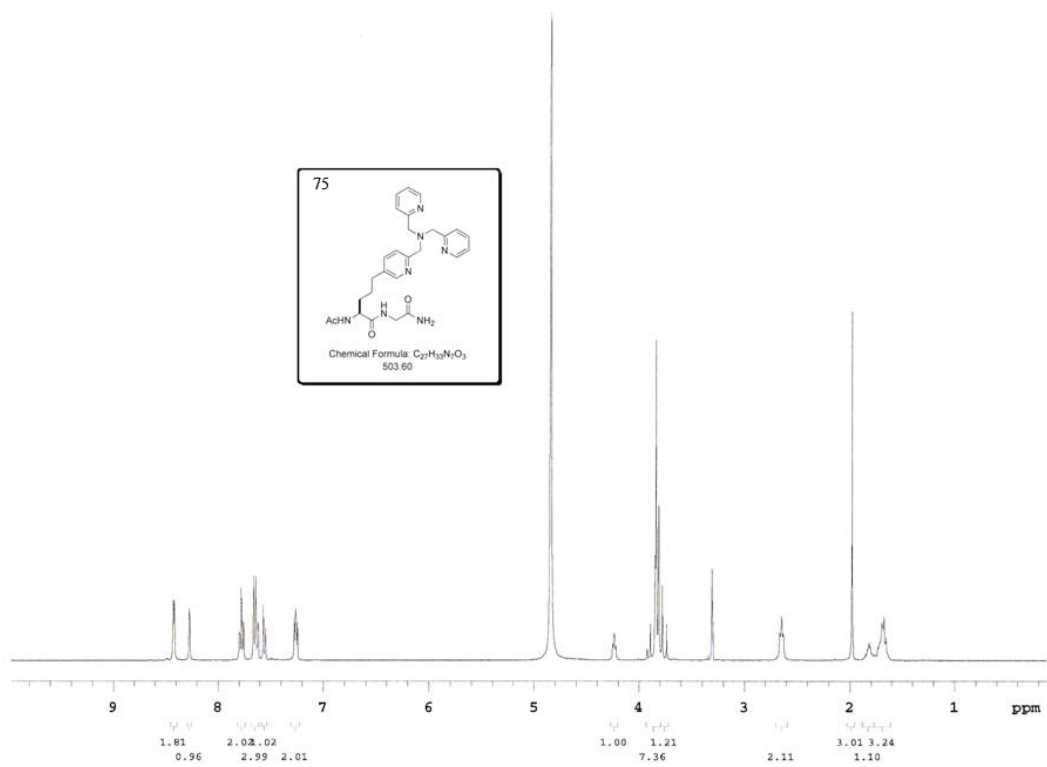


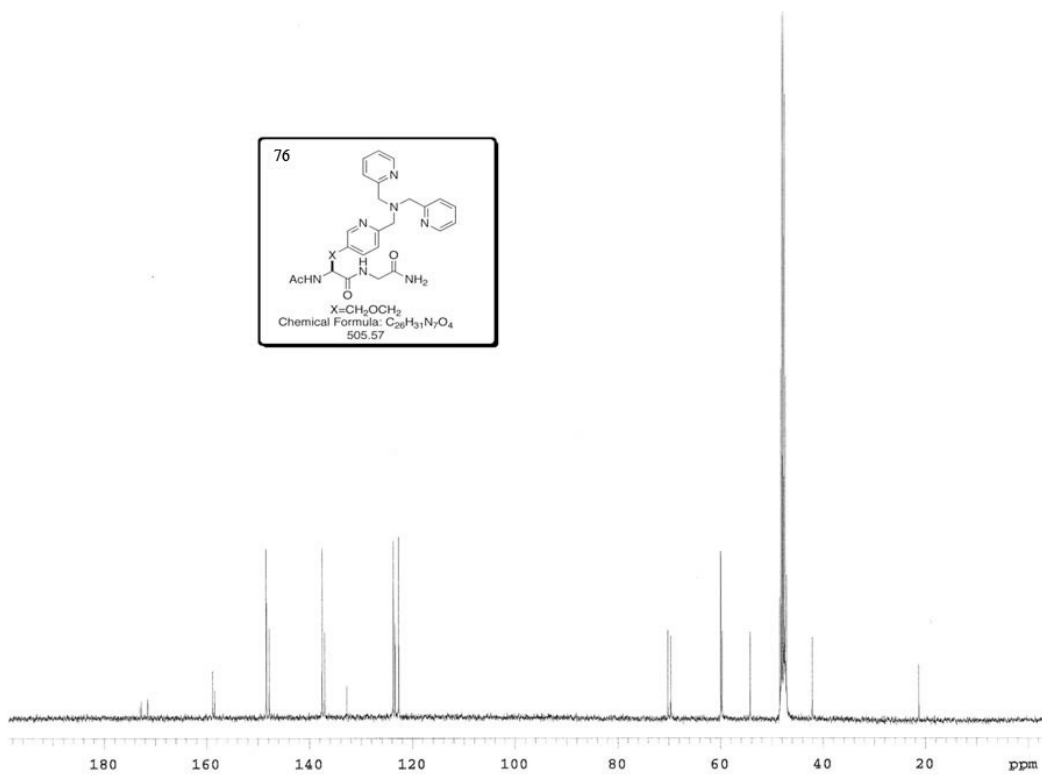
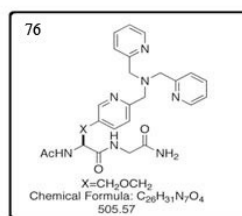
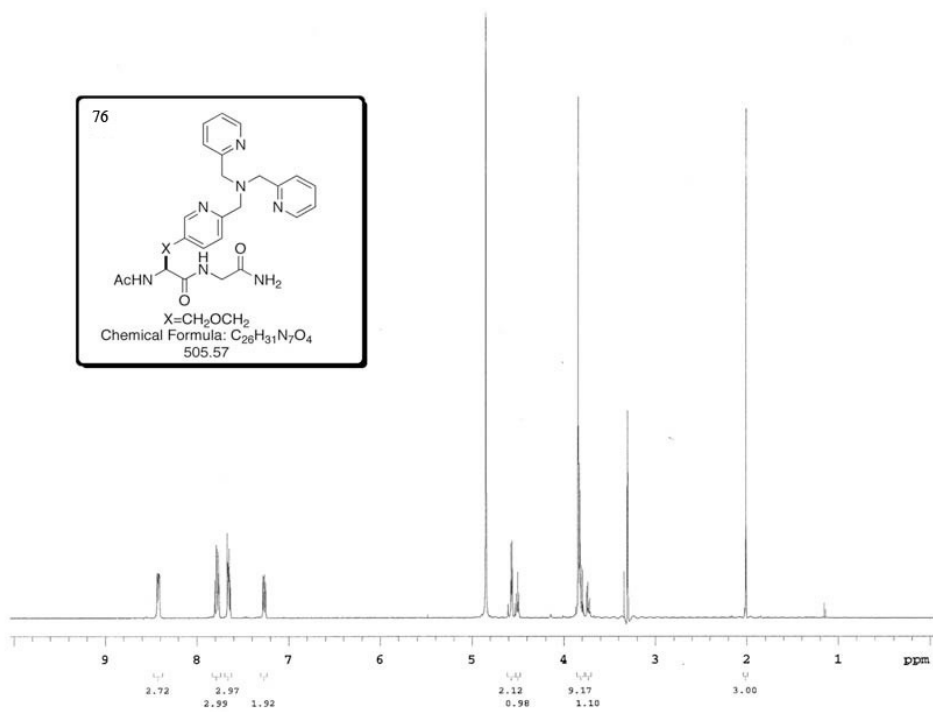
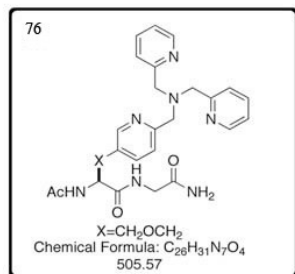


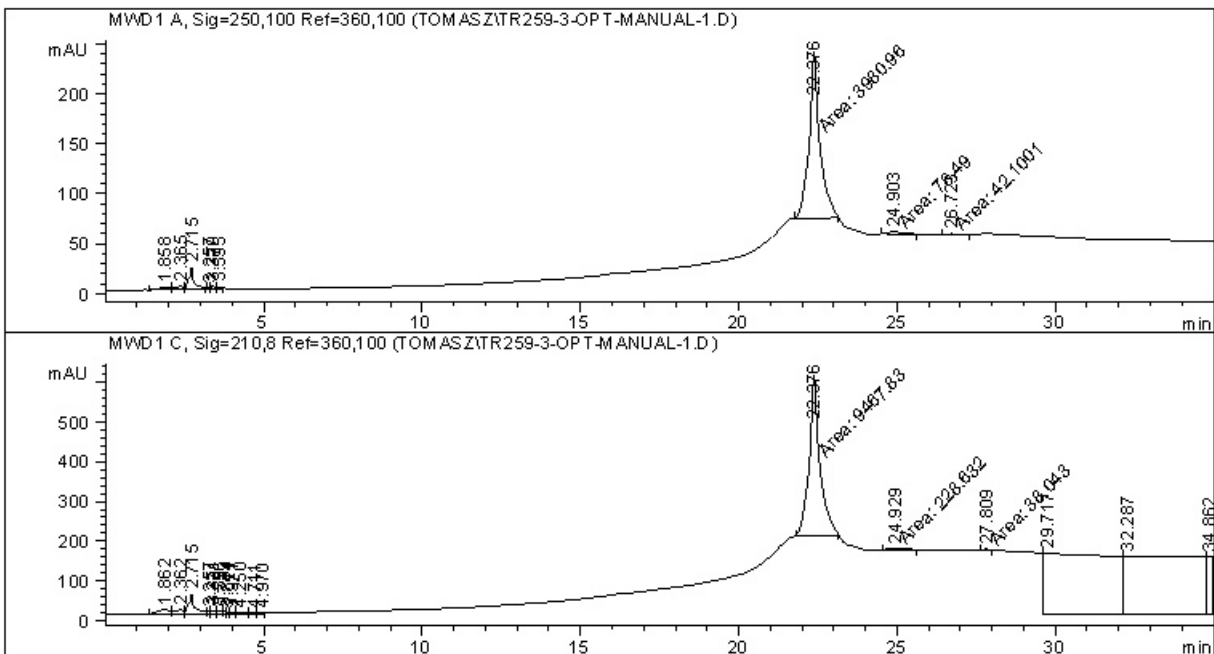
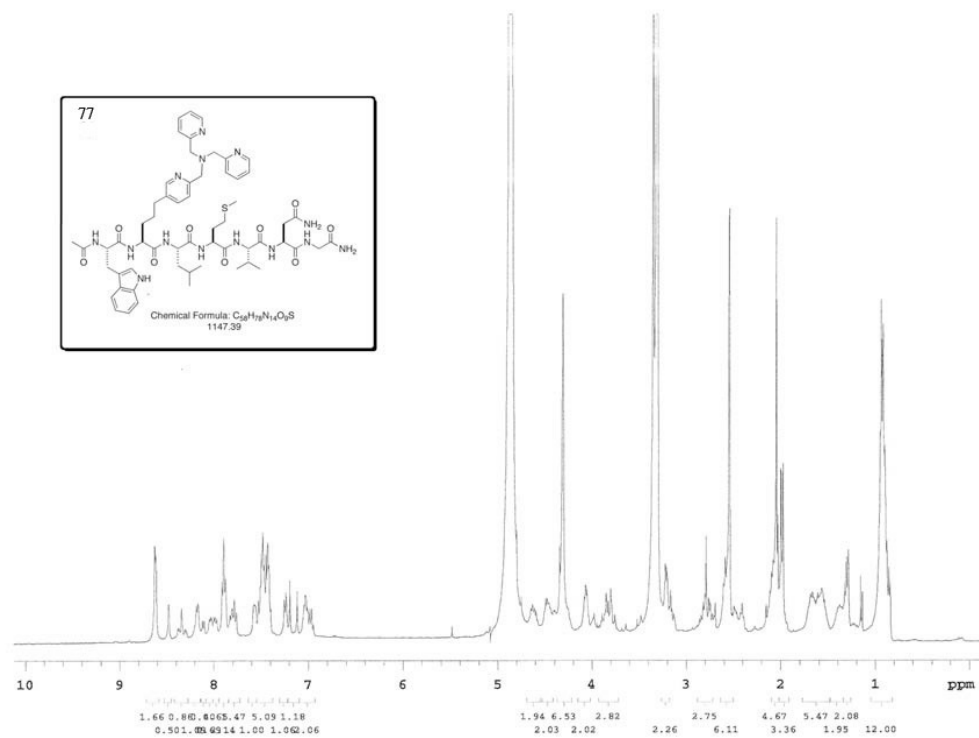




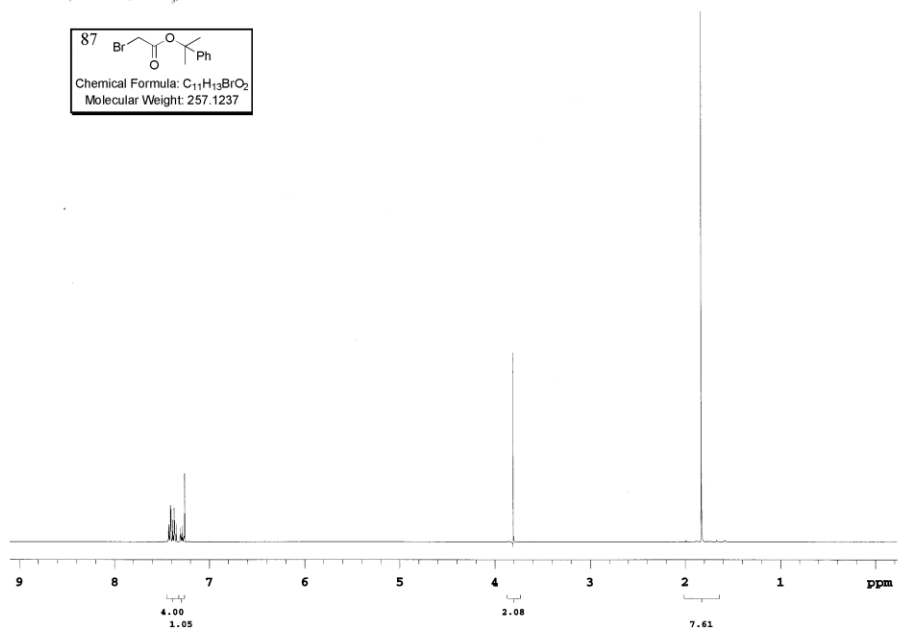
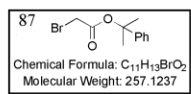
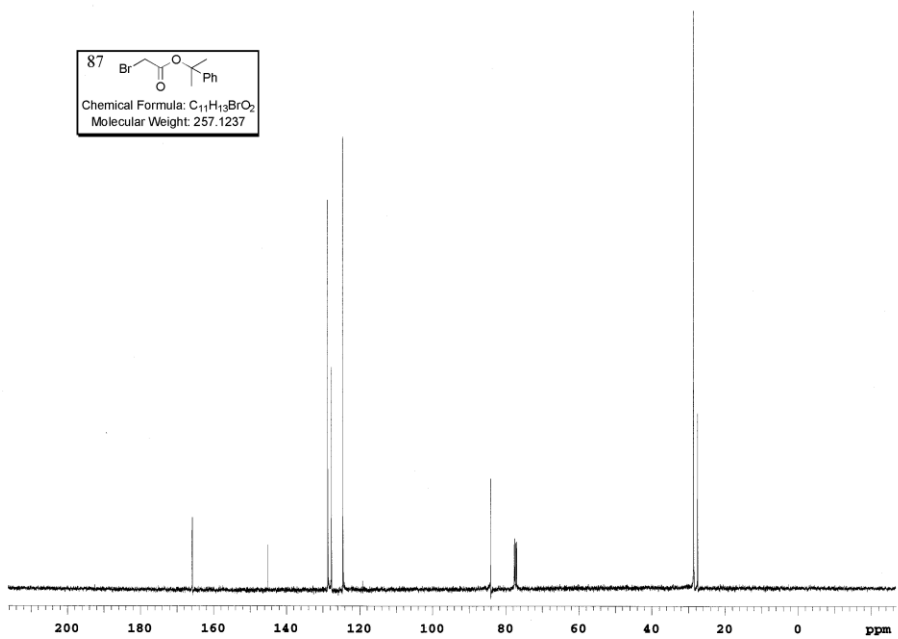
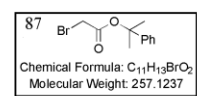


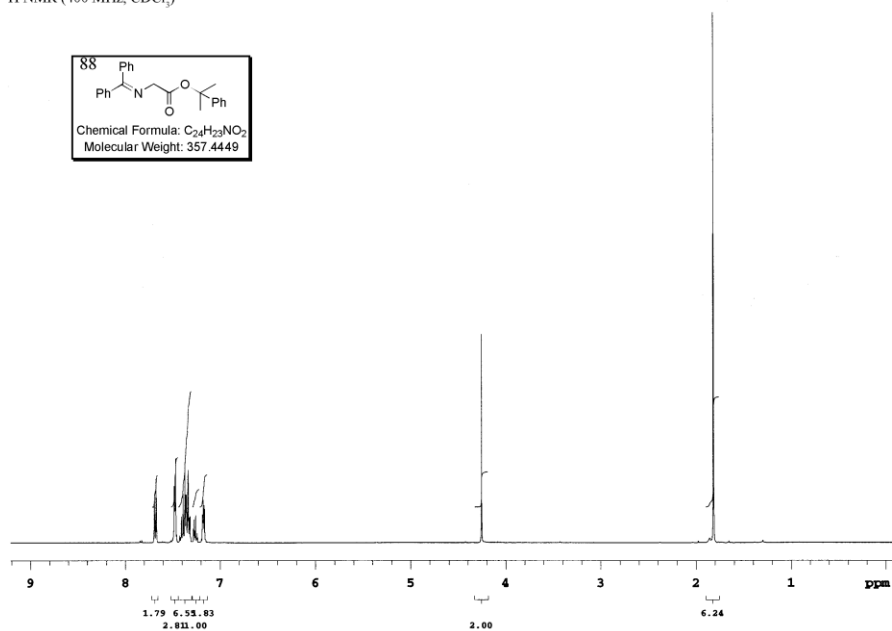
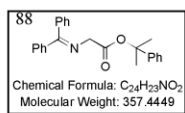
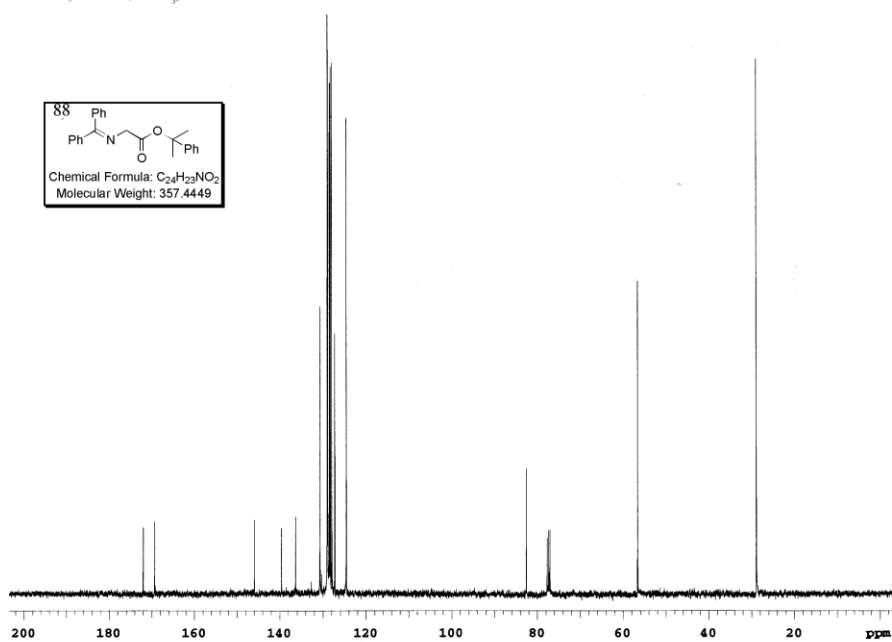
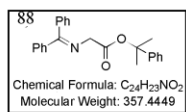


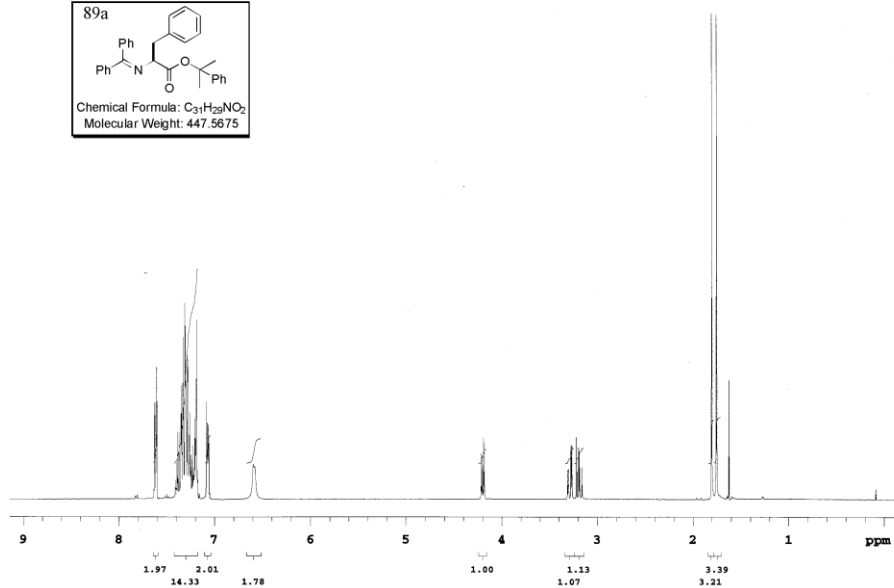
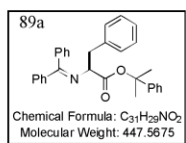
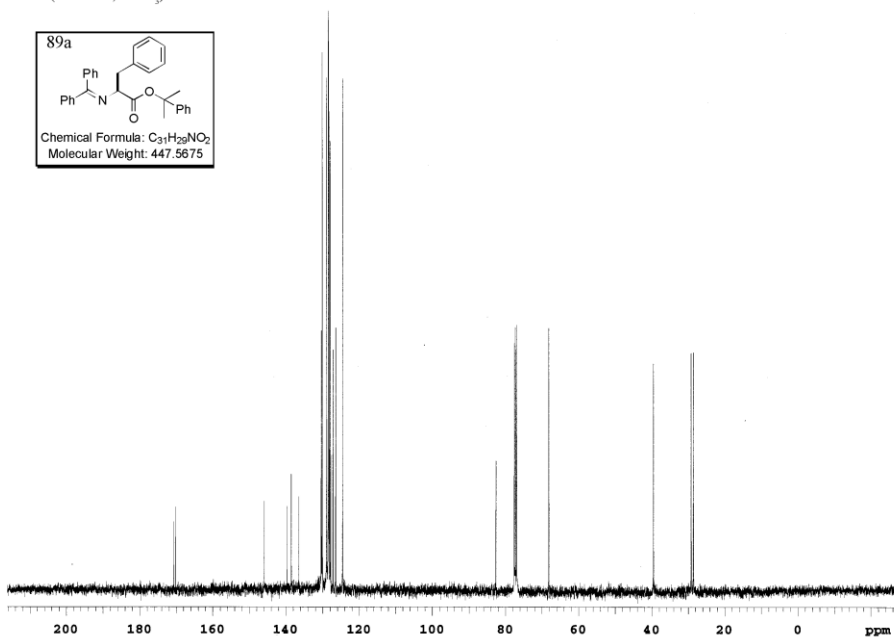
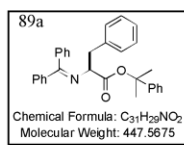


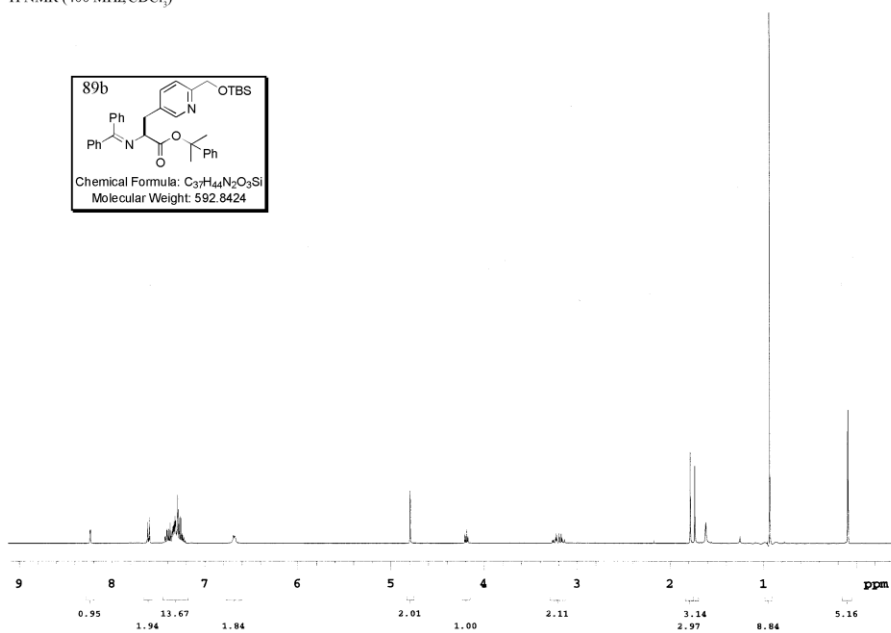
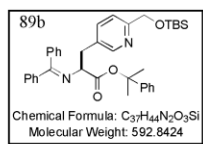
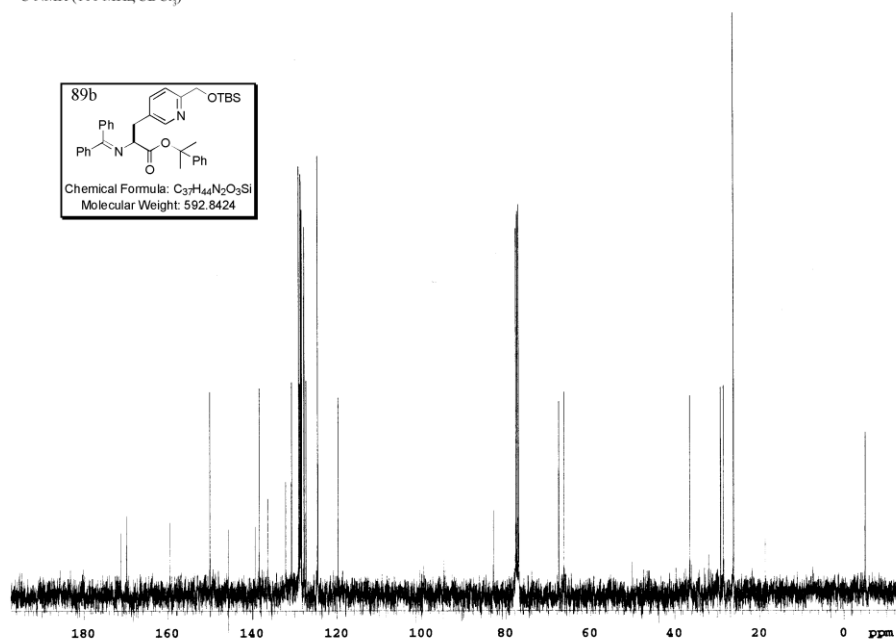
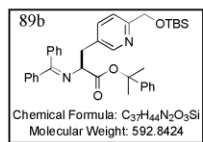


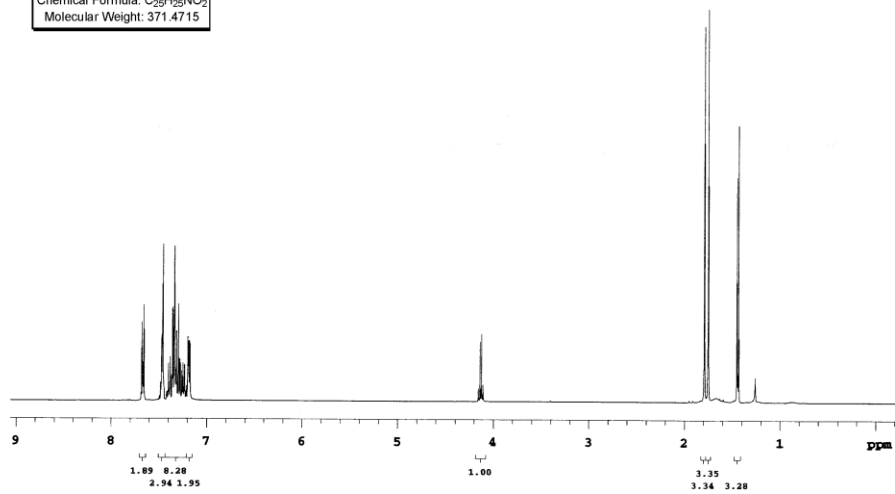
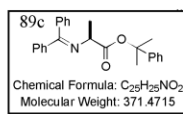
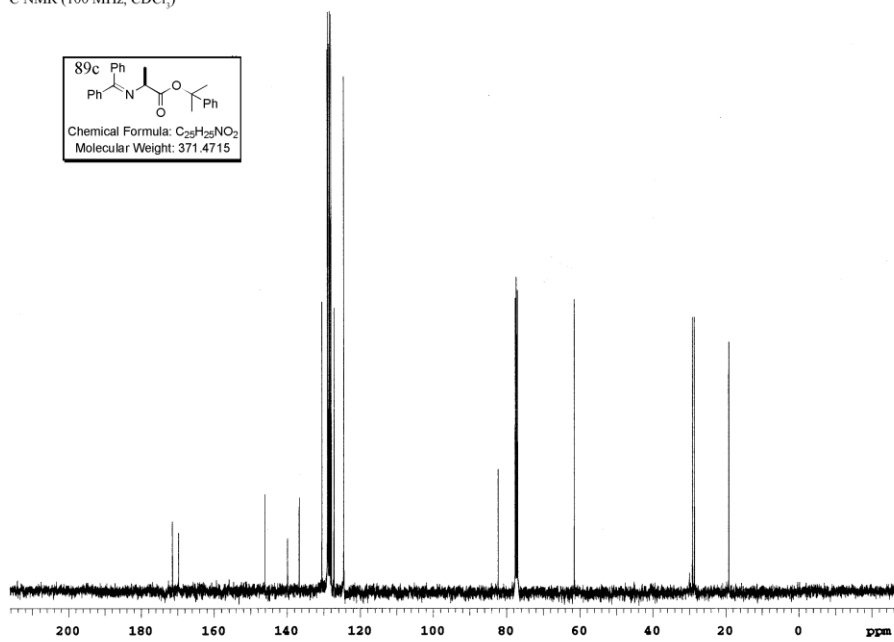
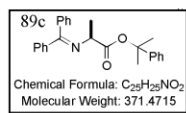
Purity of 77: HPLC chromatogram

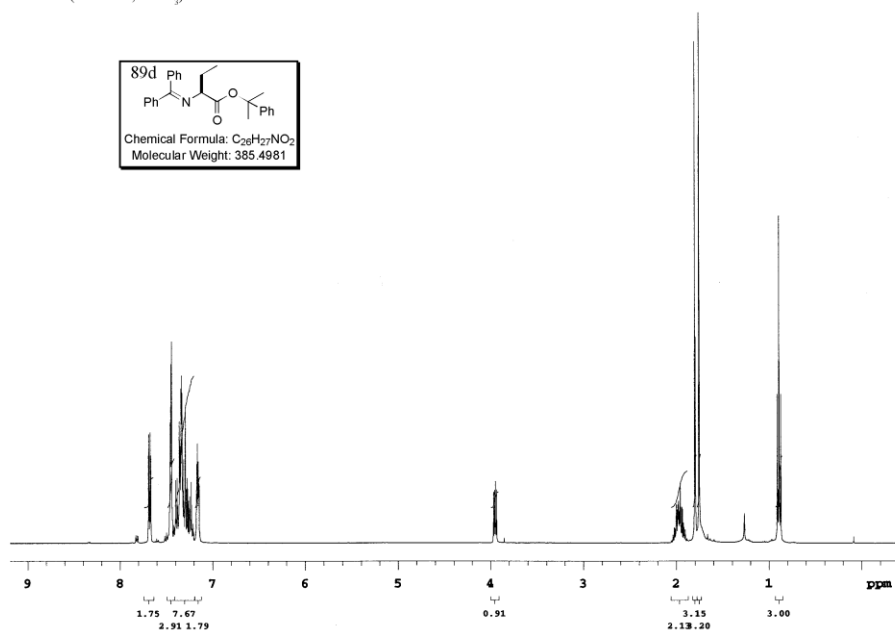
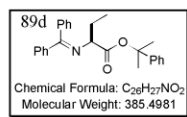
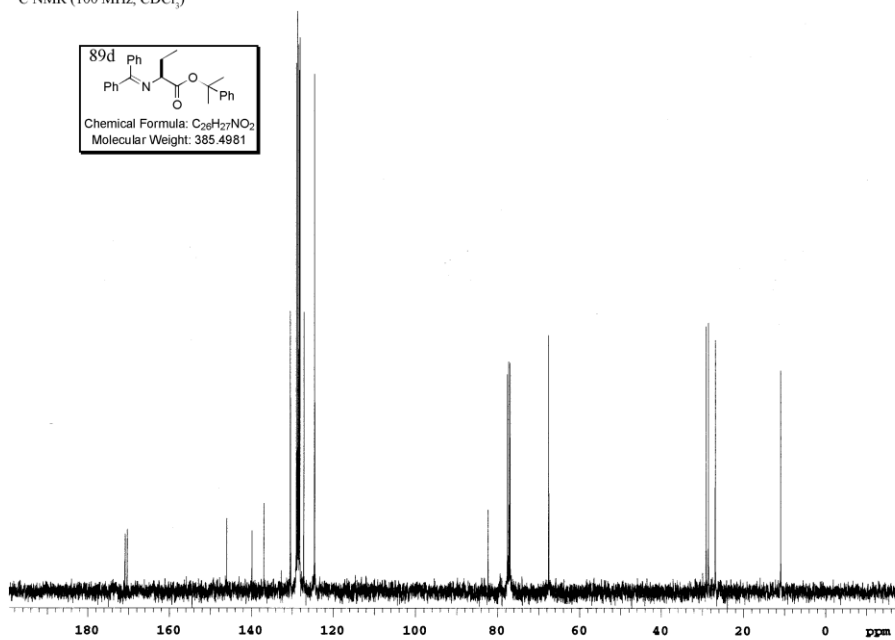
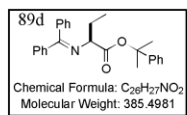
¹H NMR (400 MHz, CDCl₃)¹³C NMR (100 MHz, CDCl₃)

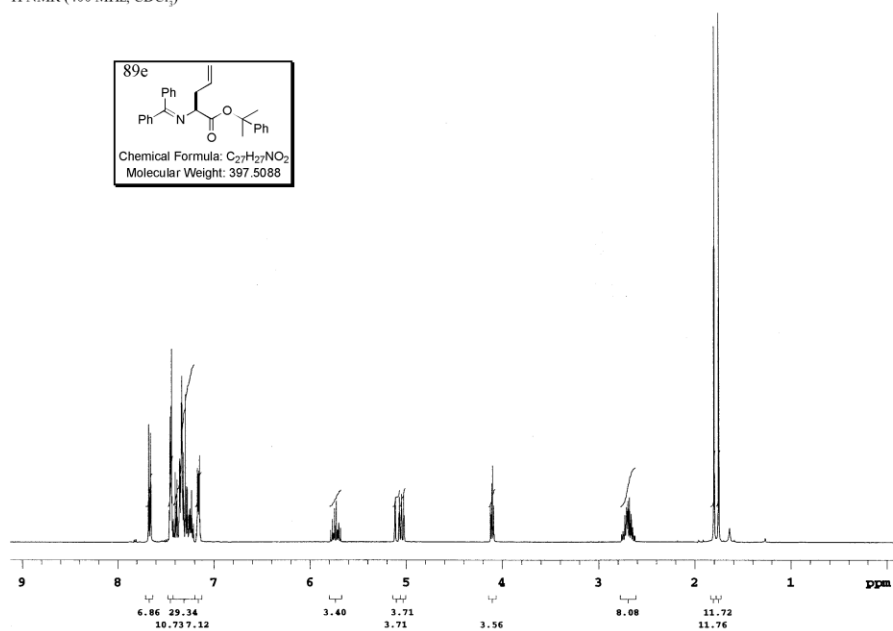
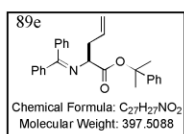
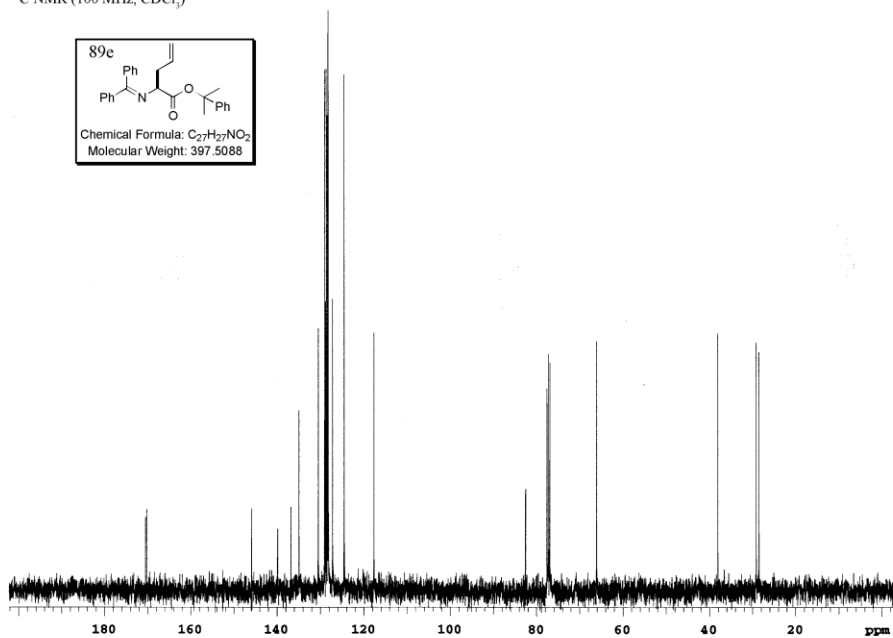
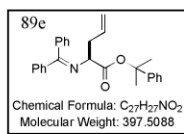
¹H NMR (400 MHz, CDCl₃)¹³C NMR (100 MHz, CDCl₃)

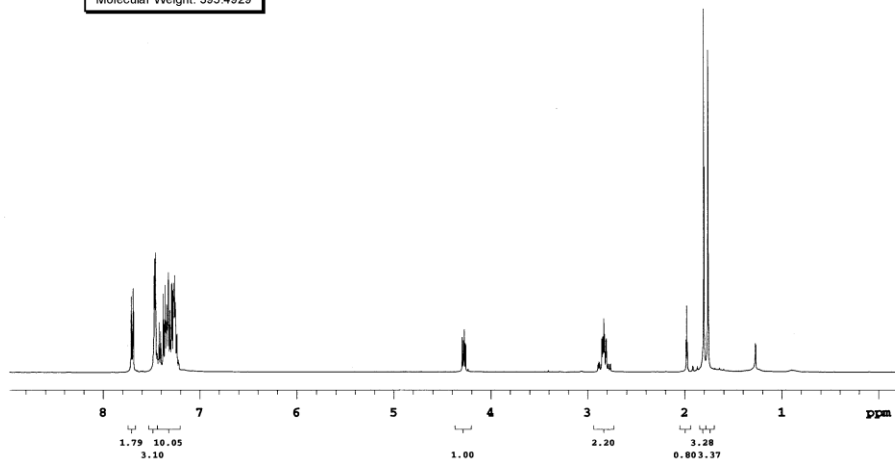
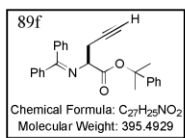
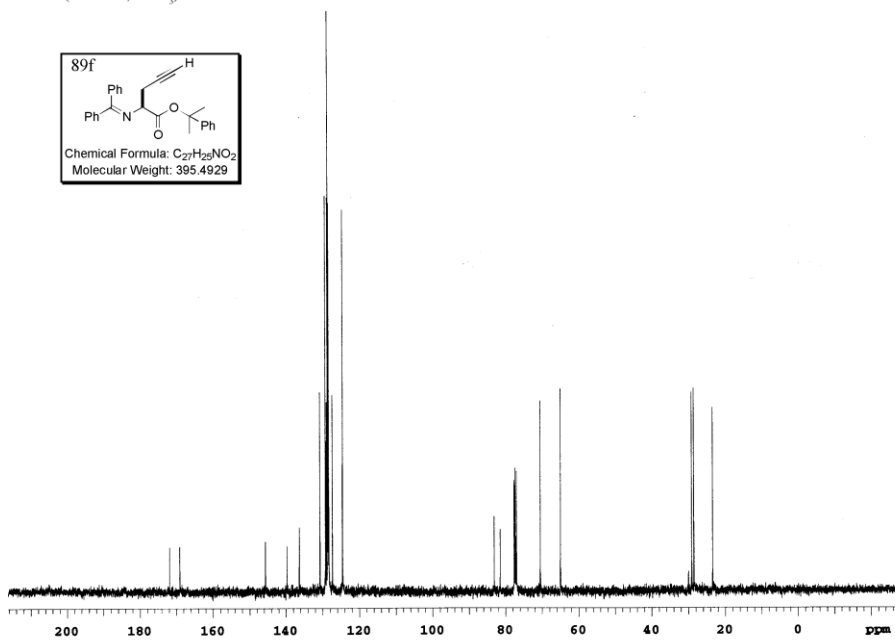
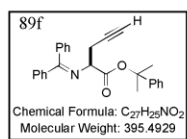
¹H NMR (400 MHz, CDCl₃)¹³C NMR (100 MHz, CDCl₃)

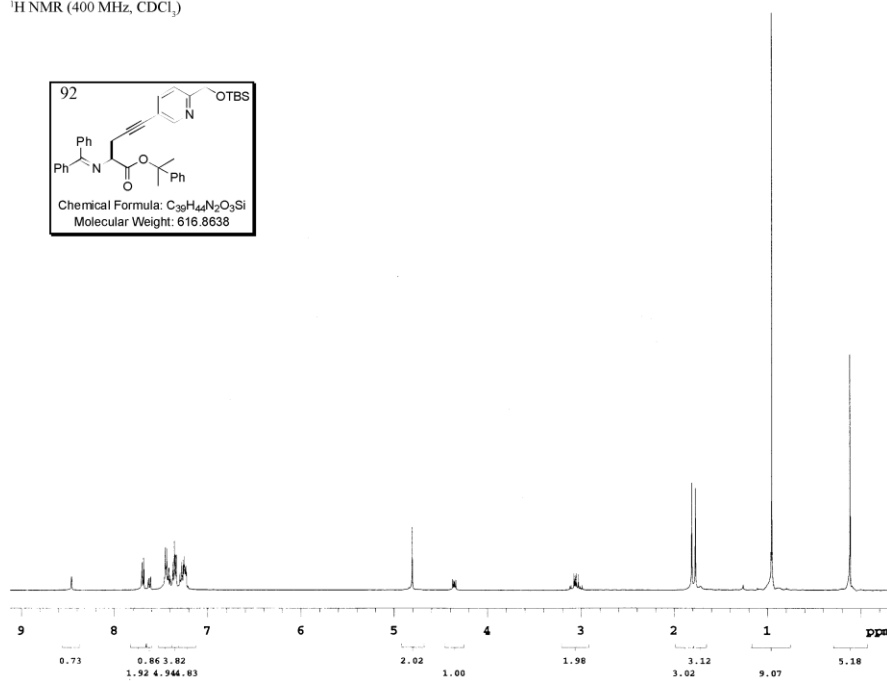
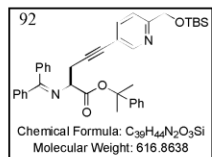
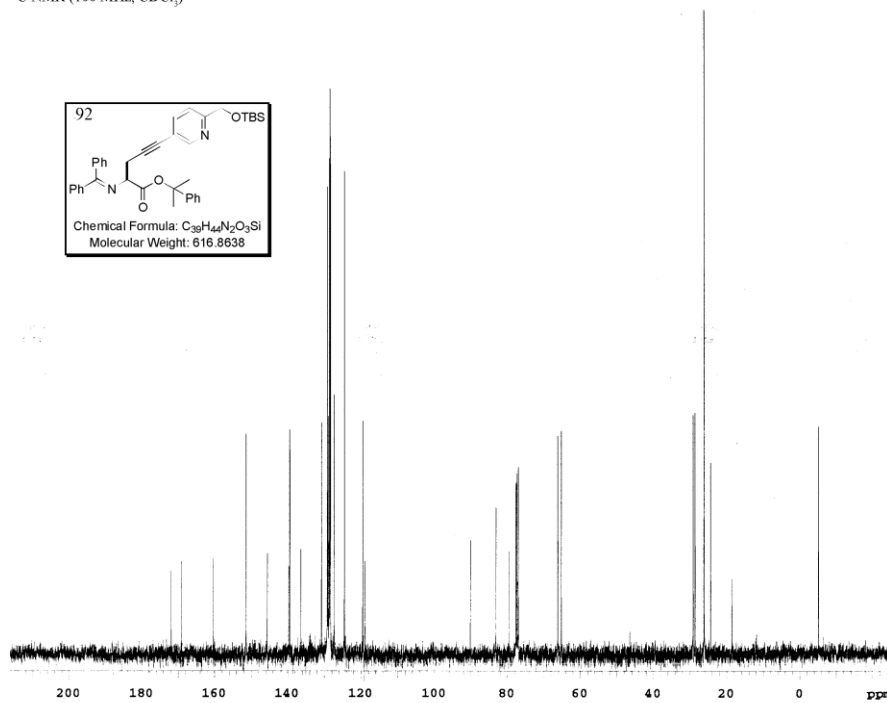
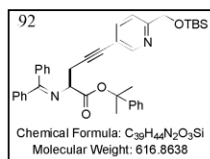
¹H NMR (400 MHz, CDCl₃)¹³C NMR (100 MHz, CDCl₃)

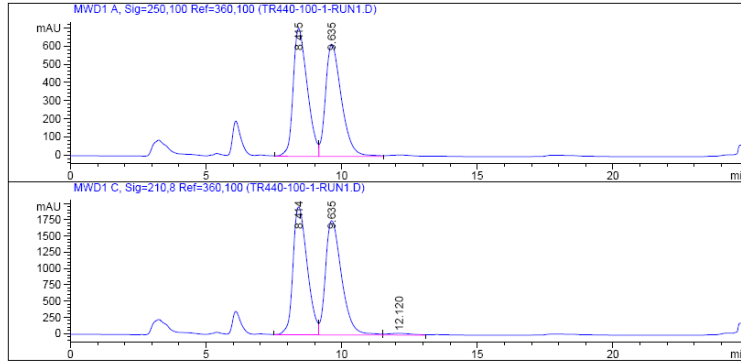
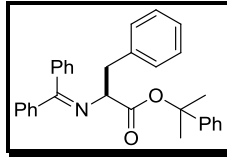
¹H NMR (400 MHz, CDCl₃)¹³C NMR (100 MHz, CDCl₃)

¹H NMR (400 MHz, CDCl₃)¹³C NMR (100 MHz, CDCl₃)

¹H NMR (400 MHz, CDCl₃)¹³C NMR (100 MHz, CDCl₃)

¹H NMR (400 MHz, CDCl₃)¹³C NMR (100 MHz, CDCl₃)

¹H NMR (400 MHz, CDCl₃)¹³C NMR (100 MHz, CDCl₃)

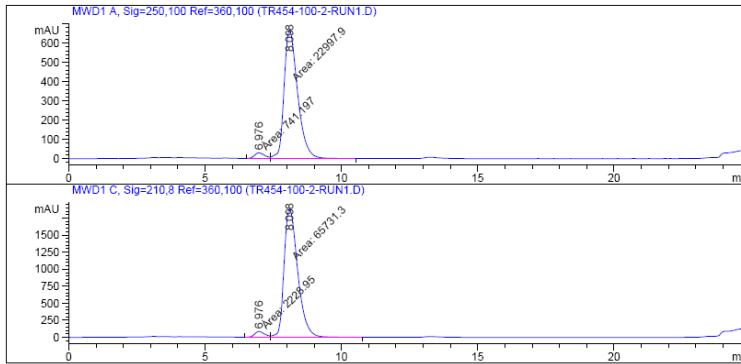
(S)-2-phenylpropan-2-yl 2-((diphenylmethylene)amino)-3-phenylpropanoate (89a) :

```

=====
                          Area Percent Report
=====
Sorted By      :      Signal
Multiplier     :      1.0000
Dilution      :      1.0000
Sample Amount  :      50.00000 [ng/ul] (not used in calc.)
Use Multiplier & Dilution Factor with ISTDs
  
```

Signal 1: MWD1 A, Sig=250,100 Ref=360,100

Peak #	RetTime [min]	Type	Width [min]	Area [mAU*s]	Height [mAU]	Area %
1	8.415	VV	0.5644	2.53885e4	704.59943	50.1218
2	9.635	VV	0.6130	2.52651e4	617.93176	49.8782



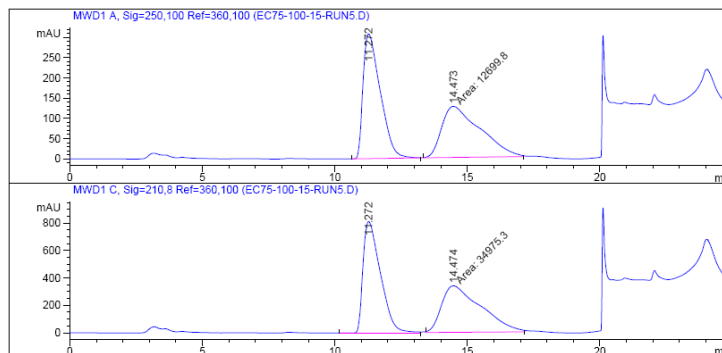
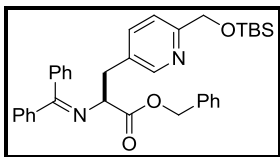
```

=====
                          Area Percent Report
=====
Sorted By      :      Signal
Multiplier     :      1.0000
Dilution      :      1.0000
Sample Amount  :      50.00000 [ng/ul] (not used in calc.)
Use Multiplier & Dilution Factor with ISTDs
  
```

Signal 1: MWD1 A, sig=250,100 Ref=360,100

Peak #	RetTime [min]	Type	Width [min]	Area [mAU*s]	Height [mAU]	Area %
1	6.976	MF	0.4229	741.19720	29.20864	3.1223
2	8.098	FM	0.5752	2.29979e4	666.39508	96.8777

**(S)-benzyl 3-(6-(((tert-butyldimethylsilyl)oxy)methyl)pyridin-3-yl)-2-
((diphenylmethylene)amino)propanoate (91) :**

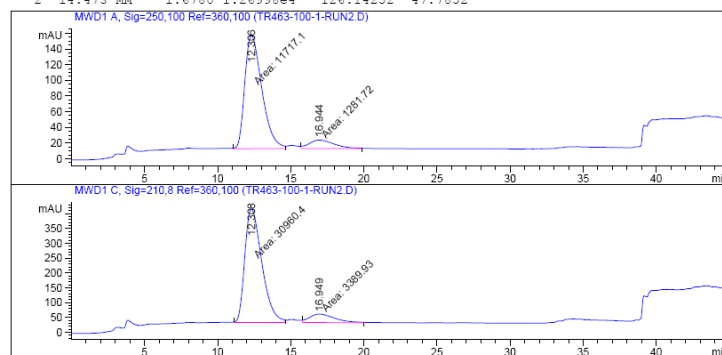


```

=====
                        Area Percent Report
=====
Sorted By      :      Signal
Multiplier    :      1.0000
Dilution      :      1.0000
Sample Amount  :      50.00000 [ng/ul] (not used in calc.)
Use Multiplier & Dilution Factor with ISTDs
  
```

Signal 1: MWD1 A, Sig=250,100 Ref=360,100

Peak #	RetTime [min]	Type	Width [min]	Area [mAU*s]	Height [mAU]	Area %
1	11.272	BB	0.6900	1.38770e4	307.77429	52.2148
2	14.473	MN	1.6780	1.26999e4	126.14252	47.7852



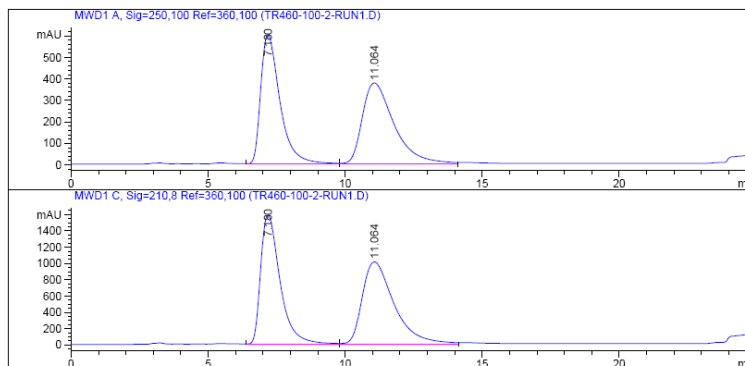
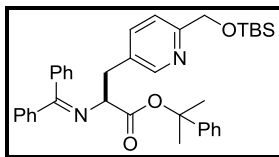
```

=====
                        Area Percent Report
=====
Sorted By      :      Signal
Multiplier    :      1.0000
Dilution      :      1.0000
Sample Amount  :      50.00000 [ng/ul] (not used in calc.)
Use Multiplier & Dilution Factor with ISTDs
  
```

Signal 1: MWD1 A, Sig=250,100 Ref=360,100

Peak #	RetTime [min]	Type	Width [min]	Area [mAU*s]	Height [mAU]	Area %
1	12.306	MF	1.3516	1.17171e4	144.48506	90.1398
2	16.944	FM	1.9785	1281.71692	10.79684	9.8602

(S)-2-phenylpropan-2-yl 3-(6-(((tert-butyldimethylsilyl)oxy)methyl)pyridin-3-yl)-2-((diphenylmethylene)amino)propanoate (89b) :

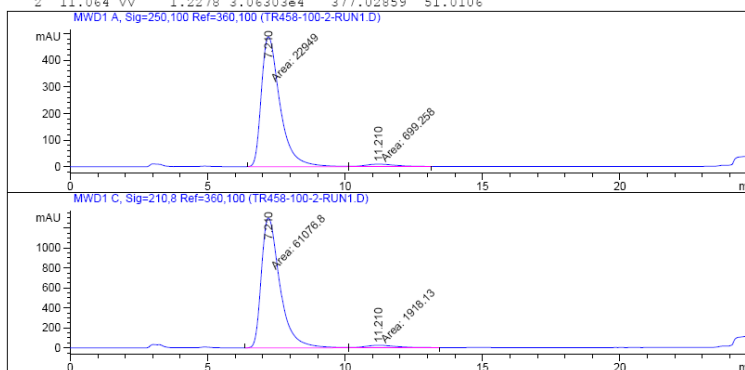


```

=====
                          Area Percent Report
=====
Sorted By      :      Signal
Multiplier     :      1.0000
Dilution      :      1.0000
Sample Amount  :      50.00000 [ng/ul] (not used in calc.)
Use Multiplier & Dilution Factor with ISTDs
  
```

Signal 1: MWD1 A, Sig=250,100 Ref=360,100

Peak #	RetTime [min]	Type	Width [min]	Area [mAU*s]	Height [mAU]	Area %
1	7.180	VV	0.7465	2.94167e4	601.60315	48.9894
2	11.064	VV	1.2278	3.06303e4	377.02859	51.0106

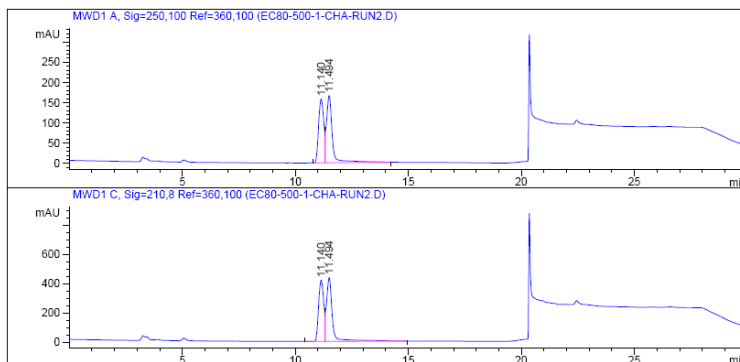
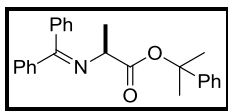


```

=====
                          Area Percent Report
=====
Sorted By      :      Signal
Multiplier     :      1.0000
Dilution      :      1.0000
Sample Amount  :      50.00000 [ng/ul] (not used in calc.)
Use Multiplier & Dilution Factor with ISTDs
  
```

Signal 1: MWD1 A, sig=250,100 Ref=360,100

Peak #	RetTime [min]	Type	Width [min]	Area [mAU*s]	Height [mAU]	Area %
1	7.210	MF	0.7826	2.29490e4	488.74872	97.0431
2	11.210	FM	1.2771	699.25775	9.12578	2.9569

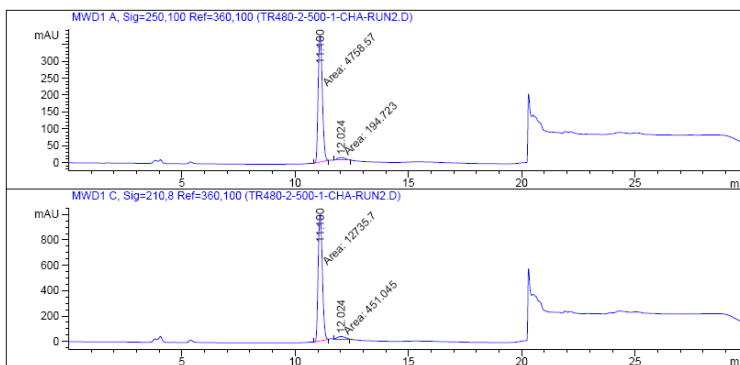
(S)-2-phenylpropan-2-yl 2-((diphenylmethylene)amino)propanoate (89c):

```

=====
                          Area Percent Report
=====
Sorted By      :      Signal
Multiplier     :      1.0000
Dilution      :      1.0000
Sample Amount  :      50.00000 [ng/ul] (not used in calc.)
Use Multiplier & Dilution Factor with ISTDs
  
```

Signal 1: MWD1 A, Sig=250,100 Ref=360,100

Peak #	RetTime [min]	Type	Width [min]	Area [mAU*s]	Height [mAU]	Area %
1	11.140	BV	0.2512	2450.17700	157.71756	44.7847
2	11.494	VB	0.2644	3020.84131	165.94911	55.2153

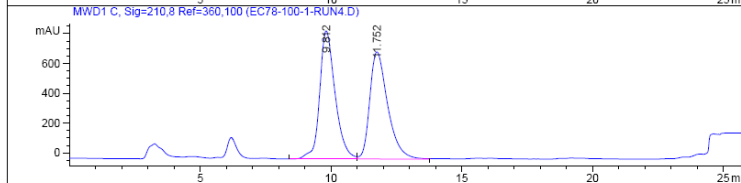
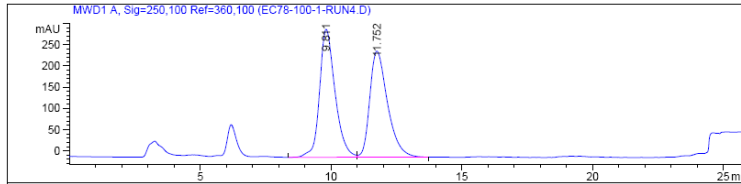
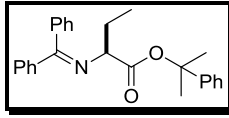


```

=====
                          Area Percent Report
=====
Sorted By      :      Signal
Multiplier     :      1.0000
Dilution      :      1.0000
Sample Amount  :      50.00000 [ng/ul] (not used in calc.)
Use Multiplier & Dilution Factor with ISTDs
  
```

Signal 1: MWD1 A, Sig=250,100 Ref=360,100

Peak #	RetTime [min]	Type	Width [min]	Area [mAU*s]	Height [mAU]	Area %
1	11.100	MM	0.2122	4758.56787	373.75891	96.0688
2	12.024	MM	0.4131	194.72266	7.85543	3.9312

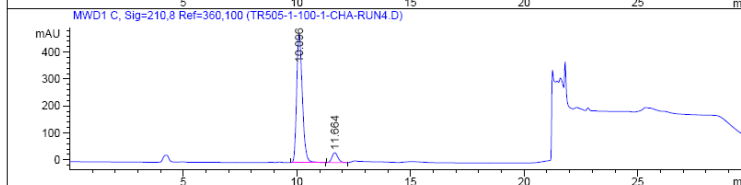
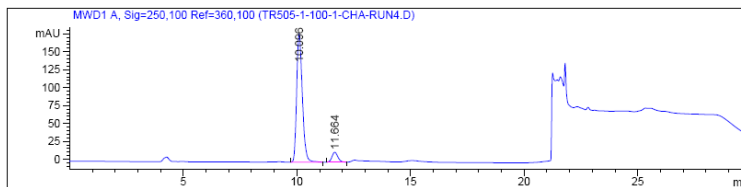
(S)-2-phenylpropan-2-yl 2-((diphenylmethylene)amino)butanoate (89d):

=====
 Area Percent Report
 =====

Sorted By : Signal
 Multiplier : 1.0000
 Dilution : 1.0000
 Sample Amount : 50.00000 [ng/ul] (not used in calc.)
 Use Multiplier & Dilution Factor with ISTDs

Signal 1: MWD1 A, Sig=250,100 Ref=360,100

Peak #	RetTime [min]	Type	Width [min]	Area [mAU*s]	Height [mAU]	Area %
1	9.811	VV	0.6124	1.23977e4	301.06070	51.2681
2	11.752	VB	0.7067	1.17844e4	249.67369	48.7319

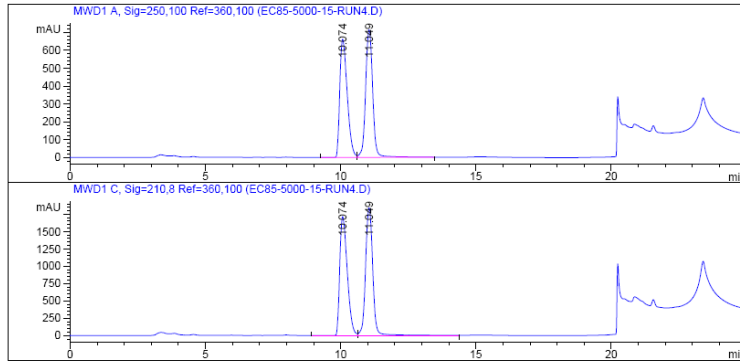
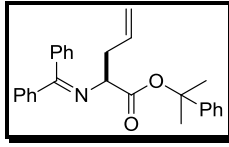


=====
 Area Percent Report
 =====

Sorted By : Signal
 Multiplier : 1.0000
 Dilution : 1.0000
 Sample Amount : 50.00000 [ng/ul] (not used in calc.)
 Use Multiplier & Dilution Factor with ISTDs

Signal 1: MWD1 A, Sig=250,100 Ref=360,100

Peak #	RetTime [min]	Type	Width [min]	Area [mAU*s]	Height [mAU]	Area %
1	10.096	BB	0.2684	3104.37109	178.95375	92.7437
2	11.664	BB	0.2772	242.88545	13.67393	7.2563

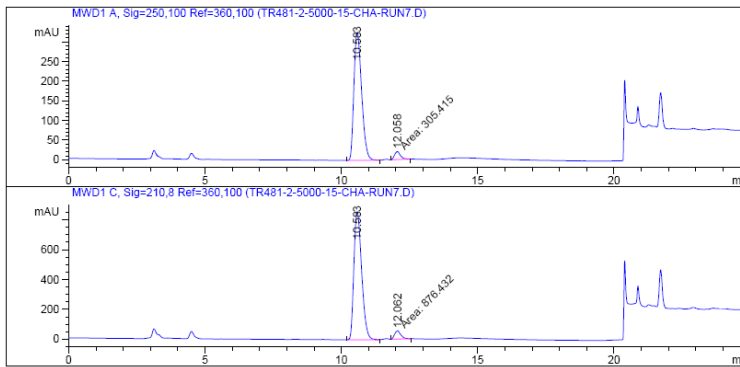
(S)-2-phenylpropan-2-yl 2-((diphenylmethylene)amino)pent-4-enoate (89e) :

```

=====
                          Area Percent Report
=====
Sorted By      :      Signal
Multiplier    :      1.0000
Dilution      :      1.0000
Sample Amount :      50.00000 [ng/ul] (not used in calc.)
Use Multiplier & Dilution Factor with ISTDs
  
```

Signal 1: MWD1 A, Sig=250,100 Ref=360,100

Peak #	RetTime [min]	Type	Width [min]	Area [mAU*s]	Height [mAU]	Area %
1	10.074	BV	0.2960	1.25991e4	662.02496	49.1652
2	11.049	VB	0.2847	1.30269e4	714.62256	50.8348

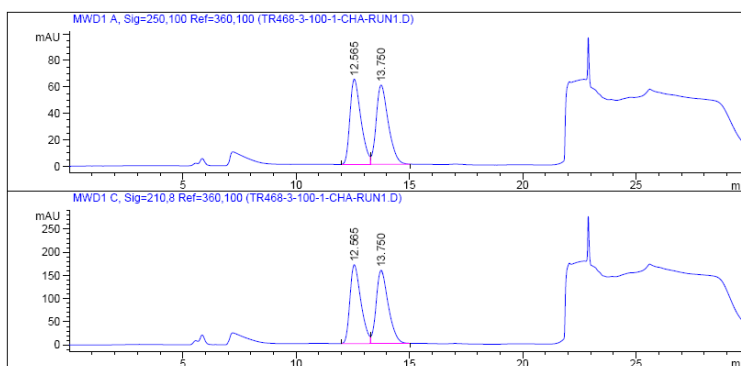
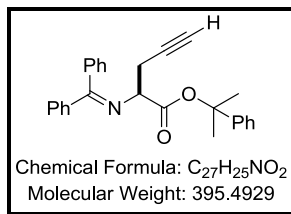


```

=====
                          Area Percent Report
=====
Sorted By      :      Signal
Multiplier    :      1.0000
Dilution      :      1.0000
Sample Amount :      50.00000 [ng/ul] (not used in calc.)
Use Multiplier & Dilution Factor with ISTDs
  
```

Signal 1: MWD1 A, Sig=250,100 Ref=360,100

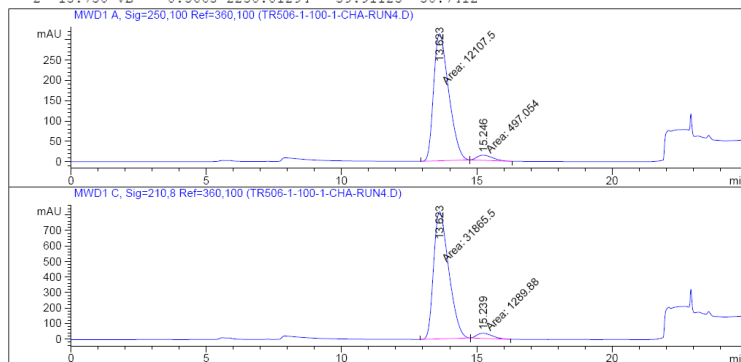
Peak #	RetTime [min]	Type	Width [min]	Area [mAU*s]	Height [mAU]	Area %
1	10.583	BV	0.3070	6401.47363	326.13348	95.4463
2	12.058	NM	0.2488	305.41464	20.46243	4.5537

(S)-2-phenylpropan-2-yl 2-((diphenylmethylene)amino)pent-4-ynoate (89f) :=====
Area Percent Report
=====

Sorted By : Signal
Multiplier : 1.0000
Dilution : 1.0000
Sample Amount : 50.00000 [ng/ul] (not used in calc.)
Use Multiplier & Dilution Factor with ISTDs

Signal 1: MWD1 A, Sig=250,100 Ref=360,100

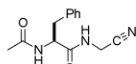
Peak #	RetTime [min]	Type	Width [min]	Area [mAU*s]	Height [mAU]	Area %
1	12.565	BV	0.5123	2164.85962	64.38284	49.2588
2	13.750	VB	0.5663	2230.01294	59.91125	50.7412

=====
Area Percent Report
=====

Sorted By : Signal
Multiplier : 1.0000
Dilution : 1.0000
Sample Amount : 50.00000 [ng/ul] (not used in calc.)
Use Multiplier & Dilution Factor with ISTDs

Signal 1: MWD1 A, Sig=250,100 Ref=360,100

Peak #	RetTime [min]	Type	Width [min]	Area [mAU*s]	Height [mAU]	Area %
1	13.623	MM	0.6467	1.21075e4	312.01645	96.0565
2	15.246	MM	0.6549	497.05380	12.64924	3.9435

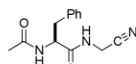
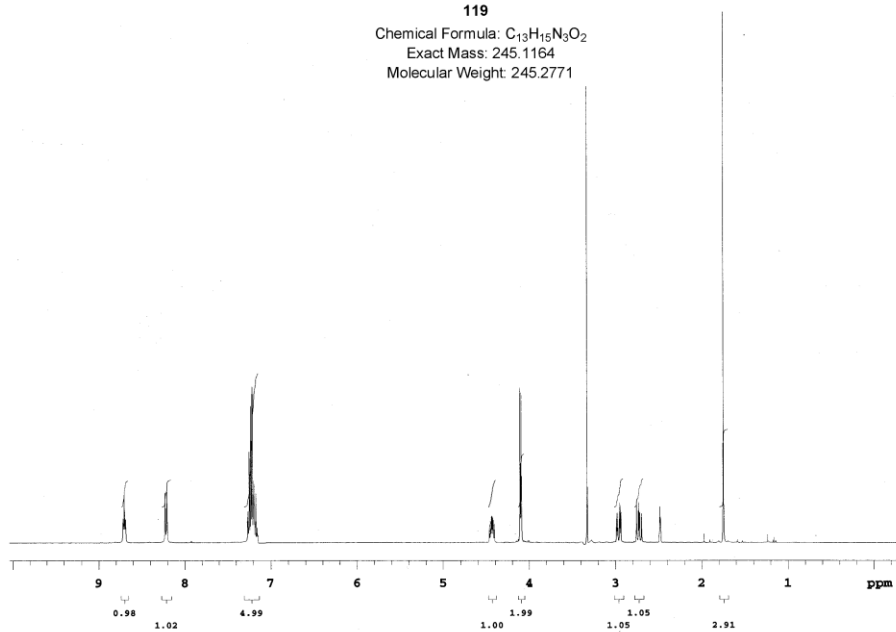


119

Chemical Formula: C₁₃H₁₅N₃O₂

Exact Mass: 245.1164

Molecular Weight: 245.2771

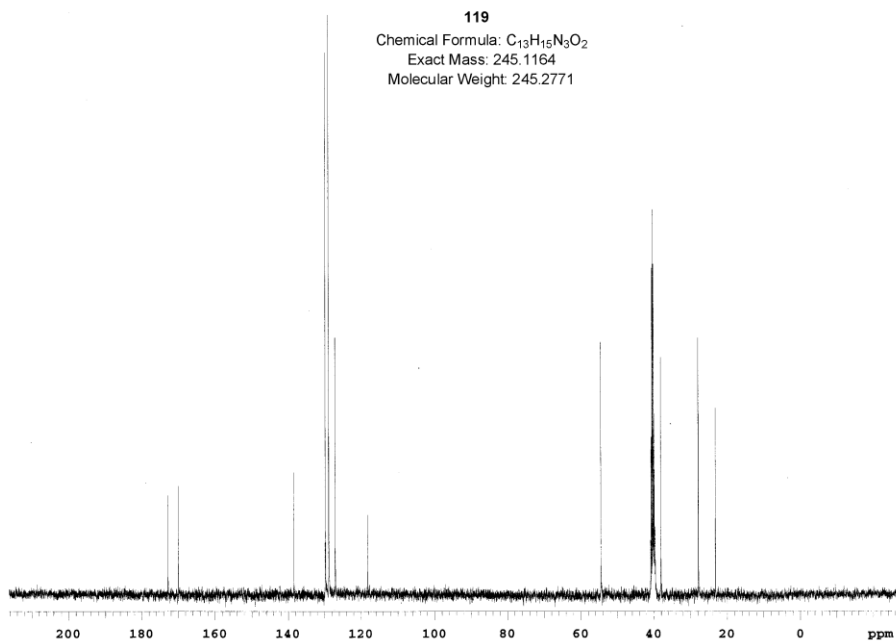


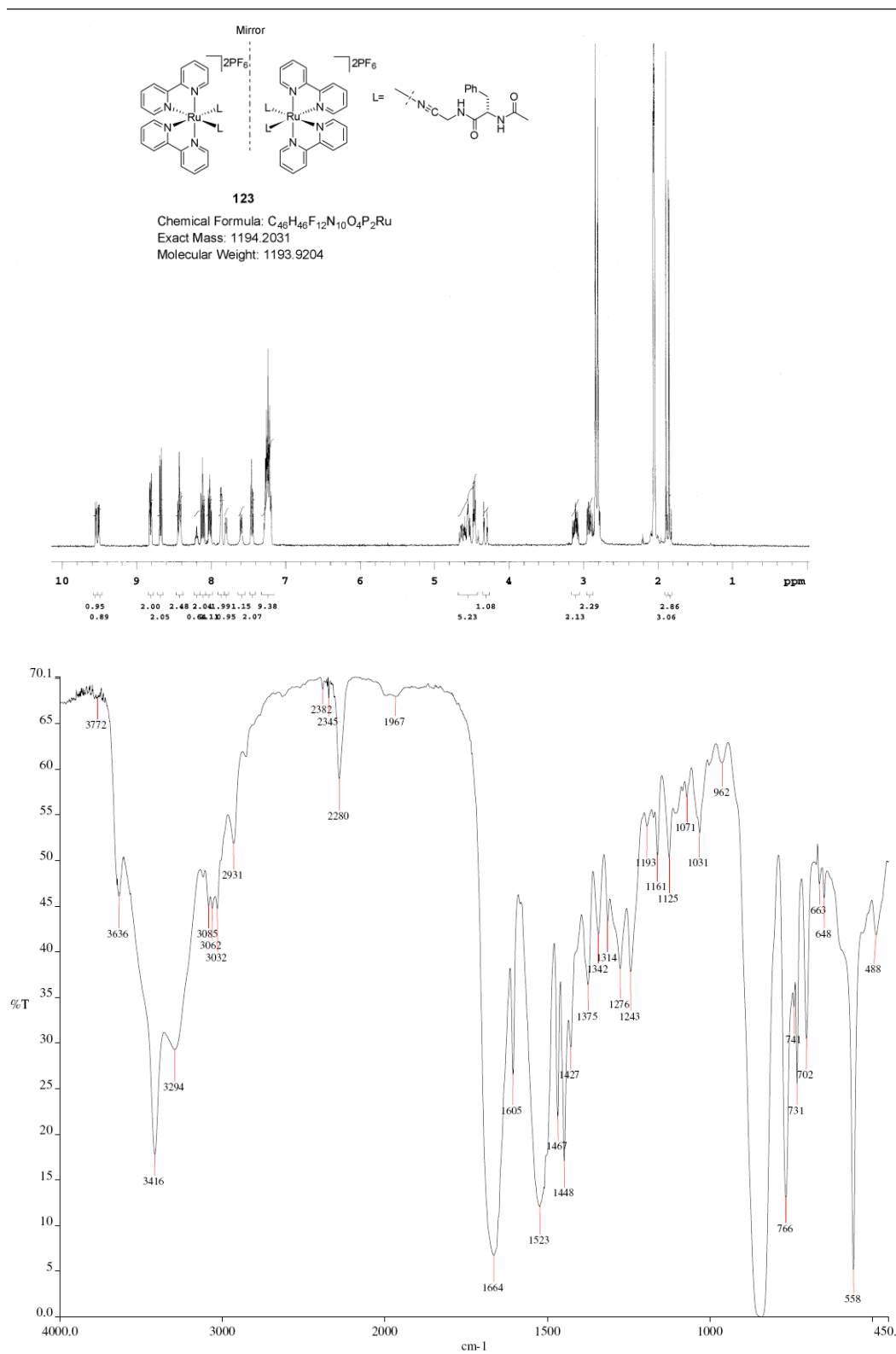
119

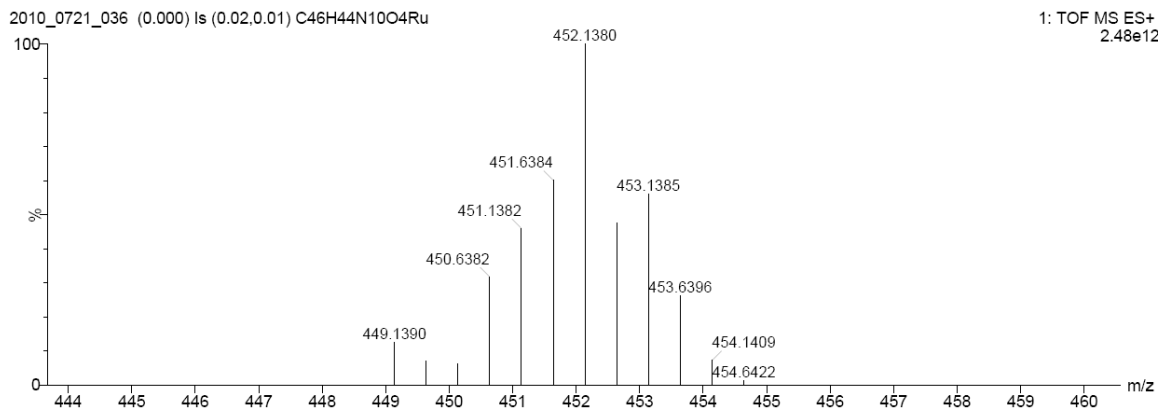
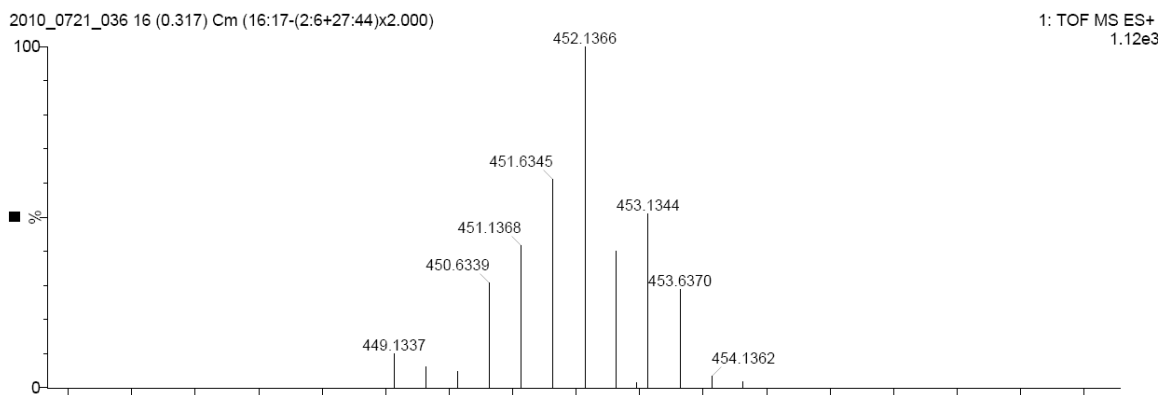
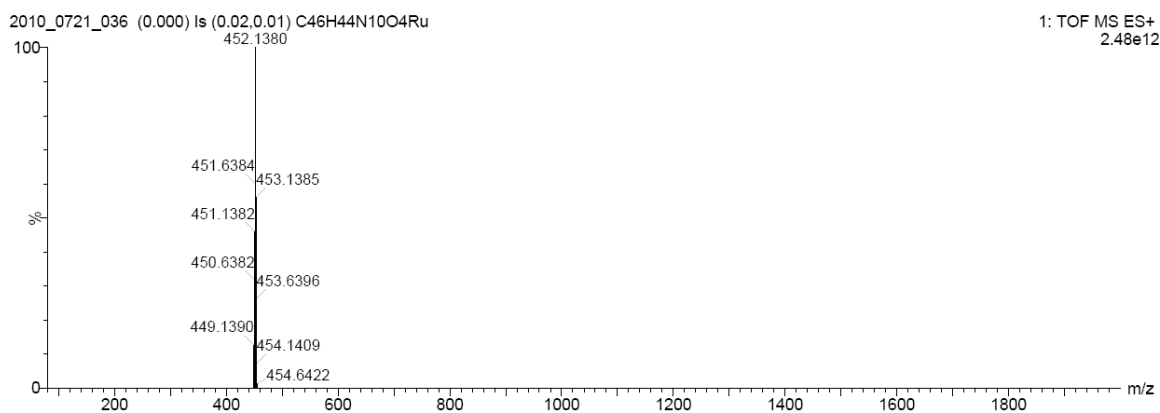
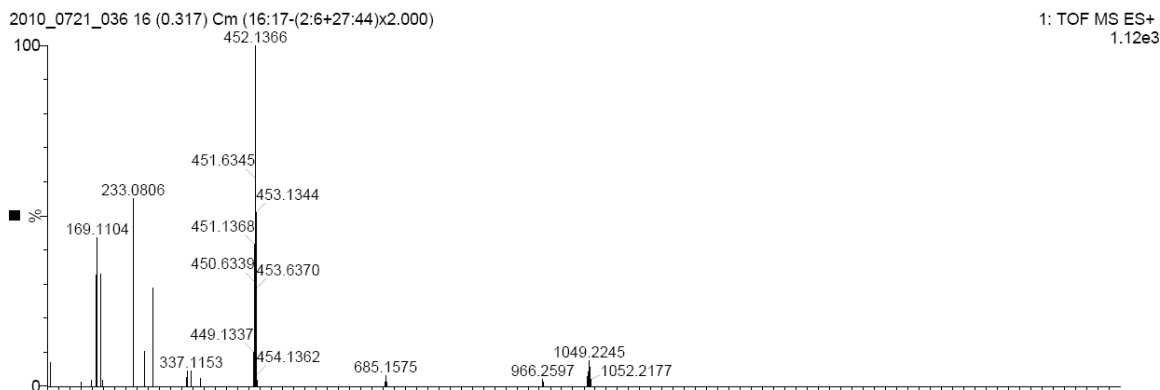
Chemical Formula: C₁₃H₁₅N₃O₂

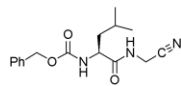
Exact Mass: 245.1164

Molecular Weight: 245.2771



IR spectrum of **123**

HRMS of **123** and Ru pattern for **123**

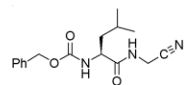
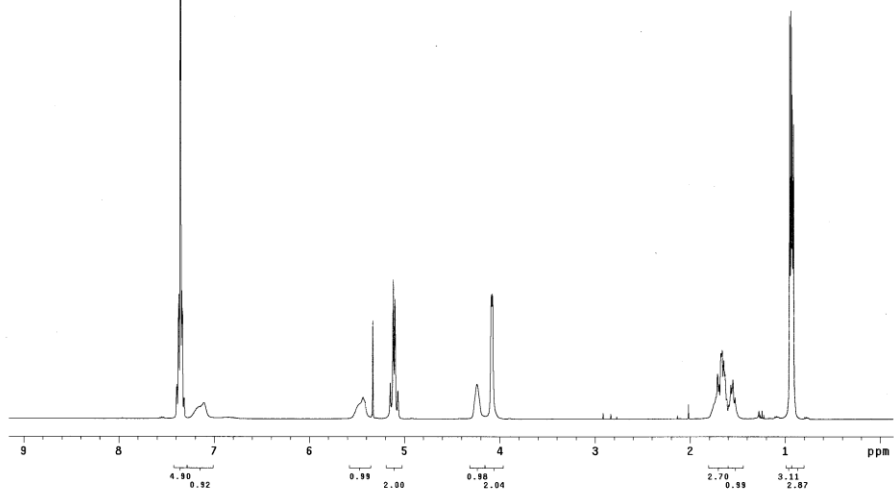


124

Chemical Formula: $C_{16}H_{21}N_3O_3$

Exact Mass: 303.1583

Molecular Weight: 303.3562

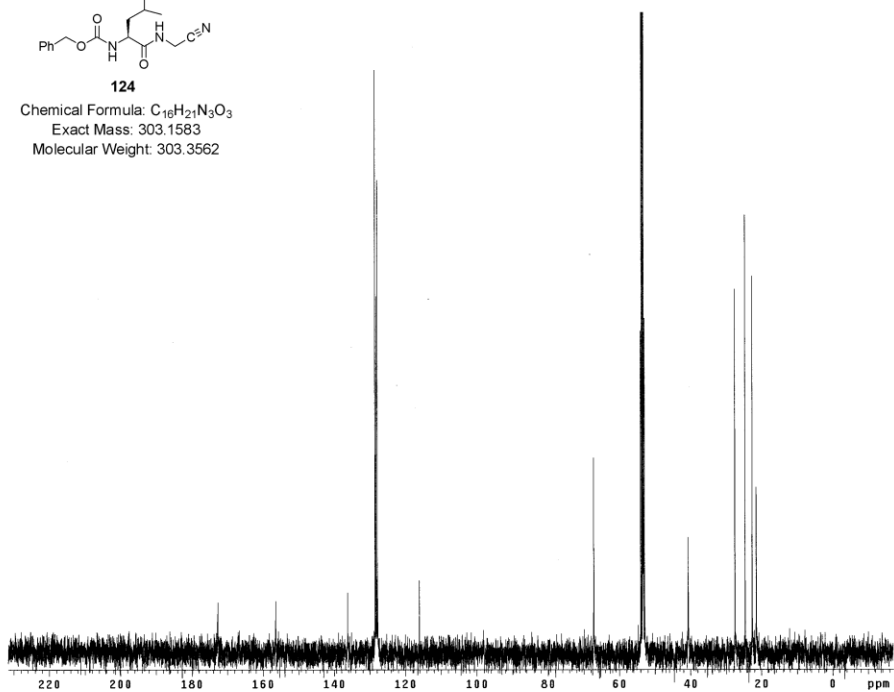


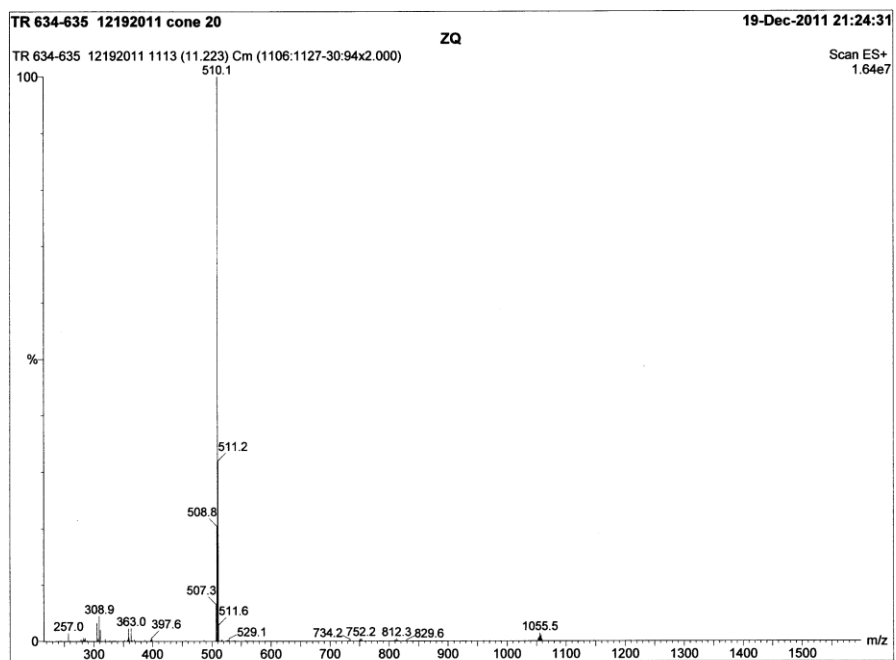
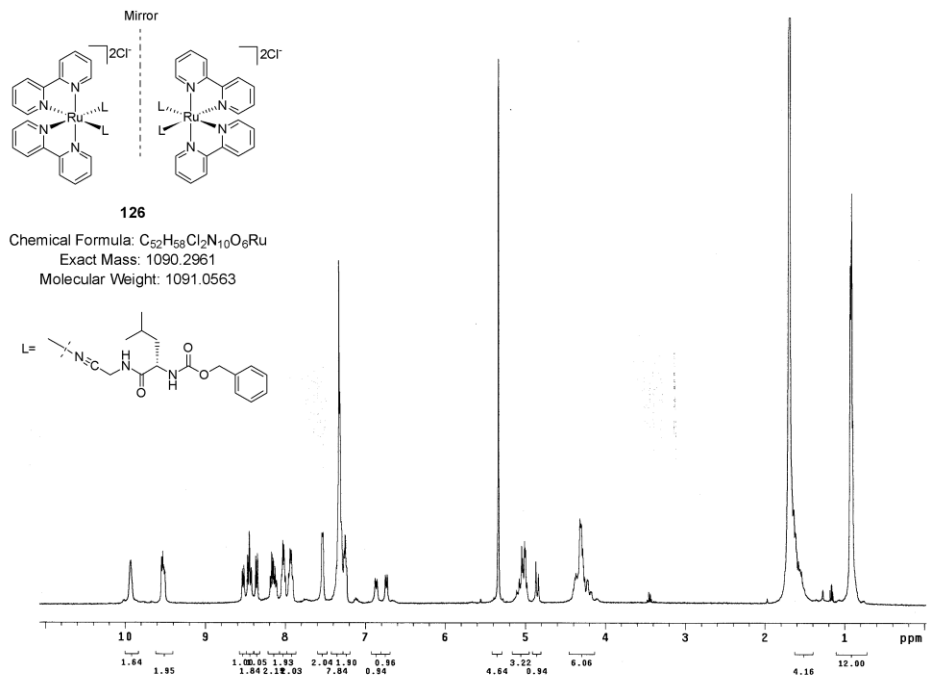
124

Chemical Formula: $C_{16}H_{21}N_3O_3$

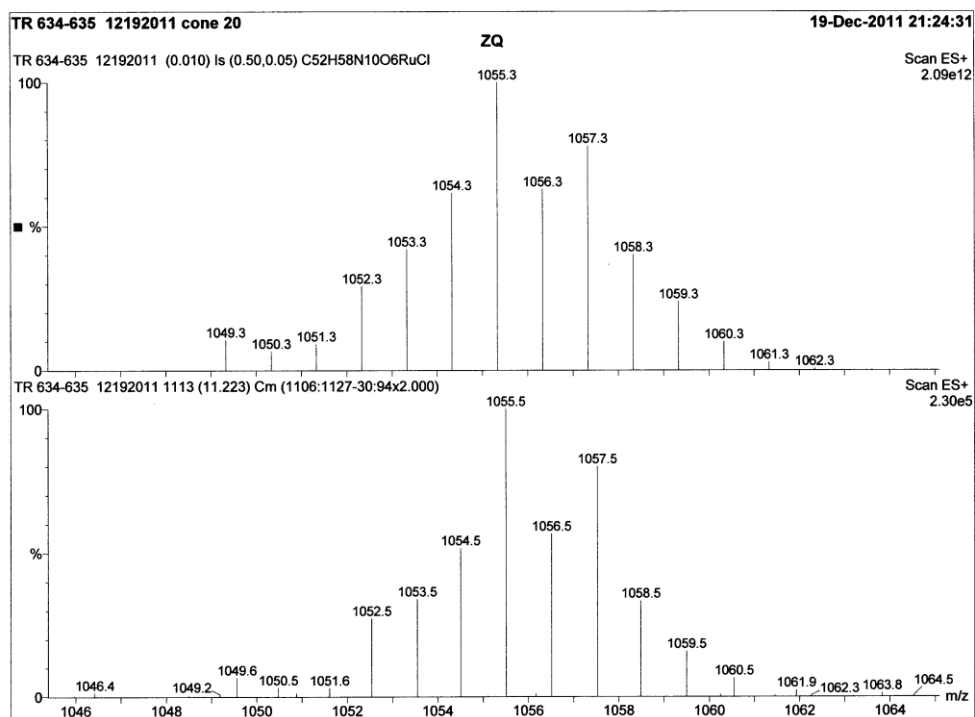
Exact Mass: 303.1583

Molecular Weight: 303.3562





LRMS of 126



LRMS of 126: Isotope pattern

REFERENCES

1. Metzler-Nolte, N., *Top. Organomet. Chem.* **2010**, *32* (Copyright (C) 2012 American Chemical Society (ACS). All Rights Reserved.), 195-217.
2. Shaw, C. F., *Chemical Reviews* **1999**, *99* (9), 2589-2600.
3. Fricker, S. P., *Dalton Transactions* **2007**, (43), 4903-4917.
4. Ghosh, D.; Pecoraro, V. L., *Current Opinion in Chemical Biology* **2005**, *9* (2), 97-103.
5. Doerr, A. J.; McLendon, G. L., *Inorganic Chemistry* **2004**, *43* (25), 7916-7925.
6. DeGrado, W. F.; Summa, C. M.; Pavone, V.; Nastro, F.; Lombardi, A., *Annual Review of Biochemistry* **1999**, *68*, 779-819.
7. Stephenson, K. A.; Banerjee, S. R.; Besanger, T.; Sogbein, O. O.; Levadala, M. K.; McFarlane, N.; Lemon, J. A.; Boreham, D. R.; Maresca, K. P.; Brennan, J. D.; Babich, J. W.; Zubieta, J.; Valliant, J. F., *Journal of the American Chemical Society* **2004**, *126* (28), 8598-8599.
8. Fischman, A. J.; Babich, J. W.; Strauss, H. W., *Journal of Nuclear Medicine* **1993**, *34* (12), 2253-63.
9. Okarvi, S. M., *Cancer Treatment Reviews* **2008**, *34* (1), 13-26.
10. Okarvi, S. M., *Medicinal Research Reviews* **2004**, *24* (5), 685.
11. Fichna, J.; Janecka, A., *Bioconjugate Chem. FIELD Full Journal Title:Bioconjugate Chemistry* **2003**, *14* (1), 3-17.
12. Liu, S.; Edwards, D. S., *Chemical Reviews* **1999**, *99* (9), 2235-2268.
13. Sardesai, N. Y.; Zimmermann, K.; Barton, J. K., *Journal of the American Chemical Society* **1994**, *116* (17), 7502-8.

14. Jeon, J. W.; Son, S. J.; Yoo, C. E.; Hong, I. S.; Song, J. B.; Suh, J., *Organic Letters* **2002**, 4 (23), 4155-4158.
15. Hamzavi, R.; Happ, T.; Weitershaus, K.; Metzler-Nolte, N., *Journal of Organometallic Chemistry* **2004**, 689 (25), 4745-4750.
16. Imperiali, B.; Roy, R. S., *The Journal of Organic Chemistry* **1995**, 60 (6), 1891-1894.
17. Imperiali, B.; Prins, T. J.; Fisher, S. L., *The Journal of Organic Chemistry* **1993**, 58 (6), 1613-1616.
18. Imperiali, B.; Fisher, S. L., *Journal of the American Chemical Society* **1991**, 113 (22), 8527-8528.
19. Imperiali, B.; Fisher, S. L., *The Journal of Organic Chemistry* **1992**, 57 (2), 757-759.
20. van den Heuvel, M.; van den Berg, T. A.; Kellogg, R. M.; Choma, C. T.; Feringa, B. L., *Journal of Organic Chemistry* **2004**, 69 (2), 250-262.
21. Abouelatta, A. I.; Campanali, A. A.; Ekkati, A. R.; Shamoun, M.; Kalapugama, S.; Kodanko, J. J., *Inorganic Chemistry* **2009**, 48 (16), 7729-7739.
22. Ekkati, A. R.; Kodanko, J. J., *J Am Chem Soc* **2007**, 129 (41), 12390-1.
23. Jackson, C. S.; Schmitt, S.; Dou, Q. P.; Kodanko, J. J., *Inorganic Chemistry* **2011**, 50 (12), 5336-5338.
24. Prakash, J.; Schmitt, S. M.; Dou, Q. P.; Kodanko, J. J., *Metallomics* **2012**, 4 (2), 174-178.
25. Prakash, J.; Kodanko, J. J., *Inorganic Chemistry* **2012**, 51 (4), 2689-2698.
26. Dilipkumar, J. N., *Wayne State University Dissertations* **2011**.
27. Stephenson, K. A.; Banerjee, S. R.; Sogbein, O. O.; Levadala, M. K.; McFarlane, N.; Boreham, D. R.; Maresca, K. P.; Babich, J. W.; Zubieta, J.; Valliant, J. F., *Bioconjugate Chemistry* **2005**, 16 (5), 1189-1195.

28. Stephenson, K. A.; Zubieta, J.; Banerjee, S. R.; Levadala, M. K.; Taggart, L.; Ryan, L.; McFarlane, N.; Boreham, D. R.; Maresca, K. P.; Babich, J. W.; Valliant, J. F., *Bioconjugate Chemistry* **2004**, *15* (1), 128-136.
29. Stephenson, K. A.; Reid, L. C.; Zubieta, J.; Babich, J. W.; Kung, M.-P.; Kung, H. F.; Valliant, J. F., *Bioconjugate Chemistry* **2008**, *19* (5), 1087-1094.
30. Ruan, F.; Chen, Y.; Itoh, K.; Sasaki, T.; Hopkins, P. B., *The Journal of Organic Chemistry* **1991**, *56* (14), 4347-4354.
31. De León-Rodríguez, L. M.; Kovacs, Z.; Dieckmann, G. R.; Sherry, A. D., *Chemistry – A European Journal* **2004**, *10* (5), 1149-1155.
32. Peuralahti, J.; Hakala, H.; Mikkala, V.-M.; Loman, K.; Hurskainen, P.; Mulari, O.; Hovinen, J., *Bioconjugate Chemistry* **2002**, *13* (4), 870-875.
33. Song, A. I.; Rana, T. M., *Bioconjugate Chemistry* **1997**, *8* (2), 249-252.
34. Jiang, H.; O'Neil, E. J.; DiVittorio, K. M.; Smith, B. D., *Organic Letters* **2005**, *7* (14), 3013-3016.
35. Cheng, R. P.; Fisher, S. L.; Imperiali, B., *Journal of the American Chemical Society* **1996**, *118* (46), 11349-11356.
36. Huang, X.; Long, E. C., *Bioorganic & Medicinal Chemistry Letters* **1995**, *5* (17), 1937-1940.
37. Rossi, P.; Felluga, F.; Scrimin, P., *Tetrahedron Letters* **1998**, *39* (39), 7159-7162.
38. Rossi, P.; Tecilla, P.; Baltzer, L.; Scrimin, P., *Chemistry – A European Journal* **2004**, *10* (17), 4163-4170.
39. Nadler, A.; Hain, C.; Diederichsen, U., *European Journal of Organic Chemistry* **2009**, *2009* (27), 4593-4599.

40. Chen, S.-Y.; Huang, Y.; Zhang, G.-L.; Cheng, H.; Xia, C.-Q.; Ma, L.-J.; Yu, H.; Yu, X.-Q., *Synthesis* **2005**, 2005 (EFirst), 888,892.
41. Fani, M.; Maecke, H., *European Journal of Nuclear Medicine and Molecular Imaging* **2012**, 39 (1), 11-30.
42. Bajusz, S.; Janaky, T.; Csernus, V. J.; Bokser, L.; Fekete, M.; Srkalovic, G.; Redding, T. W.; Schally, A. V., *Proceedings of the National Academy of Sciences* **1989**, 86 (16), 6313-6317.
43. Lee, J.; Udugamasooriya, D. G.; Lim, H.-S.; Kodadek, T., *Nat Chem Biol* **2010**, 6 (4), 258-260.
44. Mansuy, D.; Battioni, P., *Bioinorg. Catal. (2nd Ed., Revis. Expanded)* **1999**, 323-354.
45. Que, L., Jr., *Bioinorg. Catal. (2nd Ed., Revis. Expanded)* **1999**, 269-321.
46. Rohde, J.-U.; In, J.-H.; Lim, M. H.; Brennessel, W. W.; Bukowski, M. R.; Stubna, A.; Münck, E.; Nam, W.; Que, L., *Science* **2003**, 299 (5609), 1037-1039.
47. Costas, M.; Mehn, M. P.; Jensen, M. P.; Que, L., *Chemical Reviews* **2004**, 104 (2), 939-986.
48. Que, L., *Accounts of Chemical Research* **2007**, 40 (7), 493-500.
49. Nam, W., *Accounts of Chemical Research* **2007**, 40 (7), 522-531.
50. Abouelatta, A. I. Y., *Wayne State University Dissertations. Paper 153* **2010**.
51. Campanali, A. A., *Wayne State University Dissertations. Paper 194* **2011**.
52. Grapperhaus, C. A.; Mienert, B.; Bill, E.; Weyhermüller, T.; Wieghardt, K., *Inorganic Chemistry* **2000**, 39 (23), 5306-5317.

53. Lim, M. H.; Rohde, J.-U.; Stubna, A.; Bukowski, M. R.; Costas, M.; Ho, R. Y. N.; Münck, E.; Nam, W.; Que, L., Jr., *Proceedings of the National Academy of Sciences of the United States of America* **2003**, *100* (7), 3665-3670.
54. Bukowski, M. R.; Koehntop, K. D.; Stubna, A.; Bominaar, E. L.; Halfen, J. A.; Muenck, E.; Nam, W.; Que, L., Jr., *Science* **2005**, *310* (5750), 1000-1002.
55. Nehru, K.; Seo, M. S.; Kim, J.; Nam, W., *Inorganic Chemistry* **2007**, *46* (1), 293-298.
56. Bukowski, M. R.; Comba, P.; Lienke, A.; Limberg, C.; Lopez de Laorden, C.; Mas-Balleste, R.; Merz, M.; Que, L., Jr., *Angewandte Chemie, International Edition* **2006**, *45* (21), 3446-3449.
57. Sastri, C. V.; Seo, M. S.; Park, M. J.; Kim, K. M.; Nam, W., *Chemical Communications* **2005**, (11), 1405-1407.
58. Pestovsky, O.; Stoian, S.; Bominaar, E. L.; Shan, X.; Munck, E.; Que, L., Jr.; Bakac, A., *Angewandte Chemie, International Edition* **2005**, *44* (42), 6871-6874.
59. Balland, V.; Charlot, M.-F.; Banse, F.; Girerd, J.-J.; Mattioli, T. A.; Bill, E.; Bartoli, J.-F.; Battioni, P.; Mansuy, D., *European Journal of Inorganic Chemistry* **2004**, (2), 301-308.
60. Li, F.; England, J.; Que, L., *Journal of the American Chemical Society* **2010**, *132* (7), 2134-2135.
61. Kim, S. O.; Sastri, C. V.; Seo, M. S.; Kim, J.; Nam, W., *Journal of the American Chemical Society* **2005**, *127* (12), 4178-4179.
62. Kaizer, J.; Klinker, E. J.; Oh, N. Y.; Rohde, J.-U.; Song, W. J.; Stubna, A.; Kim, J.; Münck, E.; Nam, W.; Que, L., *Journal of the American Chemical Society* **2003**, *126* (2), 472-473.
63. Jabre, N. D.; Hryhorczuk, L.; Kodanko, J. J., *Inorganic Chemistry* **2009**.

64. Campanali, A. A.; Kwiecien, T. D.; Hryhorczuk, L.; Kodanko, J. J., *Inorganic Chemistry* **2010**, *49* (11), 4759-4761.
65. Prakash, J.; Kodanko, J. J., *Inorganic Chemistry* **2011**, *50* (9), 3934-3945.
66. Merrifield, R. B., *Journal of the American Chemical Society* **1963**, *85* (14), 2149-2154.
67. Marglin, B.; Merrifield, R. B., *Journal of the American Chemical Society* **1966**, *88* (21), 5051-5052.
68. Fankhauser, P.; Brenner, M., Need for Solid-Phase Thinking in Solid-Phase Synthesis. In *The Chemistry of Polypeptides*, Katsoyannis, P. G., Ed. Springer US: 1973; pp 389-411.
69. Mitchell, A. R., *Peptide Science* **2008**, *90* (3), 175-184.
70. Gordon, K.; Balasubramanian, S., *Journal of Chemical Technology & Biotechnology* **1999**, *74* (9), 835-851.
71. Gutte, B.; Merrifield, R. B., *Journal of Biological Chemistry* **1971**, *246* (6), 1922-1941.
72. Wang, S.-S., *Journal of the American Chemical Society* **1973**, *95* (4), 1328-1333.
73. Rink, H., *Tetrahedron Letters* **1987**, *28* (33), 3787-3790.
74. Barlos, K.; Gatos, D.; Kallitsis, J.; Papaphotiu, G.; Sotiriu, P.; Wenqing, Y.; Schäfer, W., *Tetrahedron Letters* **1989**, *30* (30), 3943-3946.
75. Story, S. C.; Aldrich, J. V., *International Journal of Peptide and Protein Research* **1992**, *39* (1), 87-92.
76. Thompson, L. A.; Ellman, J. A., *Tetrahedron Letters* **1994**, *35* (50), 9333-9336.
77. Dinh, T. Q.; Armstrong, R. W., *Tetrahedron Letters* **1996**, *37* (8), 1161-1164.
78. Calmes, M.; Daunis, J., *Amino Acids* **1999**, *16* (3-4), 215-250.
79. Ma, J.-A., *Angewandte Chemie International Edition* **2003**, *42* (36), 4290-4299.
80. Najera, C.; Sansano, J. M., *Chemical Reviews* **2007**, *107* (11), 4584-4671.

81. Maruoka, K.; Ooi, T., *Chemical Reviews* **2003**, *103* (8), 3013-3028.
82. O'Donnell, M. J., *Accounts of Chemical Research* **2004**, *37* (8), 506-517.
83. Mohr, J. T.; Hong, A. Y.; Stoltz, B. M., *Nat Chem* **2009**, *1* (5), 359-369.
84. Knowles, W. S.; Sabacky, M. J., *Chemical Communications (London)* **1968**, *0* (22), 1445-1446.
85. Junge, K.; Oehme, G.; Monsees, A.; Riermeier, T.; Dingerdissen, U.; Beller, M., *Journal of Organometallic Chemistry* **2003**, *675* (1-2), 91-96.
86. Fu, Y.; Hou, G.-H.; Xie, J.-H.; Xing, L.; Wang, L.-X.; Zhou, Q.-L., *The Journal of Organic Chemistry* **2004**, *69* (23), 8157-8160.
87. Junge, K.; Hagemann, B.; Enthaler, S.; Spannenberg, A.; Michalik, M.; Oehme, G.; Monsees, A.; Riermeier, T.; Beller, M., *Tetrahedron: Asymmetry* **2004**, *15* (17), 2621-2631.
88. Jia, X.; Li, X.; Xu, L.; Shi, Q.; Yao, X.; Chan, A. S. C., *The Journal of Organic Chemistry* **2003**, *68* (11), 4539-4541.
89. Reetz, M. T.; Ma, J.-A.; Goddard, R., *Angewandte Chemie International Edition* **2005**, *44* (3), 412-415.
90. Abe, H.; Amii, H.; Uneyama, K., *Organic Letters* **2001**, *3* (3), 313-315.
91. Burk, M. J.; Feaster, J. E., *Journal of the American Chemical Society* **1992**, *114* (15), 6266-6267.
92. Banphavichit, V.; Mansawat, W.; Bhanthumnavin, W.; Vilaivan, T., *Tetrahedron* **2004**, *60* (46), 10559-10568.
93. Ooi, T.; Uematsu, Y.; Maruoka, K., *Journal of the American Chemical Society* **2006**, *128* (8), 2548-2549.

94. Lygo, B.; Andrews, B. I., *Accounts of Chemical Research* **2004**, 37 (8), 518-525.
95. Hashimoto, T.; Maruoka, K., *Chemical Reviews* **2007**, 107 (12), 5656-5682.
96. Ooi, T.; Maruoka, K., *Angewandte Chemie-International Edition* **2007**, 46 (23), 4222-4266.
97. Jew, S. S.; Park, H. G., *Chemical Communications* **2009**, (46), 7090-7103.
98. O'Donnell, M. J.; Bennett, W. D.; Wu, S., *Journal of the American Chemical Society* **1989**, 111 (6), 2353-2355.
99. Corey, E. J.; Xu, F.; Noe, M. C., *Journal of the American Chemical Society* **1997**, 119 (50), 12414-12415.
100. Corey, E. J.; Noe, M. C.; Xu, F., *Tetrahedron Letters* **1998**, 39 (30), 5347-5350.
101. Lygo, B.; Wainwright, P. G., *Tetrahedron Letters* **1997**, 38 (49), 8595-8598.
102. O'Donnell, M. J.; Delgado, F.; Hostettler, C.; Schwesinger, R., *Tetrahedron Letters* **1998**, 39 (48), 8775-8778.
103. Chinchilla, R.; Mazon, P.; Najera, C., *Molecules* **2004**, 9 (5), 349-364.
104. Thierry, B.; Plaquevent, J. C.; Cahard, D., *Molecular Diversity* **2005**, 9 (4), 277-290.
105. Park, H. G.; Jeong, B. S.; Yoo, M. S.; Lee, J. H.; Park, M. K.; Lee, Y. J.; Kim, M. J.; Jew, S. S., *Angewandte Chemie-International Edition* **2002**, 41 (16), 3036-3038.
106. Chinchilla, R.; Mazón, P.; Nájera, C., *Tetrahedron: Asymmetry* **2002**, 13 (9), 927-931.
107. Lygo, B.; Allbutt, B., *Synlett* **2004**, (2), 326-328.
108. Palmer, M. J.; Danilewicz, J. C.; Vuong, H., *Synlett* **1994**, (3), 171-2.
109. Faul, M. M.; Winneroski, L. L.; York, J. S.; Reinhard, M. R.; Hoying, R. C.; Gritton, W. H.; Dominianni, S. J., *Heterocycles* **2001**, 55 (4), 689-704.
110. Kundu, B.; Shukla, S., *Collect. Czech. Chem. Commun.* **1994**, 59 (1), 231-233.

111. Diez-Barra, E.; De La Hoz, A.; Sanchez-Verdu, P., *Anales de Quimica International Edition* **1997**, *93* (3), 145-146.
112. Applegate, H. E.; Cimarusti, C. M.; Dolfini, J. E.; Funke, P. T.; Koster, W. H.; Puar, M. S.; Slusarchyk, W. A.; Young, M. G., *The Journal of Organic Chemistry* **2002**, *44* (5), 811.
113. Freedman, H. H.; Dubois, R. A., *Tetrahedron Letters* **1975**, *16* (38), 3251-3254.
114. Dehmlow, E. V., *Angewandte Chemie International Edition in English* **1977**, *16* (8), 493-505.
115. Rabinovitz, M.; Cohen, Y.; Halpern, M., *Angewandte Chemie International Edition in English* **1986**, *25* (11), 960-970.
116. Zervas, L.; Theodoropoulos, D. M., *Journal of the American Chemical Society* **1956**, *78* (7), 1359.
117. Dugave, C.; Menez, A., *The Journal of Organic Chemistry* **1996**, *61* (17), 6067.
118. Sharma, S. K.; Songster, M. F.; Colpitts, T. L.; Hegyes, P.; Barany, G.; Castellino, F. J., *The Journal of Organic Chemistry* **1993**, *58* (18), 4993.
119. Ulku, S., *Wayne State University Dissertations* **2011**.
120. Jabre, N. D.; Respondek, T.; Ulku, S. A.; Korostelova, N.; Kodanko, J. J., *The Journal of Organic Chemistry* **2010**, *75* (3), 650-659.
121. Ooi, T.; Uematsu, Y.; Kameda, M.; Maruoka, K., *Angewandte Chemie-International Edition* **2002**, *41* (9), 1551-1554.
122. Ooi, T.; Kameda, M.; Maruoka, K., *Journal of the American Chemical Society* **2003**, *125* (17), 5139-5151.
123. Wessjohann, L.; McGaffin, G.; de Meijere, A., *Synthesis* **1989**, *1989* (05), 359,363.

124. Saksena, A. K.; Girijavallabhan, V. M.; Lovey, R. G.; Jao, E.; Bennett, F.; Mc, C. J. L.; Wang, H.; Pike, R. E.; Bogen, S. L.; Chan, T.-Y.; Liu, Y.-T.; Zhu, Z.; Njoroge, F. G.; Arasappan, A.; Parekh, T.; Ganguly, A. K.; Chen, K. X.; Venkatraman, S.; Vaccaro, H. A.; Pinto, P. A.; Santhanam, B.; Kemp, S. J.; Levy, O. E.; Lim-Wilby, M.; Tamura, S. Y.; Wu, W.; Hendrata, S.; Huang, Y.; Wong, J. K.; Nair, L. G. Preparation of peptides as NS3-serine protease inhibitors of hepatitis C virus. US20070032433A1, 2007.
125. Yue, C.; Thierry, J.; Potier, P., *Tetrahedron Letters* **1993**, 34 (2), 323-326.
126. Thierry, J.; Yue, C.; Potier, P., *Tetrahedron Letters* **1998**, 39 (12), 1557-1560.
127. Pickard, P. L.; Tolbert, T. L., *Org. Synth.* **1964**, 44, 51.
128. Eils, S.; Rossen, K.; Jahn, W.; Klement, I. Imination process for the preparation of substituted N-methyleneglycinate esters from imines and leaving group-substituted acetate esters. EP1207151A1, 2002.
129. Respondek, T.; Cueny, E.; Kodanko, J. J., *Organic Letters* **2011**, 14 (1), 150-153.
130. O'Donnell, M. J.; Polt, R. L., *The Journal of Organic Chemistry* **1982**, 47 (13), 2663-2666.
131. Kodanko, J. J.; Morys, A. J.; Lippard, S. J., *Organic Letters* **2005**, 7 (21), 4585-4588.
132. Puente, X. S.; Sanchez, L. M.; Overall, C. M.; Lopez-Otin, C., *Nat Rev Genet* **2003**, 4 (7), 544-558.
133. Rawlings, N. D.; Tolle, D. P.; Barrett, A. J., *Nucleic Acids Res* **2004**, 32 (suppl 1), D160-D164.
134. Turk, B., *Nat Rev Drug Discov* **2006**, 5 (9), 785-799.
135. Koblinski, J. E.; Ahram, M.; Sloane, B. F., *Clinica Chimica Acta* **2000**, 291 (2), 113-135.

136. Stennicke, H. R.; Ryan, C. A.; Salvesen, G. S., *Trends in Biochemical Sciences* **2002**, 27 (2), 94-101.
137. Thome, M.; Schneider, P.; Hofmann, K.; Fickenscher, H.; Meinel, E.; Neipel, F.; Mattmann, C.; Burns, K.; Bodmer, J.-L.; Schroter, M.; Scaffidi, C.; Krammer, P. H.; Peter, M. E.; Tschopp, J., *Nature* **1997**, 386 (6624), 517-521.
138. Abbenante, G.; Fairlie, D. P., *Med Chem* **2005**, 1 (1), 71-104.
139. Zaman, M. A.; Oparil, S.; Calhoun, D. A., *Nat Rev Drug Discov* **2002**, 1 (8), 621-636.
140. Overall, C. M.; Lopez-Otin, C., *Nat Rev Cancer* **2002**, 2 (9), 657-672.
141. Coussens, L. M.; Fingleton, B.; Matrisian, L. M., *Science* **2002**, 295 (5564), 2387-2392.
142. James, M. N. G., *Protein Science* **1999**, 8 (3), 693-694.
143. Turk, V.; Turk, B.; Turk, D., *EMBO J* **2001**, 20 (17), 4629-4633.
144. Reinheckel, T.; Deussing, J.; Roth, W.; Peters, C., *Biological Chemistry* **2001**, 382 (5), 735-741.
145. Saftig, P.; Hunziker, E.; Wehmeyer, O.; Jones, S.; Boyde, A.; Rommerskirch, W.; Moritz, J. D.; Schu, P.; von Figura, K., *Proceedings of the National Academy of Sciences* **1998**, 95 (23), 13453-13458.
146. Mohamed, M. M.; Sloane, B. F., *Nat Rev Cancer* **2006**, 6 (10), 764-775.
147. Gocheva, V.; Joyce, J. A., *Cell Cycle* **2007**, 6 (1), 60-64.
148. Palermo, C.; Joyce, J. A., *Trends in Pharmacological Sciences* **2008**, 29 (1), 22-28.
149. Jedeszko, C.; Sloane, B. F., *Biological Chemistry* **2004**, 385 (11), 1017-1027.
150. Joyce, J. A.; Hanahan, D., *Cell Cycle* **2004**, 3 (12), 1516-1519.

151. Drake, F. H.; Dodds, R. A.; James, I. E.; Connor, J. R.; Debouck, C.; Richardson, S.; Lee-Rykaczewski, E.; Coleman, L.; Rieman, D.; Barthlow, R.; Hastings, G.; Gowen, M., *Journal of Biological Chemistry* **1996**, *271* (21), 12511-12516.
152. Garnero, P.; Borel, O.; Bytjalsen, I.; Ferreras, M.; Drake, F. H.; McQueney, M. S.; Foged, N. T.; Delmas, P. D.; Delaissé, J.-M., *Journal of Biological Chemistry* **1998**, *273* (48), 32347-32352.
153. Podgorski, I.; Linebaugh, B. E.; Koblinski, J. E.; Rudy, D. L.; Herroon, M. K.; Olive, M. B.; Sloane, B. F., *Am J Pathol* **2009**, *175* (3), 1255-1269.
154. Framson, P. E.; Sage, E. H., *Journal of Cellular Biochemistry* **2004**, *92* (4), 679-690.
155. Podhajcer, O.; Benedetti, L.; Girotti, M. R.; Prada, F.; Salvatierra, E.; Llera, A., *Cancer and Metastasis Reviews* **2008**, *27* (3), 523-537.
156. Herroon, M. K.; Rajagurubandara, E.; Rudy, D. L.; Chalasani, A.; Hardaway, A. L.; Podgorski, I., *Oncogene* **2013**, *32* (12), 1580-1593.
157. Jensen, A. B.; Wynne, C.; Ramirez, G.; He, W.; Song, Y.; Berd, Y.; Wang, H.; Mehta, A.; Lombardi, A., *Clinical Breast Cancer* **2010**, *10* (6), 452-458.
158. Bromme, D.; Lecaille, F., *Expert Opinion on Investigational Drugs* **2009**, *18* (5), 585-600.
159. Otto, H.-H.; Schirmeister, T., *Chemical Reviews* **1997**, *97* (1), 133-171.
160. Renslo, A. R.; McKerrow, J. H., *Nat Chem Biol* **2006**, *2* (12), 701-710.
161. Vasiljeva, O.; Reinheckel, T.; Peters, C.; Turk, D.; Turk, V.; Turk, B., *Current Pharmaceutical Design* **2007**, *13* (3), 385-401.
162. Yasuda, Y.; Kaleta, J.; Brömme, D., *Advanced Drug Delivery Reviews* **2005**, *57* (7), 973-993.

163. Sadaghiani, A. M.; Verhelst, S. H. L.; Gocheva, V.; Hill, K.; Majerova, E.; Stinson, S.; Joyce, J. A.; Bogyo, M., *Chemistry & Biology* **2007**, *14* (5), 499-511.
164. Mukherjee, A.; Sadler, P. J.; Begley, T. P., *Metals in Medicine: Therapeutic Agents*. In *Wiley Encyclopedia of Chemical Biology*, John Wiley & Sons, Inc.: 2007.
165. Dhar, S.; Kolishetti, N.; Lippard, S. J.; Farokhzad, O. C., *Proceedings of the National Academy of Sciences* **2011**, *108* (5), 1850-1855.
166. Pizarro, A.; Habtemariam, A.; Sadler, P., *Activation Mechanisms for Organometallic Anticancer Complexes*. In *Medicinal Organometallic Chemistry*, Jaouen, G.; Metzler-Nolte, N., Eds. Springer Berlin Heidelberg: 2010; Vol. 32, pp 21-56.
167. Peyrone, M., *Justus Liebigs Annalen der Chemie* **1844**, *51* (1), 1-29.
168. Rosenberg, B. H.; Cavalieri, L. F., *Nature* **1965**, *206* (4988), 999-1001.
169. Rosenberg, B.; Vancamp, L.; Trosko, J. E.; Mansour, V. H., *Nature* **1969**, *222* (5191), 385-386.
170. Cepeda, V.; Fuertes, M. A.; Castilla, J.; Alonso, C.; Quevedo, C.; Perez, J. M., *Anticancer Agents Med Chem* **2007**, *7* (1), 3-18.
171. Jung, Y.; Lippard, S. J., *Chemical Reviews* **2007**, *107* (5), 1387-1407.
172. Nakayama, K.; Kanzaki, A.; Terada, K.; Mutoh, M.; Ogawa, K.; Sugiyama, T.; Takenoshita, S.; Itoh, K.; Yaegashi, N.; Miyazaki, K.; Neamati, N.; Takebayashi, Y., *Clinical Cancer Research* **2004**, *10* (8), 2804-2811.
173. Komeda, S.; Casini, A., *Curr Top Med Chem* **2012**, *12* (3), 219-35.
174. Bergamo, A.; Sava, G., *Dalton Transactions* **2011**, *40* (31), 7817-7823.
175. Levina, A.; Mitra, A.; Lay, P. A., *Metallomics* **2009**, *1* (6), 458-470.
176. Clarke, M. J., *Coordination Chemistry Reviews* **2003**, *236* (1-2), 209-233.

177. Clarke, M. J., *Coordination Chemistry Reviews* **2002**, 232 (1–2), 69-93.
178. Bruijninx, P. C.; Sadler, P. J., *Curr Opin Chem Biol* **2008**, 12 (2), 197-206.
179. Ang, W. H.; Dyson, P. J., *European Journal of Inorganic Chemistry* **2006**, 2006 (20), 3993-3993.
180. Clarke, M. J.; Bitler, S.; Rennert, D.; Buchbinder, M.; Kelman, A. D., *Journal of Inorganic Biochemistry* **1980**, 12 (1), 79-87.
181. Frasca, D.; Ciampa, J.; Emerson, J.; Umans, R. S.; Clarke, M. J., *Met Based Drugs* **1996**, 3 (4), 197-209.
182. Mestroni, G.; Alessio, E.; Sava, G.; Pacor, S.; Coluccia, M.; Boccarelli, A., *Met Based Drugs* **1994**, 1 (1), 41-63.
183. Coluccia, M.; Sava, G.; Loseto, F.; Nassi, A.; Boccarelli, A.; Giordano, D.; Alessio, E.; Mestroni, G., *European Journal of Cancer* **1993**, 29 (13), 1873-1879.
184. Rademaker-Lakhai, J. M.; van den Bongard, D.; Pluim, D.; Beijnen, J. H.; Schellens, J. H. M., *Clinical Cancer Research* **2004**, 10 (11), 3717-3727.
185. Hartinger, C. G.; Zorbas-Seifried, S.; Jakupec, M. A.; Kynast, B.; Zorbas, H.; Keppler, B. K., *Journal of Inorganic Biochemistry* **2006**, 100 (5–6), 891-904.
186. Bergamo, A.; Sava, G., *Dalton Transactions* **2007**, 0 (13), 1267-1272.
187. Kapitza, S.; Pongratz, M.; Jakupec, M. A.; Heffeter, P.; Berger, W.; Lackinger, L.; Keppler, B. K.; Marian, B., *Journal of Cancer Research and Clinical Oncology* **2005**, 131 (2), 101-110.
188. Som, P.; Oster, Z. H.; Matsui, K.; Guglielmi, G.; Persson, B. R. R.; Pellettieri, M. L.; Srivastava, S. C.; Richards, P.; Atkins, H. L.; Brill, A. B., *European Journal of Nuclear Medicine* **1983**, 8 (11), 491-494.

189. Hartinger, C. G.; Hann, S.; Koellensperger, G.; Sulyok, M.; Groessler, M.; Timerbaev, A. R.; Rudnev, A. V.; Stingeder, G.; Keppler, B. K., *Int J Clin Pharmacol Ther* **2005**, *43* (12), 583-5.
190. Piccioli, F.; Sabatini, S.; Messori, L.; Orioli, P.; Hartinger Ch, G.; Keppler, B. K., *J Inorg Biochem* **2004**, *98* (6), 1135-42.
191. Pongratz, M.; Schluga, P.; Jakupec, M. A.; Arion, V. B.; Hartinger, C. G.; Allmaier, G.; Keppler, B. K., *Journal of Analytical Atomic Spectrometry* **2004**, *19* (1), 46-51.
192. Hostetter, A. A.; Miranda, M. L.; DeRose, V. J.; McFarlane Holman, K. L., *J Biol Inorg Chem* **2011**, *16* (8), 1177-85.
193. Scolaro, C.; Bergamo, A.; Brescacin, L.; Delfino, R.; Cocchietto, M.; Laurency, G.; Geldbach, T. J.; Sava, G.; Dyson, P. J., *Journal of Medicinal Chemistry* **2005**, *48* (12), 4161-4171.
194. Peacock, A. F. A.; Sadler, P. J., *Chemistry – An Asian Journal* **2008**, *3* (11), 1890-1899.
195. Guichard, S. M.; Else, R.; Reid, E.; Zeitlin, B.; Aird, R.; Muir, M.; Dodds, M.; Fiebig, H.; Sadler, P. J.; Jodrell, D. I., *Biochemical Pharmacology* **2006**, *71* (4), 408-415.
196. Phillips, A. D.; Gonsalvi, L.; Romerosa, A.; Vizza, F.; Peruzzini, M., *Coordination Chemistry Reviews* **2004**, *248* (11-12), 955-993.
197. Casini, A.; Gabbiani, C.; Sorrentino, F.; Rigobello, M. P.; Bindoli, A.; Geldbach, T. J.; Marrone, A.; Re, N.; Hartinger, C. G.; Dyson, P. J.; Messori, L., *Journal of Medicinal Chemistry* **2008**, *51* (21), 6773-6781.
198. Barton, J., *Science* **1986**, *233* (4765), 727-734.
199. Barton, J. K.; Lolis, E., *Journal of the American Chemical Society* **1985**, *107* (3), 708-709.

200. Novakova, O.; Kasparkova, J.; Vrana, O.; van Vliet, P. M.; Reedijk, J.; Brabec, V., *Biochemistry* **1995**, *34* (38), 12369-12378.
201. Erkkila, K. E.; Odom, D. T.; Barton, J. K., *Chemical Reviews* **1999**, *99* (9), 2777-2796.
202. Gill, M. R.; Thomas, J. A., *Chemical Society Reviews* **2012**, *41* (8), 3179-3192.
203. Schatzschneider, U.; Niesel, J.; Ott, I.; Gust, R.; Alborzinia, H.; Wöfl, S., *ChemMedChem* **2008**, *3* (7), 1104-1109.
204. Xu, H.; Liang, Y.; Zhang, P.; Du, F.; Zhou, B.-R.; Wu, J.; Liu, J.-H.; Liu, Z.-G.; Ji, L.-N., *JBIC Journal of Biological Inorganic Chemistry* **2005**, *10* (5), 529-538.
205. Hall, J. P.; O'Sullivan, K.; Naseer, A.; Smith, J. A.; Kelly, J. M.; Cardin, C. J., *Proceedings of the National Academy of Sciences* **2011**, *108* (43), 17610-17614.
206. Turro, C., *Proceedings of the National Academy of Sciences* **2011**, *108* (43), 17573-17574.
207. Ortman, I.; Elias, B.; Kelly, J. M.; Moucheron, C.; Kirsch-DeMesmaeker, A., *Dalton Transactions* **2004**, *0* (4), 668-676.
208. Chatterjee, D.; Mitra, A.; De, G. S., *Platinum Met. Rev.* **2006**, *50* (1), 2-12.
209. Corral, E.; Hotze, A. G.; Dulk, H.; Leczkowska, A.; Rodger, A.; Hannon, M.; Reedijk, J., *JBIC Journal of Biological Inorganic Chemistry* **2009**, *14* (3), 439-448.
210. Winterle, J. S.; Kliger, D. S.; Hammond, G. S., *Journal of the American Chemical Society* **1976**, *98* (12), 3719-3721.
211. Demas, J. N.; Harris, E. W.; McBride, R. P., *Journal of the American Chemical Society* **1977**, *99* (11), 3547-3551.
212. Miller, S. S.; Zahir, K.; Haim, A., *Inorganic Chemistry* **1985**, *24* (24), 3978-3980.

213. Mulazzani, Q. G.; Sun, H.; Hoffman, M. Z.; Ford, W. E.; Rodgers, M. A. J., *The Journal of Physical Chemistry* **1994**, *98* (4), 1145-1150.
214. DeRosa, M. C.; Crutchley, R. J., *Coordination Chemistry Reviews* **2002**, *233–234* (0), 351-371.
215. Abdel-Shafi, A. A.; Worrall, D. R.; Ershov, A. Y., *Dalton Transactions* **2004**, *0* (1), 30-36.
216. Hamblin, M. M.; Mroz, P., *Advances in Photodynamic Therapy: Basic, Translational and Clinical*. Artech House: 2008; p 600.
217. Durham, B.; Caspar, J. V.; Nagle, J. K.; Meyer, T. J., *Journal of the American Chemical Society* **1982**, *104* (18), 4803-4810.
218. Pinnick, D. V.; Durham, B., *Inorganic Chemistry* **1984**, *23* (10), 1440-1445.
219. Henderson, B. W.; Dougherty, T. J., *Photochemistry and Photobiology* **1992**, *55* (1), 145-157.
220. Dolmans, D. E. J. G. J.; Fukumura, D.; Jain, R. K., *Nat Rev Cancer* **2003**, *3* (5), 380-387.
221. Pushpan, S. K.; Venkatraman, S.; Anand, V. G.; Sankar, J.; Parmeswaran, D.; Ganesan, S.; Chandrashekar, T. K., *Curr Med Chem Anticancer Agents* **2002**, *2* (2), 187-207.
222. O'Connor, A. E.; Gallagher, W. M.; Byrne, A. T., *Photochemistry and Photobiology* **2009**, *85* (5), 1053-1074.
223. Ackroyd, R.; Kelty, C.; Brown, N.; Reed, M., *Photochemistry and Photobiology* **2001**, *74* (5), 656-669.
224. Horstkotte, E.; Schröder, T.; Niewöhner, J.; Thiel, E.; Jay, D. G.; Henning, S. W., *Photochemistry and Photobiology* **2005**, *81* (2), 358-366.
225. Rajfur, Z.; Roy, P.; Otey, C.; Romer, L.; Jacobson, K., *Nat Cell Biol* **2002**, *4* (4), 286-93.

226. Bulina, M. E.; Chudakov, D. M.; Britanova, O. V.; Yanushevich, Y. G.; Staroverov, D. B.; Chepurnykh, T. V.; Merzlyak, E. M.; Shkrob, M. A.; Lukyanov, S.; Lukyanov, K. A., *Nat Biotechnol* **2006**, *24* (1), 95-9.
227. Vitriol, E. A.; Uetrecht, A. C.; Shen, F.; Jacobson, K.; Bear, J. E., *Proceedings of the National Academy of Sciences* **2007**, *104* (16), 6702-6707.
228. Lee, J.; Yu, P.; Xiao, X.; Kodadek, T., *Molecular BioSystems* **2008**, *4* (1), 59-65.
229. Abdel-Shafi, A. A.; Beer, P. D.; Mortimer, R. J.; Wilkinson, F., *Helvetica Chimica Acta* **2001**, *84* (9), 2784-2795.
230. Zeglis, B. M.; Pierre, V. C.; Barton, J. K., *Chemical Communications* **2007**, *0* (44), 4565-4579.
231. Sitlani, A.; Long, E. C.; Pyle, A. M.; Barton, J. K., *Journal of the American Chemical Society* **1992**, *114* (7), 2303-2312.
232. Singh, T. N.; Turro, C., *Inorganic Chemistry* **2004**, *43* (23), 7260-7262.
233. Garner, R. N.; Gallucci, J. C.; Dunbar, K. R.; Turro, C., *Inorg Chem* **2011**, *50* (19), 9213-5.
234. Goldbach, R. E.; Rodriguez-Garcia, I.; van Lenthe, J. H.; Siegler, M. A.; Bonnet, S., *Chemistry – A European Journal* **2011**, *17* (36), 9924-9929.
235. Howerton, B. S.; Heidary, D. K.; Glazer, E. C., *Journal of the American Chemical Society* **2012**, *134* (20), 8324-8327.
236. Wachter, E.; Heidary, D. K.; Howerton, B. S.; Parkin, S.; Glazer, E. C., *Chemical Communications* **2012**, *48* (77), 9649-9651.
237. Betanzos-Lara, S.; Salassa, L.; Habtemariam, A.; Sadler, P. J., *Chemical Communications* **2009**, *0* (43), 6622-6624.

238. Betanzos-Lara, S.; Salassa, L.; Habtemariam, A.; Novakova, O.; Pizarro, A. M.; Clarkson, G. J.; Liskova, B.; Brabec, V.; Sadler, P. J., *Organometallics* **2012**, *31* (9), 3466-3479.
239. Garanger, E.; Boturyn, D.; Dumy, P., *Anticancer Agents Med Chem* **2007**, *7* (5), 552-8.
240. Reubi, J. C., *Endocr Rev* **2003**, *24* (4), 389-427.
241. Zaccaro, L.; Del Gatto, A.; Pedone, C.; Saviano, M., *Curr Med Chem* **2009**, *16* (7), 780-95.
242. Mező, G.; Manea, M., *Expert Opinion on Drug Delivery* **2010**, *7* (1), 79-96.
243. Barragán, F.; López-Senín, P.; Salassa, L.; Betanzos-Lara, S.; Habtemariam, A.; Moreno, V.; Sadler, P. J.; Marchán, V., *Journal of the American Chemical Society* **2011**, *133* (35), 14098-14108.
244. Zayat, L.; Calero, C.; Alborés, P.; Baraldo, L.; Etchenique, R., *Journal of the American Chemical Society* **2003**, *125* (4), 882-883.
245. Zayat, L.; Salierno, M.; Etchenique, R., *Inorganic Chemistry* **2006**, *45* (4), 1728-1731.
246. Nikolenko, V.; Yuste, R.; Zayat, L.; Baraldo, L. M.; Etchenique, R., *Chemical Communications* **2005**, *0* (13), 1752-1754.
247. Zayat, L.; Noval, M. G.; Campi, J.; Calero, C. I.; Calvo, D. J.; Etchenique, R., *ChemBioChem* **2007**, *8* (17), 2035-2038.
248. Fry, N. L.; Mascharak, P. K., *Accounts of Chemical Research* **2011**, *44* (4), 289-298.
249. Balzani, V.; Moggi, L.; Manfrin, M. F.; Bolletta, F.; Laurence, G. S., *Coordination Chemistry Reviews* **1975**, *15* (4), 321-433.
250. Van Houten, J.; Watts, R. J., *Journal of the American Chemical Society* **1975**, *97* (13), 3843-3844.

251. Wagenknecht, P. S.; Ford, P. C., *Coordination Chemistry Reviews* **2011**, 255 (5–6), 591-616.
252. Burdzinski, G.; Hackett, J. C.; Wang, J.; Gustafson, T. L.; Hadad, C. M.; Platz, M. S., *Journal of the American Chemical Society* **2006**, 128 (41), 13402-13411.
253. Chen, L. X., *Angewandte Chemie International Edition* **2004**, 43 (22), 2886-2905.
254. Liu, Y.; Turner, D. B.; Singh, T. N.; Angeles-Boza, A. M.; Chouai, A.; Dunbar, K. R.; Turro, C., *Journal of the American Chemical Society* **2008**, 131 (1), 26-27.
255. Salassa, L.; Garino, C.; Salassa, G.; Gobetto, R.; Nervi, C., *Journal of the American Chemical Society* **2008**, 130 (29), 9590-9597.
256. Borfecchia, E.; Garino, C.; Salassa, L.; Ruiu, T.; Gianolio, D.; Zhang, X.; Attenkofer, K.; Chen, L. X.; Gobetto, R.; Sadler, P. J.; Lamberti, C., *Dalton Transactions* **2013**, 42 (18), 6564-6571.
257. Farrer, N. J.; Sadler, P. J., *Australian Journal of Chemistry* **2008**, 61 (9), 669-674.
258. Löser, R.; Schilling, K.; Dimmig, E.; Gütschow, M., *Journal of Medicinal Chemistry* **2005**, 48 (24), 7688-7707.
259. Moon, J. B.; Coleman, R. S.; Hanzlik, R. P., *Journal of the American Chemical Society* **1986**, 108 (6), 1350-1.
260. Cruz, A. J.; Kirgan, R.; Siam, K.; Heiland, P.; Rillema, D. P., *Inorganica Chimica Acta* **2010**, 363 (11), 2496-2505.
261. Liu, Y.; Turner, D. B.; Singh, T. N.; Angeles-Boza, A. M.; Chouai, A.; Dunbar, K. R.; Turro, C., *Journal of the American Chemical Society* **2009**, 131 (1), 26-27.
262. Stone, K. R.; Mickey, D. D.; Wunderli, H.; Mickey, G. H.; Paulson, D. F., *Int J Cancer* **1978**, 21 (3), 274-81.

263. Podgorski, I.; Linebaugh, B. E.; Sameni, M.; Jedeszko, C.; Bhagat, S.; Cher, M. L.; Sloane, B. F., *Neoplasia* **2005**, 7 (3), 207-23.
264. Respondek, T.; Garner, R. N.; Herroon, M. K.; Podgorski, I.; Turro, C.; Kodanko, J. J., *Journal of the American Chemical Society* **2011**, 133 (43), 17164-17167.
265. Greenspan, P. D.; Clark, K. L.; Tommasi, R. A.; Cowen, S. D.; McQuire, L. W.; Farley, D. L.; van Duzer, J. H.; Goldberg, R. L.; Zhou, H.; Du, Z.; Fitt, J. J.; Coppa, D. E.; Fang, Z.; Macchia, W.; Zhu, L.; Capparelli, M. P.; Goldstein, R.; Wigg, A. M.; Doughty, J. R.; Bohacek, R. S.; Knap, A. K., *Journal of Medicinal Chemistry* **2001**, 44 (26), 4524-4534.
266. *Handbook of Photochemistry, Third Edition*. CRC Press: 2006; p pp 650.
267. Brown, G. M.; Callahan, R. W.; Meyer, T. J., *Inorganic Chemistry* **1975**, 14 (8), 1915-1921.
268. Durham, B.; Wilson, S. R.; Hodgson, D. J.; Meyer, T. J., *Journal of the American Chemical Society* **1980**, 102 (2), 600-607.
269. Ford, P. C., *Coordination Chemistry Reviews* **1970**, 5 (1), 75-99.
270. Ford, P. C., *Coordination Chemistry Reviews* **1982**, 44 (1), 61-82.
271. Ford, P. C.; Wink, D.; Dibenedetto, J., *Progress in Inorganic Chemistry* **1983**, 30, 213-71.
272. Palmer, J. T.; Bryant, C.; Wang, D.-X.; Davis, D. E.; Setti, E. L.; Rydzewski, R. M.; Venkatraman, S.; Tian, Z.-Q.; Burrill, L. C.; Mendonca, R. V.; Springman, E.; McCarter, J.; Chung, T.; Cheung, H.; Janc, J. W.; McGrath, M.; Somoza, J. R.; Enriquez, P.; Yu, Z. W.; Strickley, R. M.; Liu, L.; Venuti, M. C.; Percival, M. D.; Falgueyret, J.-P.; Prasit, P.; Oballa, R.; Riendeau, D.; Young, R. N.; Wesolowski, G.; Rodan, S. B.; Johnson, C.; Kimmel, D. B.; Rodan, G., *Journal of Medicinal Chemistry* **2005**, 48 (24), 7520-7534.

273. Ruettinger, A.; Mollenhauer, J.; Loeser, R.; Guetschow, M.; Wiederanders, B., *BioTechniques* **2006**, *41* (4), 469-473.
274. Cer, R. Z.; Mudunuri, U.; Stephens, R.; Lebeda, F. J., *Nucleic Acids Res* **2009**, *37* (Web Server issue), W441-5.
275. Tepel, C.; Bromme, D.; Herzog, V.; Brix, K., *Journal of Cell Science* **2000**, *113* (24), 4487-4498.
276. Puckett, C. A.; Ernst, R. J.; Barton, J. K., *Dalton Transactions* **2010**, *39* (5), 1159-1170.
277. Brubaker, K. D.; Vessella, R. L.; True, L. D.; Thomas, R.; Corey, E., *Journal of Bone and Mineral Research* **2003**, *18* (2), 222-230.
278. Littlewood-Evans, A. J.; Bilbe, G.; Bowler, W. B.; Farley, D.; Wlodarski, B.; Kokubo, T.; Inaoka, T.; Sloane, J.; Evans, D. B.; Gallagher, J. A., *Cancer Research* **1997**, *57* (23), 5386-5390.
279. Kingsley, L. A.; Fournier, P. G. J.; Chirgwin, J. M.; Guise, T. A., *Molecular Cancer Therapeutics* **2007**, *6* (10), 2609-2617.

ABSTRACT**METHODOLOGIES FOR ATTACHING POLYPYRIDYL LIGANDS INTO AMINO ACIDS AND SYNTHESIS AND BIOLOGICAL EVALUATION OF NOVEL LIGHT ACTIVATED PEPTIDOMIMETIC CYSTEINE PROTEASE INHIBITORS CAGED BY Ru^{II}(bpy)₂**

by

TOMASZ RESPONDEK**August 2013****Advisor:** Jeremy J. Kodanko, Ph.D.**Major:** Chemistry (Organic)**Degree:** Doctor of Philosophy

Two separate subjects are described in this dissertation. The first part describes novel methodologies for attaching polypyridyl ligands into unnatural amino acids. The first chapter describes the different possibilities for attaching metal ligands to peptides and their applications as potential imaging and therapeutic agents covered so far in the literature. It is followed in the second chapter by the description of a new method for the construction of metal-peptide conjugates through the use of three unnatural amino acids, and their adaptation to solid phase synthesis. The third chapter describes the synthesis of a novel, “optimal” substrate for the enantioselective alkylation reaction of glycine benzophenone imine derivatives. Optimization of the enantiomeric excess, scope and compatibility with acid-labile containing protecting groups are disclosed.

The second chapter presents the synthesis of the first caged cysteine protease inhibitor. After an introductory survey of different Ru and Pt complexes used as potential therapeutic cancer agents, cysteine protease inhibitors are described. The syntheses of Ru^{II}(bpy)₂ complexes

caging cathepsin inhibitors are revealed with full characterization in the following chapters. The stability of the complexes in the dark in aqueous solutions and their ability to release the inhibitors upon irradiation with visible light are shown, followed by cathepsin activity inhibition studies, *in vitro* and *in cellulo*. Finally, the toxicity of the complexes is evaluated in cell viability studies.

AUTOBIOGRAPHICAL STATEMENT

TOMASZ RESPONDEK

Education

- 2007-2013 PhD studies, Wayne State University, Detroit, USA. Expected defense in June 2013
Advisor Prof. Jeremy J. Kodanko
- 2000-2007 M.Sc. in Organic Chemistry at the National Institute of Applied Sciences (INSA) of Rouen, France
Advisor Prof. Jean-Charles Quirion

Honors and Awards

- 2010-2012 President of the Alpha Psi chapter of the PLU (Phi Lambda Upsilon)
2010 Honor Citation for Teaching Service in Chemistry
2010 Department of Chemistry travel award for the spring 2010 ACS meeting
2009-present Member of the ACS
2009-2010 Secretary of the Alpha Psi chapter of the PLU
2009-present Member of the honorary chemical society Phi Lambda Upsilon (PLU)
2009 Graduate School Citation for Excellence in Teaching
2006 The GlaxoSmithKline Certificate for Outstanding Academic Achievement in Organic Chemistry

Publications

4. Respondek T., Cueny E., Kodanko J. J. "Cumyl Ester as the C-Terminal Protecting Group in the Enantioselective Alkylation of Glycine Benzophenone Imine" *Org Lett*, **2012**, 14 (1), 150–153
3. Respondek T., Garner R. N., Herroon M. K., Podgorski I., Turro C., Kodanko J. J. "Light Activation of a Cysteine Protease Inhibitor: Caging of a Peptidomimetic Nitrile with RuII(bpy)₂" *JACS*, **2011**, 133(43), 17164-17167
2. Jabre N. D., Respondek T., Ulku S., Korostelova N., Kodanko J. J. "A Divergent Strategy for Attaching Polypyridyl Ligands to Peptides", *JOC*, **2010**, 75(3), 650-659
1. Wan Z., Yan H., Hall R. F., Lin X., Livia S, Respondek T., Widdowson K. L., Zhu C., Callahan J. F. "Design and development of arrayable syntheses to accelerate SAR studies of pyridopyrimidinone and pyrimidopyrimidinone", *Tet Lett*, **2009**, 50(3), 370-372